UNIVERSITÀ DEGLI STUDI DI MILANO

PhD in Pharmacological, Experimental and Clinical Sciences – XXXIII Cycle

Department of Pharmacological and Biomolecular Sciences

May a pharmacological modulation of lipids alter pro-tumorigenic signaling of Extracellular Vesicles? A long journey in EVs dimensional, lipidic and proteic characterization from a metastatic melanoma cell line.

Tutor

Prof. A. Corsini

Candidate

Felice Maria Accattatis

Co-Tutor

Dr. L. Arnaboldi

Coordinator

Prof. G.D. Norata

A.A.

(2019-2020)

1 Introduction

2 Aims of the Project

3 Materials and methods

Proteomics, imaging and pharmacological modulation experiments have been funded by the project EXTRALIPO “New lipid-oriented pharmacological and chemical approaches to discriminate and unravel extracellular vesicles biological functions” Bando SEED – PSR 2019 by Bellosta S, Valoti E, Straniero V, Puglisi E, **Accattatis F M** and L. Arnaboldi.

Abstract

New insights into size, protein and lipid composition may help in characterizing functionality of Extracellular Vesicles (EVs) and infer with their fast development as delivery tools. Unfortunately, despite latest size-based classifications which divide EVs in small (50-80nm) or large (80-120nm) exosomes, microvesicles (<1000nm) and the new smallest (<50nm) population (exomeres), overlapping of different EV populations and unproper separation methods impair the comprehension of their biological role. In addition (EVs) are a very attractive pharmacological target, due to their involvement in cell-cell communication in physiological and pathological conditions. Among lipids, cholesterol and BisMonoacylGlyceroPhosphate (BMP) play a paramount role in EV biogenesis since their interplay drive endosomes towards the secretory or recycling pathway. We used as model a lymph node metastatic cell line (LM-16).

1)We set up a reproducible ultracentrifugation (UC) method for a size-based separation of different EV populations by 5 UC steps, in which physical and dynamic parameters are determined by an algorithm developed by Livshits et al. 2) In vitro treatment LM-16 cells with simvastatin and/or KT182, respectively inhibitors of cholesterol biosynthesis and of BMP degradation, was carried for 3 days with 10% FCS and for 3 days in serum free conditions. In this case we only isolated two fractions according to canonical EVs isolation method, namely 10K (microvesicles) and 100K (exosomes). EVs were further characterized by Nanosight, Zetasizer, Confocal and Electron microscopy. Quantitative proteomic analysis was performed by mass spectrometry and results analyzed by Ingenuity Pathway Analysis (IPA) while lipid analysis was carried out by gas-liquid chromatography.

1) Zetasizer and TEM analysis documented the existence of 5 different EV populations, whose relative % in saturated fatty acids gradually and continuously increased from larger to smaller EV (from 37.21±0.21 to 64.79±9.47). Proteomics identified a total of 2003 proteins differentially distributed (or even unique) among the 5 EV populations (n=697, 819, 1079, 1621 and 1654, respectively). IPA analysis of these distributions revealed different characteristics signaling pathways. 2) Treatment with simvastatin (0.1µM) and KT182 (50nM) alone or in combination did not affect cell proliferation, and EVs size and counts. Proteomics identified 1294 and 1192 proteins respectively for 100K and 10K, showing different significant expression patterns, compared to control, with several proteins up- and down regulated. IPA showed that treatments specifically decreased the expression of proteins involved in cellular movement, migration, proliferation and cytoskeleton arrangement, both in 100K and 10K fractions, with typical and striking differences and patterns.

Melanoma-released EVs include vesicles of different size, fatty acid and protein composition. These differences may translate into distinct behaviors and functions in biological fluids and help to define the role of specific EV populations in physiological and pathological processes. Cholesterol and BMP modulation of melanoma cells dramatically alters the protein content of released EVs, possibly leading to altered EVs functionality, suggesting the potential of lipid modulation in reshaping tumor cell-released EVs to develop new therapeutic approaches. Finally, these results pave the road to new pharmacological treatments to modulate EVs functions or to use EVs as pharmaceutical tools or melanoma biomarkers.

Nuove scoperte nella caratterizzazione dimensionale e del contenuto lipidico e proteico delle Vescicole Extracellulari (EVs) sono di fondamentale importanza per la determinazione della loro funzionalità e conseguentemente corroborare il loro sviluppo come delivery tools o biomarcatori. Le più recenti classificazioni dividono le EVs in piccole (50-80nm) e larghe (80-120nm) (esosomi) e microvescicole (<1000nm). Recentemente è stata inoltre identificata nuova popolazione, gli esomeri (<50nm). La mancanza di metodi di separazione corretti, unita alle numerose caratteristiche fisiche e chimiche in comune fra le varie popolazioni compromettono la comprensione dei loro ruoli biologici. Le EVs rappresentano inoltre un interessante target farmacologico, dal momento che sono coinvolte nella comunicazione intracellulare sia in condizioni fisiologiche che patologiche. Fra tutti i lipidi, il colesterolo e il BisMonoacilGliceroFosfato (BMP) hanno un ruolo fondamentale nella biogenesi delle vescicole dal momento che indirizzano gli endosomi verso la via degradativa o secretoria.

Considerando le più recenti classificazioni dimensionali delle EVs in base alle abbiamo settato un metodo di ultracentrifugazione con 5 differenti passaggi, utilizzando un algoritmo sviluppato da Livshits et al., che tiene conto dei parametri fisici e dinamici sia delle EV che delle centrifughe utilizzate. 2) Al fine di alterare farmacologicamente le EVs abbiamo trattato le cellule LM-16 con simvastatina (inibitore della biosintesi del colesterolo) e KT182 (inibitore della degradazione del BMP), per 3 giorni in medium supplementato con 10%FCS e per 3 giorni senza siero. In questo caso abbiano isolato due frazioni come da metodo classico, 10K (microvescicole) e 100K (esosomi). Le EVs sono state caratterizzate con l'utilizzo di Nanosight, Zetasizer, Microscopia Elettronica e Confocale. L'analisi proteomica è stata svolta tramite spettrometria di massa e i risultati analizzati con Ingenuity Pathway Analysis (IPA), mentre l'analisi lipidica è stata svolta tramite cromatografia gas-liquido.

1)Analisi tramite TEM e Zetasizer hanno documentato l'esistenza di 5 diverse popolazioni di dimensioni diverse, la cui percentuale relativa di acidi grassi saturi incrementa in maniera graduale e continua dalle vescicole più larghe a quelle più piccole (da 37.21±0.21 to 64.79±9.47). L'analisi proteomica ha identificato un totale di 2003 proteine, distribuite in maniera differente (alcune di esse uniche per ogni frazione) fra le 5 popolazioni (rispettivamente n=697, 819, 1079, 1621 e 1654). L'analisi tramite IPA delle distribuzioni proteiche ha fatto emergere differenti pathways di trasduzione del segnale associati a ciascuna frazione. 2) Il trattamento con simvastatina (0.1μM) e KT182 (50nM), e la loro combinazione, ha dimostrato di non alterare la proliferazione cellulare, il diametro e il numero di EVs. Tuttavia la successiva analisi proteomica ha identificato 1294 e 1192 proteine per rispettivamente 100K e 10K, con vie di trasduzione del segnale over e downregulate dai trattamenti.

Concludendo, le EVs rilasciate dalle cellule di melanoma includono vescicole di differente diametro, con diverse composizioni di acidi grassi e di proteine. Queste differenze si riflettono in distinte funzionalità nei fluidi biologici e possono sicuramente chiarire i diversi ruoli di specifiche popolazioni di vescicole sia in processi fisiologici che patologici. Inoltre la modulazione dei livelli di colesterolo e BMP ha significativamente alterato il contenuto proteico delle vescicole, conferendo loro un'alterata funzionalità e suggerendo il potenziale della modulazione lipidica come nuovo approccio farmacologico. In definitiva, questi risultati possono essere utili per sviluppare nuovi trattamenti farmacologici per modulare la funzionalità delle vescicole o per utilizzarli come tool farmaceutici (ad esempio come sistemi di trasporto farmaci).

Cancer and melanoma

Cancer is one of the most widespread pathologies and the second cause of deaths in the world after cardiovascular diseases (CVD) (Istituto Superiore di Sanità); in Italy every year 363.000 new cancers are diagnosed and in 2012 deaths due to malignant tumors were 177.000 (AIRC). Cancer is mainly due to the acquisition of proliferative autonomy of the cell, which is a crucial event for neoplastic transformation. Neoplastic cells are indeed prone to produce growth factors, which in turn can act in different manners[1];

- **Endocrine**: their secretion goes into circulation to act to distant sites;
- **Paracrine***:* influencing the behavior of close cells;
- **Autocrine**: cells respond to their own stimulation.

Tumors can be classified in benign or malignant. While the first ones are capsulated, non-invasive, well differentiated and characterized by a slow growth without frequent metastasis, malignant tumors are non-capsulated, invasive, undifferentiated and characterized by a very fast growth with frequent metastasis.

Among malignant tumors, cutaneous melanoma is usually quite aggressive and represents the first cause of death among this group of tumors (7% of all tumors diagnosed in USA with an incidence of 20 times higher for white vs black people). Its anatomic distribution varies among gender, with a higher frequency in limbs, trunk and head neck district and the average age of development is 45-55 years [2]. Melanoma usually develops de novo on healthy skin, but it can also grow over a pigmentated existing benign lesion (transformation ratio 1 out of 200.000) [3].

The steps of neoplastic transformation in melanoma are the following:

1) Primitive melanoma *in situ* non invasive;
2) Primitive melanoma *invasive* without metastasis;
3) Primitive melanoma *invasive* with metastasis;
4) Metastatic melanoma.

The diffusion of melanoma is due to lymphatic dissemination into locoregional lymph nodes with spreading to organs, mainly lung, liver, central nervous system, gastrointestinal system, heart, peritoneum, adrenals, skin and skeletal apparatus [1]. Beyond the surgical removal of the malignant lesion, the first line pharmacological treatment of patients with nonresectable or metastatic melanoma characterized by the BRAF V600E mutation is mainly represented

by the kinase inhibitor Vemurafenib. Among melanomas 50-60% of patients possess a mutation of the V600e which has been linked to melanoma progression (www.melanomaitalia.org). Acquisition of resistance against vemurafenib is the main problem of melanoma pharmacological treatment, therefore other effective agents are needed for therapy.

EVs overview: history, nomenclature, theragnostic potential and limiting issues.

EVs are small vesicles, delimited by a lipid bilayer membrane, whose functions are to transport proteins, mRNA, miRNA and bioactive lipids for cell-cell communication [4]. According to the literature of the last years, all cells produce extracellular vesicles; exosomes were first described in the 40s but until 2000s they did not receive so much interest since they were thought to be just garbage bins [5].

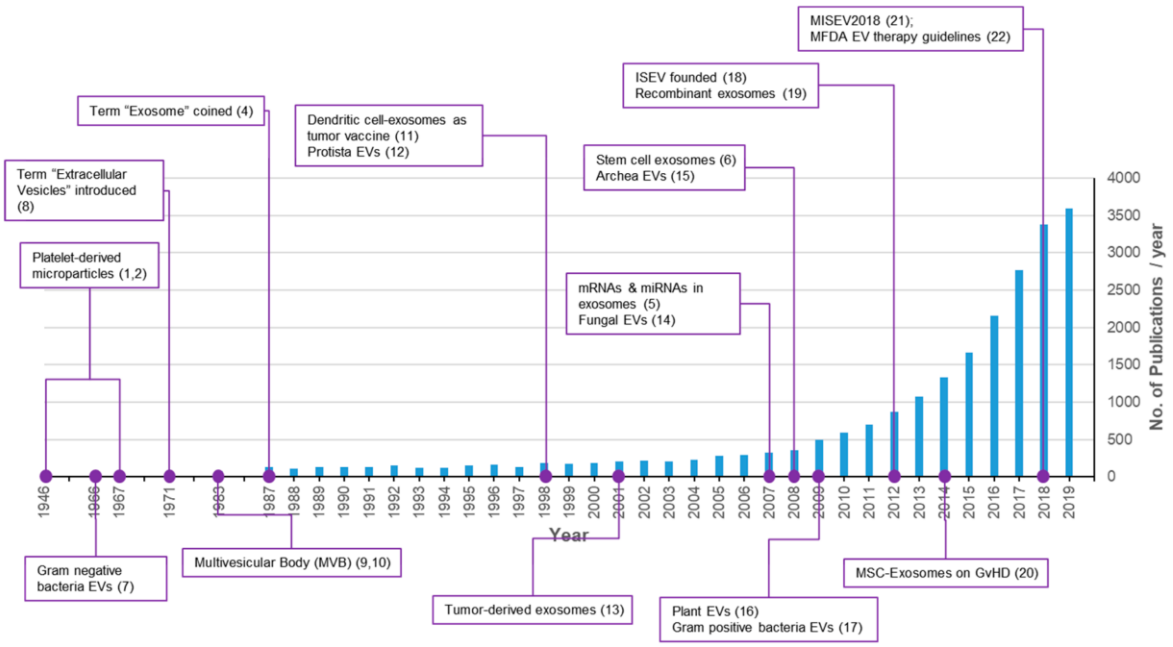

Figure 1 - History of EVs publications [5].

During last ten years, there was a huge explosion of interest, reaching 3500 publications during last year due to their great theragnostic potential, since they are involved in several transduction signal pathways both in physiological and pathological conditions. It is indeed possible to use EVs as biomarkers of early disease detection or disease progression or modify them for therapeutic goals as efficient and natural-based drug delivery systems [6]. During last years the term "exosome" became unusual and was substituted by the term Extracellular

Vesicles by the International Society of Extracellular Vesicles (ISEV). They identified various subtypes of membranous structures released by cells, and classified in exosomes, microvesicles, microparticles, ectosomes, oncosomes, apoptotic bodies and many other names. Specific issues arise when working with these "entities" whose size and amount often make them difficult to obtain as pure preparation and therefore characterize them properly [7].

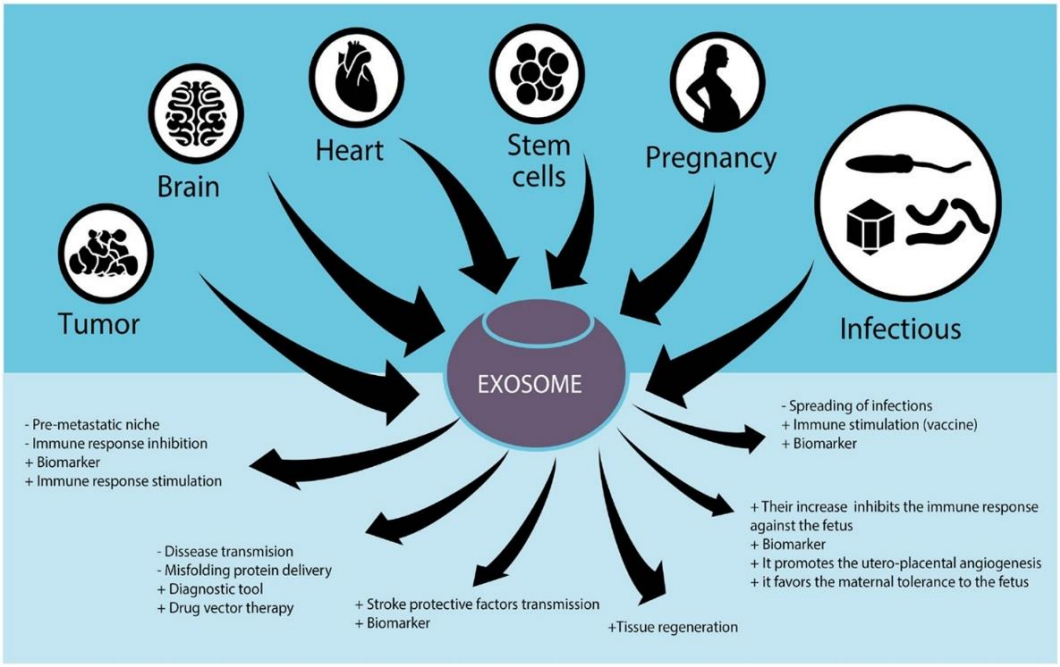

Figure 2 – Role of EVs in physiological and pathological processes [8].

Since most publications report regarding EVs focused mainly on their potential functions rather than their origin, it is still unclear which population is responsible for any given effect [4]. As highlighted in figure 2 EVs are able to play several roles in both physiological and pathological conditions as aging, immune response but also in pathological conditions as cancer, infectious and cardiovascular diseases [8]. Once secreted, EVs reach circulation and are prone to interact with recipient cells through their internalization, which leads to the activation of several and various transduction signal pathways, due to their huge enrichment in proteins, bioactive lipids and genetic materials, thus influencing physiological and pathological states of recipient cells [9]. One of the most important EVs feature is the transfer of functional cargo (miRNA, bioactive lipids and proteins) in recipient cells, with a particular tropism (e.g. ability to target specific recipient cells).

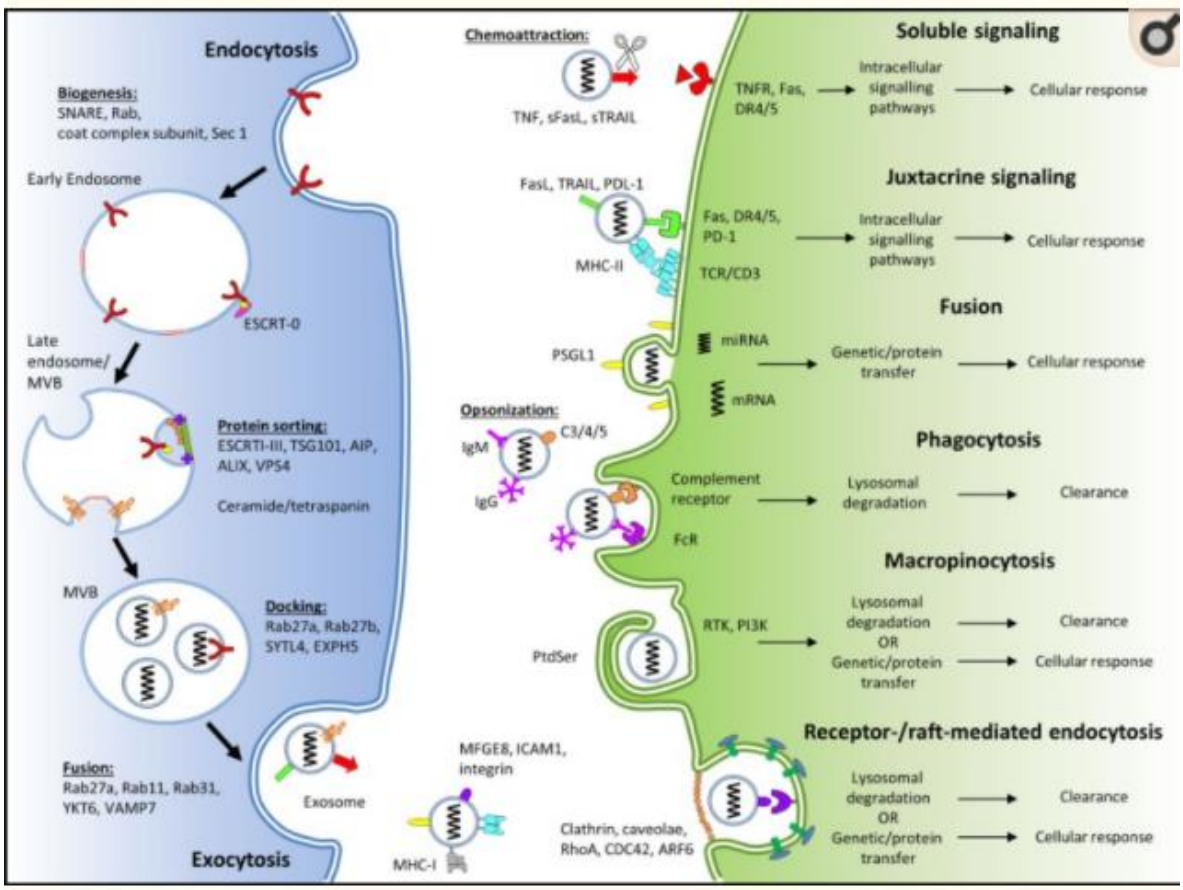

Figure 3 - Schematic representation of exosome biogenesis, internalization and cellular response [10].

EVs interaction with recipient cells utilizes various proteins expressed on their surface. As clearly explained by the figure 3 [10]. They can indeed:

1) Physically enter into the cell by fusion with plasma membrane, endocytosis phagocytosis or macropinocytosis;
2) Thanks to the presence of proteins over their surface they can bind ligands at plasma membrane level.

At any case, their content determines the activation of signaling cascades aimed at modifying behavior of recipient cells, both in pathological and in physiological conditions. In conclusion these features clearly explain the therapeutic of EVs; they can indeed be used as efficient delivery tool or as pharmacological target in EVs driven diseases [8].

Cancer and EVs, a deleterious interplay

Since it is now clear that a direct interaction between tumoral cells and their microenvironment is essential for cancer progression it is reasonable to think about a very

efficient cell-cell communication system which spreads tumoral promoters within distant and close cells. Since as mentioned EVs are small particles released by cells used to transport bioactive lipids and protein among distant and close cells it is reasonable to consider them as efficient tool of disease progression. Recent studies indeed state that EVs are fundamental to induce the formation of a pre-metastatic niche by the remodeling of extracellular matrix (ECM), they used to promote angiogenesis, to increase the proliferation of cells and to modulate the immune response on tumor environment [11] [8]. Tumoral invasion is one of the first step for metastasis cascade. Tumor-derived EVs strongly contribute to metastasis dissemination because they are prone to remodel extracellular matrix, improving tumoral cell migration [12]. They are indeed able to travel throughout the body, in all biological fluids and bind to ECM components as adhesion receptors and proteinases, (e.g. matrix metalloproteinases (MMP) and cathepsins which degrade laminin and fibronectin) [13]. On the other hand, ECM remodeling triggers the release of cytokines and growth factors which influence healthy cells of microenvironment, favoring migration and invasion of tumoral cells [12]. EVs secreted by tumoral cell lines are able to alter metabolism of healthy cells through miRNA and protein transfer; for example miR-122 contained in vesicles secreted by breast cancer is able to interact with recipient cells favoring the formation of metastasis [14]. Another important process for tumoral growth is angiogenesis, which is essential for tumoral mass to receive nutrients from blood circulation. EVs are carrier of pro-angiogenetic factors as tetraspanin-8, which is responsible to the selective recruitment of mRNA and of proteins with angiogenic features, as well as interleukin 6 (IL-6), Vascular Endothelial Growth Factor (VEGF) and MMP2 [15].

EVs classification

International Society of Extracellular Vesicles (ISEV) claimed the use of the generic term “Extracellular Vesicles” as “particles naturally released by cells which are delimited by a lipid bilayer, do not contain a functional nucleus and therefore cannot replicate” [7]. The main problem, aroused by ISEV guidelines is lack of consensus of specific markers of the different components of EVs; consensus has been only reached in defining exosomes as “particles with endosomal origin” while microparticles/microvesicles as “plasma membrane derived vesicles”[7].

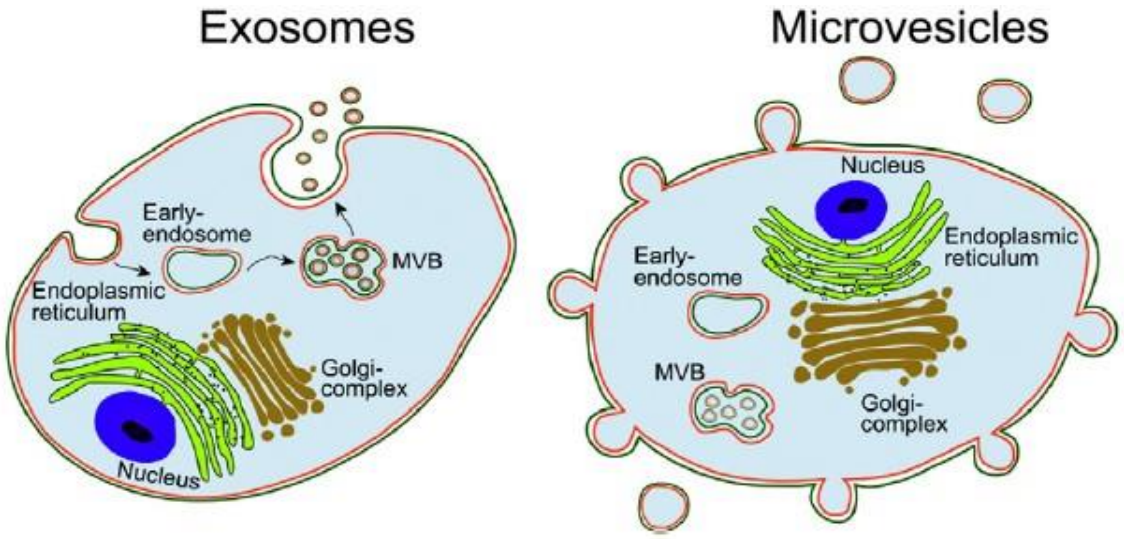

Figure 4 – While exosomes derive from the maturation of early endosomes in multivesicular bodies, microvesicles directly generate from plasma membrane budding [16].

ISEV classified vesicles according to size, one of their physical features; EVs are indeed classified in:

1) "small EVs" (sEVs) (< 100nm or < 200nm)
2) "medium/large EVs" (m/lEVs), (> 200nm) [7].

Another classification has been proposed according to their biochemical composition (CD63+/CD81+- EVs, Annexin A5-stained EVs) [7].

Nomenclature of Extracellular Vesicles and Nanoparticles

Name	Category	EV class	Size	Typical sedimentation	Protein Markers	Biogenesis
Classical exosome	Exosome	Small EV[a]	40 - 150 nm	100,000 - 200,000 × *g*	CD63 (CD81 CD9)	Multivesicular endosome
Non-classical exosome	Exosome	Small EV	40 - 150 nm	100,000 - 200,000 × *g*	(CD63- CD81- and CD9-negative)[c]	Multivesicular endosome
Classical microvesicle	Microvesicle	Large EV[b]	~ 150 - 1000 nm	10,000 - 20,000 × *g*	Annexin A1 (ARF6 Annexin A2?)	Plasma membrane budding
Large oncosome	Microvesicle	Large EV	1 - 10 µm	10,000 × *g*	Annexin A1 (ARF6 Annexin A2?)	Plasma membrane budding
ARMM	Microvesicle	Small EV	~ 40 - 100 nm	100,000 - 200,000 × *g*	ARRDC1 (TSG101)	Plasma membrane budding
Apoptotic body	Apoptotic EV	Large EV	1 - 5 µm	1,000 - 10,000 × *g*	Annexin V (PS exposure)	Apoptosis
Apoptotic vesicle	Apoptotic EV	Small to large EV	~ 100 - 1000 nm	10,000 - 200,000 × *g*	Annexin V (PS exposure)	Apoptosis
Autophagic extracellular vesicle	Autophagic EV	Small to large EV	40 - 1000 nm?	10,000 - 200,000 × *g*	LC3B-PE, p62	Unknown but autophagy-related
Exomere	Nanoparticle	Non-EV	~ 35 - 50 nm	100,000 - 200,000 × *g*	HSP90, HSPA13	Unknown
NV fractions	Nanoparticle	Non-EV	? (vaults: ~ 70 nm)	100,000 - 200,000 × *g*	Fibronectin, Histones, MVP, HSPA13	Unknown

EV, extracellular vesicle; ARMM, arrestin-domain-containing protein 1 (ARRDC1)-mediated microvesicle; PS, phosphatidylserine; NV, non-vesicular
[a]Small EVs are <200 nm in diameter; [b]Large EVs are >200 nm in diameter; [c]Hypothetical exosome not expressing CD63, CD81 and CD9

Table 1 from [17] - *Classifications of different EVs populations based on ultracentrifugation methods.*

In addition, EVs populations are nowadays classified according to the *g forces* by which they are isolated, following Thery's classical protocol [18].

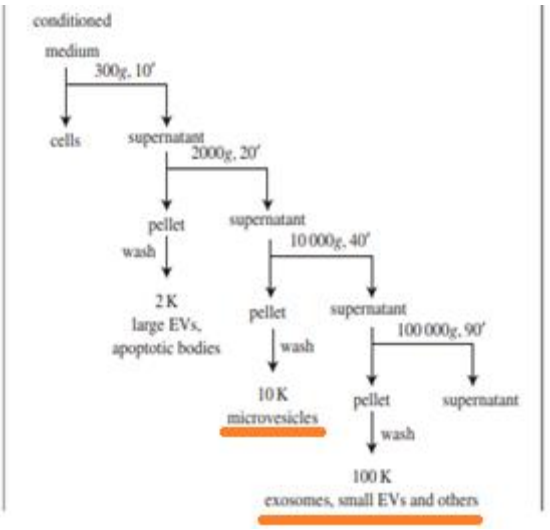

Scheme 1 – Classical ultracentrifugation protocol [18].

According to this protocol, EVs are classified in 10K pellet (microvesicles) and 100K pellet (exosomes).

In conclusion it is imperative to improve isolation and characterization methods to achieve EVs correct characterization.

Advances in dimensional EVs classification

The heterogeneity of EVs preparations makes difficult the understanding of their genesis, composition, distribution and their functions. In 2018 Zhang et al.,[19] utilized asymmetric flow field fractionation (AF4) to separate different populations of EVs based on their density and hydrodynamic properties by two perpendicular flows. They were able to optimize and adapt commonly used protocols in pharmaceutical industry to analyze polymers, macromolecules, protein complexes and viruses and to EVs.

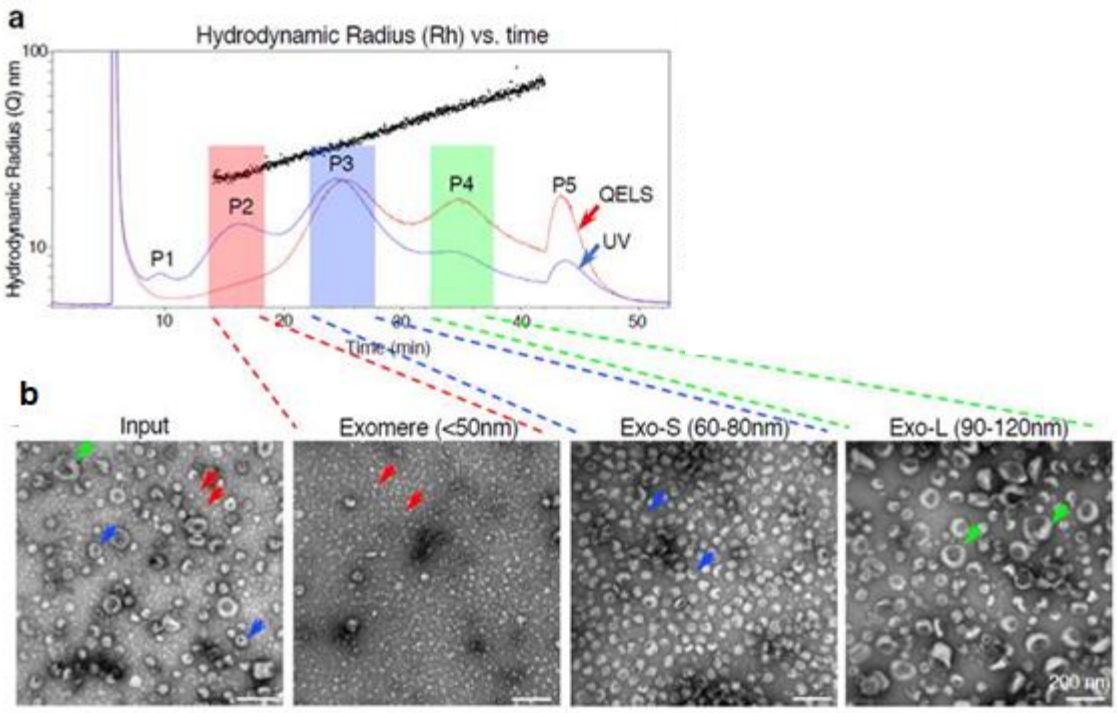

Figure 5 – Isolation methods and identification with electron microscopy and dynamic light scattering of the three resultant different populations after AF4 isolation.

AF4 represents the best way to separate different population of EVs, since it is the less-stressing method for vesicles themselves.

(a) A representative AF4 fractionation profile of vesicles. x- axis, time (min); y-axis (scale) and black dots, hydrodynamic radius (nm); red and blue lines illustrate the QELS (DLS) intensity and UV absorbance (shown on a relative scale). Different fractions have been classified in exomeres (hydrodynamic diameter <50 nm,); Exo-Small (60-80 nm); and Exo-Large (90-120 nm).

(b) Transmission Electron Microscopy images of the pre-fractionation sample (input) fractionated subpopulations (sample before separation by AF-4).

Based on these procedures they were able to identify two different classes of EVs, respectively small (60-80) and large (90-120) exosomes, together with a new population of vesicles that they called exomeres (35nm). Moreover they performed a deep analysis of the fractions, including proteomics, N-Glycosylation patterns, lipidomics, RNA and DNA profiles. They found relevant differences suggesting that these populations may have different biogenesis mechanisms and different functions in cellular communication [20]. One of the most important finding of this study is that EVs heterogeneity is not only driven by size alone, but also by cargo variations between and within each size class.

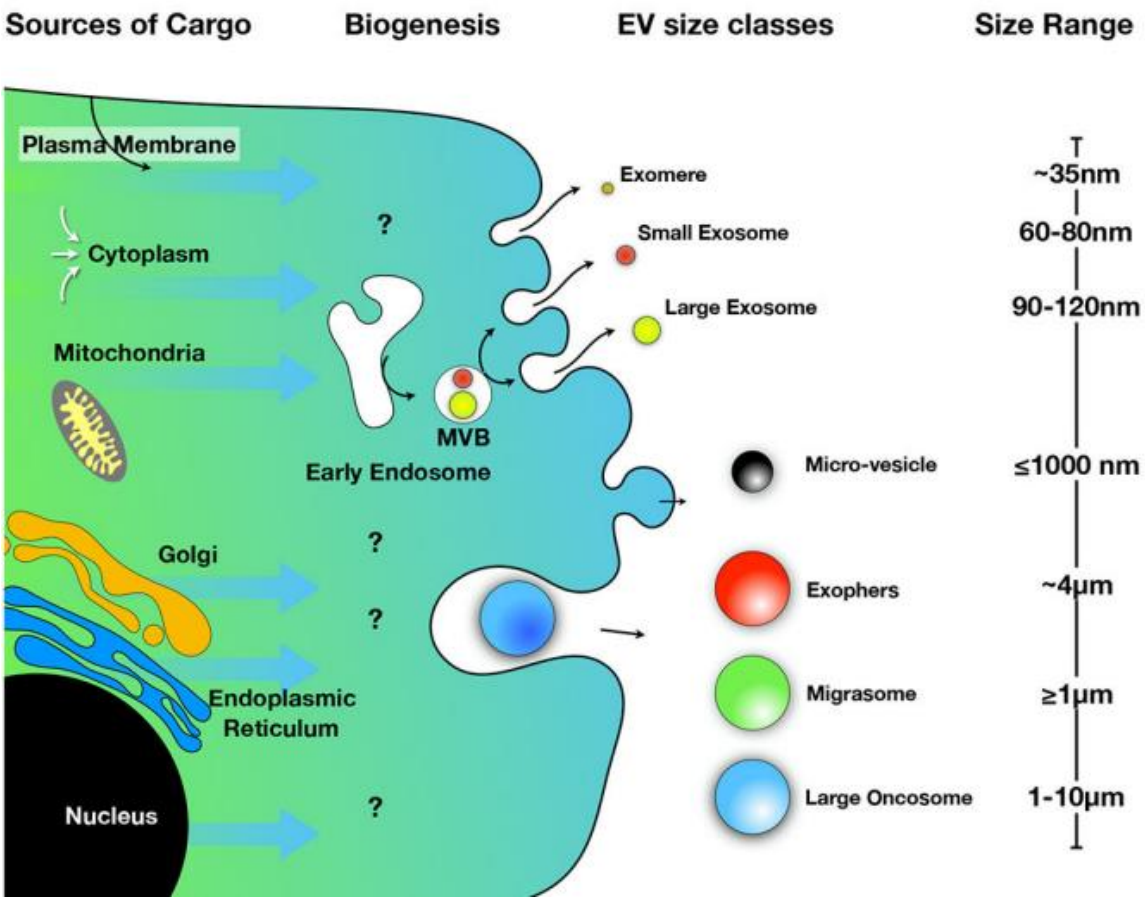

Figure 6 from [20] - *Size and biogenesis-based EVs classification.*

Another interesting hypothesis that supports the importance of the size can be explained by Multivesicular bodies (MVB) dimensions, intracellular compartments in which Intraluminal Vesicles (ILVs) (e.g. EVs with intracellular origin) are generated; MVBs have a diameter of <250nm, and contain 50-80 nm diameter internal vesicles [21] which are in the same dimensional range of a given population found by Zhang after 10 years in the following Electron Microscopy picture [21].

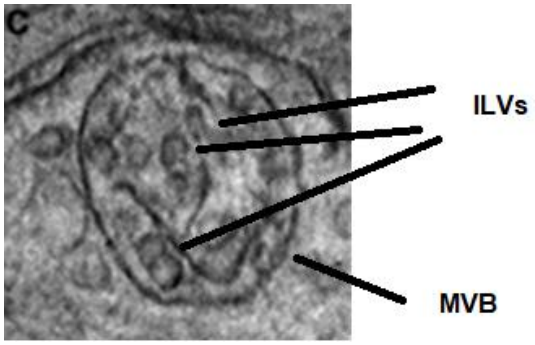

Figure 7. Electron microscopy images of a multivesicular body with 50-80 nm particles inside [21].

Altogether these data led us to think about the importance of isolating EVs by their size, and to characterize them from a lipidic and proteic point of view.

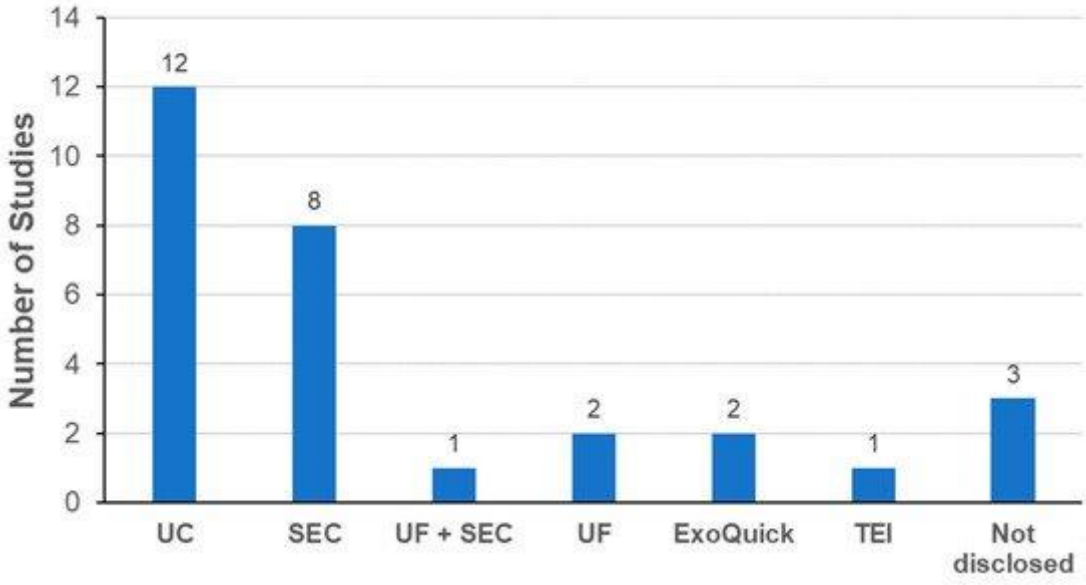

Figure 8 - Commonly used methods for EVs isolation. UC= ultracentrifugation, SEC= Size exclusion chromatography, UF+SEC= Ultracentrifugation+Size exclusion Chromatography, UF= Ultrafiltration, TEI= Total Exosome Isolation KIT, ExoQuick = commercial EVs precipitation kit and Not Disclosed = not reported [5].

Since EVs studies are mostly conducted with DC, we decided to try to optimize the separation method taking account of the presence of different population of EVs (based on Zhang's observation [19]).

Biogenesis of EVs

Exosomes "particles with endosomal origin"

The process involved in the biogenesis of the so-called exosomes was documented in the 80s, by Harding and Pan [22] which showed that small vesicles were generated from inward membrane budding of intracellular endosomes, leading to the generation of a multivesicular body (MVB) containing intraluminal vesicles (ILV); MVBs could fuse with the plasma membrane and release vesicles into the extracellular space [23].

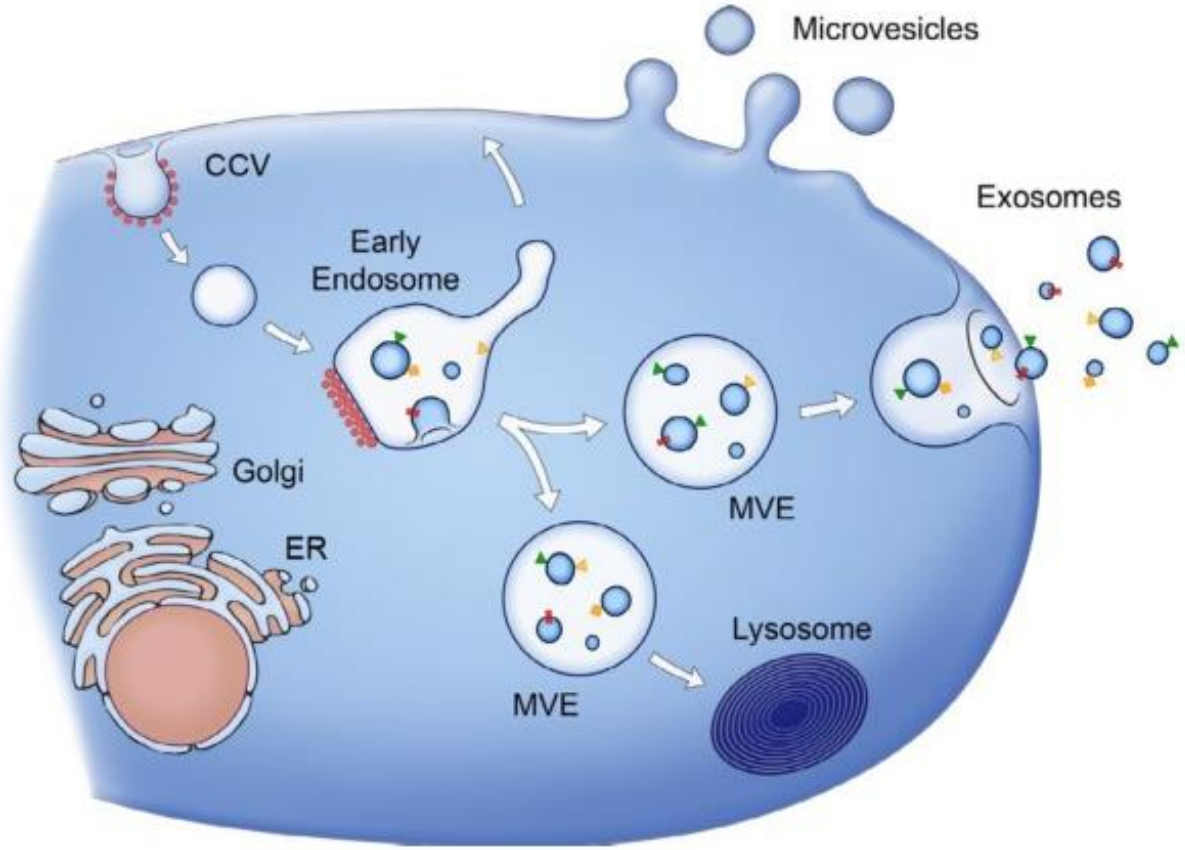

Figure 9 – While exosomes are generated thanks to an intracellular pathway, microvesicles are directly produced from plasma membrane budding [24].

Exosomal biogenesis has been well described by Hessvik NP and Llorente A [25] in their review "Current knowledge on exosome biogenesis and release".

The biogenesis of exosomes occurs within the Endosomal system and is a very complex multi-stepped process. EVs are generated into an intracellular compartment, the so-called early endosome which is generated in turn from plasma membrane invaginations.

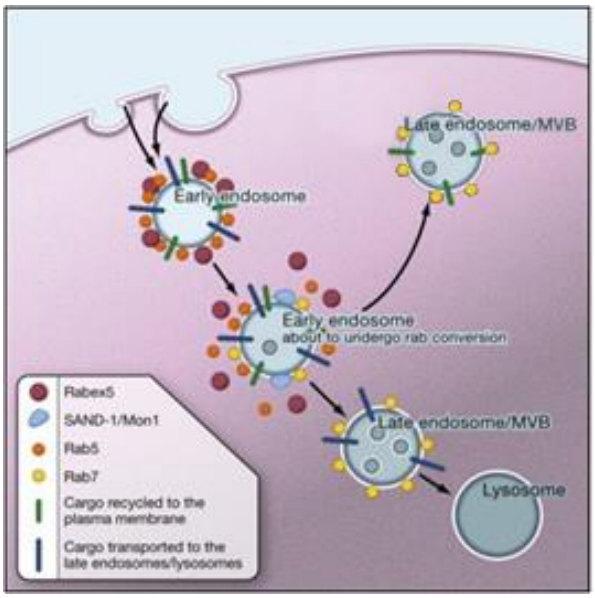

Figure 10 – Endosome Biogenesis and cycle.

Early endosome is generated from plasma membrane invaginations; after Intra Lumenal Vesicles formations this "filled" endosome is called Late endosome or Multi Vesicular Body. Afterwards it can have two different fates: the recycling one (fusion with plasma membrane and release of ILVs in the extracellular space) or the degradative one (fusion with lysosomes)

Endosomes are so classified in two main categories:

a) Early Endosome ;
b) Late Endosome or Multi Vesicular Body (MVB);

We have also to mention that MVB are not only classified on this sort of "time course EVs biogenesis" but they are also characterized by different protein content (rab 7 for Late Endosome and rab 5 and early endosome antigen 1 (EEA1) for early endosome) or by their different morphology [26].

The first phase of exosomal biogenesis is the generation of the early endosomes from plasma membrane budding (figures are adapted from [27]).

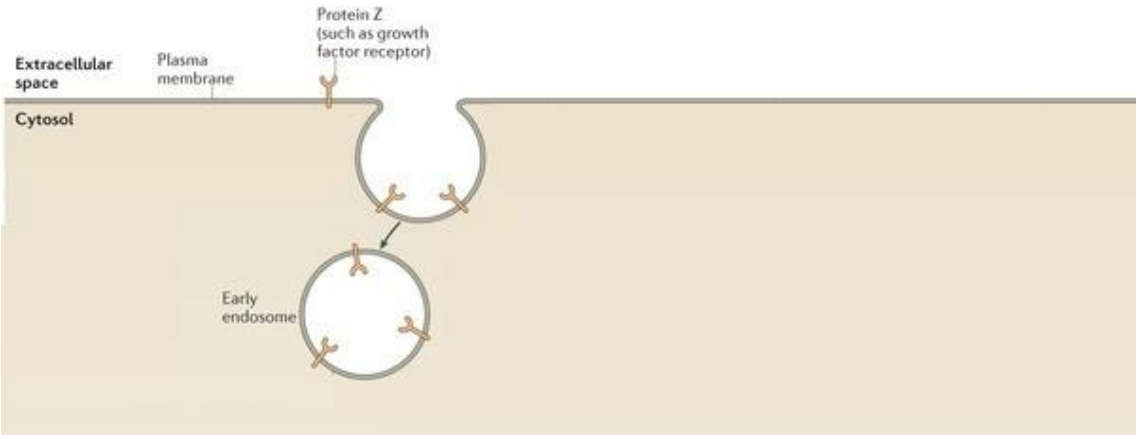

Figure 11 – Biogenesis of the early endosome; Early endosome is formed by plasma membrane invagination after interactions of specific ligands to the Z membrane protein.

After the generation of the Early Endosomes (EE) in turn are generated invaginations at the EE membrane, with the resultant generation of Intra Luminal Vesicles (ILVs) inside the endosome [25]. In these machineries, one of the crucial actor is the Endosomal Sorting Complex Required for Transport (ESCRT), a multi-enzymatic protein necessary for small-EVs biogenesis (i.e. invagination of EE membrane) and to address nucleic acids, proteins and lipids as cargo into the vesicles. ESCRT consists of four different protein complexes with different functions; ESCRT-0, -I, -II, -III and the associated AAA ATPase Vps4 complex [28]. Monoubiquitination of cytosolic domains of transmembrane protein which have been internalized by Golgi trans-portion, acts as a sort of "exit" signal which addresses proteins towards ILVs. Ubiquinated proteins in turn interact with ESCRT, for the ESCRT-dependent small-EVs generation pathway. The endosomal phosphatidyl-inositol 3P, recruits ESCRT-0 complex which binds ubiquitinated proteins. ESCRT-0 recruits in turn ESCRT-I, which incorporates ESCRT-II. Both complexes ESCRT-I ed ESCRT-II trigger the internal MVBs membrane invagination. ESCRT-II recruits in turn ESCRT-III components, which catalyze the cut of the neo-generated vesicles from the internal endosomal membrane [27]. It is important to highlight that even if ESCRTs complexes and their accessory proteins as Tsg101 (tumor susceptibility gene), and ALG-2 interacting protein X (ALIX) are recycled for the others ILVs; traces of these proteins have been found also in EVs and are therefore utilized as endosomal-derived vesicles markers. ESCRT proteins interact also with lipids or either enzymes involved in their own metabolism. Particularly ALIX binds a specific phospholipid, the so-called BisMonoacylGlyceroPhosphate (BMP) which is involved both in endosomal formation and fate; BMP is a peculiar lipid which is found only on intracellular EVs and endosomal membrane while not in cellular plasma membrane [29][30].

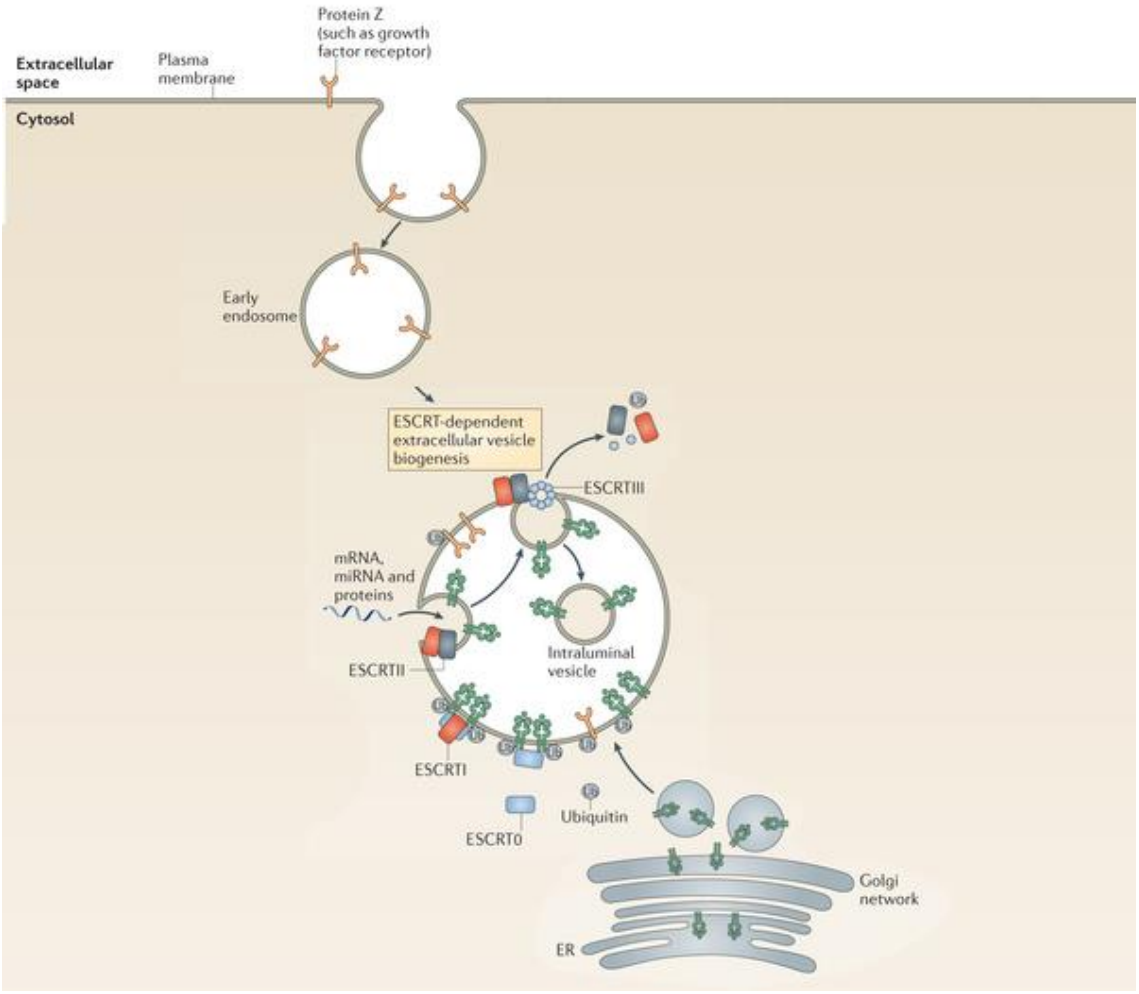

Figure 12 – Early endosome interacts with ESCRT (Endosomal Sorting Complex Required for Transport) which recruits lipids, proteins and nucleic acids fundamental for ILVs biogenesis. On the other hand ESCRT is also crucial to address the cargo inside the neo-generated particles. Internalization signal is ubiquitin which is synthetized by the Golgi.

The early endosome, now called MVB or late endosome can have two different fates [31]:

a) Fusion with plasma membrane and release of small-EVs in the extracellular space,
b) Degradation (fusion with lysosomes).

Small- EVs are released into the extracellular space after fusion of MVBs with the plasma membrane but during this process several energy barriers need to be overcome [25]. Protein–lipid and protein–protein interactions have been shown to reduce these energy barriers and facilitate fusion, as well as to provide specificity in reaching one of the two fates. Proteins involved in membrane fusion include soluble N-ethylmaleimide-sensitive factor attachment protein receptors (SNAREs), tethering factors, Rabs, and other Ras GTPases although the specific molecular machinery for fusion of MVBs with the plasma membrane is not well characterized [25].

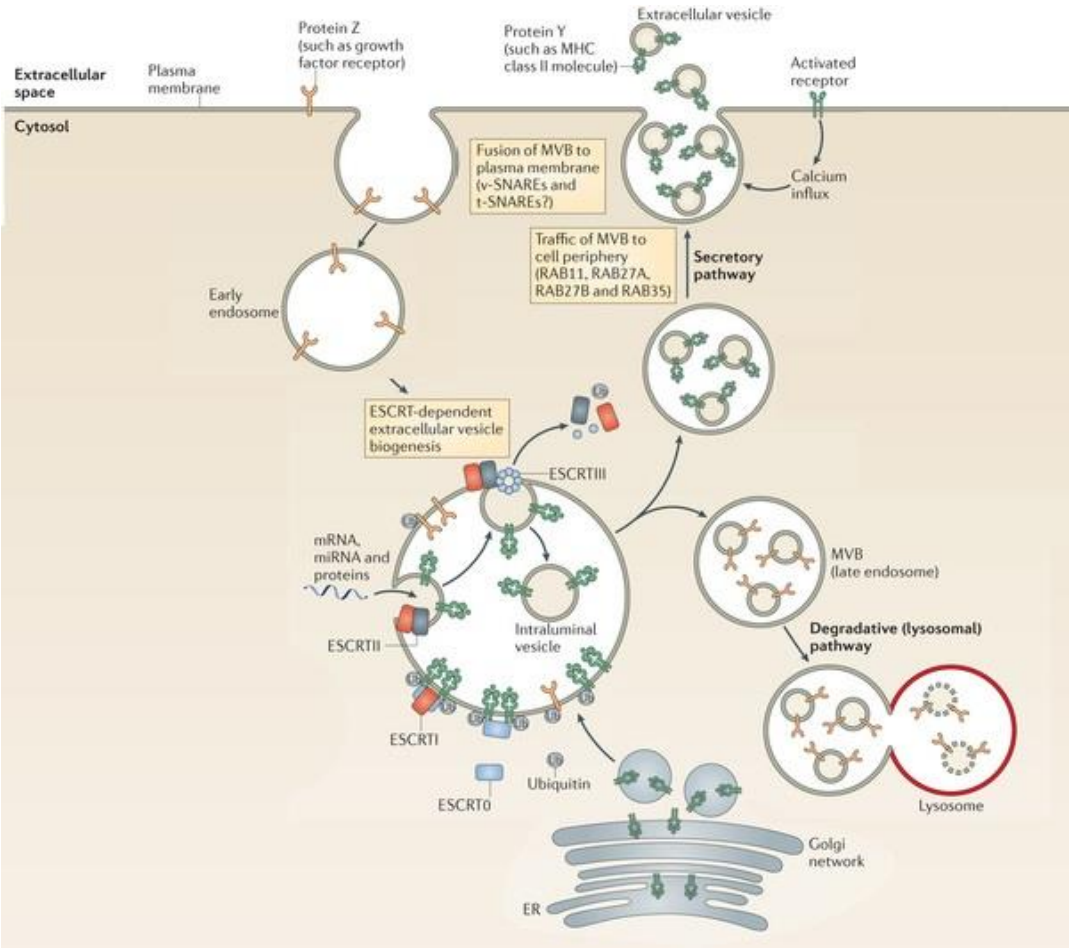

Figure 13 – Fate of MVBs.

The endosome filled with ILVs, now called late endosome or MVB may follow two different fates, the first one is the secretion while the second is the degradation of its after fusion with lysosomes.

On the other hand we have to mention that ILVs can also be generated without ESCRT complexes by the so-called ESCRT independent pathway, which seems to be dependent on the neutral sphingomyelinase (nSMAse-2). Some proteins (e.g. proteolipidic protein PLP) are addressed into ILVs independently by ESCRT thanks to the presence of microdomains which contain lipid rafts enriched in sphingolipids which in turn originate ceramides through the action of the nSMAse-2. The biogenesis of exosomes has often been described as an ESCRT-dependent or ESCRT-independent mechanism, but the pathways might not be entirely separated. These pathways might work synergistically, and different subpopulations of exosomes could depend on different machineries [25].

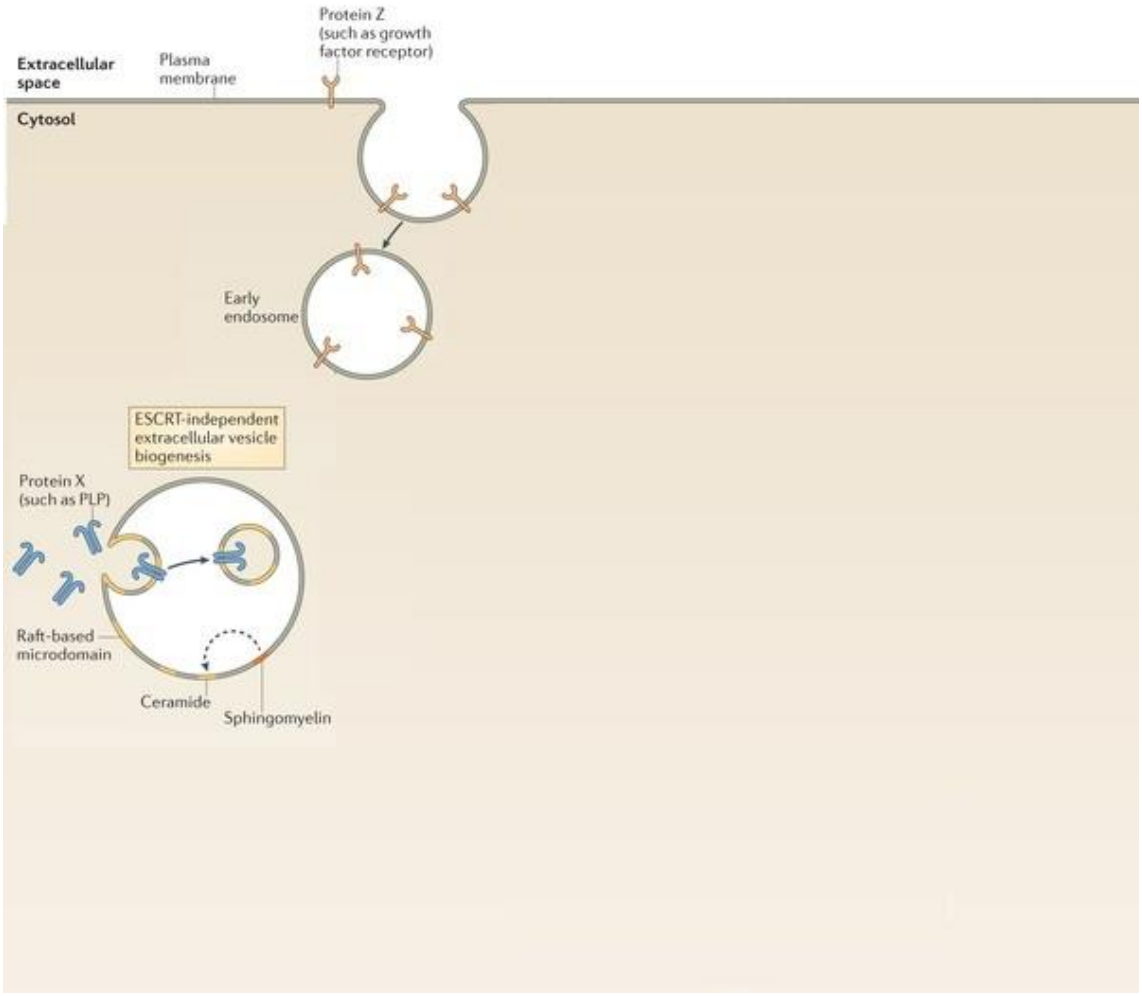

Figure 14 – ESCRT-intependent pathway.

Early endosome can interact with Proteolipidic protein (PLP) which can interact with membrane rafts for endosomal invagination resulting in ILVs generation.

Microvesicles biogenesis (plasma membrane derived EVs)

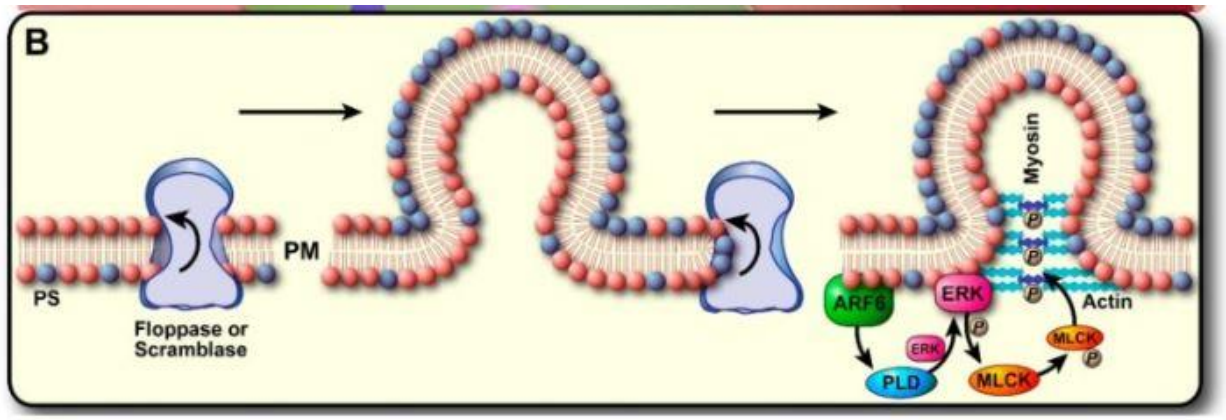

Figure 15 - Representation of molecules involved in biogenesis of microvesicles. Plasma membrane budding is initiated by a signaling cascade triggered by ARF6 through activation

and recruitment of PLD/ERK and phosphorylation of MLCK. These events lead to actomyosin contraction and pinching off the EV.

Microvesicles have an uncomplicated biogenesis, since they derive directly from plasma membrane budding. The initial curvature of plasma membrane is triggered by the recruitment of several proteins and transmembrane lipids in distinct domains. Calcium accumulation coupled with the activation of protein-degrading enzymes induce cytoskeleton degradation. Membrane gemmation is promoted by the exposure of phosphatidylserine (PS) made by specific translocases. Proteins are now transferred into the protrusion of the membrane through a signaling cascade triggered by ARF6 (ADP- ribosylation factor 6) after the activation of phospholipaseD/extracellular signal-regulated Kinase (PLD/ERK) and phosphorylation of Myosin Light-Chain Kinase (MLCK). These events trigger actomyosin contraction and therefore microvesicles generation and release [32] [33]. Conversely to these mechanisms Tumor Susceptibility Gene 101 (TSG-101) can induce ESCRT-III translocation to plasma membrane, starting the formation of the microvesicles. At the end of the process Vacuolar Protein Sorting Protein 4 (VPS4) detaches the neo-generated vesicle in extracellular environment [33].

Lipids and Extracellular Vesicles

Overview of lipids in EVs

Biological lipids are represented by a group of different water-insoluble compounds, characterized by different biological functions. Fats and oils represent the principal energy storage in several organisms while phospholipids and sterols are the main constituents of biological membranes. Other lipids exert pivotal roles as enzymatic co-factors, electron transporters, hydrophobic anchors for proteins, hormones or intracellular messengers [34].

As stated by one of the most relevant scientist in EVs field, C. Théry, “Quantifying lipids in EV preparations is another interesting possibility, because it takes into account the defining component of EVs: the lipid bilayer that defines them as vesicles [35]”. This sentence summarizes the importance of the study of the lipids that constitute and characterize EVs. EVs transport bioactive lipids, second messengers as phosphatidic acid, diglycerides, cholesterol and ceramides which are related to the biogenesis of the vesicles.

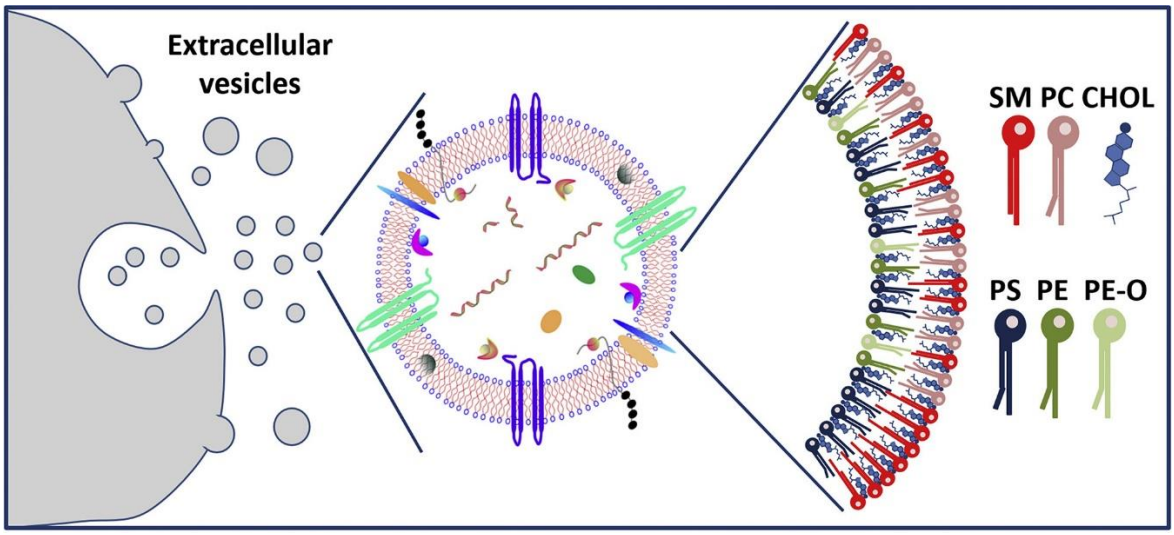

Figure 16 from [16] - *Molecular dynamic simulation of EVs membrane based upon quantitative lipidomic data for EV with a diameter between 50 and 150nm released by PC-3 cells SM= sphingomyelin, PC = phosphatidylcholine, CHOL= Cholesterol, PS= phosphatidylserine, PE= phosphatidylethanolamine, PE-O = Plasmalogens.*

Lipids represent essential components of EVs; particularly the group of A. Llorente [16] reported in their recent review the lipid composition of exosomes released by different cell types obtained by 10 different studies conducted during last years.

Table 2
Lipid composition of exosomes released by individual cell types (reprinted from [47]).

Lipids	PC-3 cells [33]		PC-3 cells + HG [62]		Oli-neu cells [65]		HepG2/C3a [66]		B-lymphocytes [64]		Mast cells [96]		Dendritic cells [96]		Reticulocytes [67]		Platelets [69]	Adipocytes [70]
	%	Factor	%	Factor	%[b]	Factor	%[b]	Factor	%	Factor	%[c]	Factor	%[e,f]	Factor	%	Factor	%	%[b]
CHOL	43.5	2.3	59	1.7	43	2.3	43	1.9	42.1	3.0	15	1.0	NR	NR	47	1.03	42.5	43
SM	16.3	2.4	9.1	2.0	8.2	1.5	9.7	10.8	23.0	2.3[e]	12	2.8	20	2.2	8.4[e]	1.31	12.5	12.5
PC	15.3	0.31	10.8	0.33	26.7	0.67	20	0.67	(20.3)[d]	(0.76)[d]	28	0.66	26	0.6	23.5	1.03	15.9	33
PS	11.7	2.1	6.9	1.2	14.9	3.0	15.6	2.4	(20.3)[d]	(0.76)[d]	(16)[d]	(1.2)[d]	(19)[d]	(1.6)[d]	5.9	0.92	10.5	1.1
PE	5.8	0.55	1.1	0.21	10.9	1.0	7.4	1.2	(14.6)[d]	(0.7)[d]	24	1.08	26	1.13	12.7	0.84	3.1	4.0
PE ethers	3.3	1.2	4.7	0.81					(14.6)[d]	(0.7)[d]							3.2	
DAG	1.5	1.5	1.1	0.92														0.8
PC ethers	0.81	0.40	0.7	0.28													1.4	
PG	0.17	0.17	0.1	0.07														
PA	0.16	1.8	0.1	0.33					(20.3)[d]	(0.76)[d]								
PI	0.13	0.13	0.3	0.16			4.1	0.18	(20.3)[d]	(0.76)[d]	(16)[d]	(1.2)[d]	(19)[d]	(1.6)[d]	2.4	1.1	5.2	2.3
Cer	0.32	1.3	0.7	1.2	NR	3.3	0.63	2.0									0.40	0.2
HexCer	0.76	3.8	2.3	2.1	NR	2.0												0.02
LacCer	0.12	3.0[a]	0.7	1.8														
Lipid analysis	MS		MS		MS		MS/GC		TLC		TLC/GLC		TLC/GLC		TLC		MS	MS
Exosome preparations[g]	SFM + SUC		SFM + SUC		SFM + SUC + SG		uFCS + SUC + IG		uFCS + SUC + SG + immunocapture		uFCS + SUC		uFCS + SUC		uFCS + SUC		SUC + IG	SFM + SUC

%: Percent of total lipid quantified. Factor: Factor of enrichment from cells to exosomes. NR: Not reported.
GLC: gas liquid chromatography; HexCer: hexosylceramide; LacCer: lactosylceramide; PG: Phosphatidylglycerol. HG. Hexadecylglycerol.

[a] Enrichments of other lipid classes are shown in Fig. 2B in reference [33].
[b] Percent CHOL was not reported; CHOL set to 43% to better compare the content of other lipid classes with the other data shown.
[c] Sum of SM and the glycosphingolipid GM3.
[d] Sum for all classes shown in parentheses and having the same numbers.
[e] Recalculated from the authors' data.
[f] CHOL not reported; the sum for the other lipid classes is 100% (including LysoPC not included in this table).
[g] Exosome preparations: Methods used to isolate the exosome preparations. SFM: serum free medium; uFCS: ultracentrifuged fetal calf serum; SUC: sequential centrifugation; SG: sucrose gradient; IG: iodixanol gradient.

Table 2 Lipid composition of exosomes released by different cell types, with enrichments of lipids vs parental cells, organized by type of lipid analysis and method utilized for exosome preparation.

As shown in the table 2 different studies confirm an enrichment from cells to exosomes of 2-3 times for cholesterol, sphingomyelin (SM), glycosphingolipids and phosphatidylserine, higher content of phosphatidylcholine and phosphatidylinositol, while phosphatidylethanolamine is quite similar [16] (% of enrichment is not reported from platelets and adipocytes since parental cells were not available). Other important lipidomics data derived from the Zhang's observation; they isolated EVs from cell media of three different cell lines (B16-F10, MDA-MB231-4175 and AsPC1, which are respectively Mus Musculus Skin Melanoma, Human Breast adenocarcinoma and Homo Sapiens Pancreas adenocarcinoma) by employing asymmetric flow field fractionation (AF4) and, as previously mentioned, they were able to identify large and small exosomes (respectively EXO-L 90-120nm and EXO-S 60-80nm) and discovered a new population of "non-membranous nanoparticles" called exomeres. They performed a deep lipidomic analysis through mass spectrometry and were able to identify eighteen lipid classes in all samples finding differences among in terms of relative frequency.

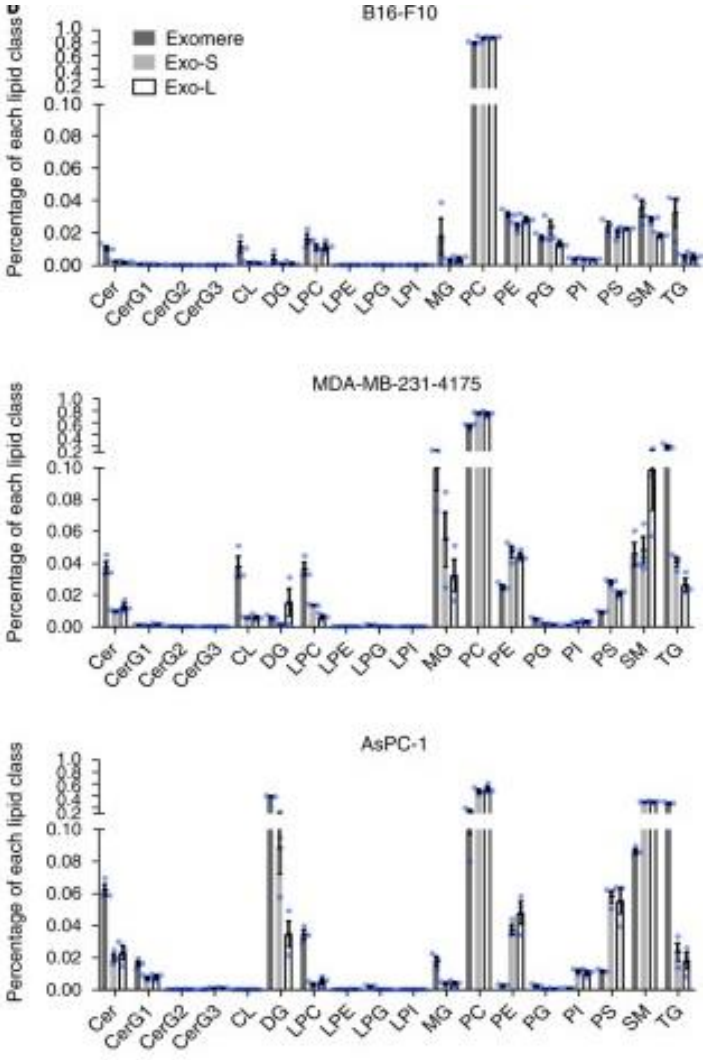

Figure 17 - Comparison of %rel of each lipid classes in Exo S, Exo L and exomeres in the three different cell lines

Phosphatidylcholine represents the main phospholipid, except for AsPC-1 exomeres, whose lower concentrations are counterbalanced by higher diglyceride and triglycerides levels. Remarkably, ceramides, triglycerides and lysophosphatidylglycerol varied significantly among all samples. Furthermore, high levels of tri-di-and monoacylclyceroles and cardiolipins, lipids characteristic of the lipid droplets and mitochondria, were found in exomeres fraction [16] maybe due to possible contaminations. Other important phospholipids as phosphatidylethanolamine and phosphatidylserine are quite similar in all exo-s and exo-l of all cell lines[19]. Unfortunately, cholesterol data were not collected in this study. A question arises from the author of this PhD thesis: how it is possible to call the exomeres “non membranous nanoparticles” while they are composed by typical membrane lipids as phosphatidylcholine and phosphatidylethanolamine?

Main Lipid Species and EVs

Fatty acids

Fatty acids are carboxylic acids with hydrocarbon chains from 4 to 36 carbons. In some fatty acids the chain is fully saturated (without double bonds) and unbranched while others contain one or more double bonds. Only few fatty acids contain three-carbon rings, methyl or hydroxyl groups. In mammalians the most common fatty acids are represented by those with unbranched chain, with a number of carbon atoms from 12 to 24. The even number of carbon atoms derives from the biosynthetic system of fatty acids. The double bond position in most fatty monounsaturated fatty acids is usually between C-9 and c-10, while in polyunsaturated ones are on C-13 and C16 [34].

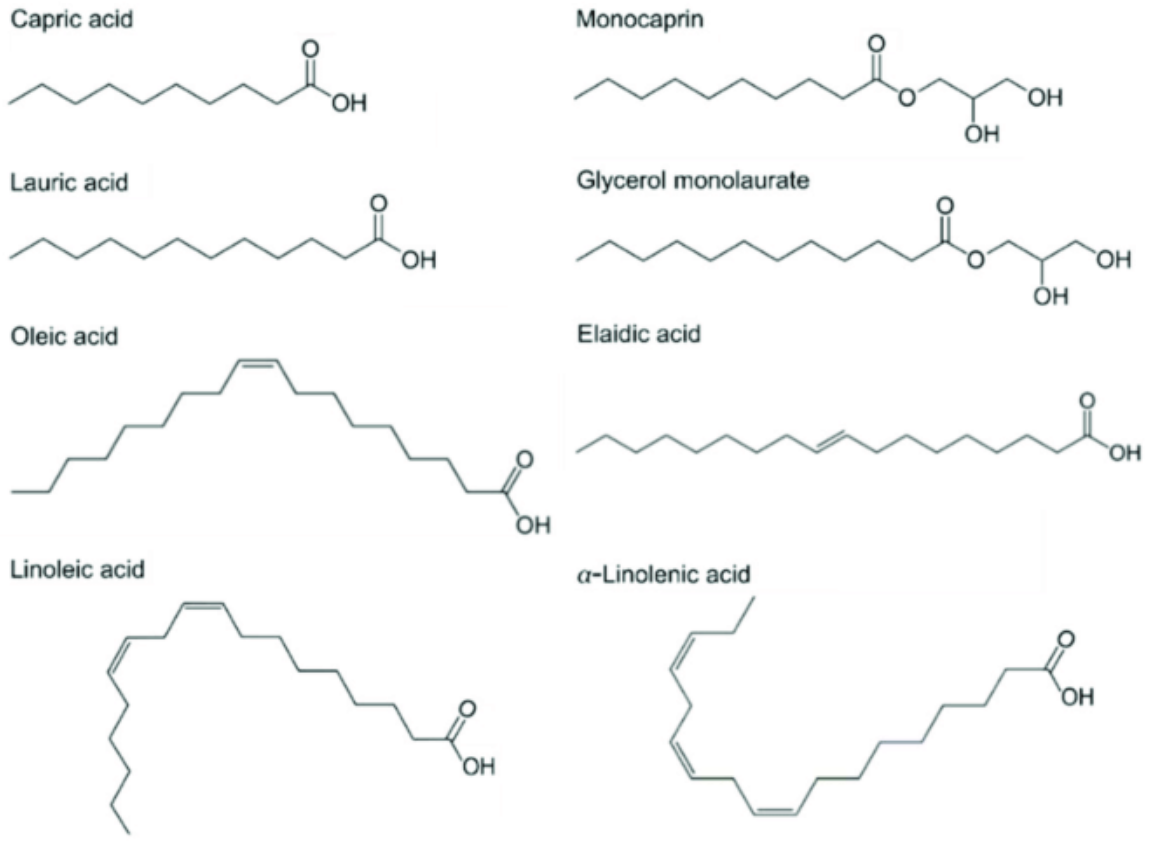

Figure 18 - Structures of common fatty acids.

The double bonds of polyunsaturated fatty acids (PUFA) are never conjugated but separated by a methylenic group and most of them are in *cis* configureuration. The physiological role of PUFA is mainly related to the position of the double bond towards the end of the chain; for this reason, since the most important bond is the aforementioned one, another kind of nomenclature is utilized, starting to count the carbons not from the classic functional group

but from the end of the chain, with the Greek alphabet letters. In this way, for example, PUFA with a double bond between C-3 and C-4 are called omega 3 [34].

Exosomes are enriched in saturated fatty acids when compared with parental cells [29], mainly due to the fact that they are enriched in phospholipids made by two saturated fatty acyl groups [30], which confer increased membrane rigidity compared to parental cells. Their membrane rigidity could be important to "protect" their functional cargo from the degradation and the stress of circulating in biological fluid. In addition to this, we have to mention that exosomes are more resistant than microvesicles against detergents, meaning that exosomes (or small-EVs) have a higher membrane lipid order [29]. EVs represent also a source of fatty acids which act as signaling molecules implicated in multiple biological functions as cancer, hemostasis, inflammation [36].

Triglycerides

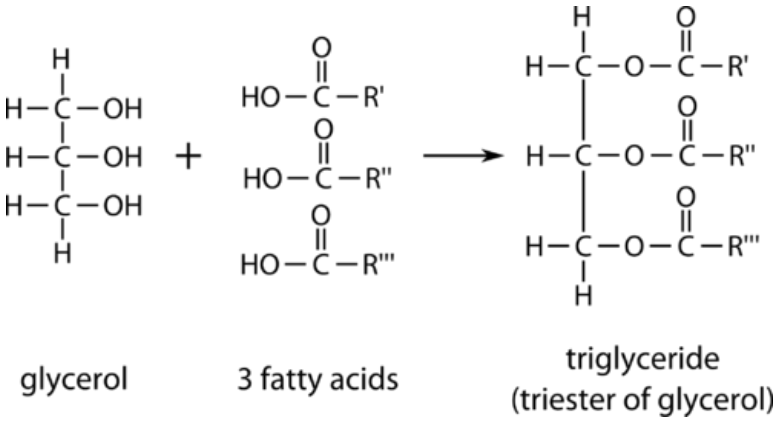

Figure 19 - Composition and structure of triglycerides.

Triglycerides (TG) are neutral esters of glycerol conjugated with long chain fatty acids. They are classified in non-complex if they possess same fatty acids in their backbone, while complex if the latter ones are different. In nature, the most abundant are the complex ones, not only for the lenght of the fatty acid but also to their unsaturation grade. TG are hydrophobic and they are completely anhydrous; for these reasons they represent the ideal reservoir of energy (mainly in adipose tissue). TG are produced in animal tissues from two precursors (acyl-CoA and L-Glycerol 3-P) with enzymatic reactions [34] and are characteristics of lipid droplets and lipoproteins, while not of the membranes; therefore the presence of these lipid species in EVs preparation should mainly due to the presence of contaminants or of improper separation [16].

Membrane lipids

Biological membranes are constituted by a lipid bilayer which acts as a protective barrier against ions and polar molecules. Membrane lipid are amphipathic, meaning that they possess both hydrophilic and hydrophobic structures. In detail, hydrophobic interactions between water and lipid molecules determine their spatial distribution in small sheets, the so-called membrane bilayer. Membrane lipids are mainly constituted by phospholipids, sphingolipids and cholesterol.

Phospholipids

In phospholipids the polar head is linked to the hydrophilic part by a phosphodiester-bond. Phospholipids present an alcohol-based classification in glycerophospholipids or phosphoglycerides (glycerol as alcohol) and sphingophospholipids (with sphingosine as backbone).

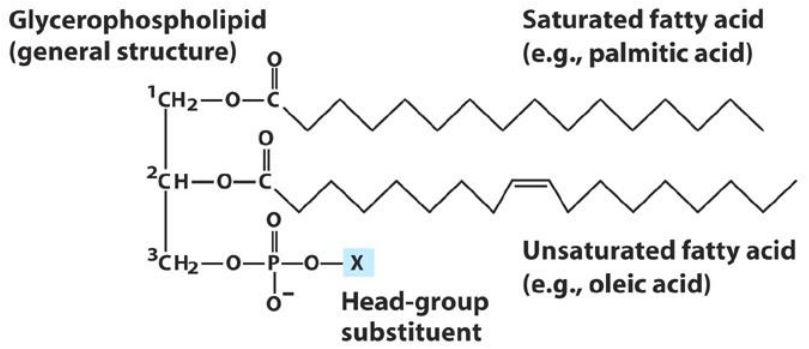

Figure 20 - Phospholipids structure.

Glycerophospholipids derive from *sn*-glycerol-3-P, in which glycerol is esterified in sn-3 with an orthophosphoric acid. In these kinds of phospholipids, glycerol is esterified with a fatty acid in *sn*-2 while different classes of compound can be inserted in *sn*-1. Based on the compound in *sn*-1, three subclasses of glycerophospholipid can be distinguished:

- 1,2-diacyl-phospholipids;
- 1-alkyl-2-acyl-phospholipids;
- 1-alkenyl-2-acyl-phospholipids.

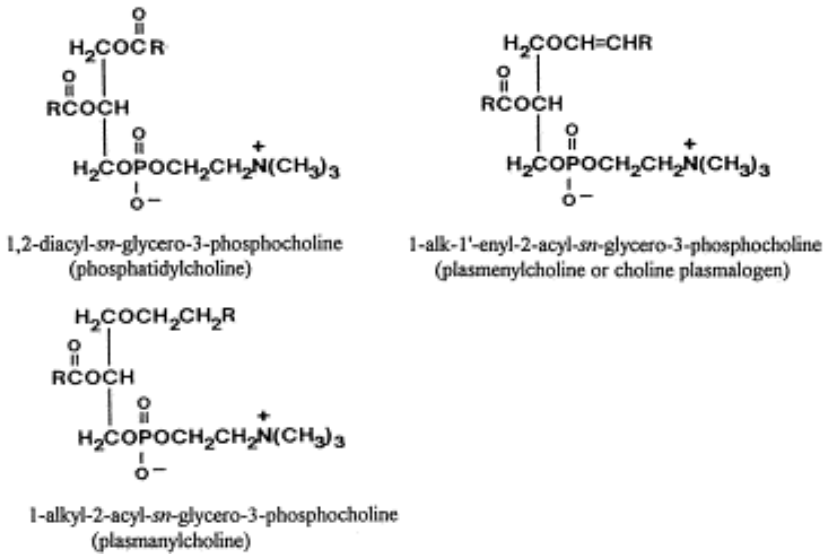

Figure 21 - Ether and ester phospholipids

Diacyl-phospholipid could be considered as phosphatidic acid-derived phospholipids with a glycerol backbone esterified in sn-1 and sn-2 with fatty acids, while in sn-3 with ortophosphoric acid. Particularly, ortophosphoric acid presents a second esterification with an alcohol (aminoalcohol or aminoacid conjugated with an alcoholic group or a carbohydrate). Consequently, diacyl-phospholipid are named with the phosphatidyl prefix, followed by the name of the esterified compound with the phosphate group (for example phosphatidyl choline, phosphatidyl ethanolamine). In phospholipids there are two kind of fatty acids, either saturated or unsaturated ones. Fatty acid in position 2 of diacyl-phosphoglycerides of cellular membrane is generally unsaturated.

Alkyl-acyl-phospholipid presents a long chain alcohol which is esterified with hydroxyl group in sn-1 of the glycerol backbone. These compounds are named 1-alkyl-2-acyl-glycero-3-phospho- followed by the name of the compound esterified to the ortophosphoric acid.

Alkenyl-acyl-phospholipids presents a vinylic ester conjugated double bond which is strongly prone to oxidation.

Phospholipids represent main components of EVs, which are in turn a great source of esterified fatty acid capable to be released by phospholipases; therefore EVs are an important source of eicosanoids, bioactive lipids with demonstrated activity both *in vitro* and *in vivo* [36]. Several groups compared the saturation of the fatty acids contained in phospholipids in exosomes with that of parental cells, and all of them agree that there is an enrichment of phospholipids with two saturated fatty acid groups in their structure [30][29]. The group of

A. Llorente performed a deep lipidomic analysis of PC-3 cells and related exosomes, finding an increase in phosphatidylcholine 14:0/16:0 and 16:0/16:0, even if the most abundant species of phosphatidylcholine were 16:0/18:1 and 16:0/16:1 [37]. They were also able to demonstrate an enrichment of 18:1 in several species in sn-2 position in exosomes released from PC-3 cells in the following species: PE 18:0/18:1, PE 16:0/18:1,PE 18:1/18:1, PI 18:0/18:1, PI 16:0/18:1, PI 18:1/18:1 and DAG 18:0/18:1 [37] [30].

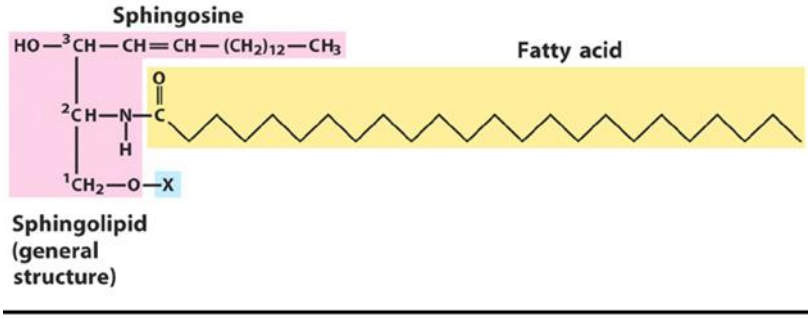

Figure 22 - Sphingolipids structure

Sphingophospholipids contain a long chain aminoalcohol called sphigosin. In spingophospholipids the aminic group of sphingosin is linked to the carboxylic group (COOH) of a fatty acid (ceramides), while the hydroxy group is esterified with the orthophosphate [38]. Sphingolipids represent important lipids for the structural integrity of exosomes, above all sphingomyelin (SM); in PC-3 cells was documented a 2.4 fold increase from cells to exosomes but, interestingly, without important changes in the relative distribution of the main substituents which compose the sphingomyelin [30][37].

Plasmalogens

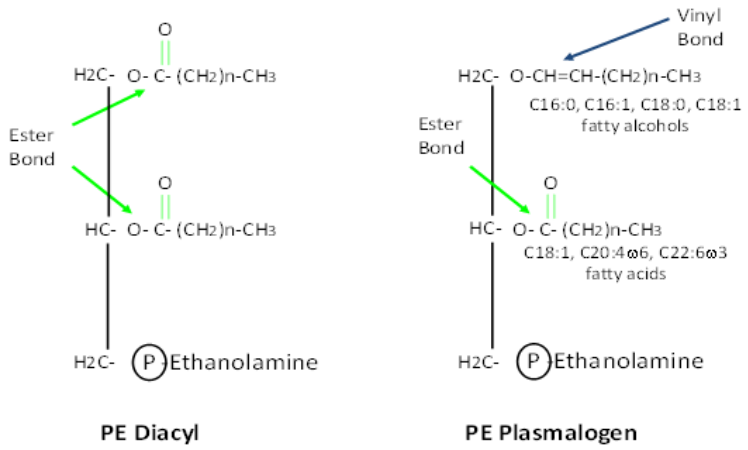

Figure 23 - Chemistry of Phosphatidylethanolamine forms

Plasmalogens are a peculiar class of membrane glycerophospholipids which contain a fatty alcohol linked through a vinyl ether bond in *sn*-1, while in *sn*-2 they are enriched in polyunsaturated fatty acids (PUFA) of the glycerol backbone. Although plasmalogens represent the 20% of the mass of all phospholipids in humans, their physiological roles are really hard to identify due to their peculiar distribution in different tissues [39]. Evidence indicate that in *sn*-1 position of plasmalogens are present fatty alcohols as 16:0, 18:0 and 18:1, which are linked to an alkyl-ether bond, in order to constitute the plasmenyl-glycerophosphate; in *sn*-2 they are enriched in PUFA, particularly 22:6ω3and 22:4ω6 [39]. Plasmalogens can reach their highest concentration in peculiar tissues as brain, neutrophils and eosinophils. Plasmalogens possess also structural roles; they are indeed related to the maintenance of physical properties of cellular membranes[40]. They are also important for membrane protein function(s) and as precursors for second-messengers lipids. Regarding the distribution in the membrane space of plasmalogens we have to mention that inside membrane itself the acyl chain of plasmalogens is oriented with an angle of 90 degrees to the membrane itself, and the presence of an ether in sn-1 contribute to make the membrane more lipophilic. In this way, the hydrogen bond reinforced between the polar heads leads to changes in lipids rearrangement inside membrane, with the relevant propension to form an inverse hexagonal phase (not a bilayer) which is an essential requirements for membrane fusion [41]. Particularly Rog and Koivuniemi compared biophysical features of diacyl and plasmalogen phosphatidylethanolamine. Results demonstrated that plasmalogens make the membrane thicker, more packed and more rigid [42]. They demonstrated also that the ether bond is able to change the orientation of the polar head, but not its position in the glycerol backbone. On the other hand, another important feature conferred by vinyl-ether is the packaging of proximal regions of *sn*-1 and *sn*-2 chains, which are more distant to the other parts of the molecule. If we take in consideration all these differences, we can claim that they have certainly a big influence in trafficking, fusion and permeability of membranes[42]. Plasmalogens accumulate in membrane rafts and are PUFA reservoir; two isoforms of PLA_2 are involved in their degradation, leading to PUFA release. One of the metabolites is a lisoplasmalogen that can be degraded or recycled by a lysoplasmalogenases with the formation of aldeheyde and phosphoglycerol. Myeloperoxidase is a protein which converts hydrogen peroxide in hypocloric acid in leukocytes, monocytes and neutrophils, contributing to to antimicrobial and cytotoxic activities of white globules. Unfortunately myeloperoxidase can react with the ether bond of plasmalogens leading to the generation of lysophospholipids with PUFA in sn-2 and 2-cloro-aldehyde with cytotoxic effects

Another important role of plasmalogen is the of protection against free radical mediated oxydative stress; vinyl bond acts indeed as suicide substrate preserving membrane PUFA integrity.

The group of Simbari [43] made a comparison between the plasmalogen content in exosomes secreted by a gastrointestinal nematode, called Heligmosomoides polygyrus, to those contained in MODE-K cells derived exosomes (gut epithelial rat cells) based on the fact that it is a naturally occurring intestinal roundworm of rodents. We have to mention that elmints do not possess the enzymes to synthesize cholesterol, thus they have to acquire it from the environment. They showed that exosomes secreted from nematodes were more rigid in comparison with those ones derived from cells, even if with less cholesterol and sphingomyelin (cholesterol is a crucial lipid that maintains membrane rigidity and one of the major component of exosomes); the lack of these two important lipids was counterbalanced by higher concentration of plasmalogens. Afterwards they decided to label exosomes with Laurdan dye; results indicated that nematode secreted exosomes possessed the same internalization ratio of the MODE-K derived exosomes, concluding that lack of cholesterol, crucial for EVs internalization was replaced and substituted in some way by increased content of plasmalogens. In addition to this, Phuyal et al. [44] demonstrated that pharmacologically-induced increase of plasmalogens at level of cell membrane leads to an enhanced release of exosomes in PC-3 cell line. They treated cells with a precursor of ether lipids, namely sn-1-O exadecylglycerol (HG). They were able to find a two times increase of ether lipids, paralleled by a 25% increase of cholesterol; this increase was reflected also in exosomes, with an increase of ether lipids. In addition to this, hexadecylglycerol treatment doubled the secretion of exosomes, without affecting their protein pattern (Alix, Tsg 101, Vinculin, Flotillin-1 and caveolin, whose concentrations were comparable between control and treated group).

In conclusion plasmalogens may act in the process of 1) biogenesis of exosomes and 2) fusion with plasma membrane independently of proteins. Other interesting data are represented by the increase of the number of multivesicular bodies with a concomitant reduction of the number ILVs inside them in HG treated group. In conclusion, studies demonstrated that ether lipids are capable to interact and therefore to modulate exosomal biogenesis and functionality.

Cholesterol

Cholesterol is a sterol characterized by cyclopenthanoperihydrophenanthrenic ring with an OH in position 3, (a secondary alcohol), with a double bond between carbon 5 and 6 and with an isoctylic lateral chain in C17. [45]. OH group in 3 is preferentially esterified with oleic or linoleic acid in the human body, while in cell most of cholesterol exists is in its free form.

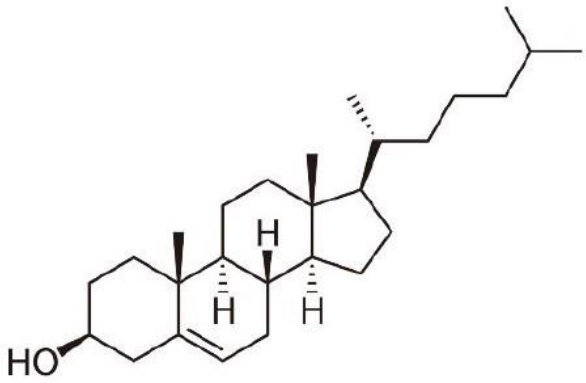

Figure 24 – Cholesterol Structure.

Cholesteryl esters are highly hydrophobic lipids, mainly present in lipoproteins or stored in cells and tissues. In healthy adults plasma concentration of total cholesterol (free+cholesteryl esters) ranges from 130 and 200 mg/100mL, of which 2/3 in its esterified form [45]. In human organism cholesterol possesses several biological functions: it is a peculiar structural component of cell membrane, myelin sheats and nerve fibers, where it regulates fluidity and permeability; it is the precursor of steroids and hormones, (testosterone, progesterone, estradiol, cortisol) vitamin D and biliary salts. The main sources of plasma cholesterol are represented by hepatic biosynthesis and gut absorption; every day humans have an average intake of about 300-700mg of cholesterol from diet, while almost the same quote is produced by de-novo biosynthesis.

.

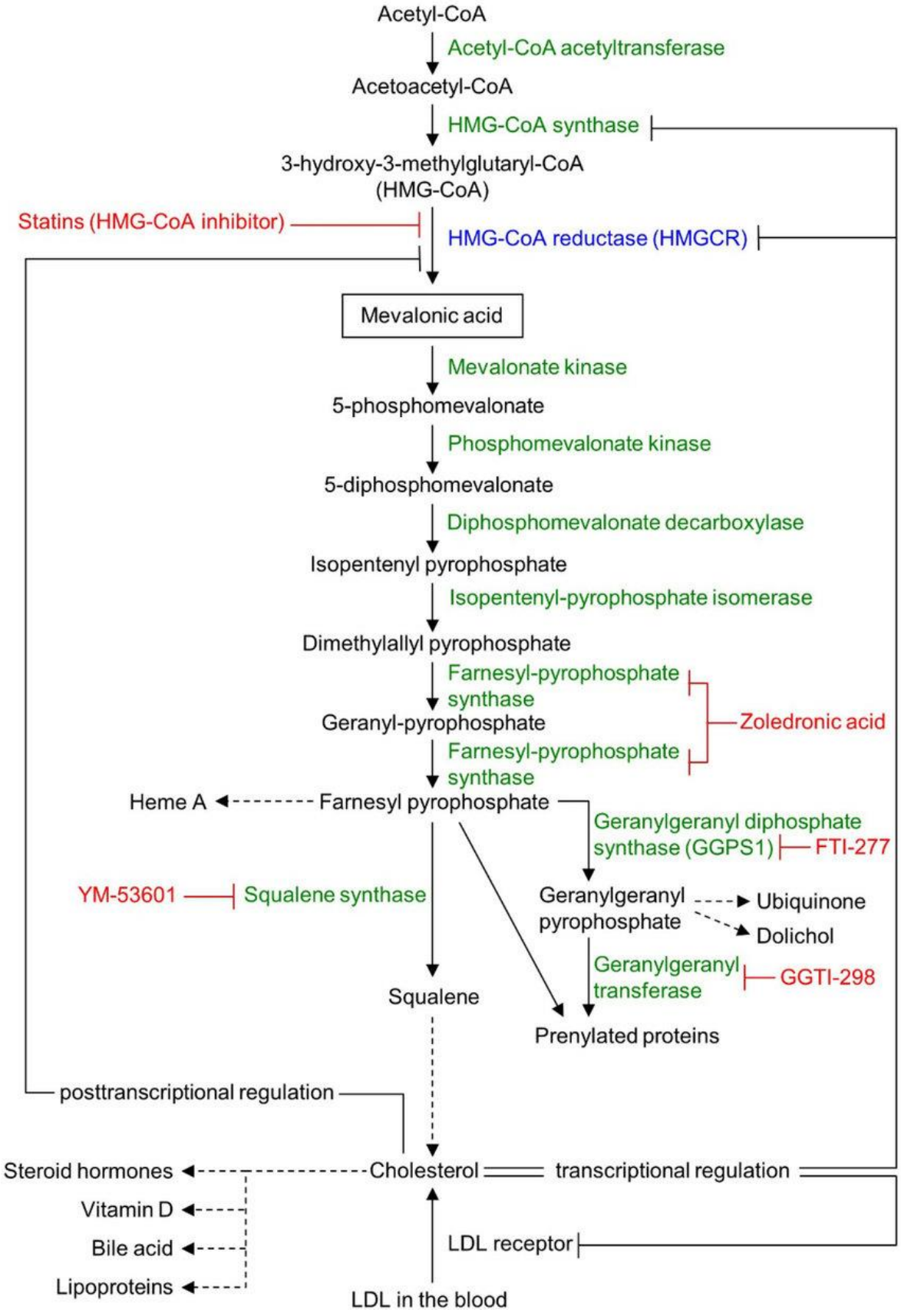

Figure 25 - Schematic view of cholesterol biosynthesis.

Almost the same amount of cholesterol is produced mainly in the liver, in hepatocytes cytoplasm (even if all cells can produce cholesterol), where a series of several biochemistry reactions originate the cholesterol molecule, which is finally released in bloodstream and distributed to tissues and organs by lipoproteins. Particularly HMG-CoA reductase is the rate-limiting enzyme of the mevalonate pathway, the metabolic pathway that produces cholesterol and isoprenoids.

Several studies indicate that EVs are enriched cholesterol when compared with parental cells, and the degree of enrichment depends on parental cells, subpopulation of EVs, and by method utilized for their isolation [46]. EVs membrane may also contain cholesterol-enriched lipid rafts.

Species	Tissue/Cell Type	Preparation	EV Isolation	Sterol Analysis	EV Type; Cholesterol Content	References
Chicken	Epiphyseal cartilage	Acutely isolated	UC	TLC	Matrix vesicles; C/PL 2-fold PM	(7)
Guinea pig	Reticulocytes	Primary	UC	TLC	EV; C/PL equal to cells	(8)
Rat	Mast cells	Line	UC	GLC	EVs; C/PL equal to cells	(9)
Human	Hepatocarcinoma, lung carcinoma, prostate cancer, fibroblasts	Line	UC	Raman spectroscopy	Exosomes; differences between lines	(10)
Mouse	Adipocytes	Line, primary	UC	Enzymatic	Exosomes; small versus large	(11)
Human	B lymphocytes	Line	—	Perfringolysin O/ Immunogold EM	Exosomes; direct staining	(12)
Human	Cervical cancer (HeLa)	Line	UC	Theonellamides/ Immunogold EM	Exosomes; direct staining; 5-fold PM	(13)
Rat	Mesenchymal stromal cells	Lines	UC	Raman spectroscopy	Exosomes; single analysis, CD9+ versus CD9−	(14)
Human	Ovarian cancer	Plasma, ascites	UC	Raman spectroscopy	Exosomes; single analysis; CD9+ (low) versus CD9− (high)	(14)
Human	Brain	Cerebrospinal fluid	UC	—	Exosomes; prominin-1	(16)
Mouse	Brain (embryonic stage)	Ventricular fluid	UC	—	Exosomes; prominin-1	(16)
Human	Colorectal cancer	Line	UC	—	Exosomes; prominin-1	(16)
Human	Eye	Lacrimal fluid	UC	—	Exosomes; prominin-1	(16)
Human	Kidney	Urine	UC	—	Exosomes; prominin-1	(16)
Human	Mouth	Saliva	UC	—	Exosomes; prominin-1	(16)
Human	Prostate epithelial cells	Seminal fluid	UC	—	Exosomes; prominin-1	(16)
Human	Lymphoma	Lines	UC, FACS	Cholesterol antibody	Exosomes; direct staining	(18)
Mouse	Microglia	Line	UC, FACS	Cholesterol antibody	Exosomes; direct staining	(18)
Human	Erythrocytes	Plasma	UC	Enzymatic	Exosomes; detergent-resistant fractions	(19)
Dog	Kidney cells	Line	FACS	Enzymatic	Toxin-induced EVs; C/L 2-fold cells	(20)
Human	Fibroblasts	Primary	FPLC	Isotope-labeled cholesterol	Microparticles; efflux	(64)
Human	B lymphocytes	Line	UC, Dynabeads	MS	Exosomes; C/L 2-fold cells	(73)
Human	Colorectal cancer	Line	UC	MS	Exosomes; C/P 5-fold cells	(74)
Mouse	Epididymis	Fluid	UC, SEC		Epididymosomes; C/PL 2-fold spermatozoa	(75)
Mouse	Leukaemia	Ascites	UC	TLC	EVs; C/PL 3-fold PM	(78)
Human	Melanoma	Lines	UC	Enzymatic	Exosomes; C/P 10-fold cells	(79)
Human	Mesenchymal stem cells	Line	UC, HPLC	Enzymatic	EVs; C/P 8-fold conditioned medium	(80)
Human	Neutrophils	Plasma	Centrifugation	TLC	EVs; C/sphingomyelin 2-fold PM	(81)
Mouse	Oligodendrocytes	Line	UC	MS	Exosomes; C/P 2-fold PM	(82)
Mouse	Osteoblast	Line	UC	TLC	Matrix vesicles; C/PL 2.5-fold PM	(83)
Human	Platelets	Plasma	UC	TLC	Microparticles; C/PL similar to PM	(84)
Human	Prostate cancer	Urine	UC	MS	Exosomes; high C/PL	(87)
Hamster	Kidney cells	Line	FPLC	Isotope-labeled cholesterol	Microparticles; efflux	(43, 65)
Human	Hepatocarcinoma, THP-1-derived macrophages	Line	UC, FACS	GC/MS	Exosomes; increased by curcumin/ U18666A	(76, 77)
Human	Prostate cancer	Line	UC	MS	Exosomes; C/PL 4-fold cells C/P 3-fold cells	(85, 86)
Mouse, human	Macrophages	Line, primary	FPLC	Isotope-labeled cholesterol	Microparticles; efflux	(43, 64, 65)
Human	Prostate epithelial cells	Seminal fluid	UC, SEC	LC-MS; TLC	Prostasomes; 55% of lipid C/PL 1.9	(88, 89)

UC, ultracentrifugation; C/PL, cholesterol-to-phospholipid ratio; GLC, gas liquid chromatography; FACS, fluorescence-activated cell sorting; C/L, cholesterol-to-lipid ratio; FPLC, fast-performance liquid chromatography; C/P, cholesterol-to-protein ratio; SEC, size exclusion chromatography.

Table 3 from [16] - *Presence of cholesterol in different cells and EVs.*

Bismonoacylglycerophosphate

Lysobisphosphatidic acid was first discovered several years ago, in 1967 by Body and Gray, as a structural isomer of the phosphatidyl glycerol (PG). In the early 70s it was renamed bis(monoacylglycero)phosphate (BMP) [47].

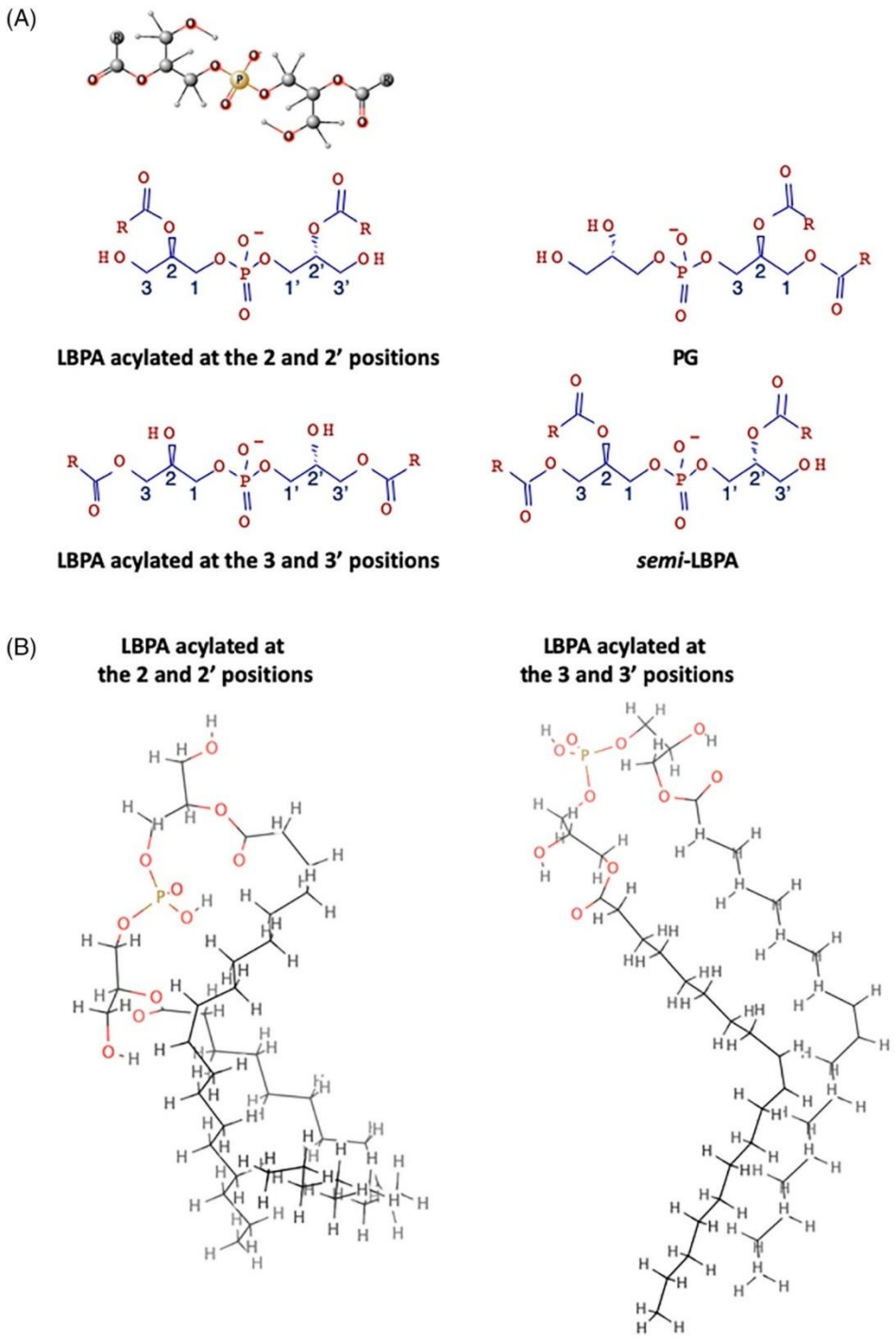

Figure 26 from [47] - *Different BMP isomers and precursors.*

Evidence demonstrated that BMP is ubiquitously distributed in cells and tissues of high eukaryotic cells, while not in prokaryotes and plants [47]. As shown by Kobayashi et al., [48] in the internal membranes of late endosomes (established by immunogold labeling of O cell crysosections), 15% of total phospholipids is represented by BMP. In addition this unique lipid and forms specialized domains in endosomal membrane; furthermore these domains are involved in sorting of the late endosomes and ligands bearing lysosomal enzymes (e.g. BMP levels can address endosome toward secretory or recycling pathways) [48]. Kobayashi et al., were also able to make the unique antibody against BMP which is still commercialized and that we utilized for our experiments. BMP is present only on the peripheral membrane of the late endosomes and on intraluminal vesicles, even if in the latter ones it accounts only 1% of total phospholipid; interestingly it has been demonstrated that BMP is not present on plasma membrane surface [29]. In human bodies, BMP is enriched into the liver. BMP content may lead us to discriminte vesicles having endosomal origin from these which originates from plasma membrane [29]. Independently on the position of the fatty acid on the glycerol backbone, BMP composition can be very different among different tissues, cell types or organelles. "This unusual composition must confer very distinctive properties, suggesting quite specific functions, most of which have yet to be revealed", as stated by W.Christie (www.lipidmaps.org) .

Fatty acid	Rat liver lysosomes	Human liver	Rabbit lung macrophages	Rat uterine stromal cells	Rat testis	BHK cells
16:0	3	6	4	6	5	4
18:0	1	5	6	3	3	trace
18:1	5	57	47	30	5	83
18:2	6	10	29	2	1	6
20:4		6	4	4		
22:4				6	5	
22:5(*n*-6)	} 4		} 2	3	70	
22:5(*n*-3)				8	trace	
22:6(*n*-3)	69	9	1	36	5	
Reference	1	1	2	3	3	4

1, Wherrett, J.R. and Huterer, S. *Lipids*, **8**, 531-533 (1973); 2, Huterer, S. and Wherrett, J. *J. Lipid Res.*, **20**, 966-973 (1979); 3, Luquain, C. *et al.*, *Biochem. J.*, **351**, 795-804 (2000); 4, Brotherus, J. and Renkonen, O. *Chem. Phys. Lipids*, **13**, 11-20 (1974).

Table 4 - Fatty acid composition (%of the total) of BMP extracted from different tissues. (www.lipidmaps.org)

BMP functions

Thanks to its negative charge at low lysosomal pH (between 4.5 and 5), BMP can stimulate the activity of lysosomal lipid-degrading enzymes, such as a-SMase, acid ceramidase, acid lipase and acid phospholipase A2. BMP is also crucial in cargo sorting by stimulating degradation and sorting of lipids (www.lipidmaps.org). BMP-rich membranes are also able to degrade sphingolipids and to regulate the fate of endosomal cholesterol [47]. Indeed it is well-known that cells acquire cholesterol by the endocytosis of LDL, but very little is still known about the mechanisms involved in the transport of endosomal cholesterol inside the cell [49]. Literature demonstrates that BMP and cholesterol are functionally related; BMP plays an important role in cholesterol transport [50]; for example in Niemann-Pick type C disorder where cholesterol accumulation is paralleled by increased BMP; moreover both BMP and cholesterol play an important role in migration and fusion of multivesicular endosomes towards the plasma membrane [29].

Particularly important for my PhD project is the work made by Pribasnig et al., (2015) [46]. Since BMP plays a key role in degradation and sorting of lipids in acidic organelles, they investigated which enzyme may be responsible for BMP catabolism/degradation. They showed that α/β hydrolase domain-6) containing 6 (ABHD-6) is responsible for the 90% of BMP hydrolase activity detected in the liver, and that knockdown of ABHD6 increases hepatic BMP levels. In addition, live cell imaging experiments revealed that ABHD6 colocalizes with early endosomes/lysosomes. ABHD-6 plays also a role in development of obesity and liver steatosis; it has been demonstrated that its pharmacological inhibition and/or knockdown protects mice from high-fat-diet induced obesity and hepatic steatosis [51].

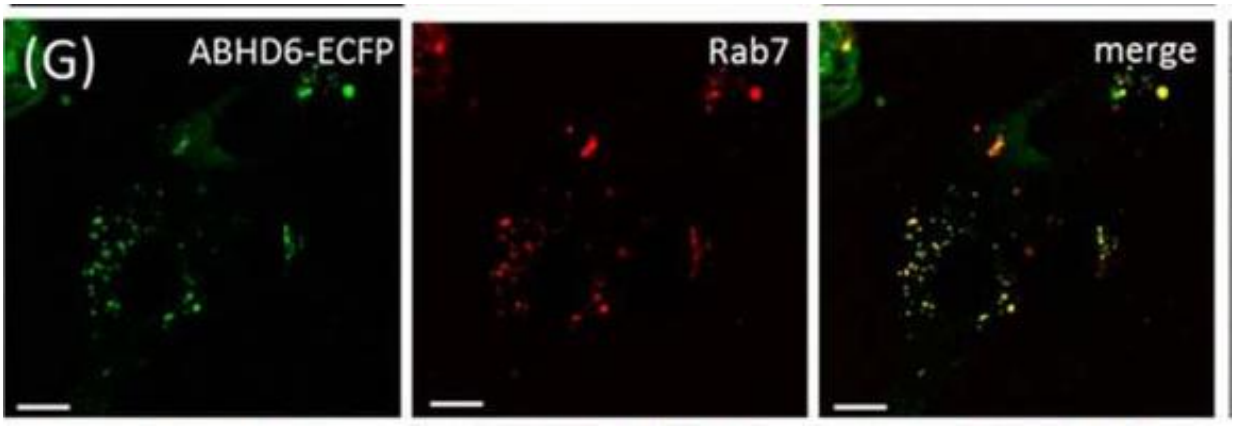

Figure 27 - Confocal microscopy analysis showed co-localization of ABHD6 and Rab7

(canonical endosomal marker).

Pribasnig et al., treated AML12 hepatocytes with KT182 (a potent inhibitor of ABHD6) for 4hrs and measured the incorporation of 3H-labeled oleic acid into BMP. Under these conditions, KT-182 increased the incorporation of the radioactive oleic acid into BMP by 48% in comparison with control cells, indicating that BMP metabolism is affected by the activity of the enzyme.

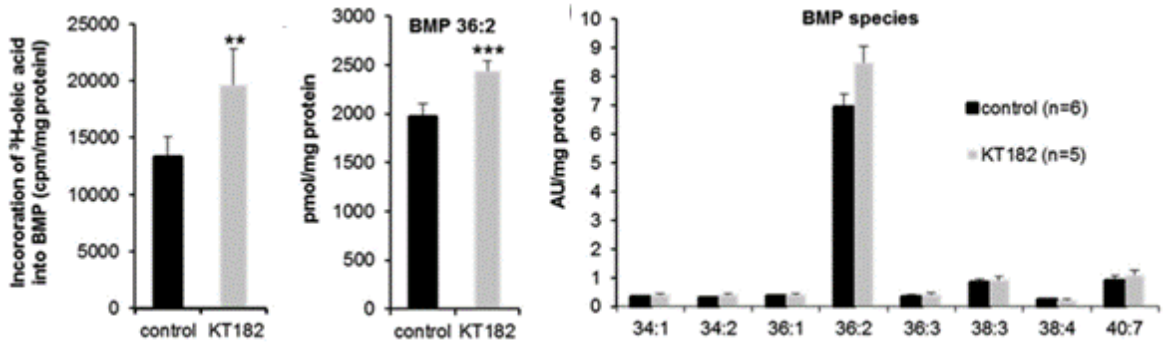

Figure 28 - Incorporation of oleic acid in different BMP species (expressed in counts minute/protein) of treated vs control cells.

In conclusion, ABHD6 is strictly related to BMP concentrations in cells, and it is particularly enriched in late endosome and lysosomes, which are crucial organelles for EVs biogenesis.

Lipids as pivotal component for EVs Biogenesis and Functions, cholesterol and BMP role in EV biogenesis

As seen before ILVs biogenesis occurs from inward buddings of the late endosomes, which leads to the generation of several 30-150 nm particles, while microvesicles directly generate from plasma membrane budding.

Microvesicles are generated from disruption of the plasma membrane lipid organization, by modification due to a cholesterol/sphingomyelin binding protein which cooperates with proteinase 3; their binding with phosphatidyl serine promotes the formation of microvesicles [29] .

As previously mentioned ILV biogenesis involves several cross talking between lipid molecules and the Endosomal Sorting Complex Required for transport proteins [29]. BMP is indeed abundant in intraluminal membranes of late endosomes but not in early endosomes [52]. Due to its cone-shaped structure, BMP can induce membrane asymmetry, favoring the

formation of ILVs in late endosomes[46]. BMP specifically interacts with ALIX (multifunctional protein involved in endocytosis, multivesicular body biogenesis), by the presence of a flexible loop contained in the ALIX Bro1 domain, suggesting a pivotal role in ESCRT-dependent ILV generation into the late endosome [53]. Another interconnection between cholesterol and BMP has been found by Chevallier and colleagues [49]. They found that Alix down-expression decreases both BMP levels and the luminal vesicle content of late endosomes, together with a reduction of cellular levels of cholesterol. We can conclude that BMP levels controls the levels of Cholesterol in the endosomal system [49].

EVs can originate from two cellular membrane compartments, very different in their lipid composition (e.g. endosomes and plasma membrane), suggesting that different amount of cholesterol may be required for their biogenesis [46]. Specific compartments of the endosomal system are enriched in cholesterol, leading to the production of ILVs; afterwards MVBs are transported by microtubules to the cell membrane where they fuse and release small-EVs [46].

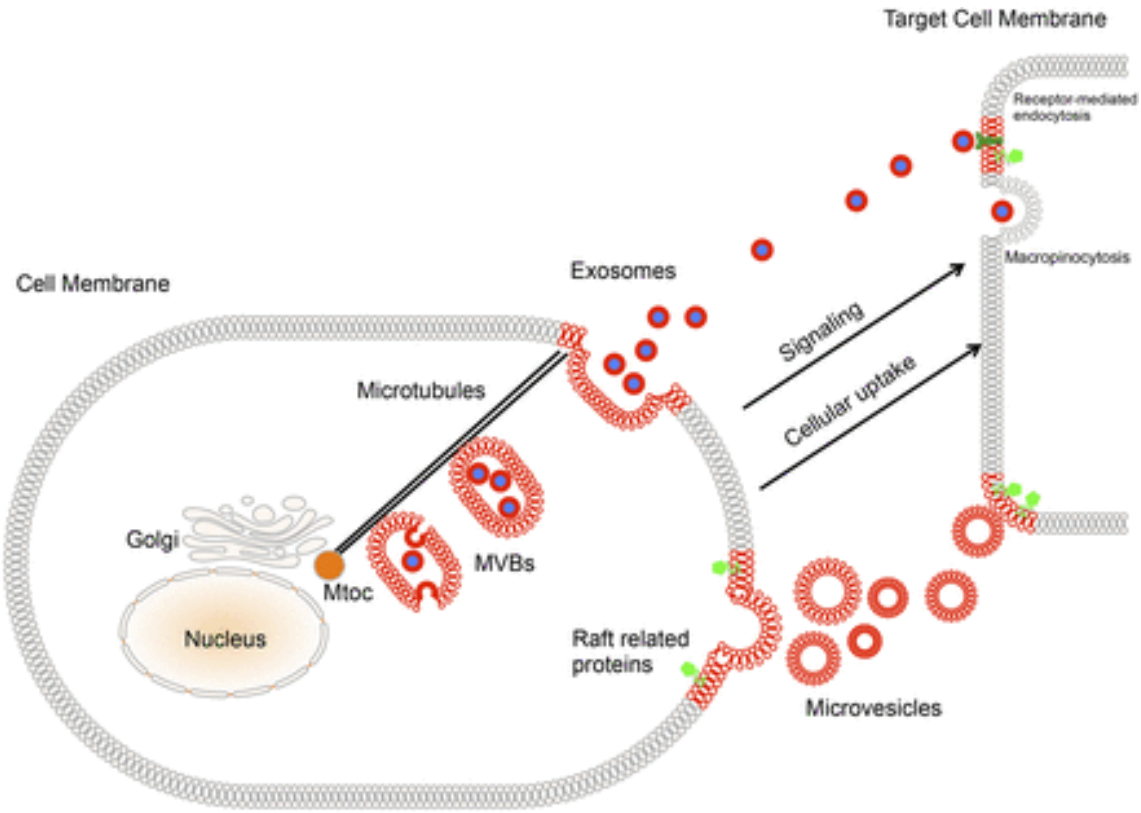

Figure 29 - Contribution of cholesterol to the journey of EVs; membranes rich in cholesterol are designed in red

In order to prove the existence of different endosomal populations in cells, Möbius et al.,[54] utilized perfringlosyn O, a cholesterol binding protein conjugated with fluorescent probe, to label cholesterol. They were able to demonstrate not only that in cells there were cholesterol positive and negative MVBs but interestingly, only those that were enriched in cholesterol undergo towards the secretory pathway, suggesting that cholesterol content of MVBs controls the release of EVs [46]. The neo-generated late endosome, filled with its cargo moves along the microtubule organizating center (mTOC) (figure 29 and 30) through a dynamic process regulated by cholesterol itself. The release of exosomes requires transport of MVBs along microtubules toward the plasma membrane, process in part controlled by cholesterol levels [46]. Release of EVs, as demonstrated by several studies, is highly cholesterol-dependent. Treatment of oligodendrocyte-like cells with cyclodextrin-bound cholesterol enhances the release of exosomes [55]. In addition, in a recent study, simvastatin, an inhibitor of HMG CoA-reductase, was tested for its effect on exosome secretion under various settings and was found to reduce the secretion of exosomes from various cell types [56].

Once reached the plasma membrane, late endosome fuses with the latter one leading to the release of exosomes into the extracellular space.

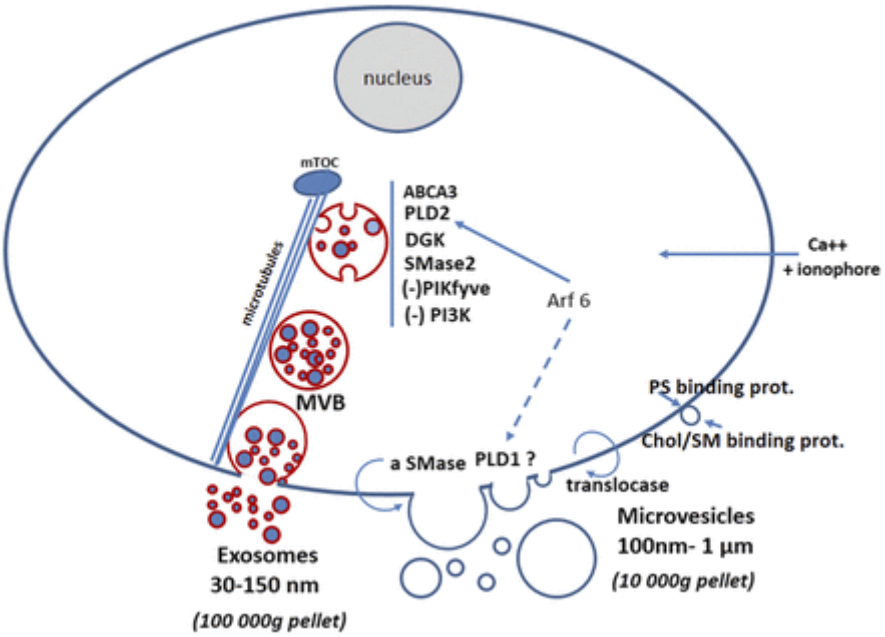

Figure 30 - Lipid-related molecules required for EVs Biogenesis, isolated by ultracentrifugation with canonical protocol developed by Théry [18]. *EVs production needs lipid transporters as ABCA3 (ATP-binding cassette sub-family A member 3), PLD2 (Phospholipase D2), DGK (Diglyceride kinase) and nSMase2 with the inhibition of PI3K*

(Phosphoinositide 3-kinase) and PIKfyve (*FYVE finger-containing phosphoinositide kinase)*[46]. *Microvesicles production is instead enhanced by the translocation to the outer leaflet of plasma membrane of a-SMase and by the sphingomyelin/cholesterol binding protein* [29]. *Particularly important is the BisMonoacylGlyceroPhosphate, highlighted in red, a crucial lipid that discriminates exosomes from microvesicles since its intracellular localization is proper only of late endosomes and lysosomes* [54][57].

In conclusion, pharmacological modulation of BMP\cholesterol concentrations, can be considered as a novel and promising therapeutic strategy by affecting EVs biogenesis, release or functionality.

Briefly, the biogenesis of Microvesicles and Exosomes, from a "lipidic" point of view may be coordinated, even if the molecular pathways involved in their formation are different [29]. In conclusion, although studies reported the importance of lipids themselves and their related enzymes, we still are at the early phase of the understanding of these complex mechanisms.

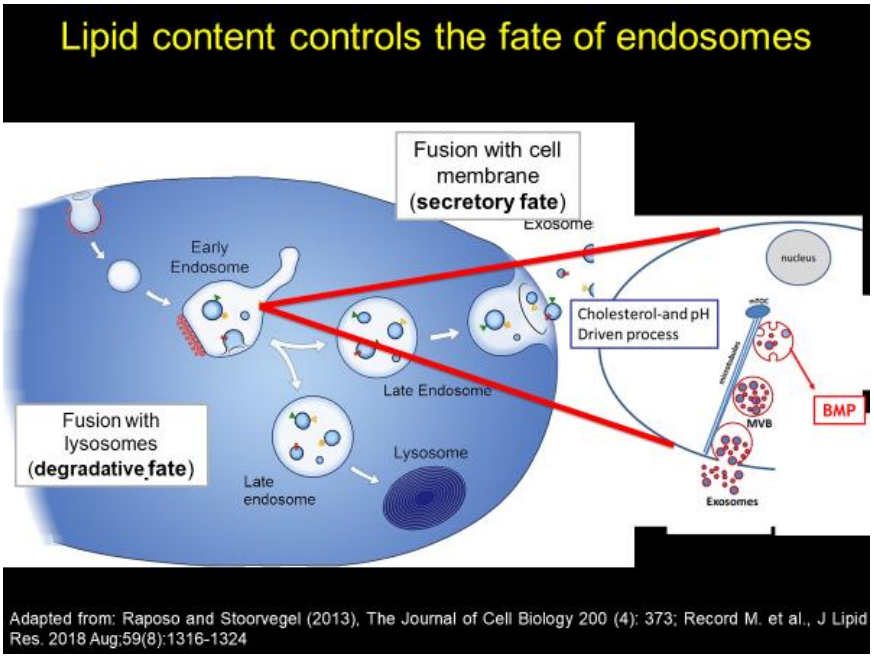

Figure 31 - Cholesterol and BMP ratio addresses endosomes towards the recycling or degradative pathway.

State of the art of EVs pharmacological modulation

Since it has been clearly established that EVs participate in cell-cell communication in physiological conditions and that impairment of their functionality and altered secretion

leads to different pathologies, they represent a very attractive pharmacological target. Inhibition of EVs release can be also useful as research tool, for example by inhibiting the release of a determined population of vesicle to obtain pure preparation for subsequent analysis. Particularly to achieve these purposes, with the preliminary data of this thesis work we were able to be funded by UNIMI with the project EXTRALIPO "New lipid-oriented pharmacological and chemical approaches to discriminate and unravel extracellular vesicles biological functions" Bando SEED – PSR 2019. However the high complexity of EVs biogenesis, together with their heterogeneity represent the big challenge [58].

EVs pharmacological modulation has been categorized in:

1. Compounds which interact with EV trafficking;
2. Compounds that affect lipid metabolism [58].

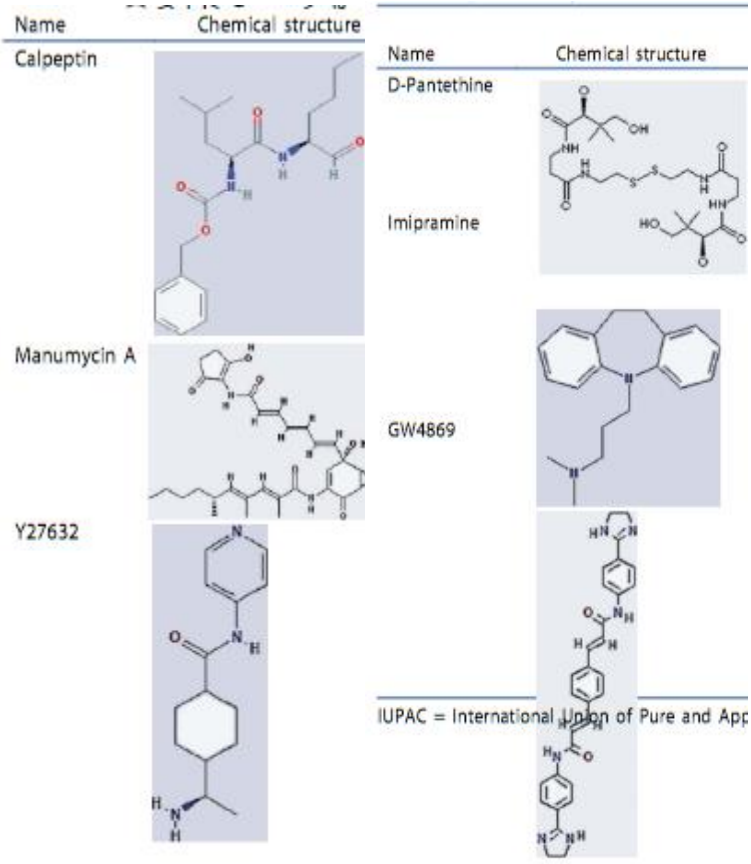

Figure 32 from [58] - *Structures of common drugs which interact with EVs biogenesis.*

GW4869 is a well-known inhibitor of nSMAse, an enzyme involved in ESCRT-independent EVs biogenesis pathway; particularly GW4869 demonstrated to reduce cardiac dysfunction after myocardial infarction through the impairment of exosome release (Biemmi et al., 2018, Circulation vol. 134. Suppl 1). Suppression of exosome secretion with GW4869 reduced

hypoxic exosome-induced migration and invasion of normoxic Colorectal cancer cells [59] and blockade of exosome generation with GW4869 dampened the sepsis-induced inflammation and cardiac dysfunction in mice [60]. On the other hand there are different results: for example Phuyal et al [61] demonstrated that GW4869 does not affect EVs release in PC3 cells.

Based on these findings we considered to utilize this compound even in our cell line but discording results together with its very poor solubility (0.2 mg/ml) aroused some doubts. Several authors used to incubate cells with GW4869 in a range from 5 up to 20 uM, while the max concentration that can be reached utilizing 0.1% of DMSO is 0.346uM.

Due to our extensive experience the field of cholesterol pharmacological modulation, we decided to utilize simvastatin to modulate cholesterol concentrations in parental cells. Simvastatin is an inhibitor of HMG- CoA reductase, the key enzyme of cholesterol biosynthetic pathway [62].

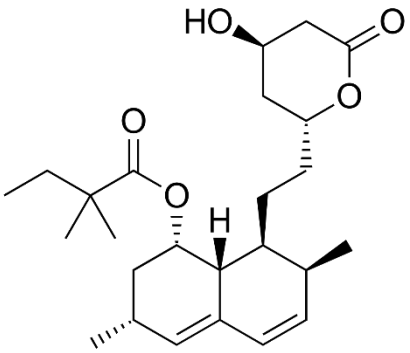

Figure 33 - Simvastatin Structure (lactone form).

HMG-CoA reductase is a transmembrane glycoprotein anchored to the endoplasmic reticulum whose functionality is regulated by 3 different mechanism:

1. *Transcriptional*, through SREBP2 (sterol regulatory element-binding protein)
2. *Phosphorylation/dephosphorylation* by a cAMP-dependent kinase and phosphatases.
3. *Reduction of half-life* in response of high cholesterol concentrations.

Statins specifically inhibit this enzyme reducing biosynthesis of cholesterol (they are well known drugs largely used in clinic for the treatment of hypercholesterolemia). In addition statins are able to inhibit protein prenylation (through the inhibition of mevalonate, farnesol and GGOH), which is a vital process, necessary for the achievement of several cellular processes as proliferation, migration, apoptosis and gene expression, the so-called

"pleiotropic effects of statins", which have been demonstrated in *in vitro* and *in vivo* models but not in clinics.

Recent clinical evidence demonstrated that statins reduced the mortality by 15% in all cases of cancer compared to non-utilizers, and preclinical studies showed that the inhibition of proliferation may affect cancer metastasis with both cholesterol dependent- and independent- mechanisms [63]. Simvastatin was also shown to alter exosome formation and secretion, reducing their secretion *in vitro* [56]. These data, together with the crucial role of cholesterol in EVs biogenesis and functionality, made statins a very useful and attractive tool to better improve the knowledge in EV field.

Together with cholesterol BMP has a pivotal role in EVs biogenesis and functionality. Very little is known about its biosynthesis but for as concern its degradation it has been established that ABHD6 is responsible for 90% of its hydrolyzation. ABHD6 expression is increased in different kinds of cancer as bone, prostate, leukemia and Burkitt lymphoma, thus providing it as a suitable therapeutic target [64]. In addition ABHD6 has also been implicated in pathogenesis of metabolic syndrome, inflammation, insulin secretion, obesity, adipose browning and brown adipose activation in animal model [65].

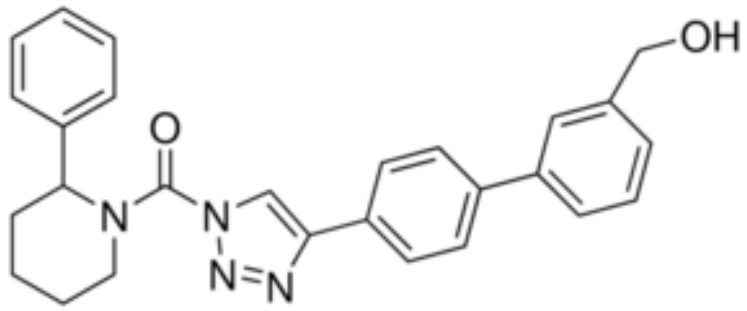

Figure 34 - KT182 structure

KT182 is a very potent, orally bioavailable and selective inhibitor of ABHD6, characterized by a great solubility in DMSO (20mg/ml). Evidence demonstrated that the compound is able to increase BMP levels through ABHD6 impairment both *in vitro* and *in vivo* [46][51].

We therefore decided to utilize KT182 as tool to reduce BMP degradation and to assess whether its modulation is able to alter the number or released EVs or to modulate their functionality.

Proteins and EVs

EVs are small particles which carry a broad amount of different proteins; depending on cell

type, EVs possess a specific subset of proteins which account for their fates and functions [4]. The main problem about EVs characterization is that different populations display similar appearances, overlapping size and similar composition that make difficult to ascertain their origin and therefore their functions [4]. Unfortunately at the moment MISEV 2018 guidelines analyzed all protein data present in literature and stated that since isolation were performed differently among all works and above all from different cellular sources of EVs,it is still not possible to propose "specific and universal markers" for any type of EVs. Thus MISEV2018 did not propose any molecular marker that specifically characterize EV subtype [7].

Unravelling proteins contained in EVs preparations may have several interesting applications:

1. they can indeed be helpful to find biomarkers for EVs origin and consequently subtype;
2. they can useful to understand their functions;
3. can be used for disease biomarker into patients.

These purposes can be achieved with recent and important improvements both in EVs isolation techniques and dimensional characterization and by the huge improvements in mass spectrometry-based proteomic tools. Several proteomics have been performed during last years to achieve EVs characterization.

Kowal et al., 2016 [66]	DUC, DGC, immuno-isolation
Zhang et al., 2018 [19]	(AF4)
Jeppsen et al., 2019 [17]	DUC, DGC
Crescitelli et al., 2020 [67]	DUC, DCG

DUC= Differential Ultracentrifugation, DGC= Differential gradient ultracentrifugation, AF4= Flow field fractionation.

Kowal et al were able to identify proteins specifically enriched in EVs and defined a set of five protein categories (as explained in following figure) displaying different relative abundance in distinct EV populations. They utilized density gradient centrifugation followed by differential ultracentrifugation. Particularly they propose cd63 as marker for small vesicles.

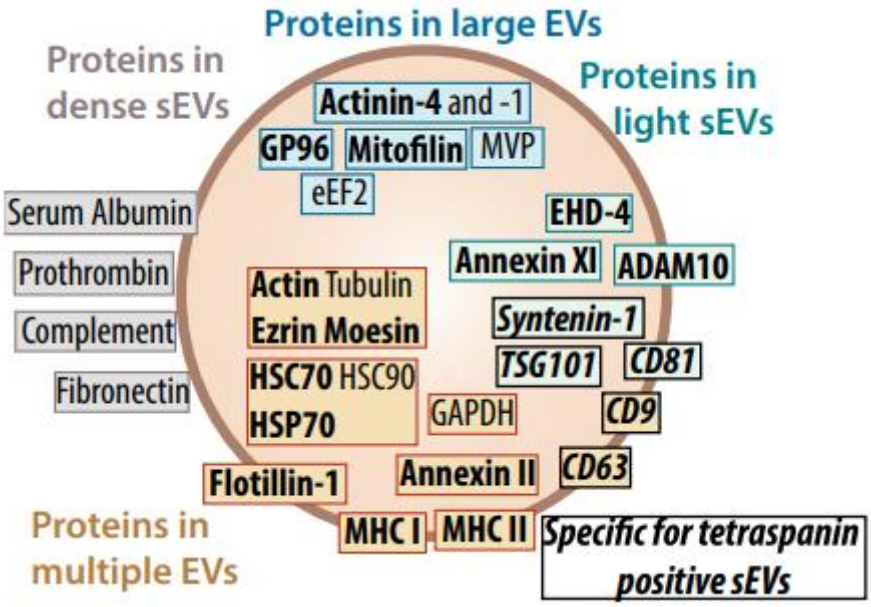

Figure 35 from [66] - *Proteins recovered by Kowal et al in different EVs fraction. Brown: proteins shared by several types of EVs. Green: proteins specifically enriched in light sEVs, including those specific of the tetraspanin-enriched endosome-derived exosomes, and ubiquitously present in all sEVs. Grey: proteins co-isolated with the small EVs. Blue: proteins specifically enriched in large and medium-sized EVs* [66].

Zhang's work [19] was the first and the unique work to perform a proteomic analysis after Flow Field fractionation isolation of EVs, in which they were able to isolate three different vesicles populations, respectively exomeres, small exosomes and large exosomes as previously reported; they were able to identify unique and common proteins among the different fractions obtained by AF4 from two different tumoral cell lines.

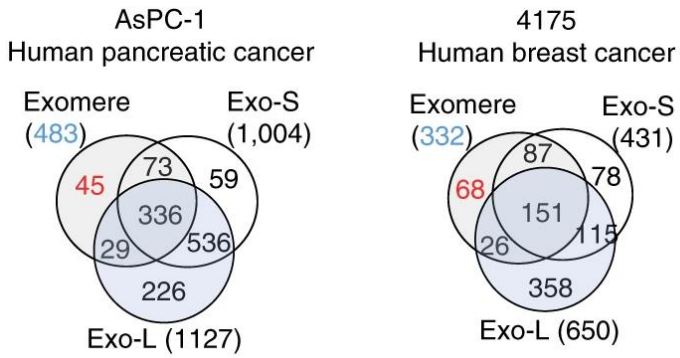

Figure 36 – Venn diagram of different and common proteins contained in exomeres, small and large exosomes, of two different cell lines [19].

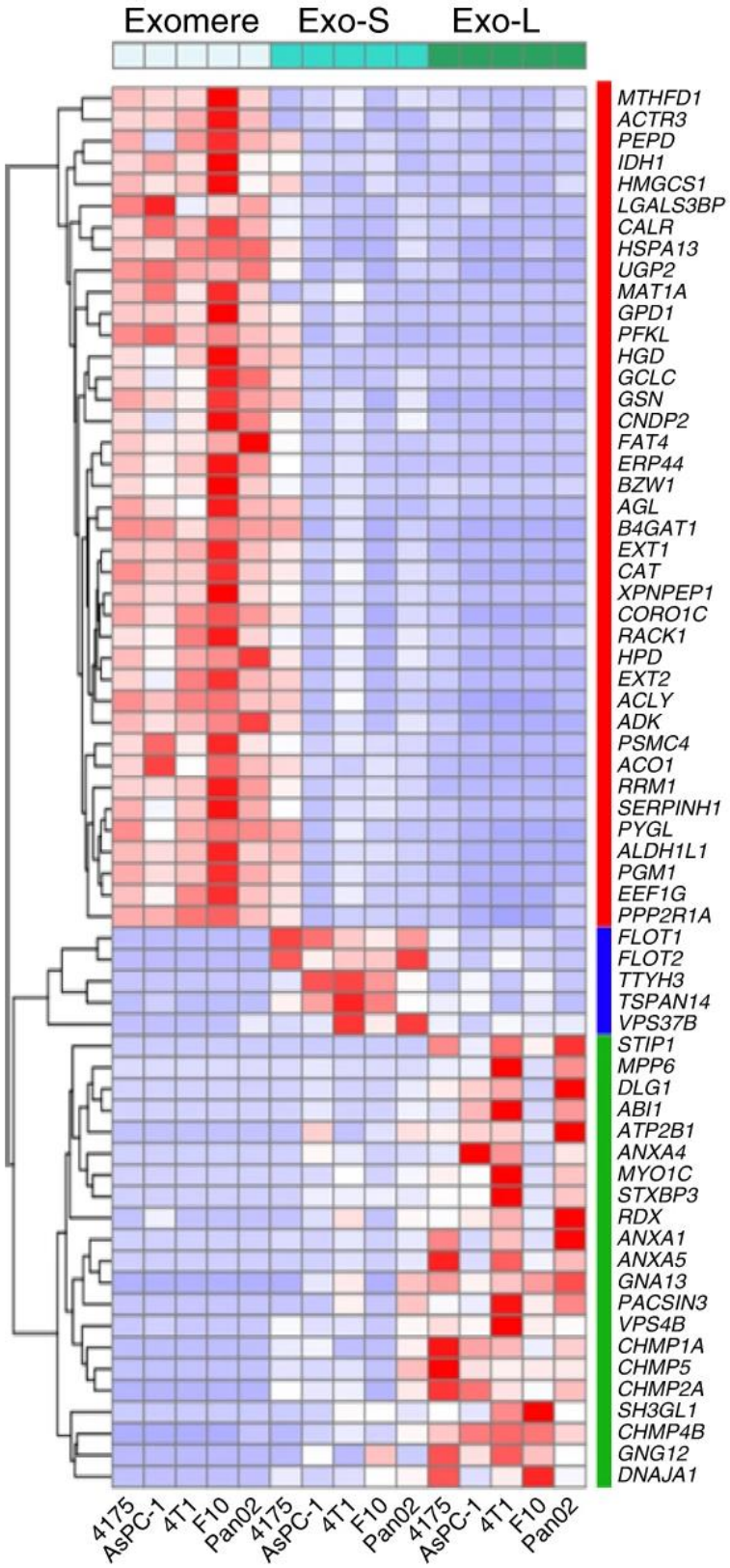

Figure 37 - Heatmap illustration of unique proteins specifically associated with exomeres, Exo-S and Exo-L [19].

They analyzed classical EV markers as flotillins, CD9, CD63, CD81, Alix1, Tsg101, HSC70

(HSPA8) and Hsp90 finding that flotillins (FLOT1 and FLOT2) represented bona fide markers of Exo-S, while HSP90AB1 was preferentially associated with exomeres. Although CD9, CD63 and CD81 demonstrated specific association with Exo-S/L subsets, they all showed a cell type- and particle-dependent preferential expression. In addition, rab proteins were only present in small and large EVs while not in exomeres.

Jeppsen et al in "Reassessment of Exosome Composition" proposed annexin A1 and annexin A2 as novel markers for microvesicles; both proteins were absent from classical CD63, CD81 and CD9 positive exosomes. Jeppsen claimed that "many of the presumed component of exosomes from Kowal [66] and Zhang [19] were absent from classical exosomes expressing CD63, CD81 and CD9.

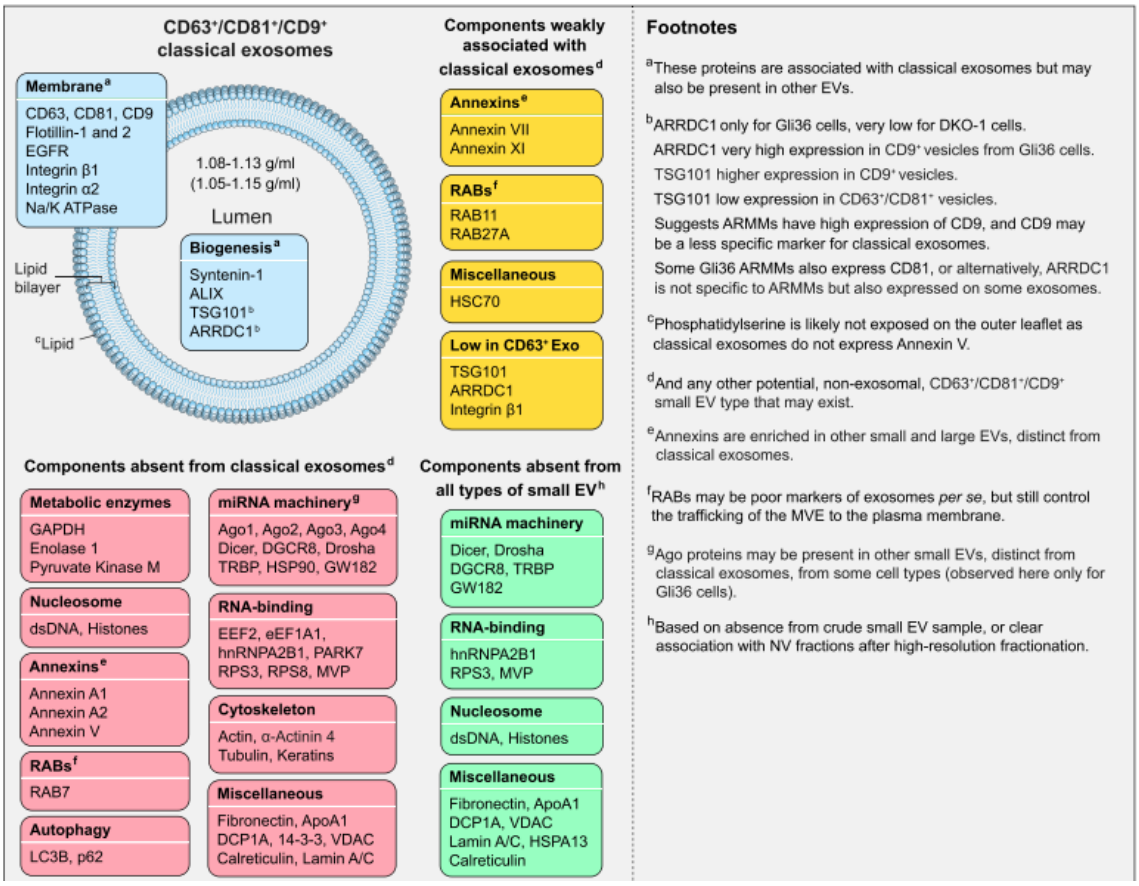

Figure 38 Schematic illustration of revised composition of CD63/CD81/CD9-positive classical exosomes based on the data generated in Jeppsen's study [17].

Crescitelli et al [67] conduced an interesting study in which they isolated EVs directly from melanoma tumor tissues for *ex vivo* experiments.

They isolated EVs by performing classical ultracentrifugation in order to obtain two different pellets, respectively microvesicles (10K) and exosomes (100K); afterwards they performed

on the same pellets density gradient centrifugation in order to obtain 1) low density small EVs, 2) high density small EVs, 3) low density large EVs and 4) high density large EVs 5) large EVs (10K) 6) small EVs (100K)

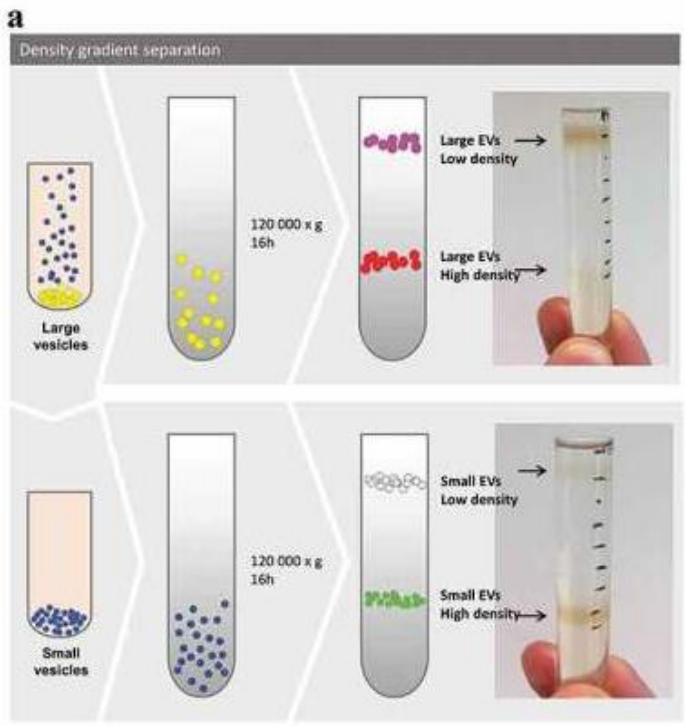

.

Figure 39 – Schematic representation of different EVs population isolated by melanoma tissues through ultracentrifugation followed by density gradient centrifugation.

Despite authors confirmed the presence of classical canonical EV marker in all fractions; it is important to report that these data do not accord with Kowal's observation whose work claimed that CD63 was a tetraspanin characteristic only of small vesicles.

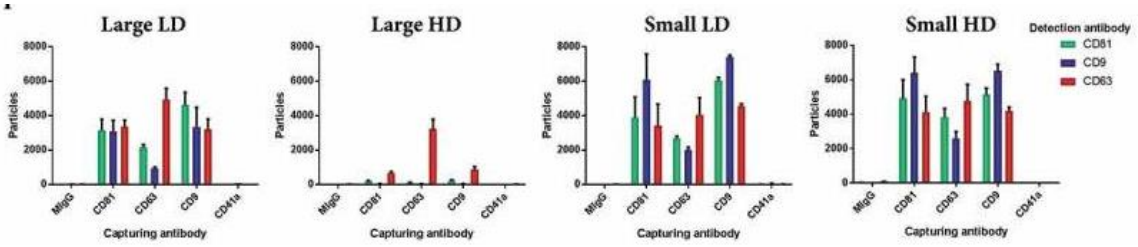

Figure 40 – Classical canonical markers present in the different populations of EVs isolated from melanoma tissues with Exoview system [67].

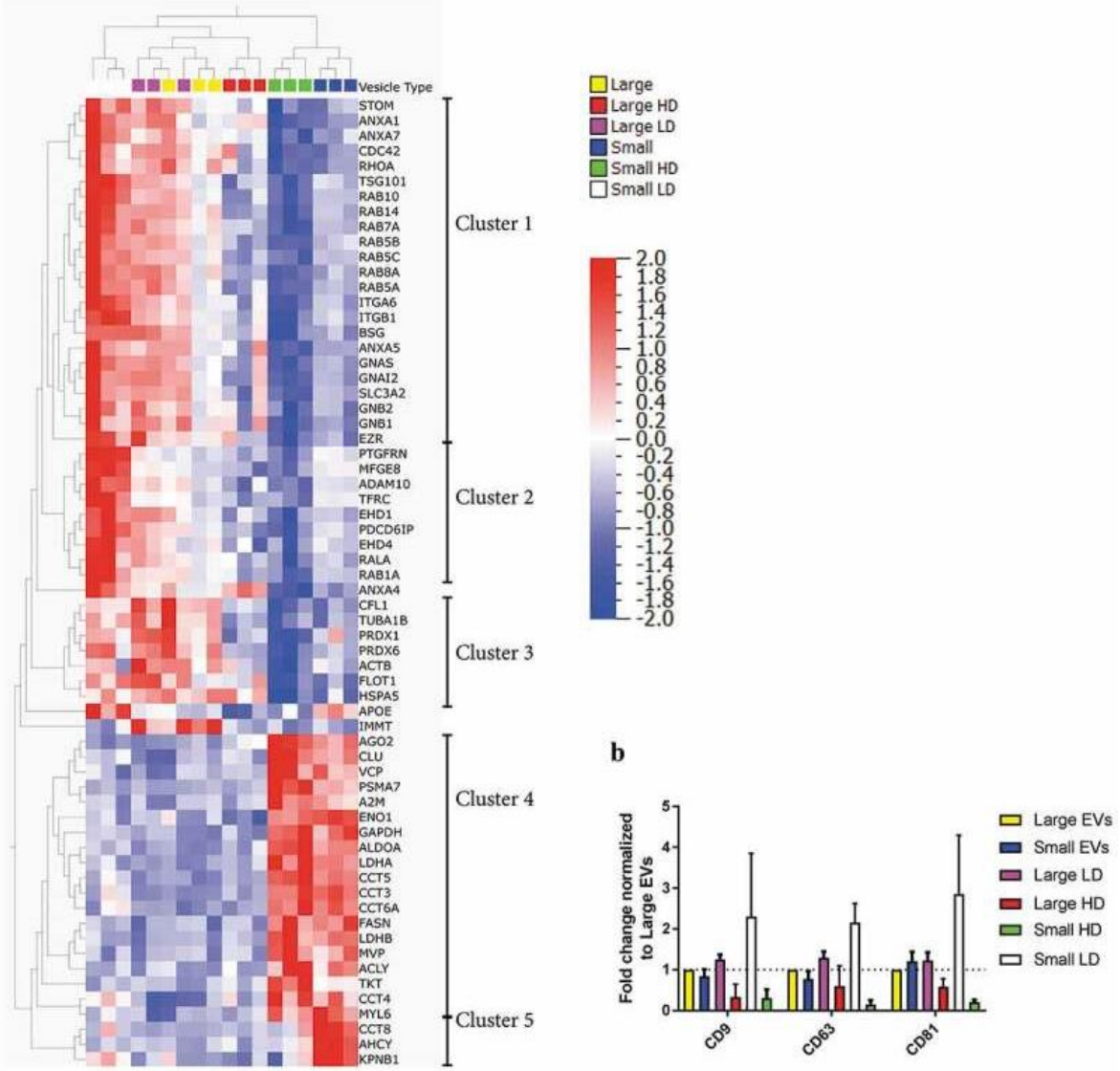

.

Figure 41 – Heatmap of protein pattern found in different EVs populations from metastatic melanoma tissue [67].

Crescitelli et al., showed that flotillin-1 were enriched in both large and small Low Density EVs, while ADAM10 and EHD4 were exclusively enriched in small Low Density EVs as previously reported by Kowal [66] suggesting that these proteins might be part of endosomal-derived vesicles (also called exosomes). The only protein enriched in large EVs and large LD EVs was the mitochondrial inner membrane protein mitofilin confirming again Kowal's observations [66]. Argonaute 2 proteins was found to be enriched in small HD EVs confirming Jeppsen's observations [17].

As reported by Crescitelli et al., “This highlights the need to perform proteomics studies that include several different subpopulations of EVs in order to determine both the shared and unique protein markers for these subpopulations”. In conclusion, proteomics, coupled with software that unravel the functionalities of a complete protein pattern can be used to improve knowledge in EVs role in cancer development and progression and therefore utilized to find new pharmacological targets or new biomarkers for early disease detection.

Aims of the project.

AIM 1) The first part of my PhD project was dedicated at setting up the experimental conditions to isolate extracellular vesicles, a necessary approach to produce valuable materials (cells, EV) and quality data, since we did not have any experience in this field. We quickly realized that the various EVs fractions overlap by their size/protein and lipid content, making very difficult their correct separation and therefore the comprehension of their physio-pathological roles. Another question that aroused was: how it is possible to isolate, following classical protocols, only two populations of vesicles, namely 100 K (exosomes) and 10K (microvesicles), while both MISEV guidelines and Zhang's findings unraveled the presence of more than two populations? To overcome these problems, we improved the existing isolation method of different EVs populations based on their size through ultracentrifugation. We based our first aim on Zhang's observations [19], developing a differential ultracentrifugation method consisting of 5 different ultracentrifugation steps, whose time and g forces were calculated with Livshts' algorithm [68], leading us to obtain 5 distinct population of vesicles.

AIM 2) After their correct isolation, second aim was intended to define differences in terms of lipid classes and protein content between parental cells and the different EVs populations. The differences may help in unraveling different EVs characteristics as membrane fluidity, signaling, EVs internalization in recipient cells, enzyme or protein functionality and distribution of canonical EVs markers among the different fractions. In addition a "lipid and a protein picture" of different population of biological vesicles may be really helpful in:

1) recreate synthetic lipid nanoparticles as much as possible close to the biological ones
2) characterize the internalization mechanisms beyond the cooperation of lipid, proteins and physical characteristics (e.g. dimension, rigidity).

Several Covid vaccines are now being developed as mRNA incapsulated in lipid nanoparticles of 100nm and we strongly believe that our efforts would be really interesting in this field. Moreover, the fractionation of EVs in five different populations will help us to understand the specific origin of the different vesicles, overcoming the problem raised in the first aim, due to the presence of different lipids and proteins which derive from distinct sites of the parental cell. In addition, this second aim is also intended to unravel the different roles of the different EVs populations, through a deep proteomic analysis made by Ingenuity Pathway Analysis software (IPA).

AIM 3) Since our lab is specialized in lipids, their metabolism and pharmacological modulation we aimed to administrate drugs affecting lipid metabolism, particularly cholesterol and bismonoacylglycerophosphate, which cooperate for EVs biogenesis/secretion. It is really interesting to assess if a depletion of cholesterol and an increase of BMP may lead to an altered release of vesicle number from the cell (quantitative hypothesis) or to the release of dysfunctional EV (qualitative hypothesis) conferring them less aggressiveness in cancer progression. In both cases, data can be utilized to assess if pharmacological modulation of lipid metabolism of parental cells can be used as alternative therapeutic strategy for cancer treatment. To achieve this aim we utilized simvastatin and KT182 with the goal to compare naïve EVs vs pharmacologically-treated ones.

Materials and Methods

Cell lines

Even if my PhD project was focused on melanoma, we decided to further utilize other different tumoral cell lines, all derived from metastasis of primary tumors. In addition, we decided to utilize tumoral cell lines since it is well-known that they produce more EVs, if compared with non-tumoral cell lines and moreover they are immortalized, thus they do not have a different production of vesicles due to cell passaging and suffer less from senescence.

LM-16 cell line

LM-16 cell line was kindly provided by the laboratory of Immunoterapia Dei Tumori Umani of the Istituto Nazionale dei Tumori Milano. LM-16 is a lymph-node metastasis derived from an extracapsular invasion from a female 39-years old patient, whose primary tumor was in the trunk [69].

Culture cell conditions are: RPMI 1640 (Roswell Park Memorial Institute medium, Euroclone) supplemented with 10% fetal calf serum (FCS) (Euroclone), L-glutamine 1mM, penicillin and streptomycin 100U/mL (Euroclone). Cell line was maintained at 37°C, 5% di CO_2 in 150mm dishes.

MDA-MB-231 cell line

MDA-MB-231 cell line is a pleuric effusion of a triple negative mammary adenocarcinoma, which is characterized by the lack of the overexpression of the estrogen receptor, progestinic receptor and HER2 receptor (epidermal growth factor 2). This cell line was isolated from a caucasian 51-year old female.

Cell culture conditions are: DMEM (Dulbecco's Modified Minimum Essential Medium, Euroclone), supplemented with 10% FCS (Euroclone), L-glutamine 1mM, penicillin and streptomycin 100U/mL (Euroclone).

PC-3 cell line

PC-3 cell line is derived from a IV grade prostate adenocarcinoma, kindly provided by Dr. Gomaraschi (UNIMI) and Prof A. Llorente (Oslo University Hospital). PC-3 is derived from a bone metastasis of a prostate carcinoma derived from a 62 years-old caucasian man.

PC3 cells were cultured in RPMI 1640 (Roswell Park Memorial Institute medium, Euroclone) + 10% di FCS Euroclone 1mM L-glutamine, 100U/mL penicillin and streptomycin. Cella were incubated at 37°C, 5% CO_2 in 150mm dishes.

Determination of cell number by coulter counter

In order to determine the number of cells used in our experimental conditions we utilized the Beckman Z1 Coulter Counter.

Cells are taken up in aliquots of the suspensions by a mechanic pump, letting cells to pass through a little hole, surrounded by two electrodes: the interruption of conductivity between the two electrodes is recorded by the instrument and the signals are converted in number of cells.

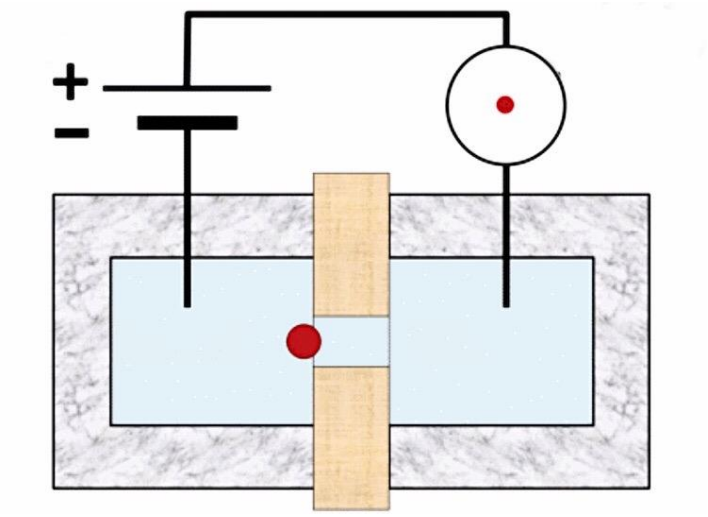

Figure 42 - Schematic representation of coulter counter.

After removing cell media from dishes, cells have been washed with PBS to remove all residues of FCS and then is added a proper volume of trypsin to detach the cell layer. After few minutes needed to achieve the proteolytic action of the enzyme, we resuspended cells in a medium solution with 10% FCS (to block the trypsin) with a glass Pasteur, avoiding the formation of cell clumps. We then resuspended 500 µL of the aforementioned suspension in

Beckman coulter counter dedicated becker, filled with 20ml of saline solution (ISOTON, Beckman). After gently resuspension cells were ready for the count into the instrument. Results were normalized by an appropriate dilution factor to reach the correct concentration of original suspension.

Doubling time determination of cell lines

In order to determine the growth curves of each cell line we seeded 35mm Petri dishes, incubated at 37°C with 5% CO_2, Samples were counted respectively at 24, 48, 72 and 96 hrs.

In detail, we removed the medium to 3 different dishes and washed them with 2ml of PBS. After PBS removal, cells have been resuspended in 1ml of trypsin. The solution has been resuspended with a glass pipette to avoid cell clumps and then resuspended in 1mL of medium supplemented with 10% FCS to block the proteolytic action of trypsin. Afterwards, 500µL of the solution have been resuspended in 20ml of isoton and cells counted with Coulter Counter. Thanks to an online tool (https://www.doubling-time.com/compute.php) it is possible to determine cell growth rate and therefore their doubling time.

$$DoublingTime = \frac{duration * \log(2)}{\log(FinalConcentration) - log(InitalConcentration)}.$$

Figure 43 - Formula for doubling time determination.

Cell culturing for proteomics and lipidomics experiments

Cells have been cultured in 150mm dishes, under sterile conditions, incubated with 15ml medium plus 10% FCS for 3 days at 37°C with 5% CO_2.

At day 0, we seeded 12 million cells/150mm dish in medium supplemented with 10%FCS; day 1 we replaced media with fresh one, supplemented with FCS 10%.

After 3 days we removed the medium and we washed twice the cells with respectively 15 and 10ml of PBS, in order to remove all vesicles and contaminants of the fetal calf serum. After that, cells have been incubated for 3 further days with 12 ml of serum-free medium.

At day 6, medium has been collected and processed with the EVs isolation protocol, while cells have been counted or utilized for further analysis (e.g. lipid composition and proteomics).

For proteomics of pharmacologically treated cells, at day 1 and day 3 we added fresh solutions of compounds.

Dose-finding experiments: MTT, cell proliferation and cholesterol biosynthesis.

At day 0 60.000 LM-16 cells were seeded in 35mm petri dishes, incubated with RPMI1640 medium supplemented with 10% FCS. Twenty-four hours later (day one) the medium was changed to one containing or not pharmacological treatments (simvastatin, KT182) supplemented with 10% FCS, and incubation was continued for further 3 days. At time 0, immediately before the addition of compounds, three dishes were counted with Coulter Counter. After 3 days of incubation (day 3), cells were washed twice with PBS and media was replaced with serum free one and incubated with the compounds for further 3 days; at day 6 cell proliferation was evaluated by counting cells after their trypsinization using a Coulter Counter model ZM. In separate dishes cholesterol synthesis has been evaluated with the same experimental conditions by measuring the incorporation of 14C acetate into free cholesterol. 3H was used as internal standard. At day 6 cells have been washed twice with PBS and protein suspended in 2 ml 0.1M NaOH. Extracts have been seeded over TLC silica plate to isolate only free cholesterol. Radioactivity was measured with scintillation cocktail.

Ultracentrifugation method

We first developed the ultracentrifugation method according to the algorithm developed by Livshts et al., (http://vesicles.niifhm.ru/) by calculating times and g-forces of the different centrifugation steps. First purification steps have been performed as reported by Thery[18]. We set the density of the particles to 1,15 g/cm^3 and density and viscosity of the medium to respectively 1g/cm^3 and 1.55 cP; We set parameters in order to obtain particles with the theoretical diameter of: minor than 50nm, 50-80nm, 80-120nm, 120-200nm and bigger than 200nm. Samples have been processed with Beckman L-60 Ultracentrifuge in a Beckman 50.2 TI rotor. We utilized 26.3 mL polycarbonate bottle with cap assemply, 25x89mm.

Theoretical diameter	Relative centrifugal force	Time at vmax
(F1) Min 50	100.000g	287 min
(F2) 50-80	100.000g	46 min
(F3) 80-120	100.000g	18 min
(F4) 120-200	100.000g	8 min
(F5) 200>	48339g	6 min

Table 5 - Times and relative centrifugal forces to achieve the precipitation of the desired theoretical diameter with 50.2TI rotor.

Following the classical protocol which requires a "wash" of resulting pellets, each sample has been resuspended in 0.1µm filtered saline solution and centrifuged with "adapted times" (table 6) with the aforementioned tool in a TLA 100.3 rotor in Beckman Optima MAX-TL ultracentrifuge. We utilized 3-5mL open-top thickwall polycarbonate tube 13x51mm.

Theoretical diameter	Rcf	Time at vmax
(F1) Min 50	100.000g	151 min
(F2) 50-80	100.000g	24 min
(F3) 80-120	100.000g	9 min
(F4) 120-200	52.000g	6 min
(F5) 200>	17.000g	7 min

Table 6 - Times and relative centrifugal forces to achieve the precipitation of the desired theoretical diameter with the 100.3 rotor.

Fractions 10K (microvesicles) and 100K (exosomes), (10K and 100K are common names widely used to identify 10.000g pellet "microvesicles" and 100.000g pellet, "exosomes") have been isolated following classical protocol [18] as follows:

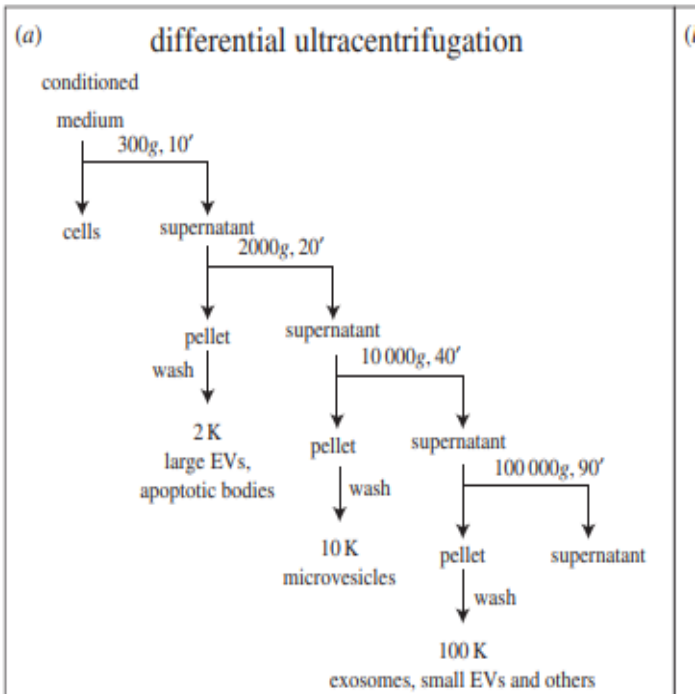

Figure 44 – Thery's protocol to isolate two different population of EVs.

Lipid extraction and GLC analysis

Lipids have been extracted following Folch's method [70]. Each sample has been resuspended with 500µL of 0.1µm filtered NaCl. Extractions have been performed in inert pyrex glass tubes utilizing $CHCl_3$ and CH_3OH 2:1; in detail we utilized 800µL of chloroform and 400µL of methanol. Samples have been mixed for two hours at 4°C; after the first step of extraction vials have been centrifuged at 2500 rpm x 10minutes to separate organic fraction from the aqueous one. This process has been repeated three times.

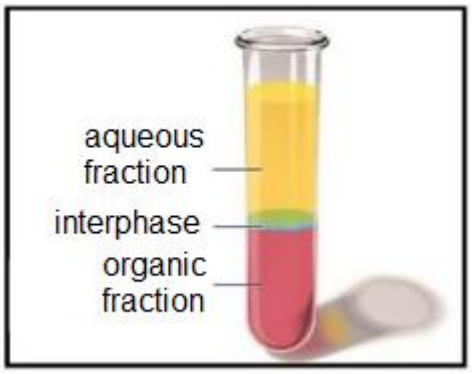

Figure 45 – Representation of lipid extraction.

a) To detect free cholesterol, an aliquot of the total lipid extract has been concentrated and injected without derivatization in a gas-liquid chromatography DANI 1000 (Dani, Milano, Italy) equipped with a flame ionization detector and a HTA autosampler (HTA, Brescia, Italy). Experimental conditions are as follows:

- chromatographic column DB-5 (Service T.L. Milano), 30 m length, 0,32 mm diameter, 0,25 micron film.

- oven temperature from 220 to 310 (heating rate 20°C/minute), total run length 8 minutes.

- constant inlet pressure 1,20 bars (hydrogen flow as carrier gas); inlet temperature from 200 to 320 (at 500 degrees/minute).

- detector temperature 350°C.

Free cholesterol mass has been quantified after peak identification and after comparing its area under the curve with that of stigmasterol (internal standard), by automated integration using a dedicated software (Clarity, Prague, Czech Republic). Free cholesterol mass has been normalized by sample protein content, evaluated by the bicinchoninic acid, and expressed as ug/mg protein.

b) To analyse fatty acid profile, total lipid extracts have been concentrated and methylated by methanolic HCl 3N for two hours at 80°C. After lipid extraction with hexane/water 200/800 ul, the methyl esters have been injected in a gas-liquid chromatography DANI 1000 (Dani, Milano, Italy) equipped with a flame ionization detector and a HTA autosampler (HTA, Brescia, Italy).

Experimental conditions are as follows:

- chromatographic column MEGA-5 (Mega Columns Legnano), 30 m length, 0,25 mm diameter, 0,15 micron film

- oven temperature: from 150 to 190°C (heating rate 8°C/minute); from 190 to 210 at 4°C/minute and from 210 to 320°C at 12°C/minute; 6 minutes hold), total run length 25 minutes

- constant inlet pressure 0,80 bars (hydrogen flow as carrier gas); inlet temperature from 150 to 250 (at 500 degrees/minute).

- detector temperature 330°C.

Total fatty acid profile of cells and EV fractions has been determined by comparing the retention times of the peaks with those obtained by running a dedicated mixture of methylated fatty acids (FAME MIX 37, Sigma-Aldrich) and their area determined by automated integration by a dedicated software (Clarity, Prague, Czech Republic). The relative % of each fatty acid has been calculated by comparing the AUC of each fatty acid with the value of the AUC of all the peaks.

For as concern lipid subclasses analyses of cells, cholesteryl esters, triglycerides, free cholesterol and free fatty acids, a proper amount of internal standard was added for each category and lipid extracts have been seeded over TLC silica plates, developed with the following solution: acetic acid, dietylether and hexane 1:20:80. Bands corresponding to the aforementioned lipids have been scraped and derivatized with methanolic HCl solution, respectively 2hrs 80°C for CE, 30 min 80 °C for TG, 5 minutes 80 °C for FFA, while FC was directly analyzed after extraction in hexane\isopropanol 3:2. We then utilized Clarity Software to determine area under curves of each fatty acid and of free cholesterol. AUC of internal standards was utilized to determine the mass of lipid class contained in samples.

Total phosphorus content has been extracted by hexane/isopropanol 3:2 and quantified by Ames' phosphorus detection assay: the extracts have been dried under nitrogen and heated

at 180°C overnight with 300ul of sulphuric acid 1N. After the addition of 5 H_2O_2 drops samples were heated again at 180 C for 2 hours until dark coloration disappeared. 300ul of water, 100ul of vitamin C 1% and 600ul of ammonium molybdate 0.5% in H_2SO_4 were added and phosphorus have been quantified after spectrophotometric analysis in 96-wells plates and calculated, calculated in nanomoles and normalized by total protein content.

Dimensional analyis

Electron Microscopy

After EVs isolation each fraction has been further characterized by electron microscopy. We decided to resuspend EVs in saline solution (0.9% NaCl pH 7.4) in order to avoid interaction of organic phosphorus contained in PBS with uranyl-acetate utilized for the staining; in addition we previously filtered saline solution with 0.1um filter, to eliminate any kind of contamination and crystal salts. Electron Microscopy (EM) is considered as one of the gold standards for EVs characterization by imaging [71].

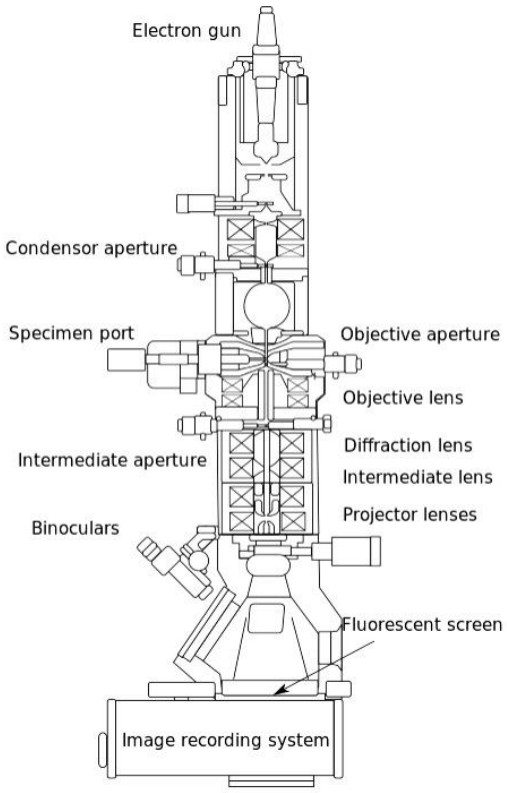

Figure 46 - Electron Microscopy representation.

EM requires the adsorption of samples on a small and thin copper grid. Thanks to the facility of EM of Oslo University Hospital and Dr K. Sagini we were able to set-up a valid method to correctly stain the 5 fractions. We then utilized these methods thanks to EM facility of UNIMI thanks to Dr. N. Santo. We first charged grids putting them in filter paper with mat face up, then inserted in the grids in the machine and waited for the vacuum (1x10-1) and set the pulse for 20 sec at 20 mA; after that we incubated grids with 5 or 10 µl of samples in NaCl 0.9% filtered 0.1um for 5 minutes followed by 4x 1 minute washes in water. At this point samples have been stained for 7 minutes in 1% uranyl-acetate (UAc 50 µl drop) and washed 30 sec in H_2O. The final step was letting grids dry for 10-20 min on the bench.

In EM analysis, a flux of high-energy electrons is sent to the sample in vacuum conditions; a series of electromagnetic lenses control electron flux to obtain the magnification of the images of the samples. Samples are adsorbed on a thin and little copper grid which is mounted in a support in the middle of the column [72].

We utilized uranyl-acetate for EVs staining which is able to bind the phosphorus of the phospholipids. The final image is the result of the combination of the atoms and molecules which deviate the electrons against those ones which let electrons to pass through them. In this way the image will be characterized by different scales of grey corresponding to different spatial distribution on the sample [72].

Zetasizer

Zetasizer is an instrument developed by Malvern which utilizes different techniques of dynamic light scattering to determine the characterization of particles in suspensions [73]. Light scattering is a consequence of the interaction of light with the electric field which characterizes a small particle or molecule. Dynamic light scattering is able to record the brownian motion of suspended particles: biggest particles move slower than smaller ones. [74].

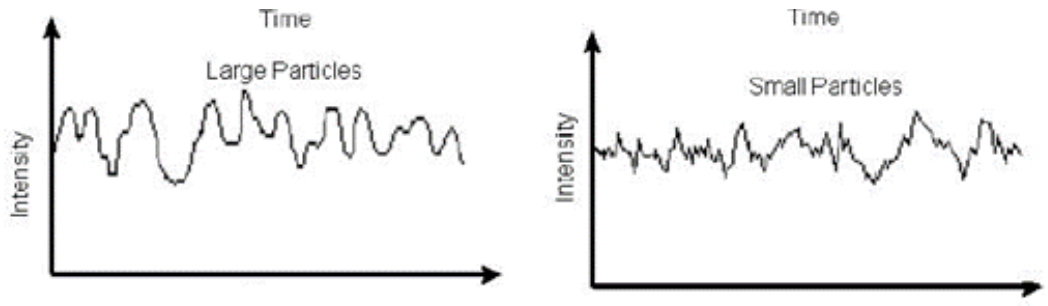

Figure 47 – Differences in Brownian motions of large and small particles.

A particular algorithm combines Rayleigh and Mie's theories letting the software to determine the hydrodynamic radius of the particles in suspension by measuring their physical behavior in solution [73]. Particularly hydrodynamic radius corresponds to the equivalent diameter of a sphere which is moving in a water suspension; the molecules of water indeed surround the particles forming a sort of "outer layer" which is "translated" in bigger dimensions compared to the effective ones of the particles. Hydrodynamic radius depends on not only particle dimensions but also on their surface, on the molecules that compose their surface and on concentrations and ions present in the suspension solution. Consequently, different surfaces together with different solutions at different temperature may change the Brownian motion of particles. For these reasons it is crucial to properly set up the instrument with refracting index of the particle and of the dispersant, viscosity (centiPoises) of the dispersant, absorption and refractive index of the particles.

Figure 48 – Zetasizer parameters typical settings. RI- refractive Index.

Samples solutions are inserted in the instrument through a particular cuvette; laser illuminates the particles and Zetasizer records how the light is refracted. Analysis gives a dimensional distribution which can be expressed in number, volume or intensity [74].

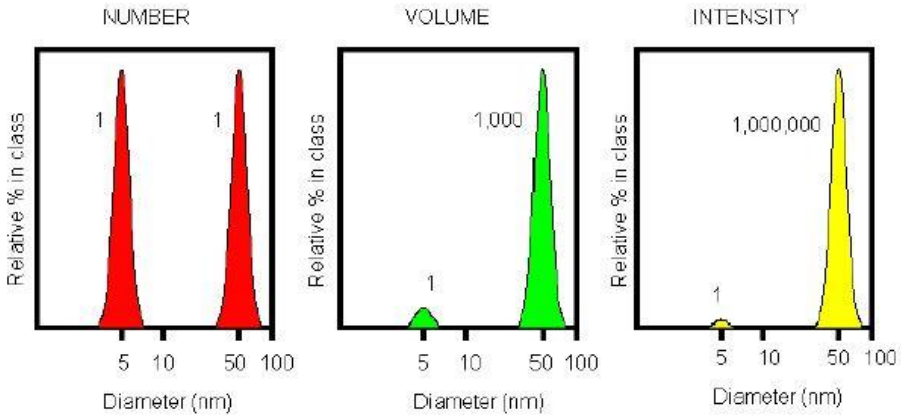

Figure 49 – Different distribution of the same sample expressed in number, volume and intensity.

What is the difference between intensity, volume and number distributions? A very simple way of describing the difference is to consider a sample that contains only two sizes of particles (5nm and 50nm) but with equal numbers of each size particle. The first graph shows the result as a number distribution representing two peaks of the same size (1:1) since there

are equal number of particles. In volume graph the area of the peak for the 50nm particles is 1000 times larger the peak for the 5nm (1:1000 ratio). Since the volume of a 50nm particle is 1000 times larger than that of the 5nm. In the last intensity graph, the area of the peak for the 50nm particles is now 1.000.000 times larger than the peak for the 5nm (1:1000000 ratio), because large particles scatter much more light than small particles. The intensity of scattering of a particle is proportional to the sixth power of its diameter (from Rayleigh's approximation) [73]. Anyway, the basic distribution obtained from a DLS measurement is intensity and therefore all other distributions are generated from this data.

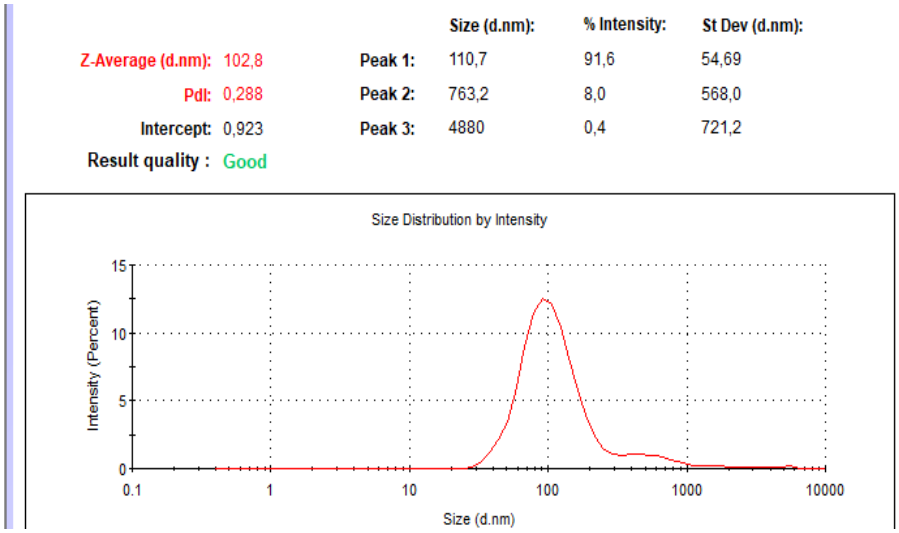

Figure 50 - Example of analysis performed with Zetasizer.

Zetasizer expresses the diameter of the suspended particles with the Z average value. Z average is the intensity-weighted mean diameter derived from the analysis, which is considered the best way to represent the intensity average particle diameter, while PdI is a dimensionless measure of the broadness of the size distribution calculated from the cumulants analysis. As established by the following table PdI between 0.08 and 0.7 are considered as mid-range values in which the algorithms at its best operates.

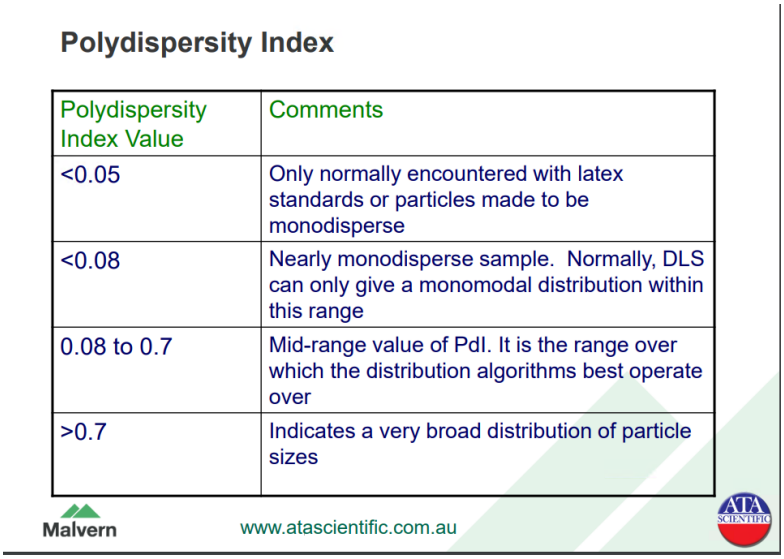

Table 7 from Malvern - The meaning of polydispersity index.

Nanosight

Nanosight is an instrument which is capable to measure the Brownian motion of suspended particles, translating it in a distribution which accounts of size and particle concentration. [75]. Correctly setting up the camera and sample image prior to capturing the video are essential to achieve valid results. We increased the Camera Level until all the particles in the sample can be seen clearly but no more than 20% are saturated (colored pixels). Initial focus is set with the manual control on the side of the Nanosight; we adjusted focus in order to obtain an image as close as possible to b.

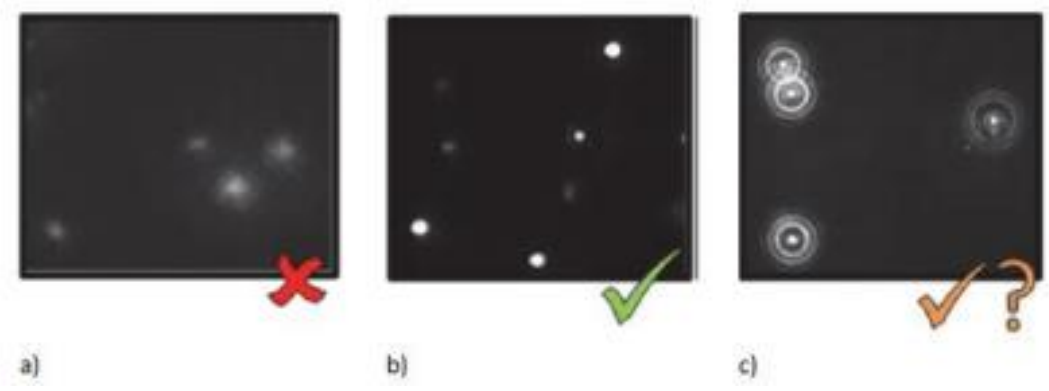

Figure 41- Optimal settings for nanosight analysis. The image should be as close as possible to B.

Nanosight instrument best operates with particle concentrations in the range of ~10^7 – 10^9 particles/ml, which approximately correspond to 20-120 particles in the field of view. Lower

concentrations require longer capture and analysis time to produce statistically significant results. When using the syringe pump, 3 repeats of sufficient length are needed to ensure reliable analyses. After recording videos we adjusted detection threshold. The lower the setting the more centers will be found; however if detection threshold is too low, 'noise' can also be tracked. On the other hand if the setting is too high, dimmer particles will be excluded. For the best analysis, we identified the center of each particle by reducing the detection threshold to a level to include as many particles as possible and within the following restrictions: in the bottom right of the image there is a count of the number of red crosses. This should be between 10 and 100 for good conditions; ideally between 20 and 50. When considering the image by eye, some of the red crosses may not appear to be distinct particles. Ideally there should be <5 (Dr. R. Santoliquido, quick guide for Nanosight users)

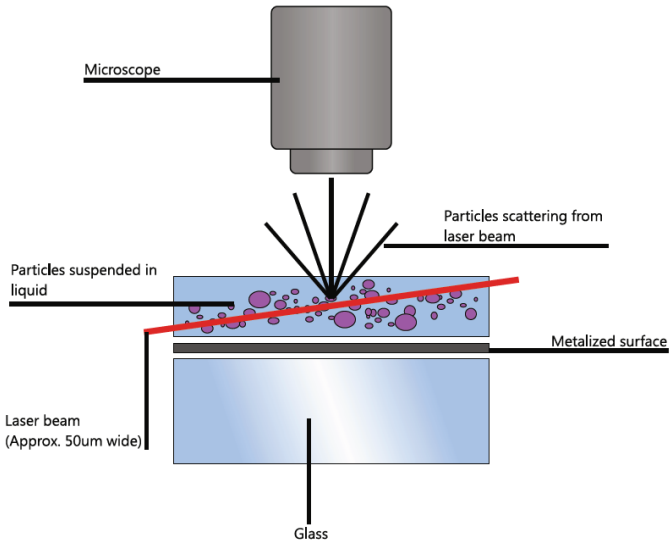

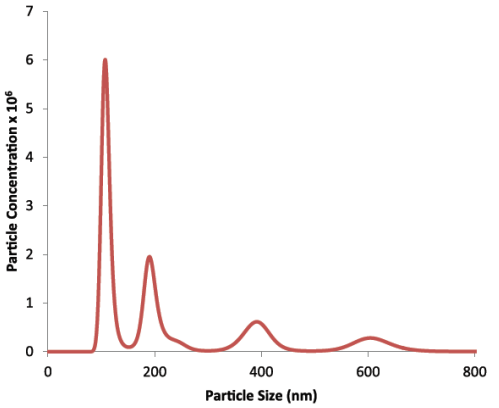

Graph of a sample with distinct peaks at 100 nm, 200 nm, 400 nm and 600 nm.

Figure 42 – How does Nanosight work? [75].

Confocal Microscopy Images

At day 0 we seeded 15000 cells/well in 24 wells plates with glass microscopy dishes. At day one we and incubated them with compounds (simvastatin and KT182) in 2ml of medium with the same experimental conditions reported in previous paragraphs. At day 7 we removed medium and fixed cells (without washing with PBS in order to not alter the intracellular morphology of organelles) with 500uL of 4% paraformaldehyde for 20 min. We then washed with 3x10' of PBS under shaking. We permeabilized cells with 1ml of 0.1% triton in PBS for 15min and washed again with PBS for 3 times. At this point we saturated non-specific sites with 5% BSA + triton 0.1% in PBS for 1 hour. We then incubated cells

with primary antibodies plus triton 0.1% in PBS for 30min and washed for 3x10min with PBS before incubating cells with secondary antibodies for 1 hour. After washing again with PBS we added 5uL of DAPI on microscope slide and gently fixed the glass microscopy dishes on its surface. Slides have been dried at 4°C before microscopy analysis. Primary antibodies were MABT837 Sigma-Aldrich Anti-LBPA Antibody, clone 6C4 and R4779 Sigma-Aldrich Anti-Rab7 antibody produced in rabbit.

Dilutions Utilized:

• anti-mouse LBPA 1:100.

• anti-rabbit RAB7 1:200.

• Alexafluor 488 (anti mouse, green) 1:1000.

• Alexafluor 555 (anti rabbit, red).

Super resolution images of BMP and Rab7 were acquired with the Nikon A1 laser scanning confocal microscope using the N-SIM structured light super resolution module and with the 100x oil immersion objective (NA 1.2). LBPA= green RAB7= red. Analyses have been carried out thanks to Dr. M. Ascagni of UNIMI.

Colorimetric Nanoplasmonic Assay (CONAN)

Colorimetric Nanoplasmonic assay [76] is cost-effective and fast colorimetric assay for probing protein contaminants and determining the concentration of EV preparations.

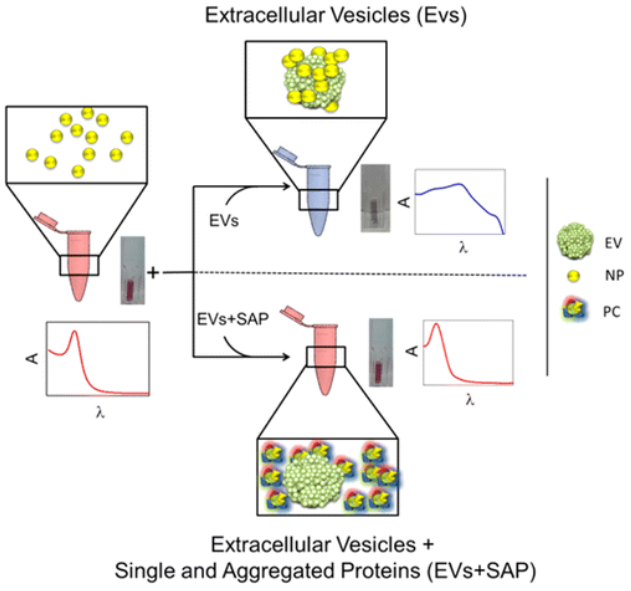

Figure 43 – Scheme of Conan Technique [76].

As represented in figure 43 from Maiolo et al.[76], nanoplasmonic assay consists of 5 μL of a 6 nM water dispersion of 15 nm gold nanoparticles (NPs), stabilized by citrate anions. Gold NPs bind the EV membrane in pure EV preparations while this phenomenon is inhibited in presence of single and aggregated protein contaminants (SAP). SAP-NP interaction keeps NPs dispersed, inhibiting NP-EV interactions. The two different conditions are optically characterized by a specific switch. In conclusion, blue color of the solution means protein purity while we obtain red shift in presence protein contaminants. The assay optical properties (blue and red coloration) were quantitatively investigated by UV/vis/NIR spectroscopy.

High resolution mass spectrometry

Samples (EVs pellets and Cells) have been resuspended in ammonium bicarbonate (AMBIC) and total protein content determined by BCA Pierce assay. Proper amount of samples was seeded in 96 wells-plates, as well as proper concentration of albumin as calibration scale, and incubated with BCA reagents (50:1) for 30 min at 37 degrees until violet coloration appears. Absorbances have been read at 562 nm in plate reader. Reduction have been performed with 5mM DTT (dithiothreitol) followed by a 30 min 52°C incubation with Thermomixer (600 rpm). Alkylation has been performed with 15mM of IAA followed by 20min incubation with Thermomixer. Samples have been finally digested by trypsin at a 1:20 ratio against total protein concentration and incubated 37°C overnight with Thermomixer. The following day 1-2uL of TFA 50% were added. Equal concentration of each samples was injected. All samples have been analyzed at UNITECH OMICs (University of Milano, Italy) using: Dionex Ultimate 3000 nano-LC system (Sunnyvale CA, USA) connected to Orbitrap Fusion™ Tribrid™ Mass Spectrometer (Thermo Scientific, Bremen, Germany) equipped with nano electrospray ion source. Peptide mixtures were pre-concentrated onto a Acclaim PepMap 100 – 100μm x 2cm C18 (Thermo Scientific) and separated on EASYSpray column ES802, 25 cm x 75 μm ID packed with Thermo Scientific Acclaim PepMap RSLC C18, 3 μm, 100 Å. The temperature was setting to 35°C. The peptides were eluted with: Gradient: from 96% buffer A (0,1% formic acid in water) to 95% buffer B (0,1% formic acid in water/acetonitrile (2/8). Total gradient: 110 min. Constant flow rate: 300 nL min−1 . Total run: 144 min. One blank was run between samples to prevent sample carryover. MS spectra were collected over an m/z range of 375 – 1500 Da at 120,000 resolutions, operating in the data dependent mode, cycle time 3 sec between masters scans. HCD was performed with collision energy set at 35 eV. Polarity: positive.

Ingenuity Pathway Software analysis

The networks, functional analyses, were generated through the use of IPA (QIAGEN Inc., https://www.qiagenbioinformatics.com/products/ingenuity-pathway-analysis) by Laboratorio Immunoterapia dei Tumori Umani (Istituto Nazionale dei Tumori, Milano) by Dr E. Vergani and M. Rodolfo. Values are expressed in % of proteins encoding for a determined function or as Z score enrichment.

1.1 Statistical analysis.

Differences have been computed by 1-way anova statistical test, followed by Tukey's test for multiple comparison using Graphpad Prism. The following p values were considered statistically significant *= $p < 0,05$, ** $p < 0,01$ *** $p < 0,001$.

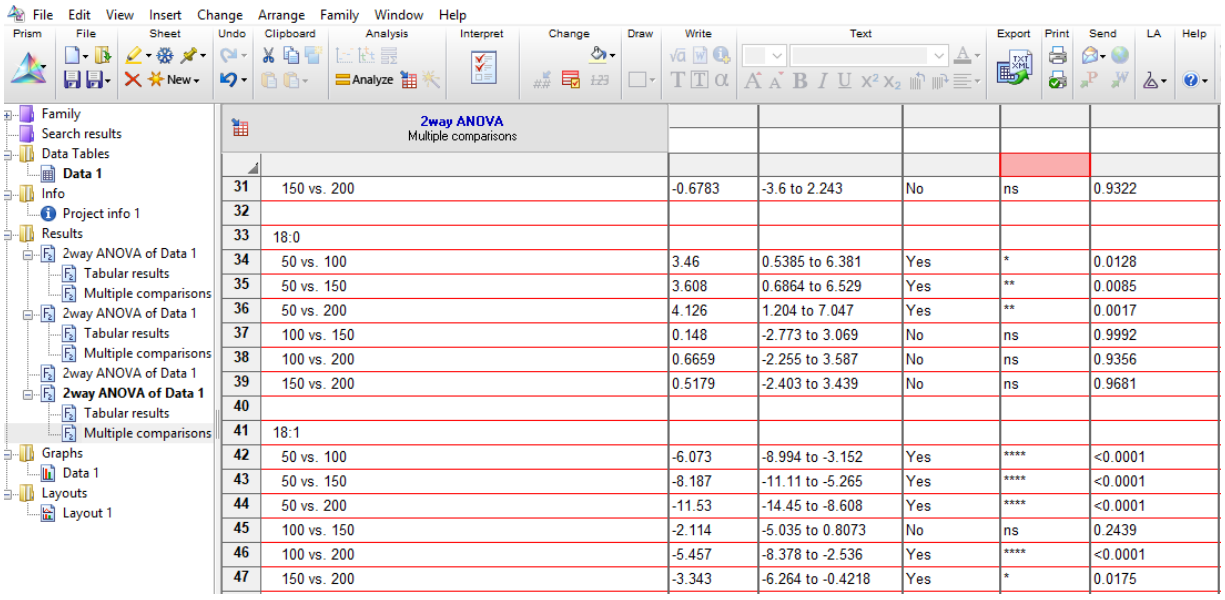

2way ANOVA
Multiple comparisons

31	150 vs. 200	-0.6783	-3.6 to 2.243	No	ns	0.9322
32						
33	18:0					
34	50 vs. 100	3.46	0.5385 to 6.381	Yes	*	0.0128
35	50 vs. 150	3.608	0.6864 to 6.529	Yes	**	0.0085
36	50 vs. 200	4.126	1.204 to 7.047	Yes	**	0.0017
37	100 vs. 150	0.148	-2.773 to 3.069	No	ns	0.9992
38	100 vs. 200	0.6659	-2.255 to 3.587	No	ns	0.9356
39	150 vs. 200	0.5179	-2.403 to 3.439	No	ns	0.9681
40						
41	18:1					
42	50 vs. 100	-6.073	-8.994 to -3.152	Yes	****	<0.0001
43	50 vs. 150	-8.187	-11.11 to -5.265	Yes	****	<0.0001
44	50 vs. 200	-11.53	-14.45 to -8.608	Yes	****	<0.0001
45	100 vs. 150	-2.114	-5.035 to 0.8073	No	ns	0.2439
46	100 vs. 200	-5.457	-8.378 to -2.536	Yes	****	<0.0001
47	150 vs. 200	-3.343	-6.264 to -0.4218	Yes	*	0.0175

Figure 44 – Example of statistical analysis made by Graphpad Prism.

Results

Cell growth curve determination

We first determined doubling time of the three different cell lines utilized, building a growth curve, in order to choose the best conditions to isolate Extracellular Vesicles from cell culture media.

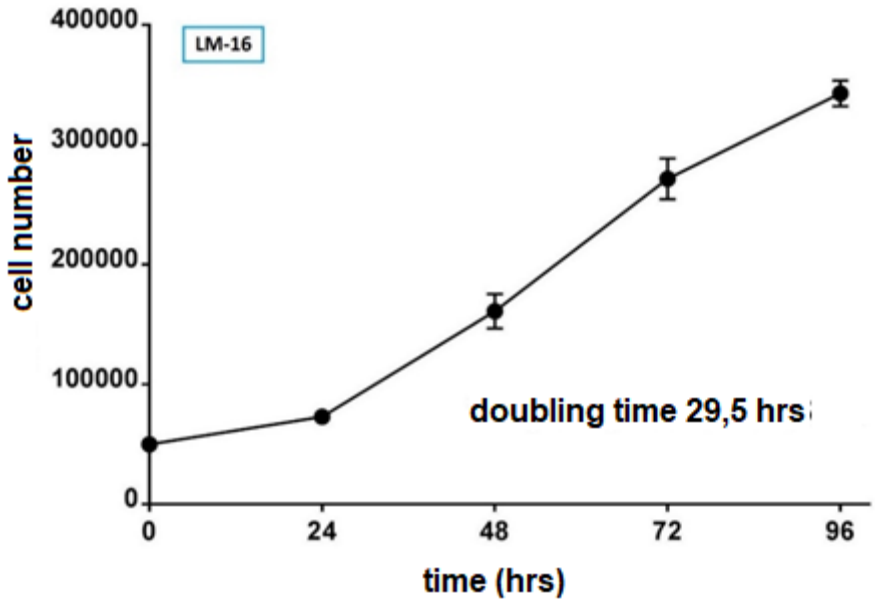

Figure 45 – LM 16 cell growth curve

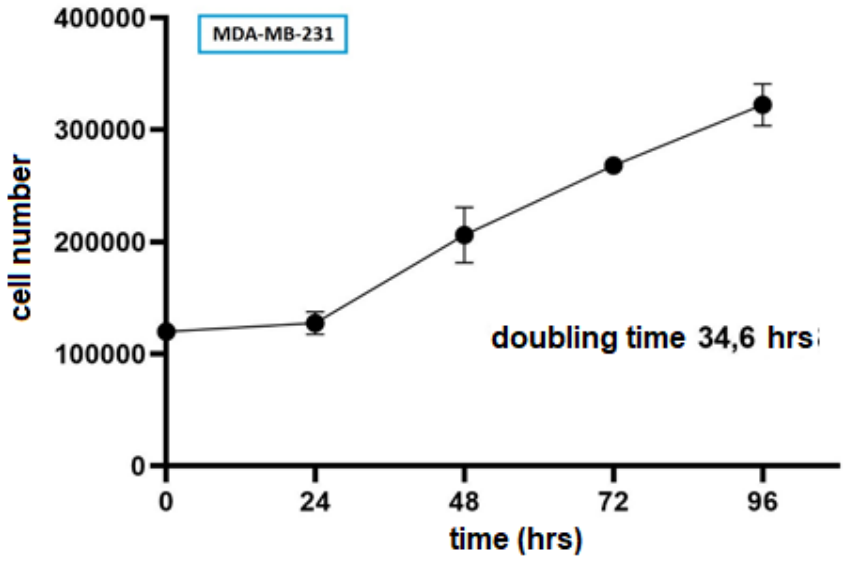

Figure 46 - MDA-MB-231 growth curve.

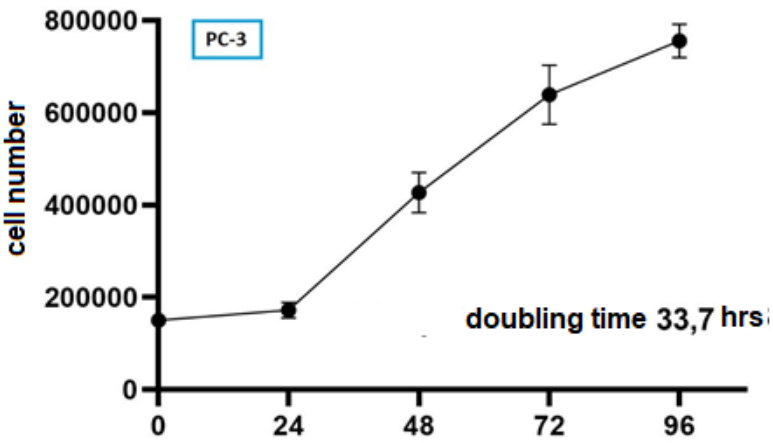

Figure 47 - PC-3 growth curve.

As shown in these graphs, growth curves are quite similar with comparable doubling times. We aimed to isolate EVs from cells with similar doubling time in order to control as much as possible proliferation variables in our experiments.

Lipid analysis of LM-16 cell line

Lipid extracts from LM-16 cell line have been analyzed through Thin Layer Chromatography (to separate different lipid classes) and Gas Liquid Chromatography (for quali-quantitative analysis) in order to evaluate LM-16 lipid composition in detail.

Total lipids

First of all, we characterized the fatty acid composition derived from total lipid extract of LM-16 cells, in order to have a sort of global "picture" of the fatty acids, both intracellular and membrane ones.

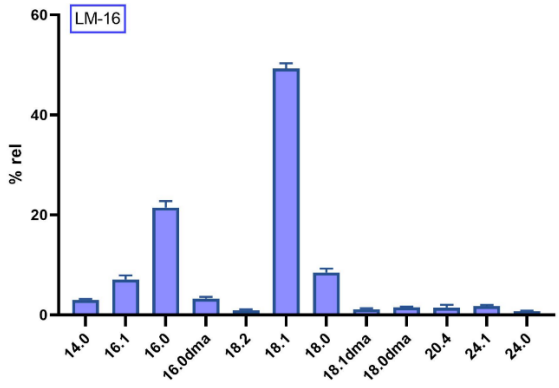

Figure 48 – Fatty acid profile derived from total lipid extract of LM-16 cells (n=5).

As clearly explained by the graph, fatty acids derived from total lipid extract range from 14 to 24 carbon atoms with a wide range of saturated fatty acids (SFA), monounsaturated fatty acids (MUFA), polyunsaturated fatty acids (PUFA) and PLASMALOGENS (PLASM) indicated in their dimethylacetal form (DMA). As expected, most abundant fatty acids are palmitic acid (16:0), stearic acid (18:0) and oleic acid (18:1); the latter one is the most abundant one among all FAs

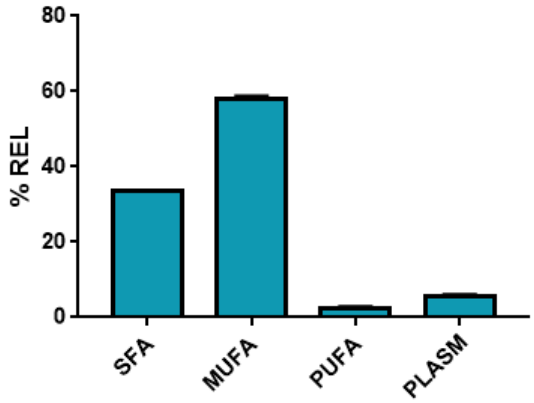

Figure 49 – SFA, MUFA, PUFA and PLASMALOGENS derived from total lipid extract.

Summarizing relative mass of fatty acids we obtain the following %rel: 33,61±0.21 for SFA, 58.11±0.73 for MUFA, 2.39±0.49 for PUFA and 5.59±0.51 for Plasmalogens.

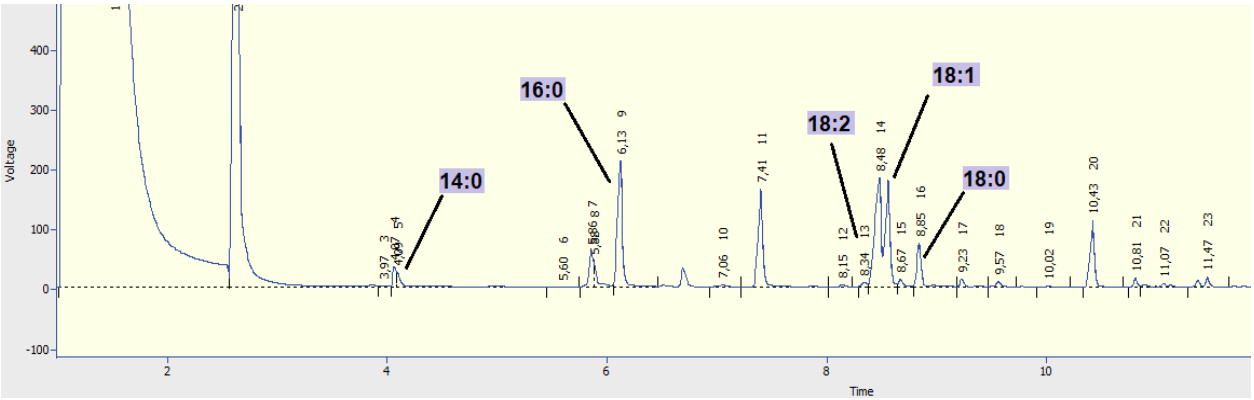

Figure 50 – Example of chromatogram derived from total lipid extract of LM-16 cells.

Cholesteryl esters

We wanted first to assess the behavior of lipid subclassess under serum deprivation (i.e. condition required for EVs isolation from cell culture media).

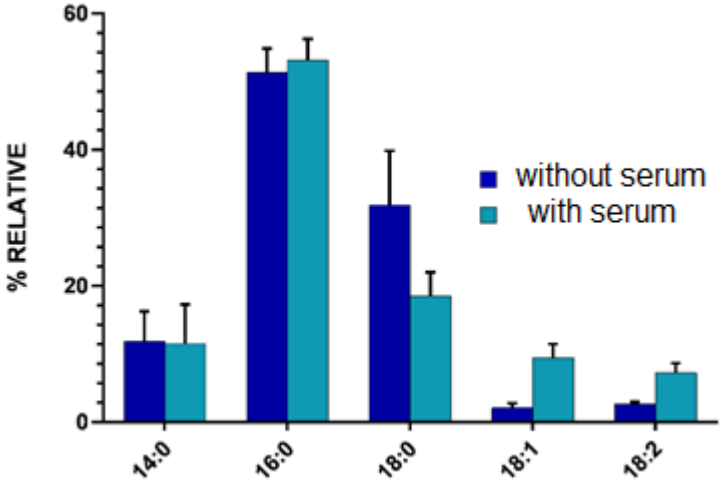

Figure 51 – % rel of fatty acids in CE with or w/o fetal calf serum supplementation.

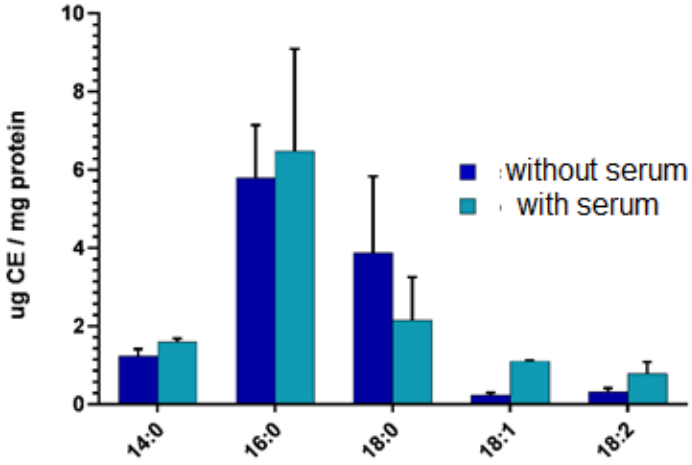

Figure 52 – Mass of fatty acids in CE with and w/o serum.

Most abundant fatty acids in cholesteryl esters are represented by myristic (14:0), palmitic (16:0) and stearic (18:0) acid. There is also a little amount of oleic acid (18:1) and linoleic acid (18:2). We can conclude that there is a general increase in mass for FAs comparing serum treated vs. w/o serum. Total mass of CE w/o serum is 11,1530 ± 0,725 µg/mg protein.

Triglycerides

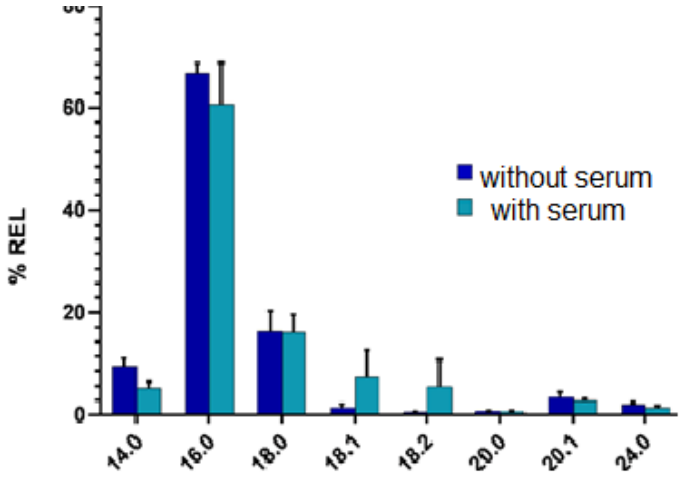

Figure. 53 – % rel of fatty acids derived from triglycerides

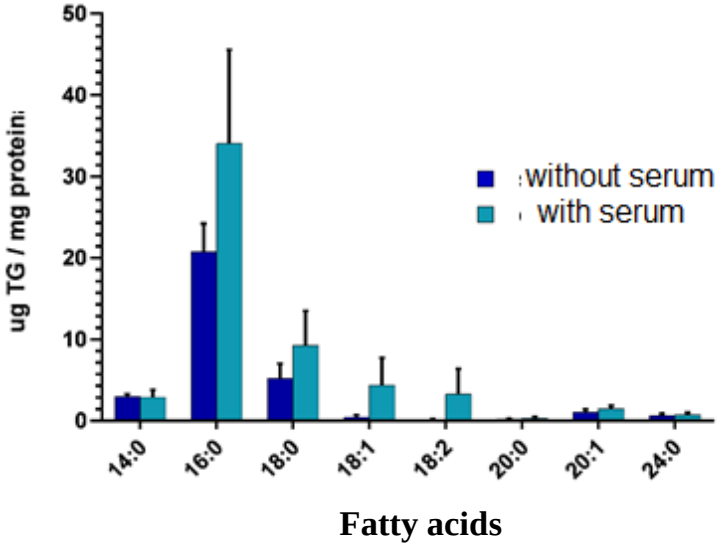

Figure 54 – Mass of fatty acids derived from triglycerides.

Even in this case, most abundant fatty acids are palmitic (16:0) and stearic (18:0). For as concern the serum supplemented cells there is a higher amount of UFA (18:2 and 18:1). In conclusion, there are differences in quali-quantitative analysis of FAs derived from

triglycerides. Generally, as expected, there is an increase of fatty acids in serum supplemented cells compared to not supplemented ones. Summarizing the masses of the different FAs we obtain a total mass of 31,4448 ± 0,829 μg/mg protein for triglycerides.

Free-fatty acids

In this case we reported free fatty acids only in serum free conditions, since preliminary results did not show any difference in this lipid class.

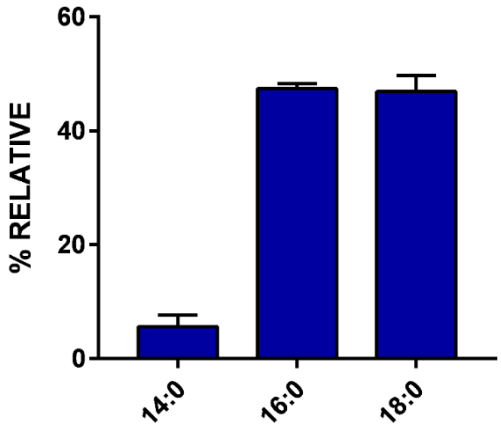

Figure. 55 - %rel of free fatty acids in cells.

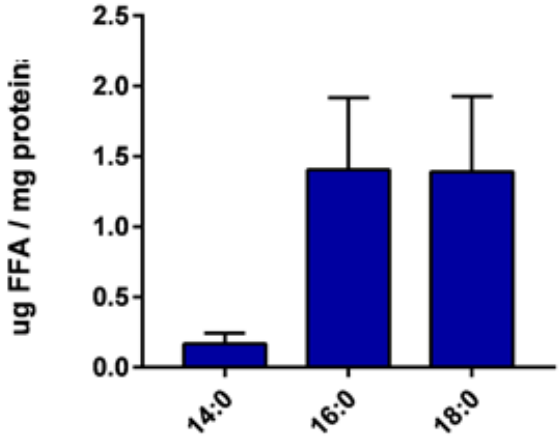

Figure. 56 – Free fatty acids mass in cells.

The mass of free fatty acids in LM-16 cells are 2,9660 ± 0,374 μg/mg protein. As we can see from the graph, they are only composed by saturated fatty acids (14:0 myristic, 16:0 palmitic and 18:0 stearic)

Phospholipids

By utilizing Ames' colorimetric assay, we determined phosphorus total mass of LM-16 cells, 0,2181 ± 0,041 μmoles/mg protein.

Free cholesterol

By GLC analysis we calculated the mass of cholesterol. After addition of a known quantity of stigmasterol as internal standard. Free cholesterol mass in LM-16 cells is 37,203 ± 2,98 μg/mg which corresponds to 0,096± 0,008 μmol/mg protein.

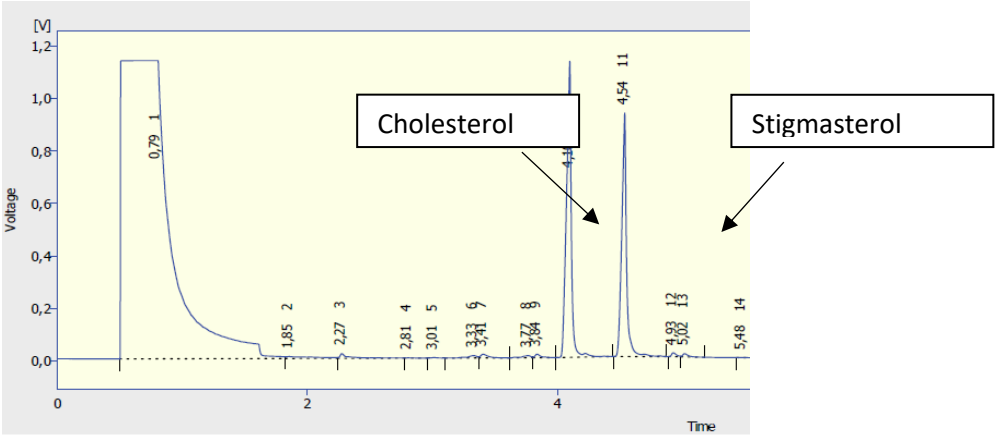

Figure. 57 – Example of chromatogram of the analysis of FC.

Free cholesterol/phospholipid ratio

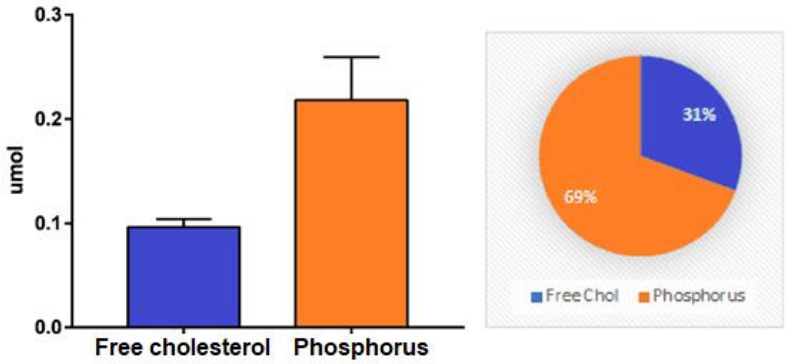

Figure. 58 – Phoshpolipid\choleserol ratio in LM-16 cells.

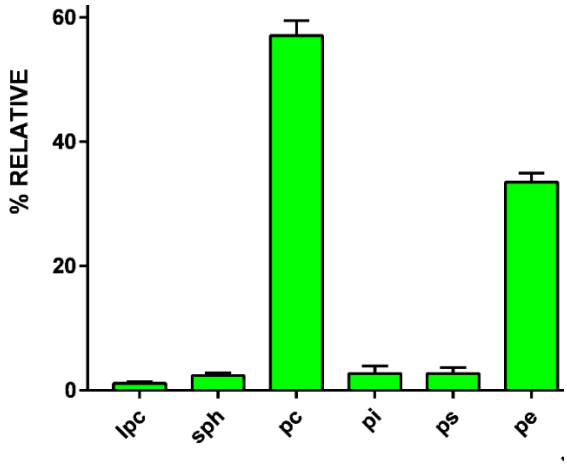

Figure. 59 – Relative % of phospholipid classes in LM-16 cells

LPC=lysophosphatidylcholine SPH=sphingomyelin PC=phosphatidylcholine PI=phosphatidylinositol PS=phosphatidylserine PE=phosphatidylethanolamine.

As is shown by both graphs, phospholipids are the main constituents of LM-16 cells (31 vs 69%, expressed in μmol/mg protein). The ratio is 2,27 ± 0,22 Relative composition of Phospholipid in cells.

After separation of the total extract by Thin Layer Chromatography we were able to analyze the relative content of phospholipids in LM-16 cells. The most abundant ones are phosphpatidylcholine and phoshpatidylethanolamine with a % rel of respectively 57.1% ± 2.4 e 33.5% ± 1.47.

Overview of cellular lipid composition (n=7)

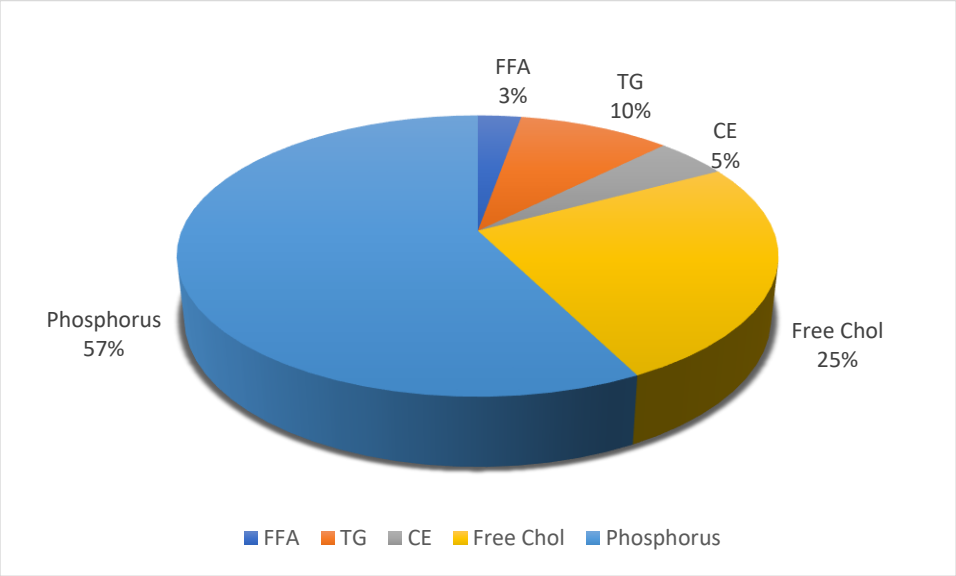

Figure. 60 – Lipid profile of LM-16 cells,57% phospholipids, 25% free chol, 10% triglycerides, 3% free fatty acids, 5% cholesteryl esters.

As expected, free cholesterol and phospholipids are the main component of these cells, followed by triglycerides, cholesteryl esters and free fatty acids.

Fatty acids derived from total lipid extract of the three different cell lines

We also analyzed the fatty acids profile from two further different tumoral cell lines since it could be interesting to compare them with the composition of their secreted EVs. We decided to utilize two further cancer cell lines, MDA-MB231 and PC-3 since the project was related to cancer-derived EVs. These extracts contain all fatty acids derived from all categories of cell lipids, as previously shown for LM-16 cells (e.g. fatty acids derived from phospholipids, triglycerides, cholesteryl esters and others).

Analyses have been performed after 3 days of starvation with medium without serum for LM 16 and MDA-MB231 and 1day starvation for PC-3 cells (since they did not survive in 3 days serum free conditions) in order to utilize the same conditions utilized for EVs collection.

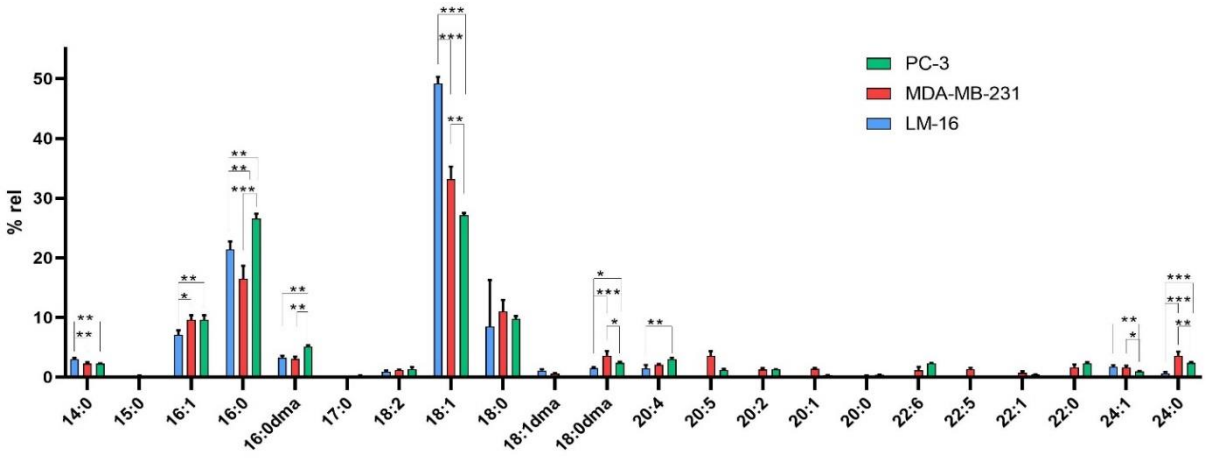

Figure 61 – Comparison of fatty acids and alcohols derived from total lipid extracts. As expected, the three different cell lines possess different lipid profiles.

The graph clearly shows that most of the fatty acids contained into the three cells range from 14 to 24 atoms of carbons, with a wide range of saturated fatty acids (SFA), unsaturated (UFA), polyunsaturated (PUFA) and fatty alcohols, derived from plasmalogens in their dimethylacetal form (DMA). Most abundant fatty acids are palmitic acid (16:0) stearic acid (18.0) and their unsaturated counterparts, respectively palmitoleic (16.1) and oleic acid (18:1), even if in different %rel for each cell. Differences in this composition are expected due to different roles and source of these cell lines. Other fatty acids which are notable to mention are myristic one (14:0) and arachidonic (20:4). The graph shows also a different %rel of the fatty alcohols derived from plasmalogens.

Categorizing fatty acids in SFA, MUFA, PUFA and DMA we are able to see a different grade of saturation among the three different cell lines.

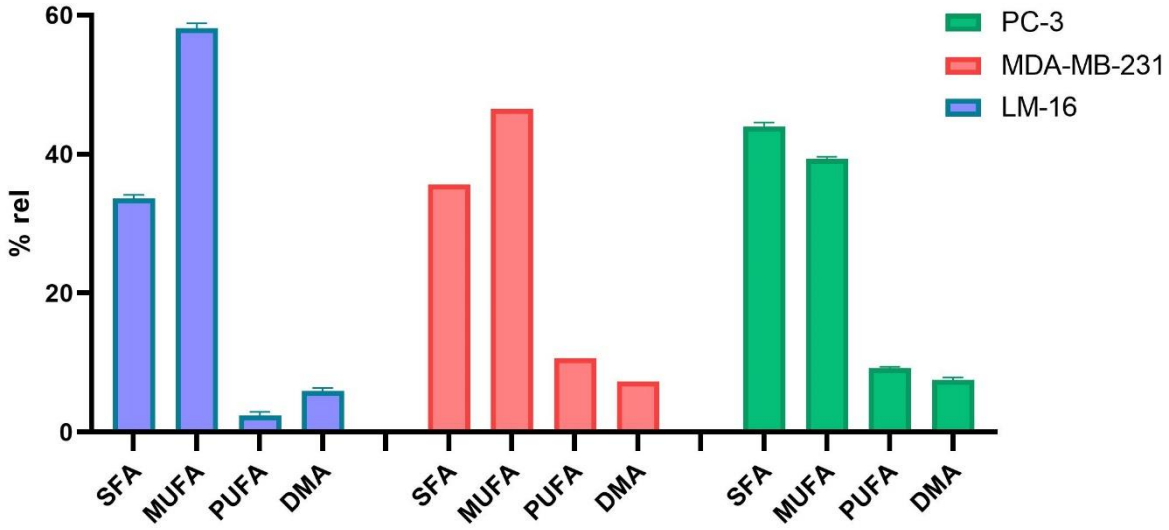

Figure 62 - SFA, MUFA PUFA and DMA (plasmalogens) comparison among 3 different cell lines.

We can conclude that each cell line possesses its unique lipid profile: LM-16 and MDA-MB-231 are indeed mainly enriched in MUFA while PC-3 are enriched in SFA. Interestingly MDA-MB-231 and PC-3 cell line contain three-times more PUFA compared to LM-16 while plasmalogens are almost the same in the three different cell lines.

Determination of the more affordable and appropriate method to isolate different extracellular vesicles subpopulations

In the first part of my PhD project we aimed to set the most appropriate conditions to isolate different EVs populations based on their size, according to their dimensional classification. For this reason we tried different approaches. First we isolated particles following Thery's protocol by filtration followed by ultracentrifugation [18] in LM-16 cells.

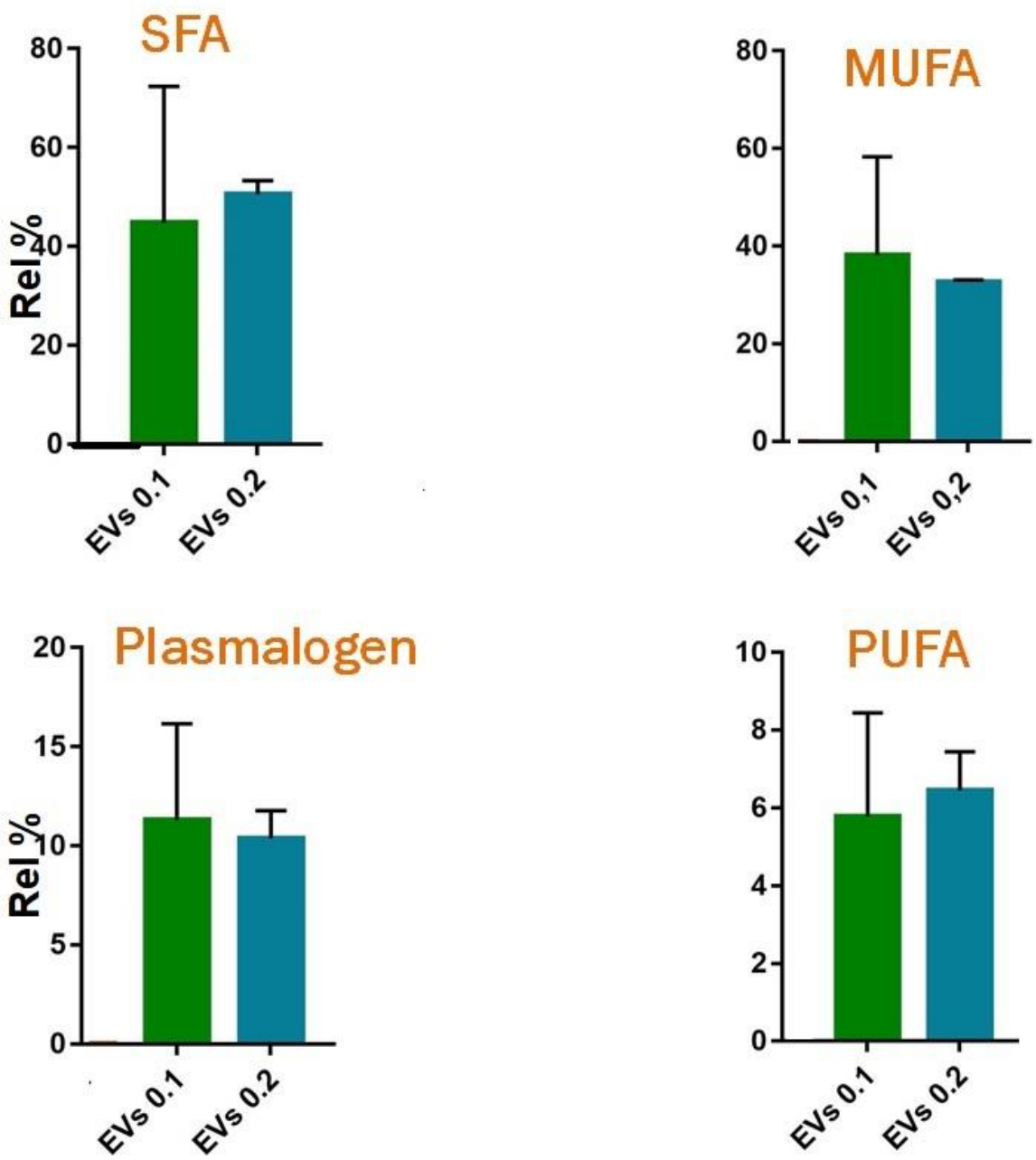

Figure 63 - %rel of in SFA, MUFA, PUFA and plasmalogen of filtered EVs derived from LM-16 cell line.

Two types of filtrations were utilized:

- 0.1um Polyvinylidene fluoride (PVDF) filter;
- 0.2 um (Polyethersulfone) PES filter.

Applying this protocol, we obtained for 0.1 um filtered particles a huge standard deviation. Probably this problem was due to the fact that we utilized 0.2 um PES filters and PVDF 0.1 um filters; indeed, based on the experience of our lab we already knew that filters membrane

material can interact differently with lipids (e.g. major component of Extracellular Vesicles), so, we would have added another confounding factor, maybe selecting a population with a certain lipid profile rather than another. For all these reasons we decided to avoid the use of filtration for EVs isolation.

A journey into centrifuges; size-based isolation of different populations of EVs through differential ultracentrifugation with a lipid-based development approach

The development of this protocol started when we realized that MISEV guidelines [7] proposed a size based classification in small EVs" (sEVs) (< 100nm or < 200nm) and "medium/large EVs" (m/lEVs), (> 200nm), while Thery's classical method of isolation let us to obtain a mixture of all these different populations.

Cell media contain a mixture of particles that differ in size, densities and sedimentation rates; for EVs isolation the most used method is differential ultracentrifugation, in which the supernatant is centrifuged by several subsequent steps. The main limitation is represented by the co-isolation of small particles when isolating large particles leading to significant contamination problems [68].

In 2015 Livshits et al., [68] performed a theoretical analysis of differential centrifugation focusing on forces, time and all parameters that influence the precipitation of particles in suspension.

$$v = g_{eff}\frac{d^2}{18\eta}(\rho - \rho_{solv}) \qquad g_{eff} = \omega^2 R$$

Figure 64 - Equation of the velocity of a particle within the centrifugation tube, as determined by the balance of centrifugal force, Archimedes floatation and Stokes viscous drag force.

In order to build our isolation protocol we utilized the online tool developed by the aforementioned group available at http://vesicles.niifhm.ru/.

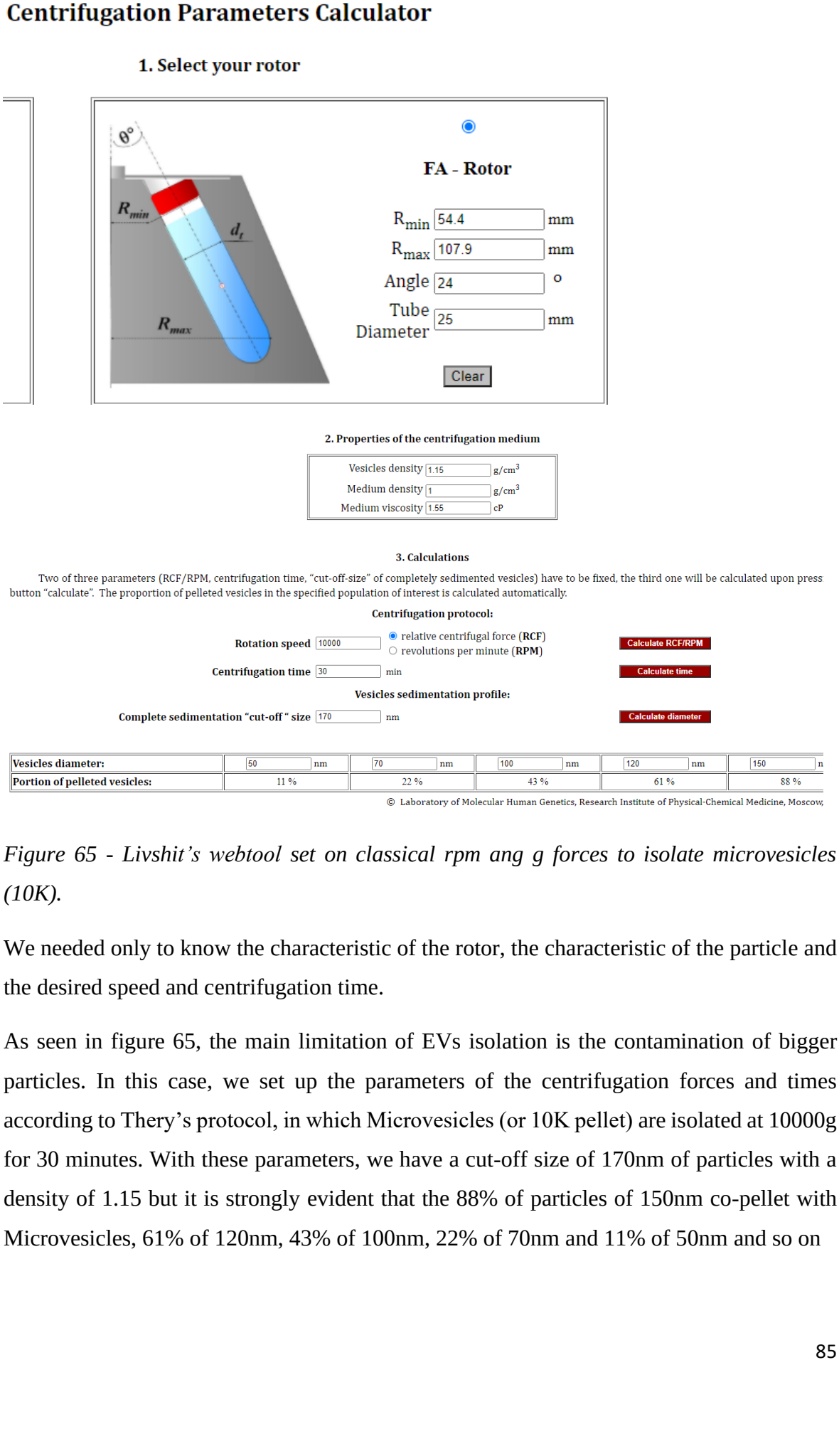

Figure 65 - Livshit's webtool set on classical rpm ang g forces to isolate microvesicles (10K).

We needed only to know the characteristic of the rotor, the characteristic of the particle and the desired speed and centrifugation time.

As seen in figure 65, the main limitation of EVs isolation is the contamination of bigger particles. In this case, we set up the parameters of the centrifugation forces and times according to Thery's protocol, in which Microvesicles (or 10K pellet) are isolated at 10000g for 30 minutes. With these parameters, we have a cut-off size of 170nm of particles with a density of 1.15 but it is strongly evident that the 88% of particles of 150nm co-pellet with Microvesicles, 61% of 120nm, 43% of 100nm, 22% of 70nm and 11% of 50nm and so on

First attempt

In order to achieve a better separation of different population of EVs we developed our protocol, trying different set-ups to obtain the best possible separation.

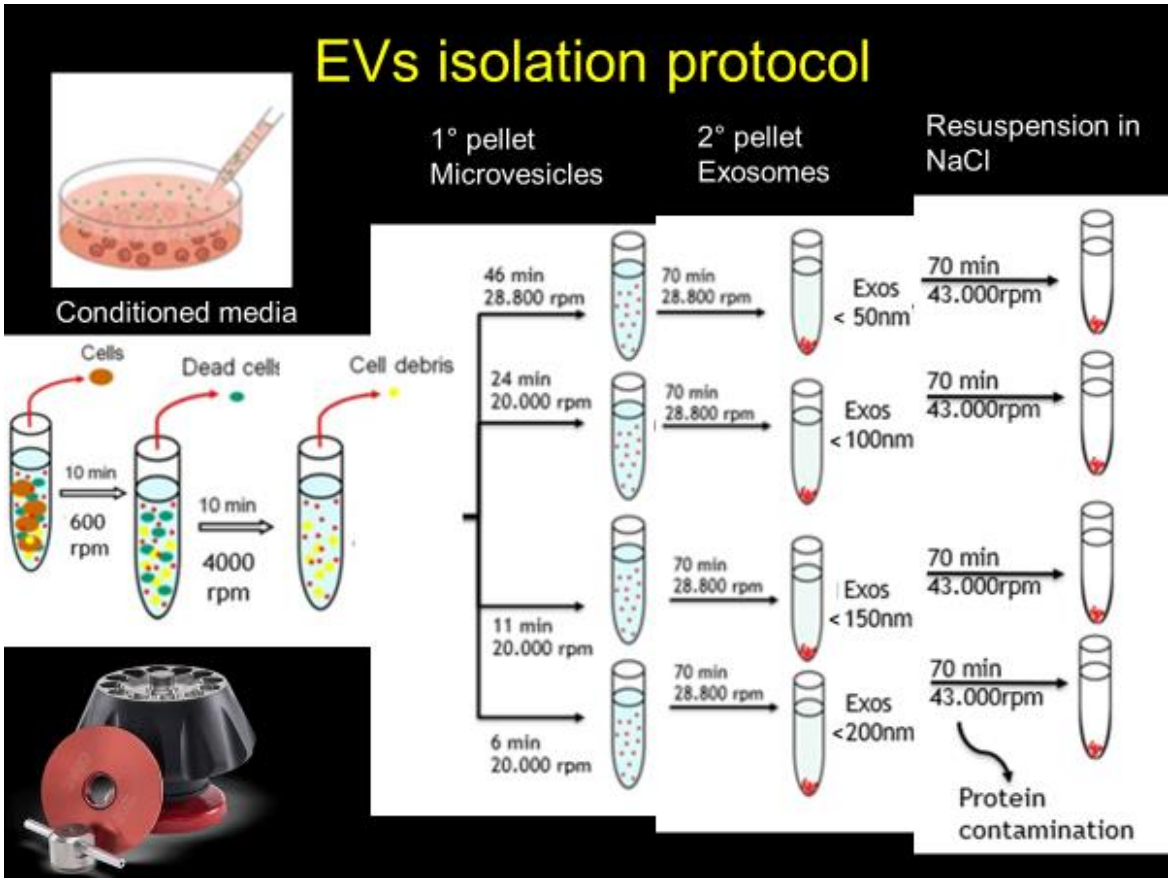

Figure 66 – Schematic representation of the first protocol that we developed. We utilized common set up to isolate cells, dead cells and cell debris, and changed g forces and time of centrifugation in order to obtain our desired cut-off.

As reported in figure 66, these conditions have been utilized for our first EVs "differential isolation". We performed subsequent centrifugation in order to obtain 8 different pellets, which theoretically contain respectively: <50nm, <100nm, <150nm, <200nm (for Exosome portion) and >50nm, >100nm, >150nm, >200nm (for Microvesicles portion). We then analyzed fatty acid content of the pellets through GLC analysis.

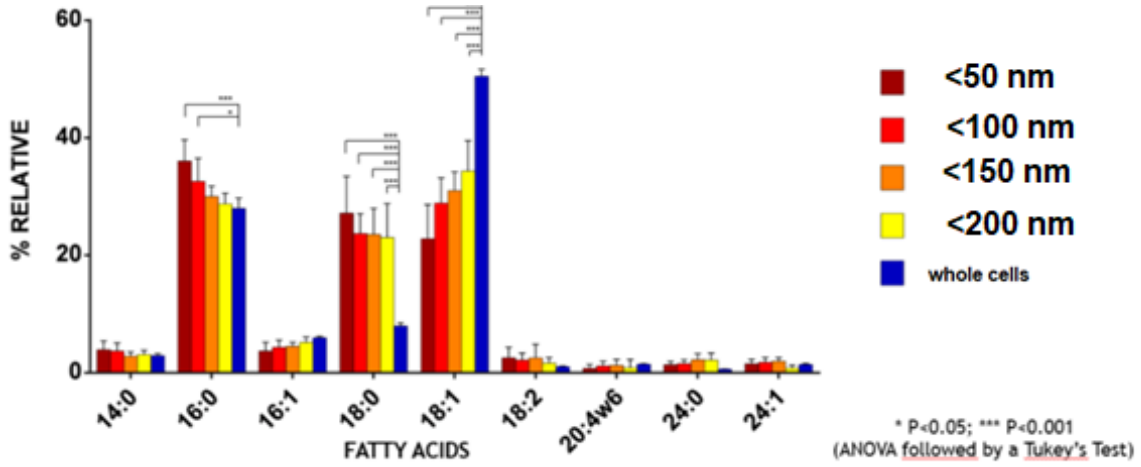

Figure 67 - Ffatty acid profile of LM-16 derived fractions and cells, (mean of 11 experiments).

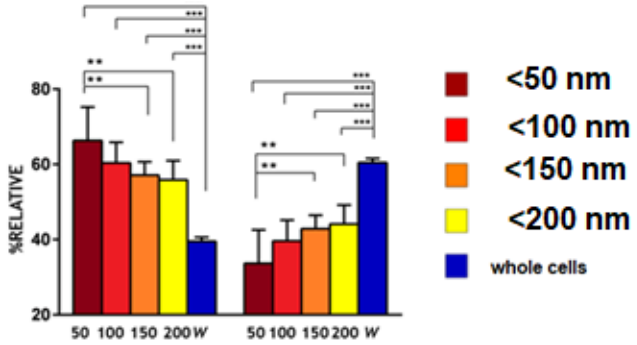

Figure 68 - Profile of SFA and UFA in whole cells and fractions.

EVs contain a broad range of important saturated fatty acids as myristic (14:0), palmitic (16:0), stearic (18:0(and lignoceric (24:0). Moreover graphs clearly show that the increase of saturated fatty acid is paralleled by the decrease of their theoretical dimensions and by the decrease in UFA.

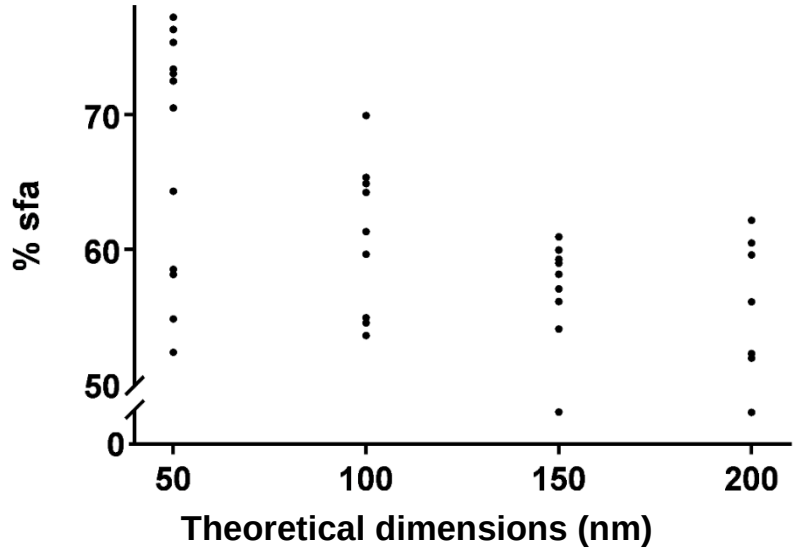

Figure. 69 – Dispersion graph of fatty acids enrichment related to theoretical variation of vesicles size (n=11).

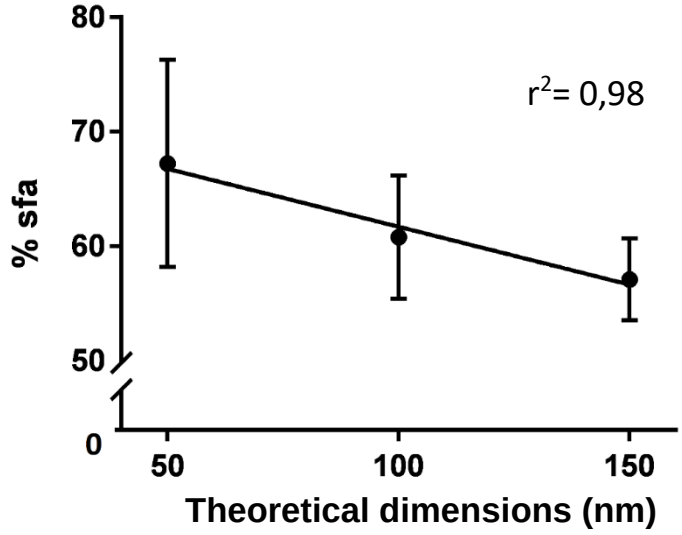

Figure. 70 – Linear correlation between the increase of dimensions and decrease of % rel of saturated fatty acids in the dimensional interval of small EVs (50-150nm) n=11.

As seen in the graphs, we can establish a linear relation between dimensional increase counterbalanced by decrease in SFA. (r^2=0,98).

Second attempt

At this point, we aimed to further optimize the isolation method, since we realized that each portion contains smaller, or bigger particles.

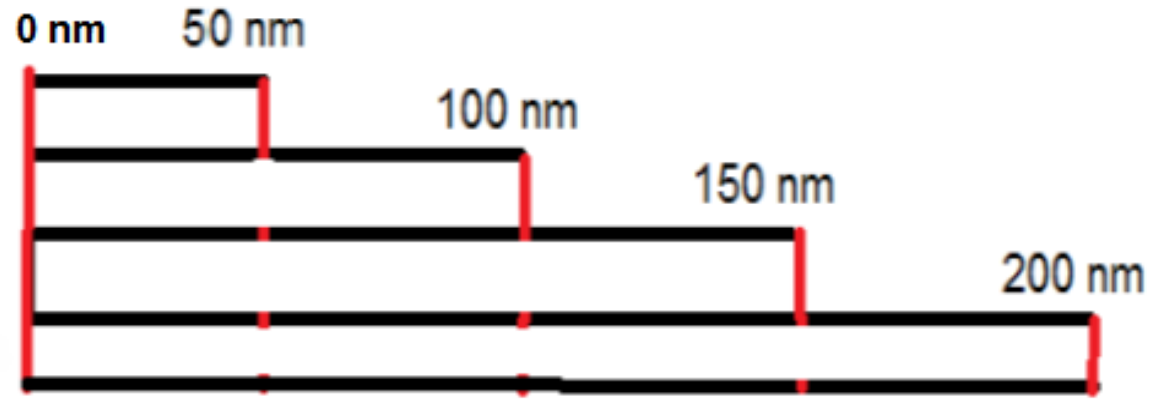

Figure 71 – schematic representation of the particles isolated during our "first attempt".

Indeed as shown in the figure above,<100nm portion still contains the 50, <150 contains the 100 and the 100 and so on. For these reasons, in order to obtain the most possible "clean" samples we decided to develop a "sequential and differential ultracentrifugation". We set up the parameters to obtain 5 different fractions.

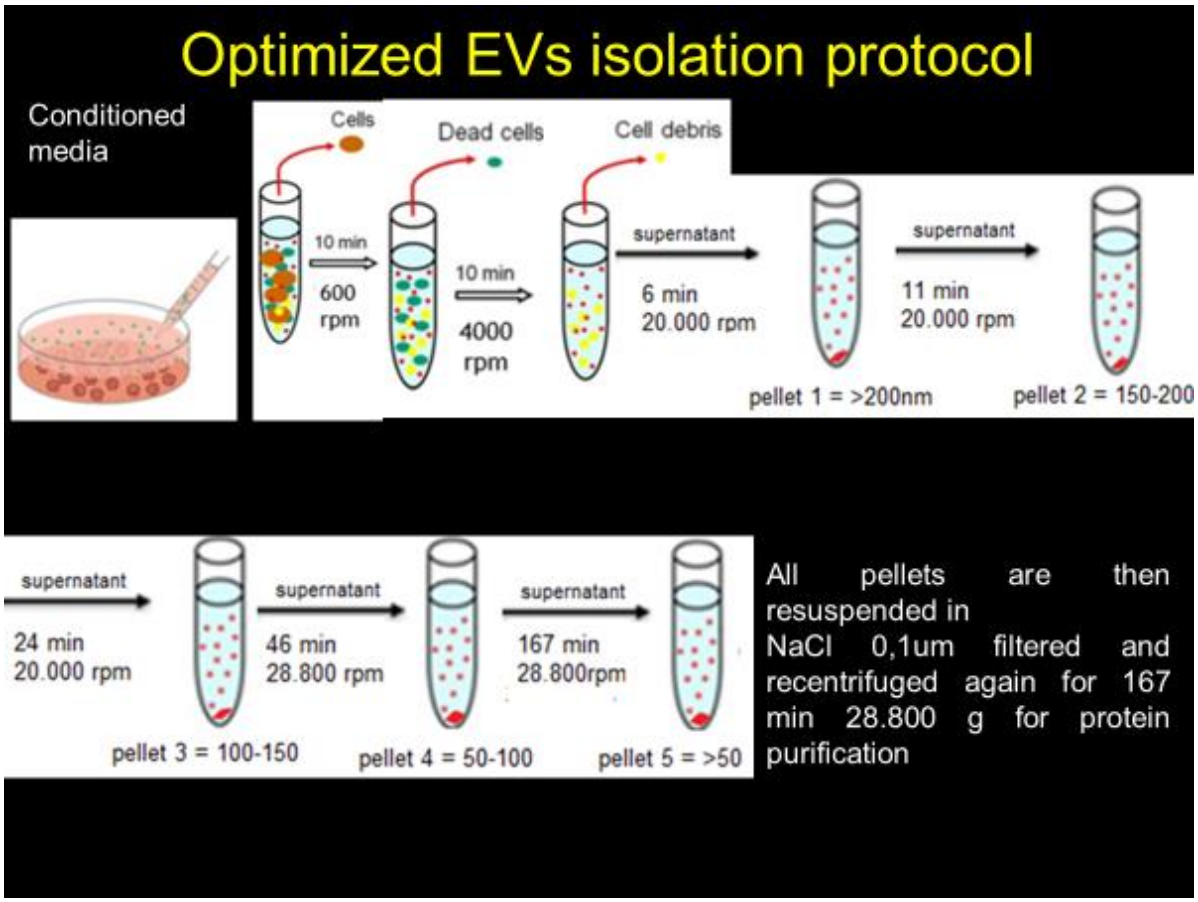

Figure 72 – Subsequent centrifugation protocol developed for our second attempt.

With this protocol, we centrifuged the supernatant 5 different times, after removing cell debris and dead cells; each time we collected the 5 different pellets which contain the theoretical expected portion of >200nm, 150-200nm, 100-150nm, 50-100nm, >50nm. We decided to utilize these cut-offs according to MISEV guidelines.

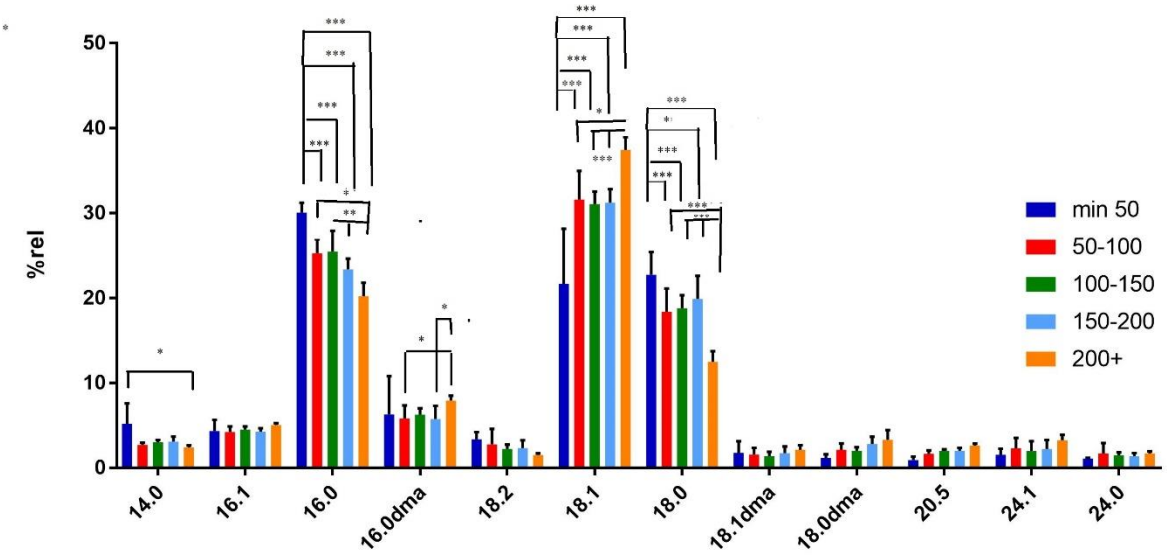

*Figure 73 - Fatty acids and alcohols derived from total lipid extracts of the 5 EVs fractions isolated from LM-16 cells *= p < 0,05, ** p < 0,01 *** p < 0,001.*

We then analyzed the fatty acids profiles derived from total lipid extracts of each fraction and as shown in figure 73 we found several significant differences among the different fatty acids (n=5).

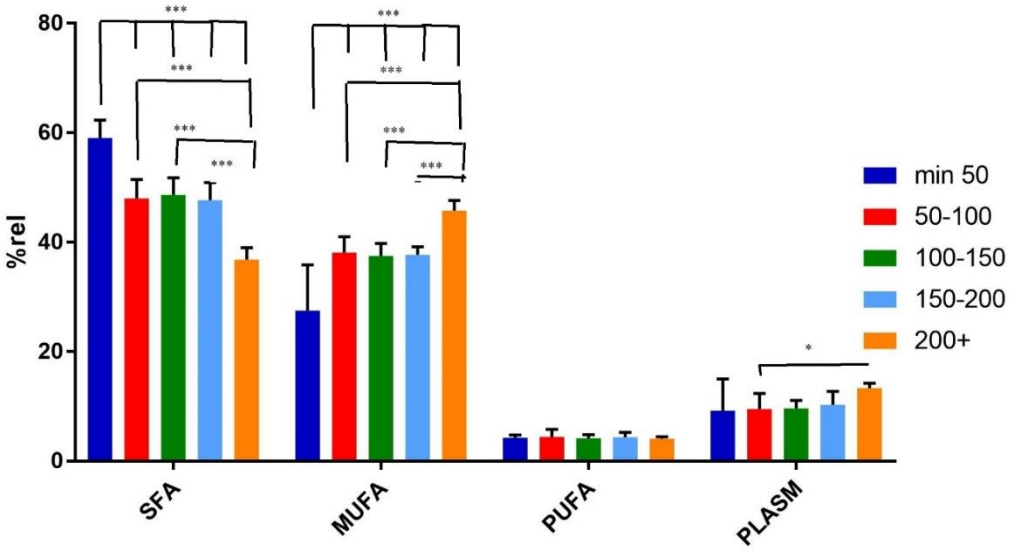

*Figure 74 - Fatty acid profile categorized for their grade of insaturation of the 5 fractions *= p < 0,05, ** p < 0,01, *** p < 0,001.*

With these experimental conditions we were not able to detect differences among 50-100, 100-150 and 150-200 fractions.

We then analyzed cholesterol/phospholipids content.

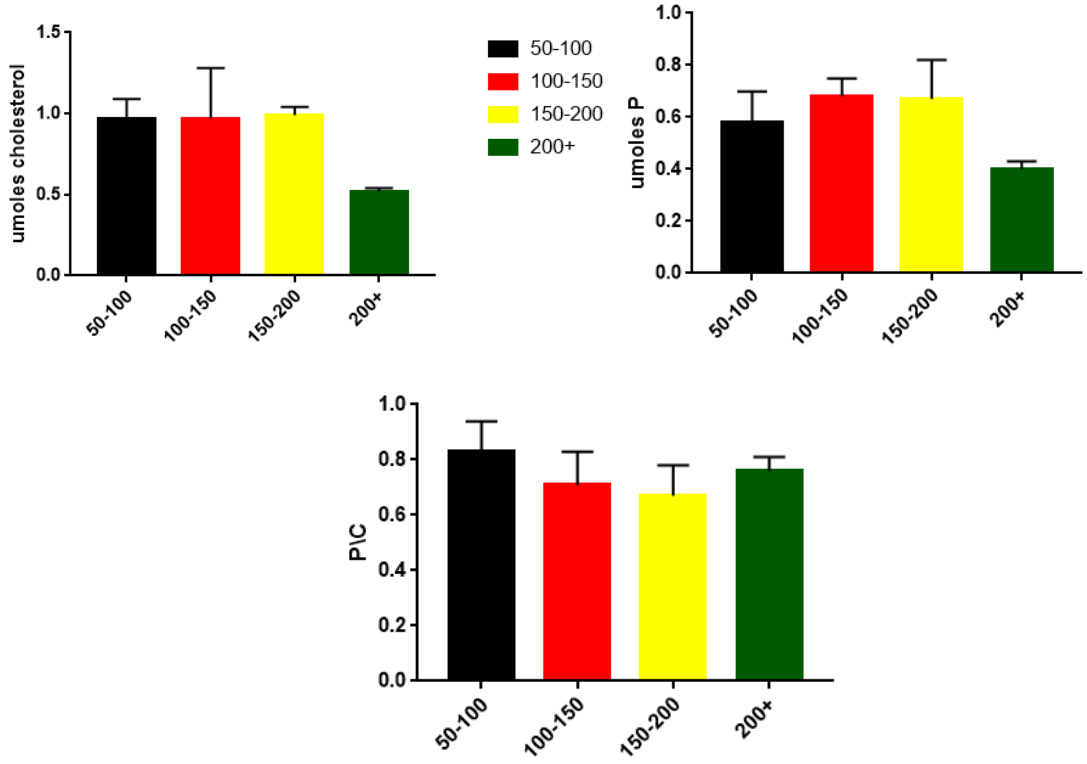

Figure 75 – umoles of cholesterol, umoles of phosphorus and their ratio obtained in the different 5 EVs fractions.

We reported similar amount of both cholesterol and phospholipids. Unfortunately we did not have data regarding min than 50, due to sample paucity.

For these reasons we decided to further improve our separation protocol following Zhang's observations [19].

Third attempt

We set up the parameters in Livshits' tool to obtain min 50, 50-80, 80-120, 120-200 and 200+ theoretical EVs diameters.

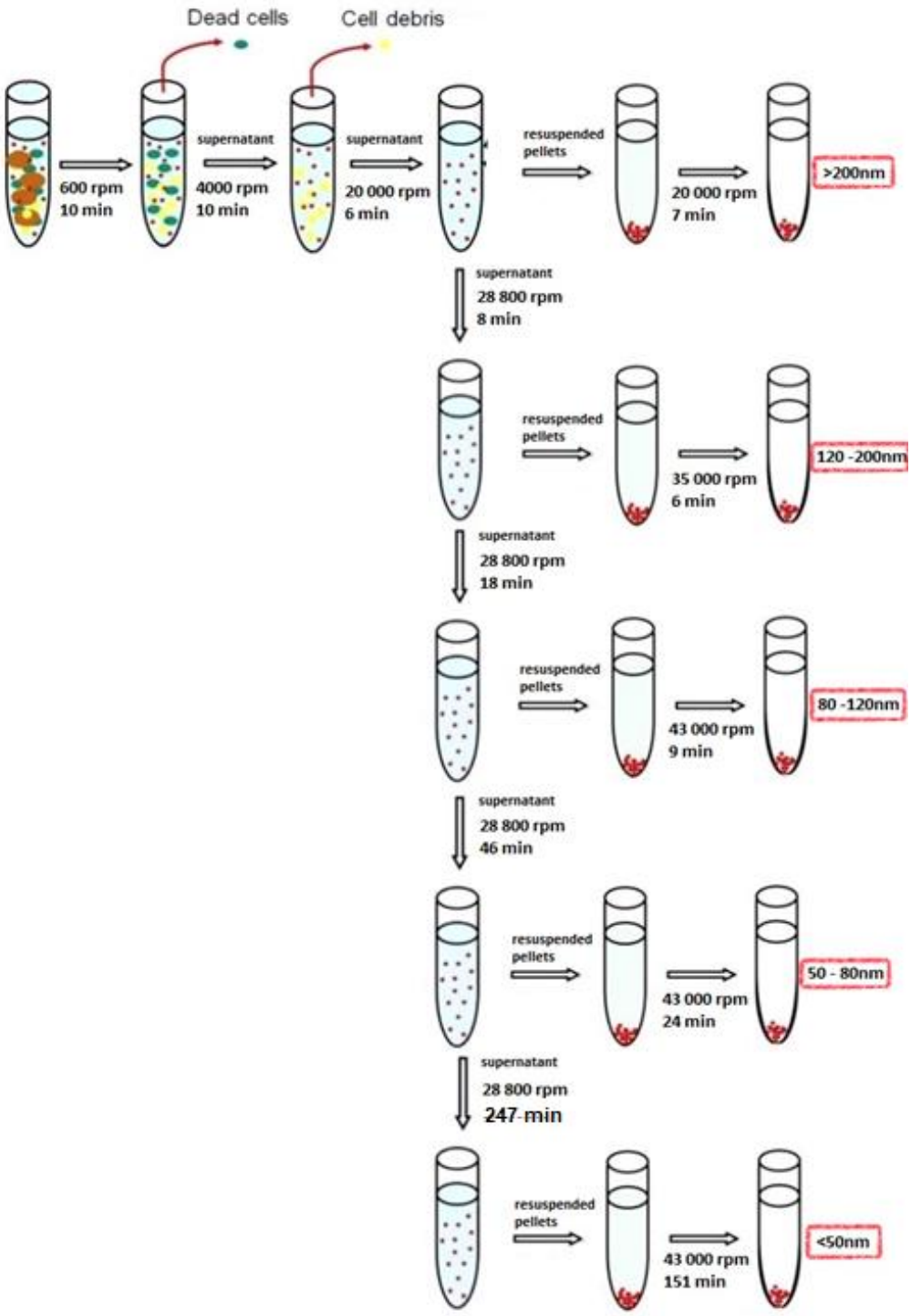

Figure 76 – Scheme of our isolation protocol developed utilizing Cut-offs as suggested by Zhang's observations.

In detail we performed the first centrifugation steps following classical protocol to remove dead cells and cell debris; after those passages we centrifuged supernatant following g forces

and time in the aforementioned figure with 50.2ti rotor; each pellet has been resuspended in NaCl 0.1um filtered and centrifuged again for wash step in TLA 100.3 rotor. After the isolation of different EVs population according to Zhang, we analyzed fatty acid profile again.

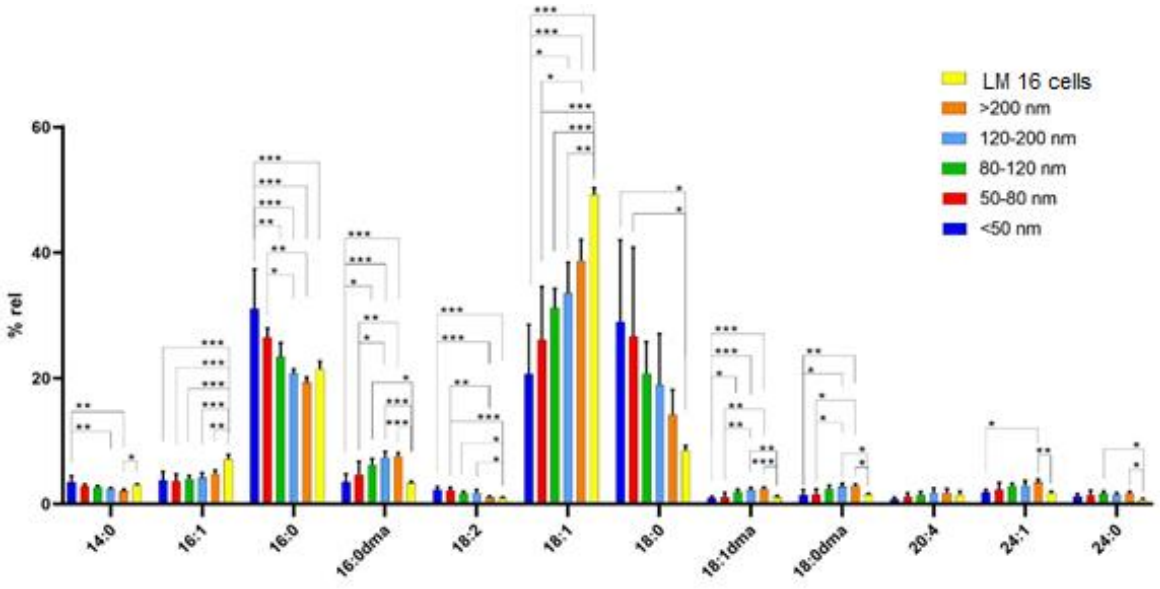

Figure 77 - Fatty acid profile of LM16 cell derived vesicles with Zhang's cutoffs ∗= p < 0,05, ∗∗ p < 0,01, ∗∗∗ p < 0,001.

We were able to find again several differences among the different fatty acids; if compared with the previous analysis we clearly see an improvement among the differences of the most abundant and important fatty acids as for example palmitic acid 16:0, stearic acid 18:0, and oleic acid 18:1.

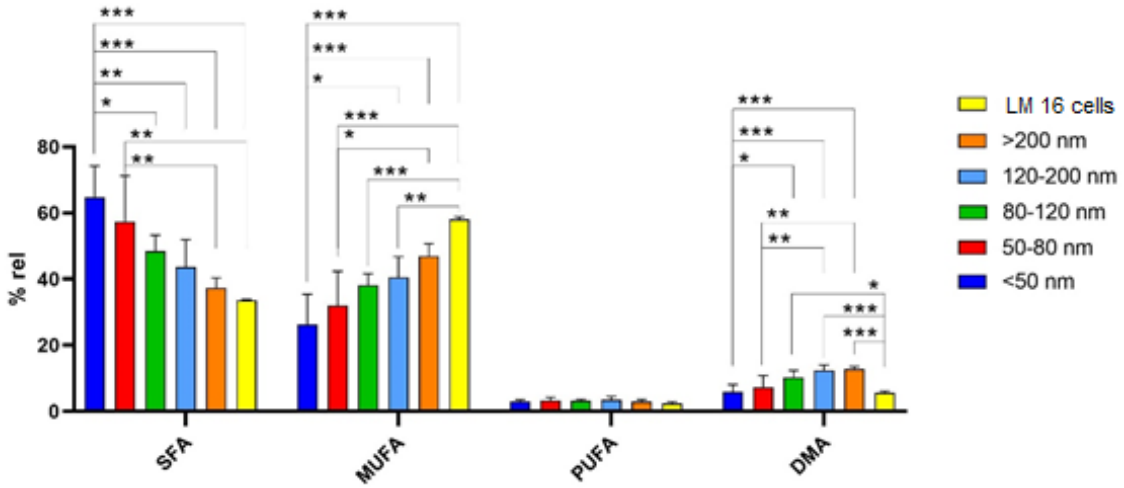

Figure 78 - FA categorized for their grade of insaturation ∗= p < 0,05, ∗∗ p < 0,01, ∗∗∗ p < 0,001.

		min 50			50-80			80-120	
SFA		64.79	9.47		57.41	13.83		48.38	4.93
MUFA		26.3	9.1		32	10.34		38.08	3.52
PUFA		3.03	0.5		3.27	0.97		3.16	0.49
PLASM		5.88	2.24		7.32	3.54		10.3	2.08
		120-200			**200+**			**LM-16 cell**	
SFA		43.62	8.31		37.36	3.02		33.61	0.21
MUFA		40.56	6.2		46.92	3.8		58.11	0.73
PUFA		3.46	1.01		2.88	0.66		2.39	0.49
PLASM		12.35	1.65		12.84	0.72		5.59	0.51

Table 8 - % rel and standard deviations of fatty acids according to their grade of insaturation in 5 different fractions and parental cells (n=5).

Differences were even more evident summarizing fatty acids according to their grade of insaturation; we have indeed several significant differences among the 5 fractions isolated according to Zhang's observation even more if compared with the previous cut-offs. For all these reasons that we choose to continue with these cut-offs to perform further analysis (dimensional analysis and proteomics).

We further analyzed lipid content (cholesterol and phospholipids).

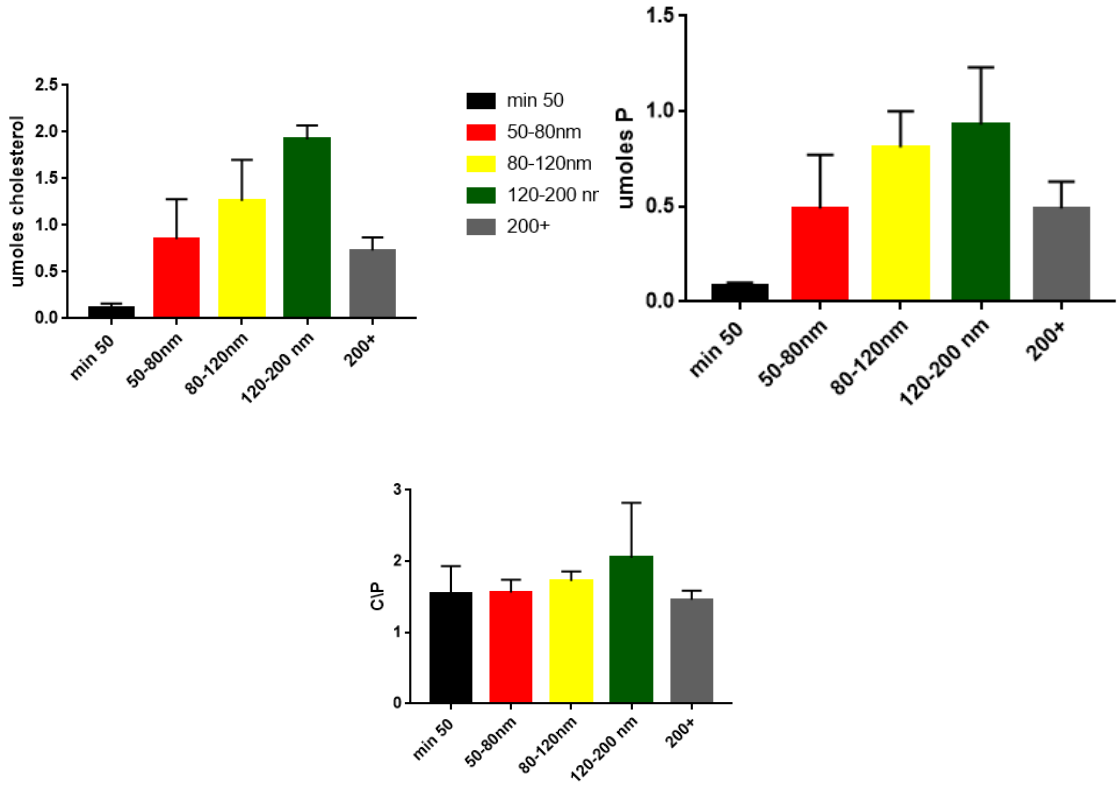

Figure 79 - Micromoles of phosphorus, cholesterol and their ratios.

It is clearly shown in figure 79 that there are differences in terms both cholesterol and phosphorus content among the different fractions. Interestingly, it seems that there are no several differences in term of cholesterol\phospholipids ratios.

Are fatty acids a distinctive EVs signature for each cell line?

In order to further demonstrate if Saturated Fatty Acid enrichment in smaller EVs could be a common feature, we performed the same isolation protocol on EVs derived from two other tumoral cell lines: Prostate Carcinoma 3 (PC-3) and Breast Cancer Adenocarcinoma cells (MDA-MB231).

As before, we analyzed the % rel of fatty acids derived from total lipid extracts of the 5 fractions and those from parental cells and we compared them.

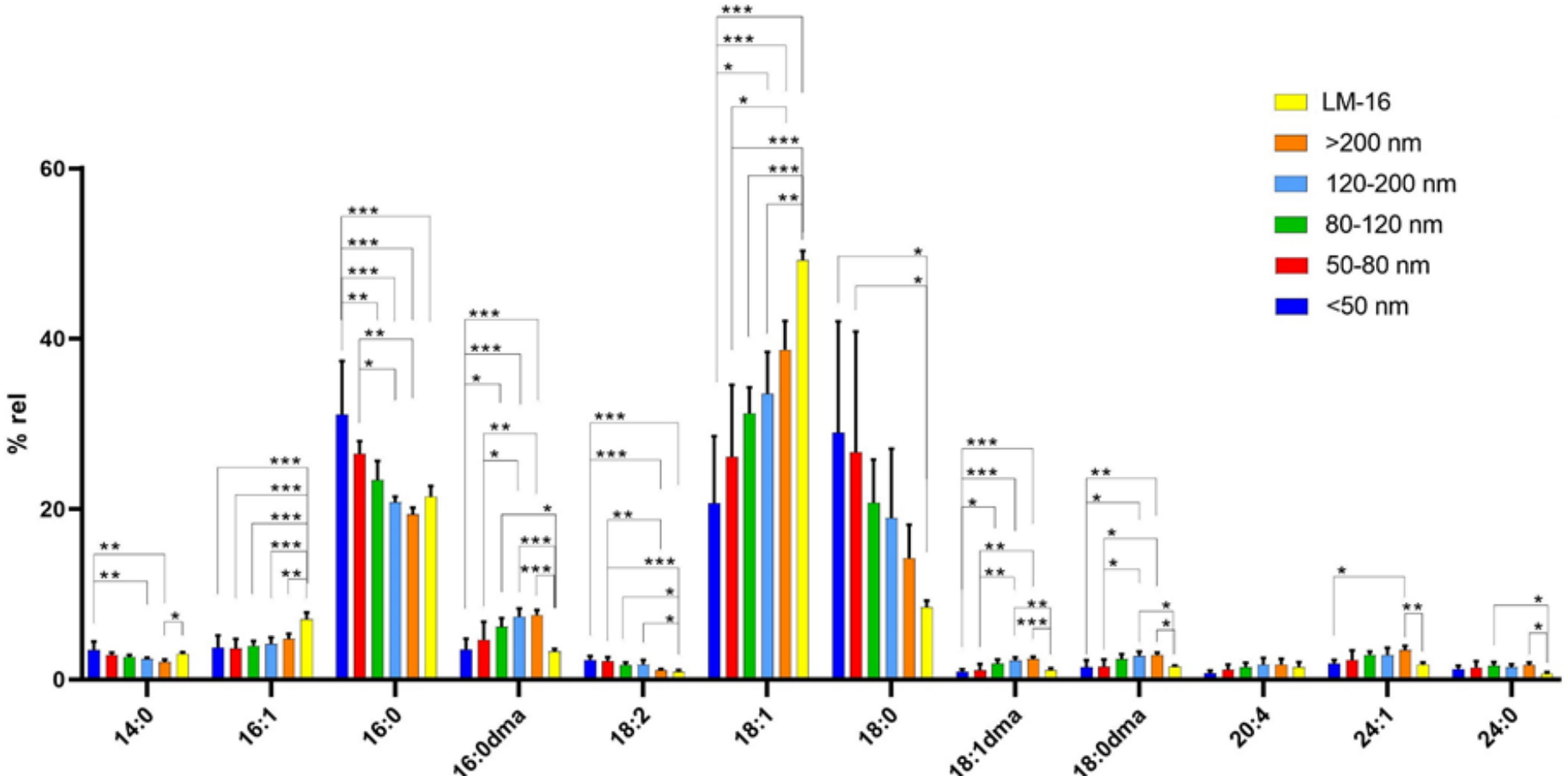

Figure 80 - % rel of fatty acids and alcohols of LM-16 cells and derived EVs subpopulations.

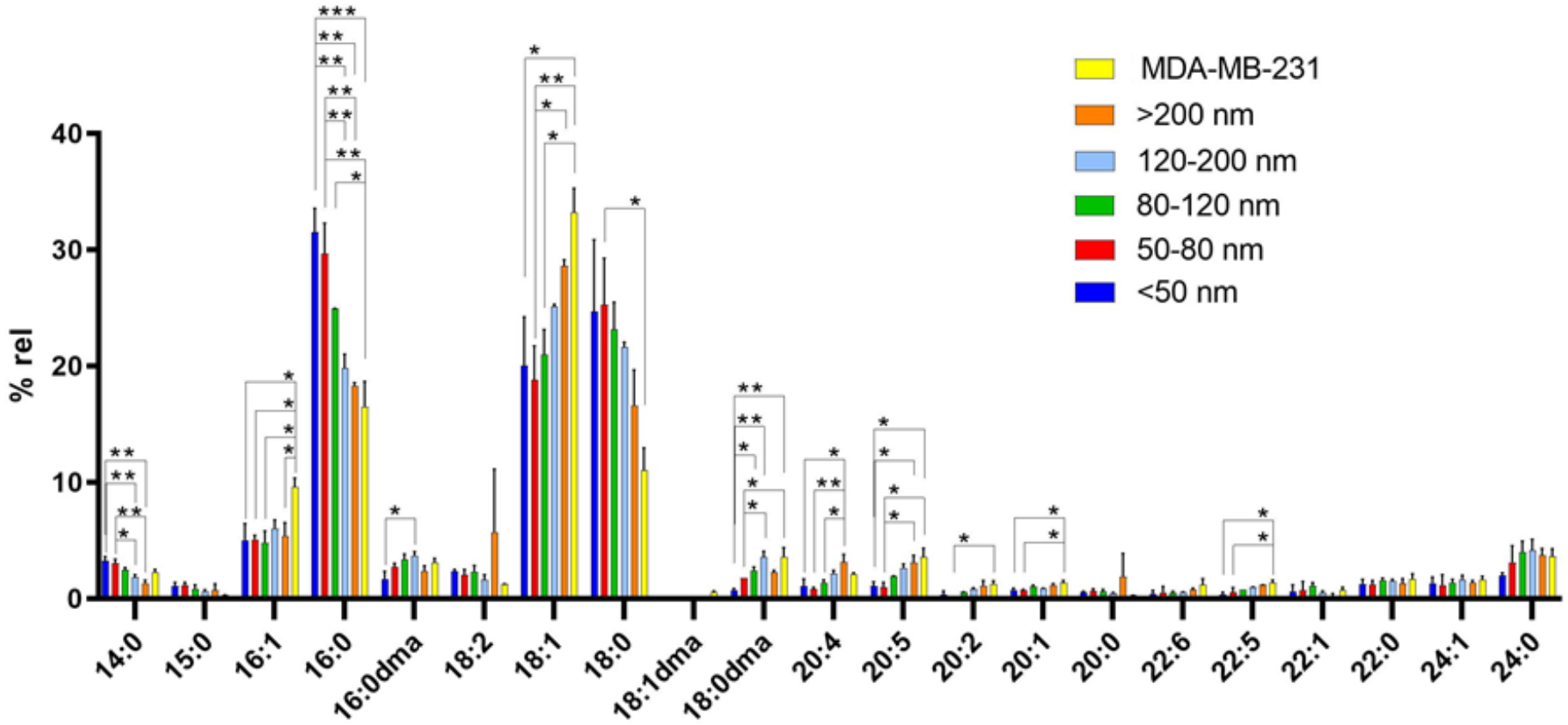

Figure 81 - % rel of fatty acids and alcohols of MDA MB 231 cells and derived EVs subpopulations.

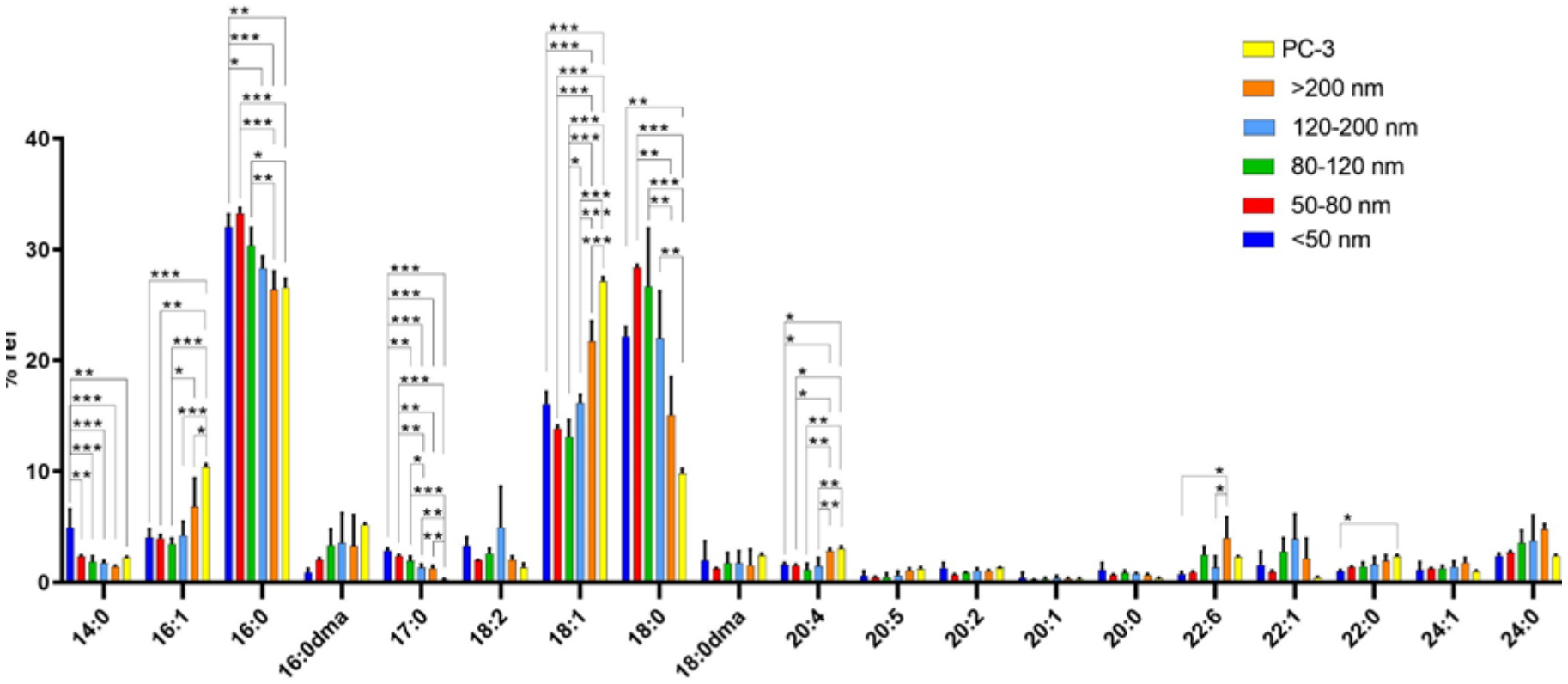

Figure 82 - % rel of fatty acids and alcohols of PC3 cells and derived EVs subpopulations.

All cells are characterized by a broad range of fatty acids from 14:0 (myristic acid) to 24:0 (lignoceric acid) The most abundant fatty acids in all EVs fractions secreted by the three different cell lines are palmitic (16:0) and stearic (18:0).

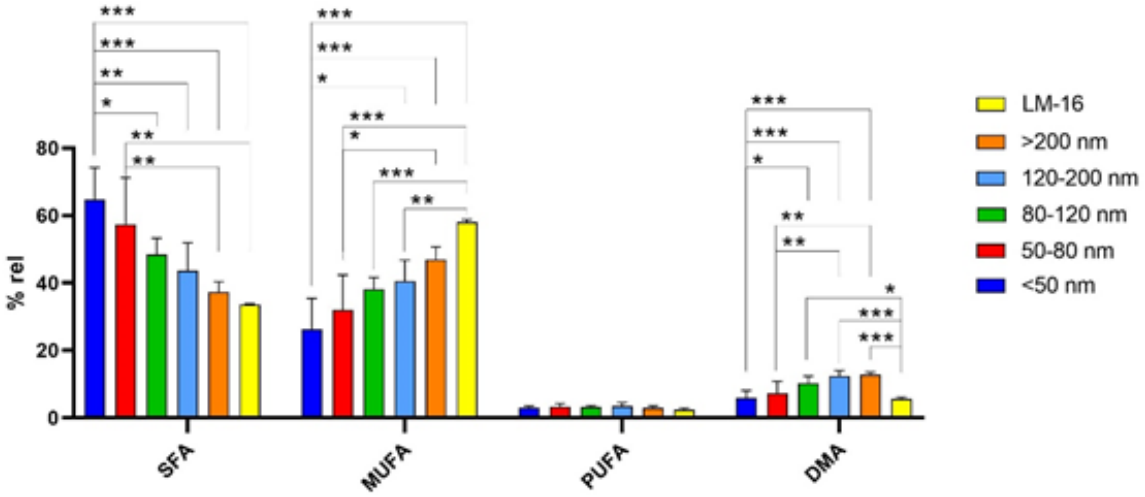

*Figure 83 – Saturated, monounsaturated, polyunsaturated and dimethylacetal (Plasmalogens) fatty acids and alcohols in LM-16 cells * = p < 0,05, ** p < 0,01, *** p < 0,001.*

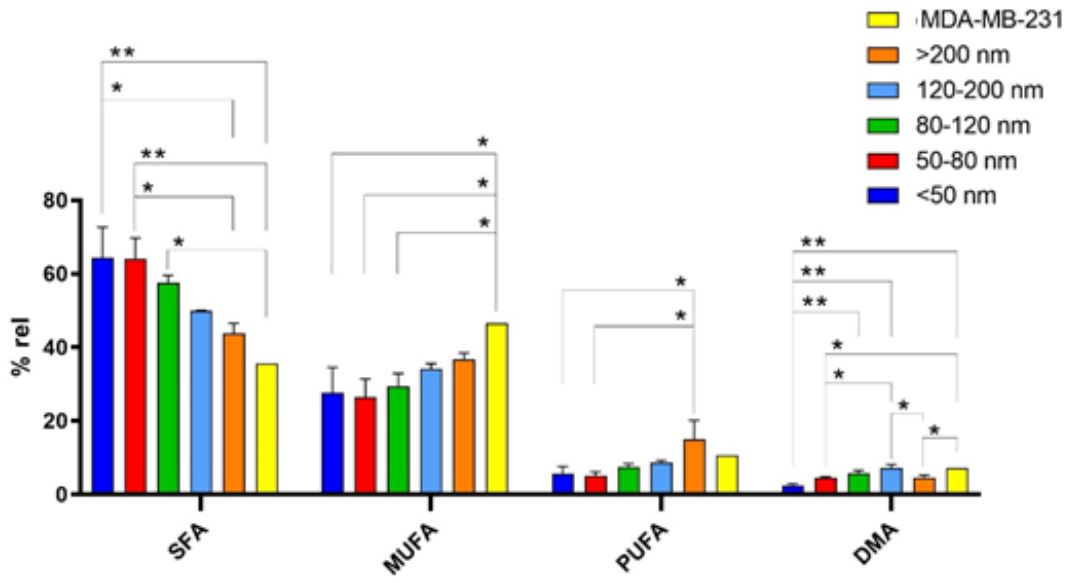

*Figure 84 – Saturated, monounsaturated, polyunsaturated and dimethylacetal (Plasmalogens) fatty acids and alcohols in MDA-MB231 cells * = p < 0,05, ** p < 0,01, *** p < 0,001.*

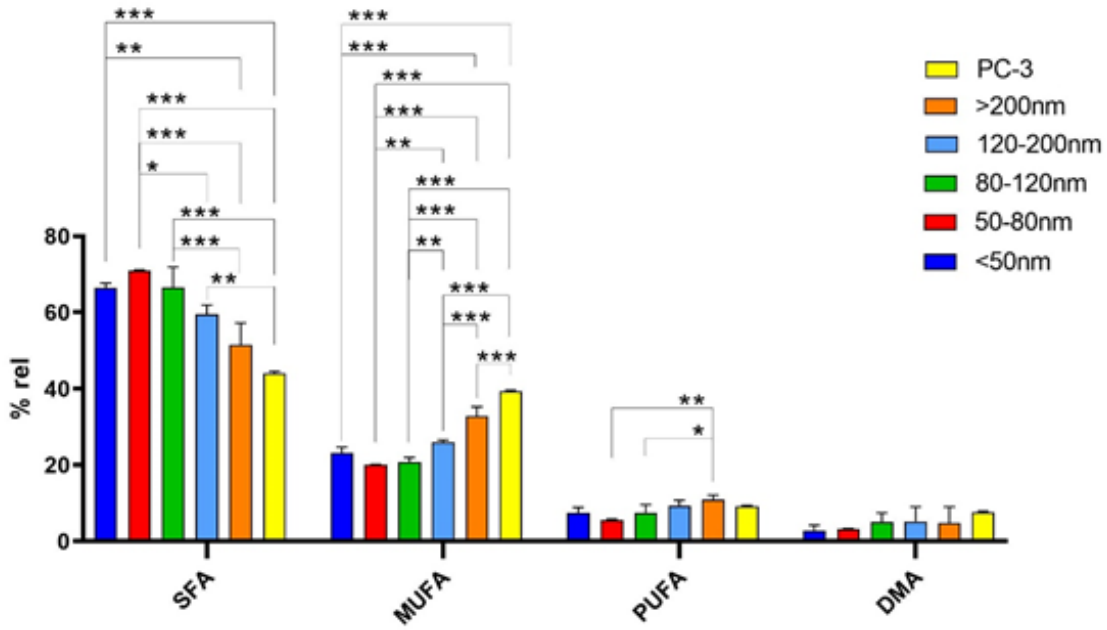

*Figure 85 – Saturated, monounsaturated, polyunsaturated and dimethylacetal (Plasmalogens) fatty acids and alcohols in PC-3 cells * = $p < 0,05$, ** $p < 0,01$ *** $p < 0,001$.*

Figures 83, 84 and 85 clearly show that the relative percentage of saturated fatty acids increases with theoretical size decrease; the trend is balanced by an opposite profile concerning unsaturated fatty acids. This behavior is common to all fractions of all three different cell lines, together with the similarity of biggest theoretical fraction with FA composition of parental cells. Relative % of polyunsaturated fatty acids and plasmalogens are also different in a significant manner, even if in minor extent.

Dimensional analysis

TEM ANALYSIS

LM-16 derived vesicles

Our second aim was to characterize these different fractions obtained by different ultracentrifugation settings by a dimensional point of view. Among the possibilities we utilized Electron Microscopy (EM). In order to take good pictures we had to change the classical protocol utilized to stain exosome in Oslo University Hospital. Thanks to the collaboration of Dr. Sagini and the facility of Electron Microscopy in Oslo, we optimized the classical method to stain the 5 different fractions.

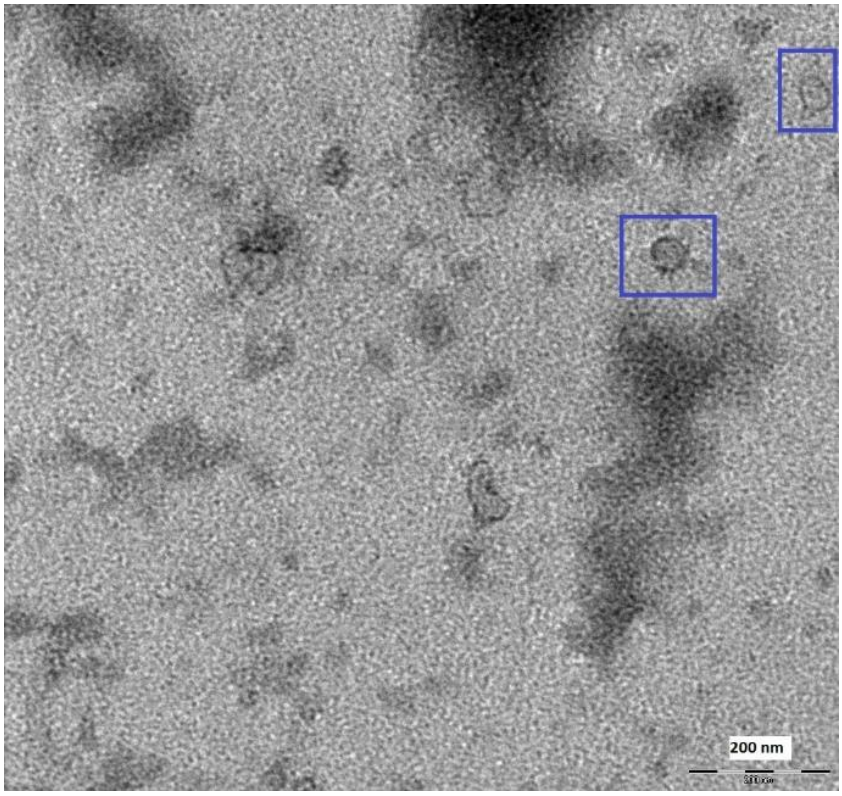

Figure 86 – EM picture of fraction corresponding to theoretical diameter of minor than 50nm.

Figure 86 shows the fraction obtained by highest speed and longest time centrifugation fraction, corresponding to exomeres with a theoretical diameter of <50nm nm. This fraction has to be considered the most difficult to purify, since it is contaminated by bigger particles, or proteins that co-pellet at these times and g-forces. In addition, this fraction seems to be the most homogeneous in terms of particles dimensions. Since it is very difficult to make conclusions about the presence of exomeres in this fraction we decided to utilize also atomic force microscopy (AFM) thanks to our collaboration with Dr. Ridolfi of the University of Bologna and CNR Firenze.

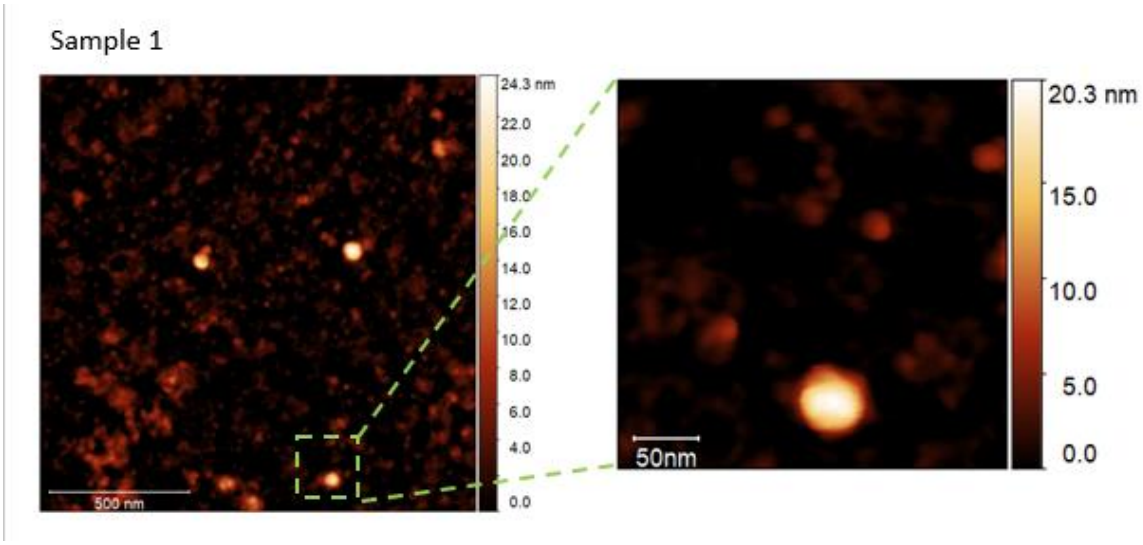

Figure 87 – Data of AFM analysis.

Preliminary AFM analysis confirms the presence of very small particles (20.3nm) in the highest centrifugation speed fraction.

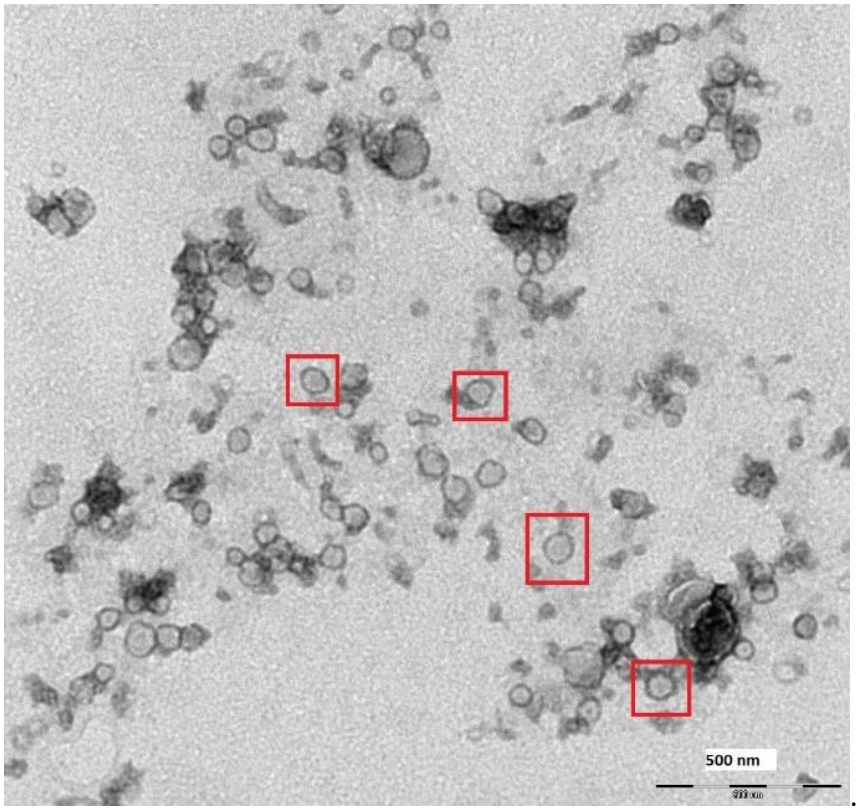

Figure 88 - EM picture of the fraction corresponding to the theoretical diameter of 50-80 nm.

In this image, we can observe the presence of bigger vesicles than those ones in the previous fraction. Almost all particles are smaller than 100nm. In addition to this, it is possible to see and confirm a typical EVs behavior: the agglomeration among particles which makes tricky the dimensional characterization with Nanosight and Zetasizer.

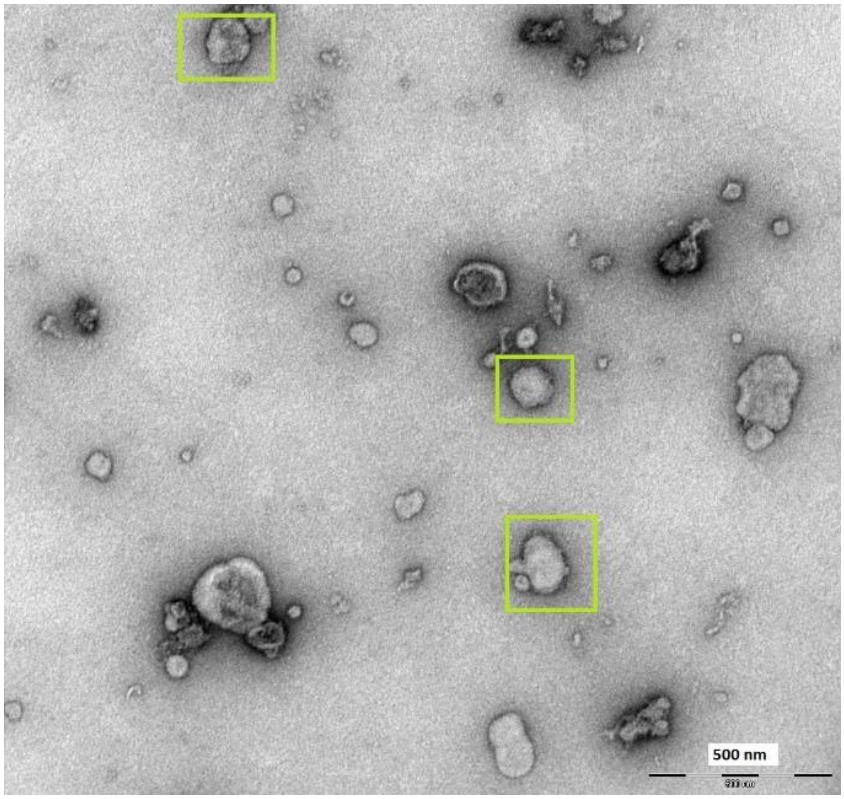

Figure 89 - EM picture of the fraction corresponding to the theoretical diameter of 80-120 nm.

The analysis of this picture unravels us the presence particles of the desired theoretical range;

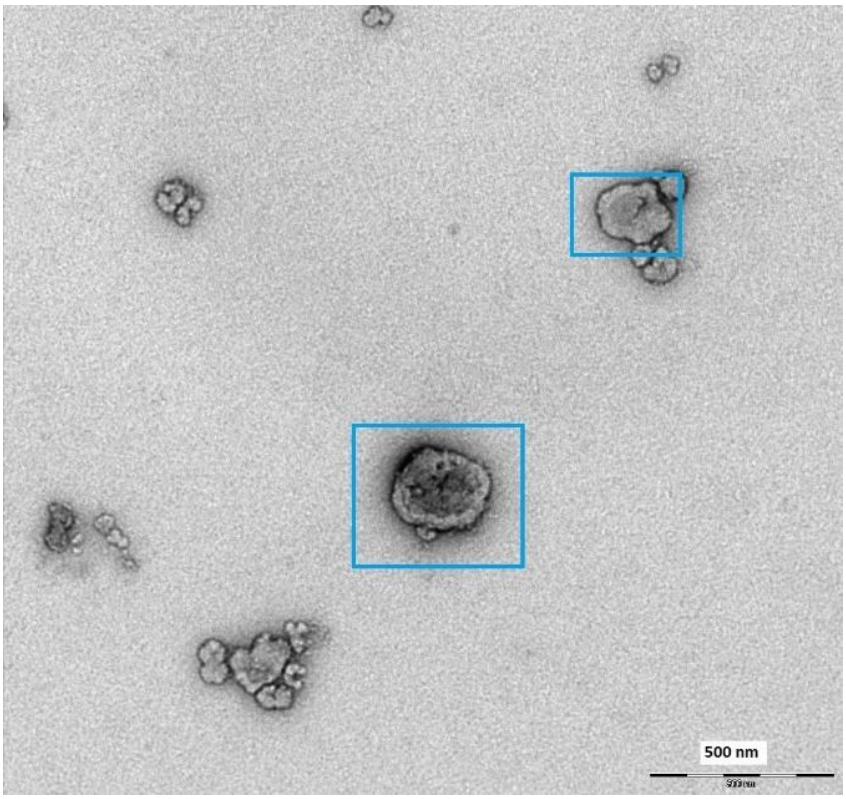

Figure 90 - EM picture of the fraction corresponding to the theoretical diameter of 120-200 nm.

Even in this picture, we observe an increase of the dimensions of the particle contained in the sample, even if contaminated with smaller ones, which are present as agglomerates. These small aggregates appear as particles without a regular shape.

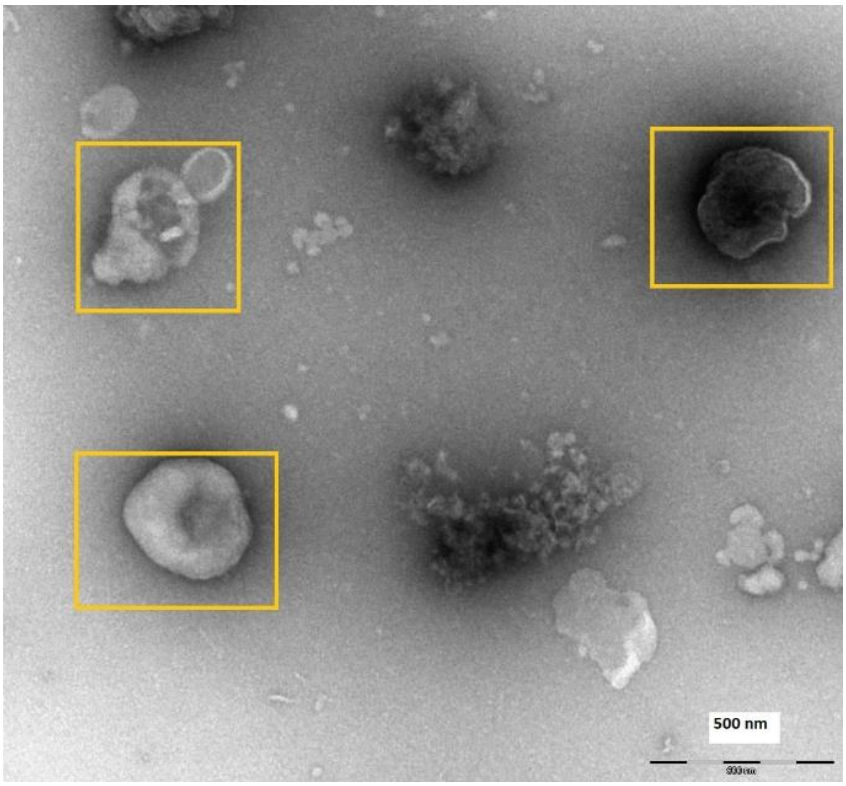

Figure 91 - EM picture of the fraction corresponding to the theoretical diameter of 200+.

Last image is referred to microvesicles or bigger particles. In this case the isolated fraction correspond to the theoretical one, even if with debris or smaller fractions.

With this fraction is evident the deformation of the shape probably due to limitations of the EM staining. Another issue is the accumulation of uranyl acetate in some particles compared to other one, which confers them a darker aspect.

Afterwards, we reported some measurements made on the particles recovered in all fractions.

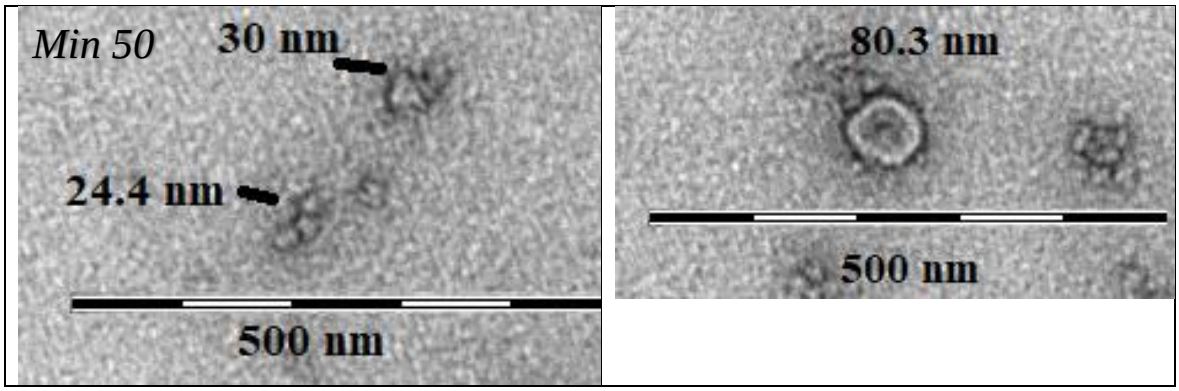

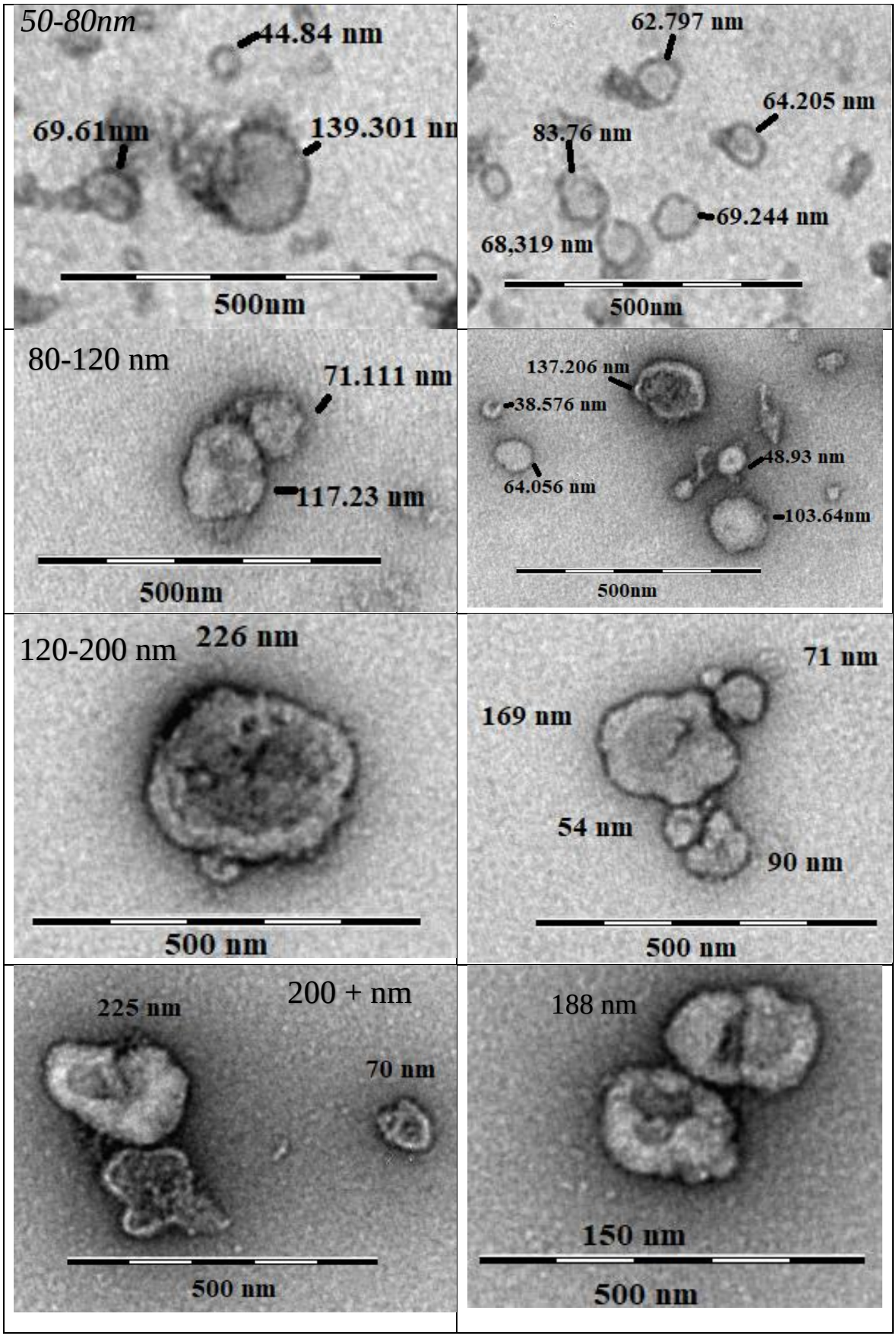

Table 9 – Diameters measured by ImageJ of particles in EM pictures of the 5 fractions.

In conclusion Electron Microscopy analysis of LM-16 derived vesicles confirms the theoretical radiuses decrease predicted by the tool; the increase of speed and centrifugation times is paralleled by the decrease of the theoretical dimensional range.

Highest speed and time centrifugation pellet unraveled the presence of very little particles with a mean diameter of about 27 nm. Particles appear with a circular shape, meaning that they are not debris of bigger particles or of cells (debris cannot close and form small particles). Samples are also "contaminated" by the presence of bigger particles, even if in not relevant quantities.

In 50-80 fraction we obtained a mixture of vesicles with a mean diameter of about 67 nm with a great circular shape even if they tend to aggregate; as shown in the picture we observe also the presence of both bigger (139.301 nm) and smaller (44.84 nm) particles.

In conclusion the decrease of the mean diameter of recovered particles is paralleled by the increase of centrifugation speed and times. Bigger particles tend to lose their round shape, making difficult the determination of the radius.

PC-3 derived vesicles

During my period at the Norwegian Institute for Cancer Research I utilized PC-3 cancer cells to perform experiments. All 5 fractions isolated from PC-3 cell lines have been analyzed with Electron Microscopy and the dimensional analysis was obtained by TEM exosome analyzer software which allows us to calculate a sort of distribution of the particles.

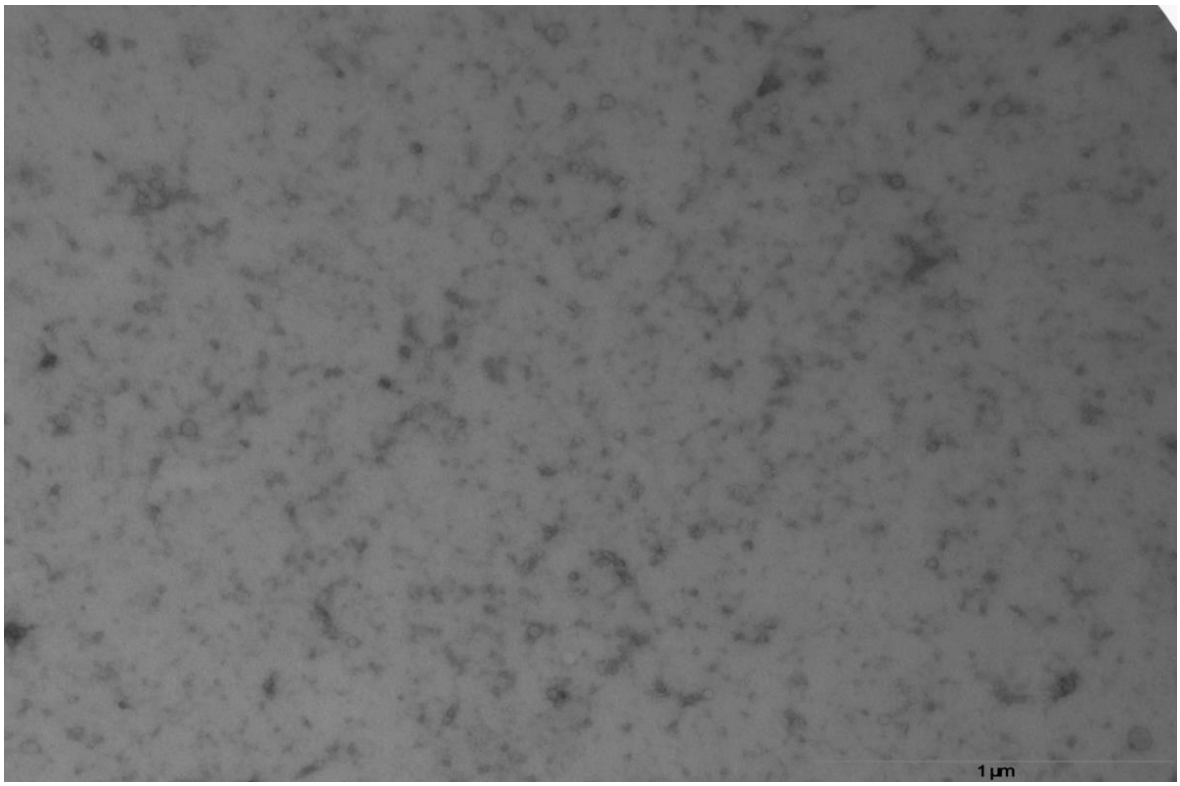

Figure 92 - EM image of the smallest fraction theoretically corresponding to min 50 nm.

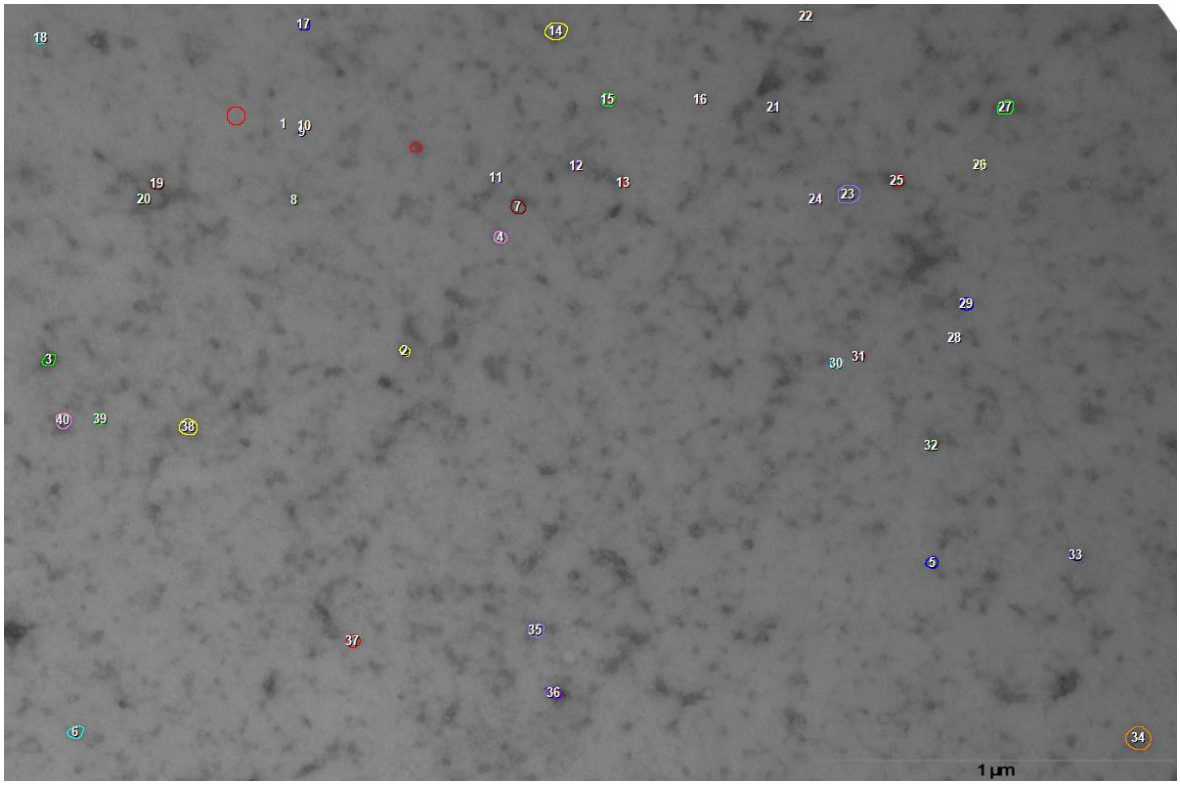

Figure 93 – the same EM image analyzed by TEM exosome analyzer software.

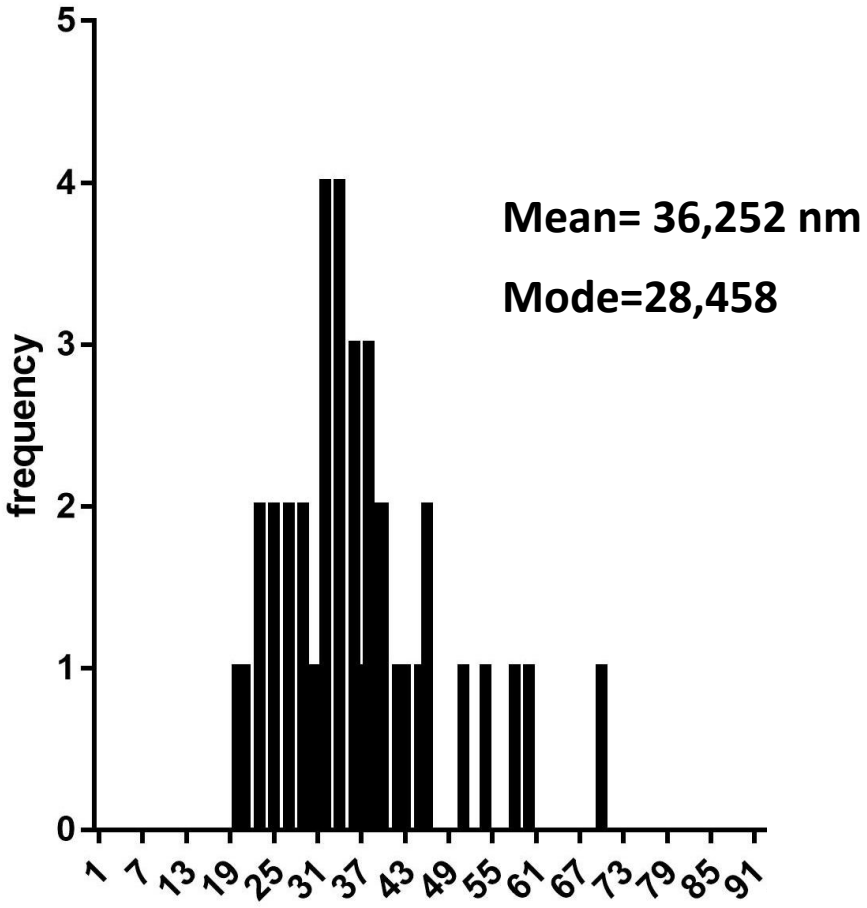

Figure 94 – Distribution of particles diameters contained in fraction corresponding to less than 50 nm theoretical diameter.

The smallest fractions isolated by Ultracentrifugation contains small particles with a mean of 36,252 nm and a mode (most frequent particle) of 28,458 nm. The image clearly shows that it is the most difficult fraction to isolate and purify, since it is contaminated by protein aggregates and/or big particles residuals derived from previous ultracentrifugation steps. On the other hands this fraction seems to be very homogeneous in terms of vesicles dimensions as previously documented by LM-16 derived EVs.

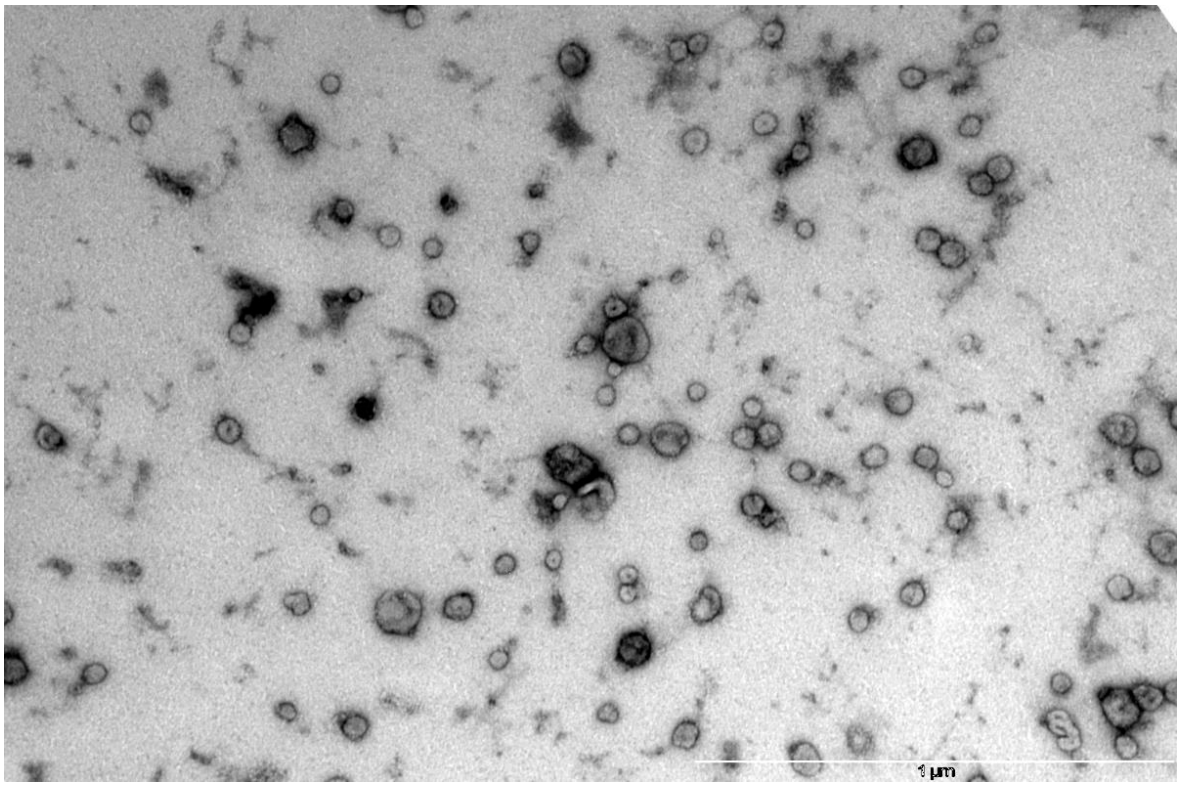

Figure 95 - EM image of the fraction theoretically corresponding to 50-80 nm.

Mean 47,82nm

Mode 48,50nm

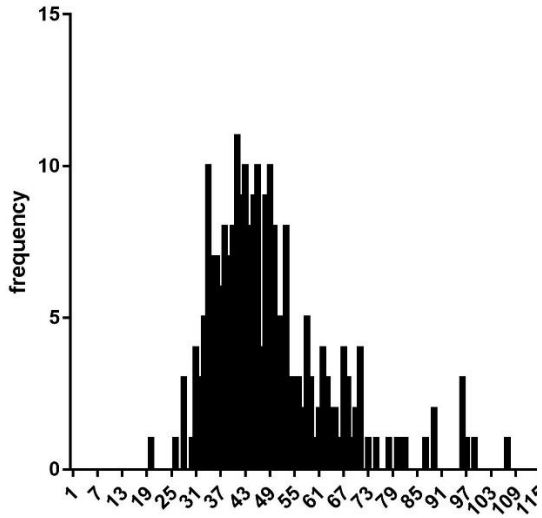

Figure 96 - Frequency graph of 50-80 nm theoretical fraction.

Fraction which theoretically corresponds to 50-80 nm clearly shows an increase both in mean and mode when compared to the previous one, with a mean of 47,82 nm and a mode of 48,50nm.

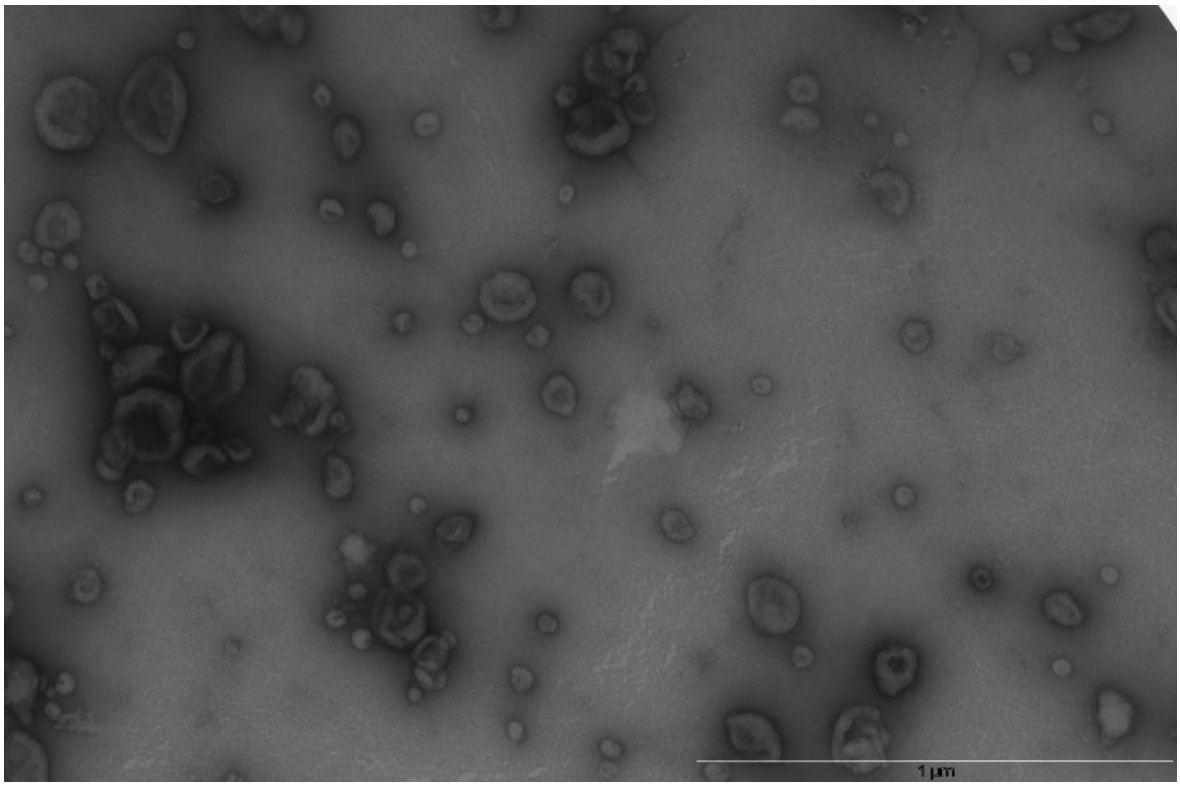

Figure 97 - EM image of the fraction theoretically corresponding to 80-120 nm.

Mean 62,229 nm

Mode 47,258 nm

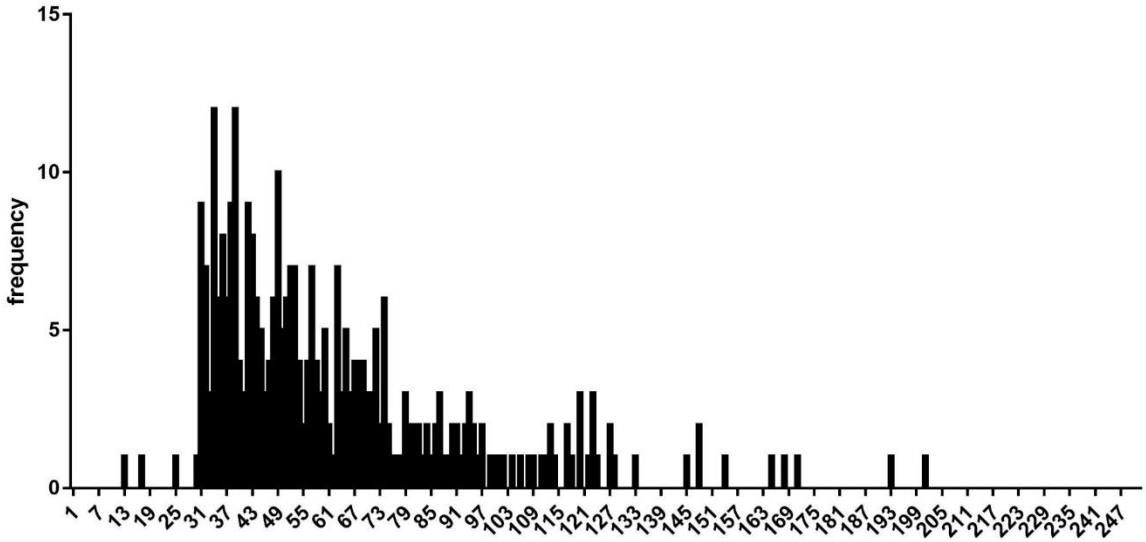

Figure 98 - Frequency graph of 80-120 nm theoretical fraction.

In this fraction we can observe more heterogeneity compared with the previous ones; we are indeed able to find bigger but also smaller particles than the theoretical size. Some vesicles

seem to be deformed probably due to their minor resistance and rigidity than the smaller ones; we have also to mention that their different shape can be due to the adsorption of particles over the copper grids for EM analysis.

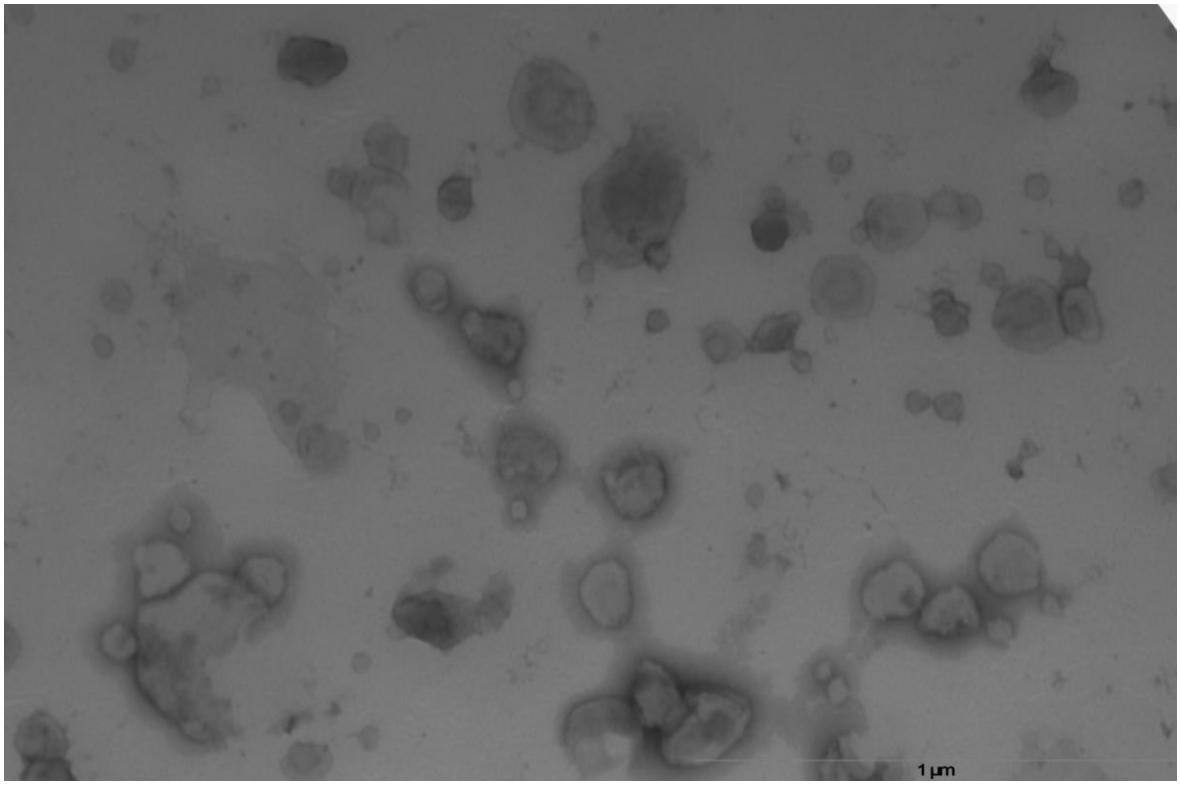

Figure 99 - EM image of the fraction theoretically corresponding to 120-200 nm.

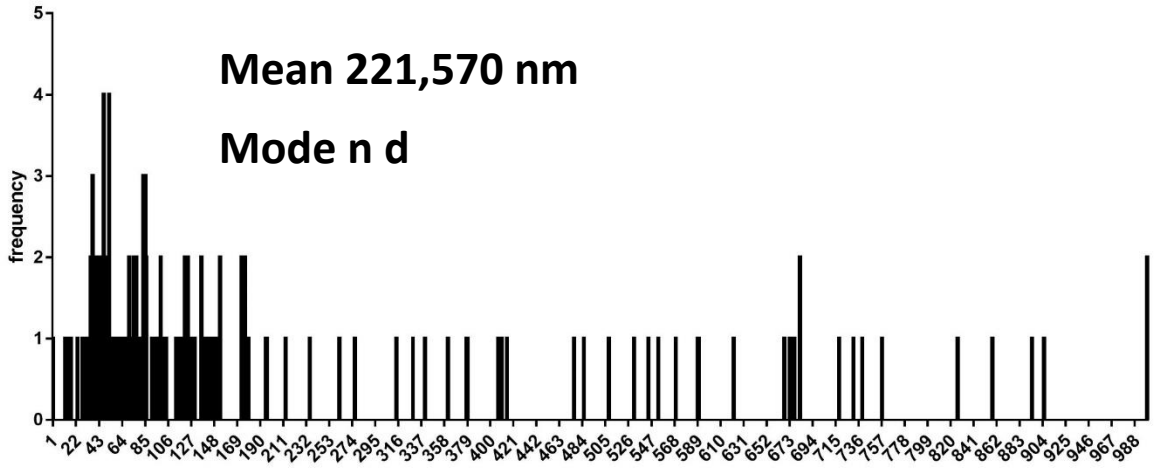

Figure 100 - Frequency graph of the 120-200nm theoretical fraction.

The 120-200 theoretical fraction appears highly heterogeneous; indeed even if the peak is always shifted to the left of the distribution, there are particles up to 1000nm.

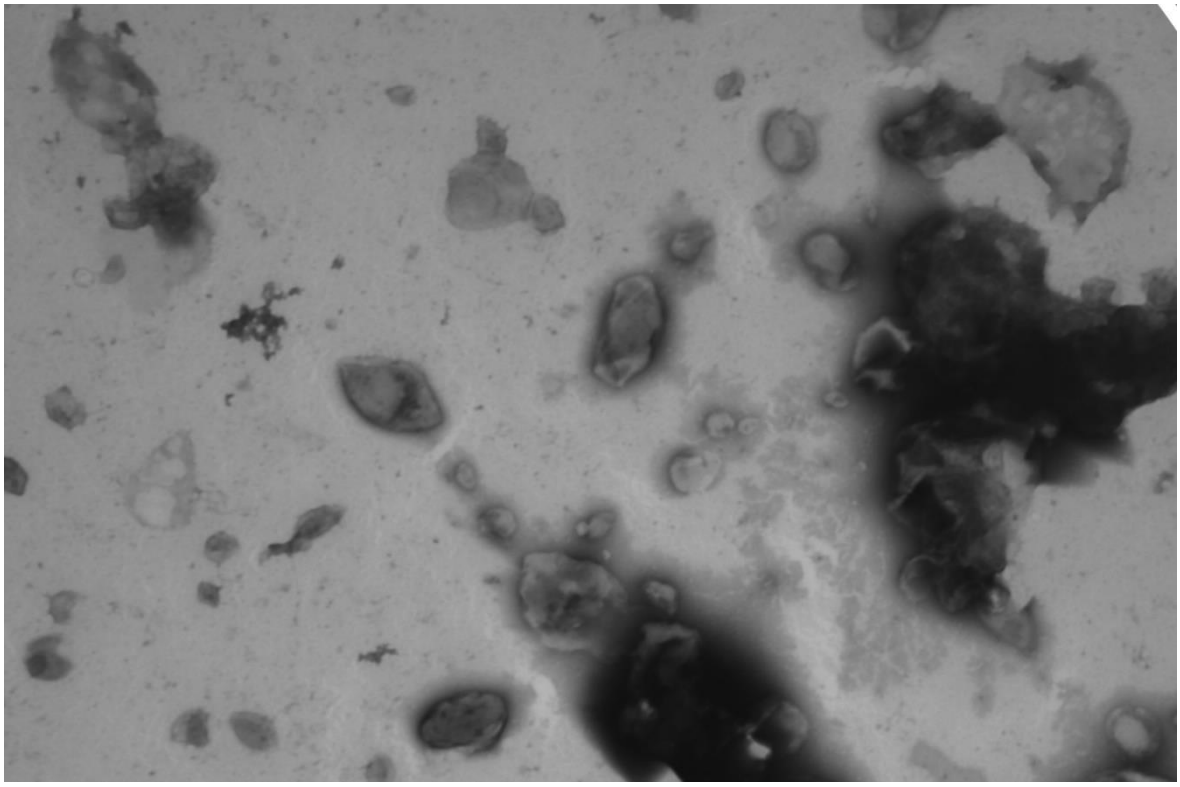

Figure 101 - EM images of fraction theoretically corresponding to 200+ fraction.

The last picture shows the 200+ fraction which theoretically contains the so-called microvesicles. Even in this case there is the presence of smaller particles than those of the desired interval. Due to the presence of these huge black spots, we decided to not take in consideration the distribution.

Theoretical diameter	Mean (nm)	Mode (nm)
Min 50	36.25	28.46
50-80	47.82	48.5
80-120	62.23	47.26
120-200	221,57	n.d.
200+	n.d.	n.d.

Table 10 – Summary of dimensional data obtained by EM analysis of PC-3 derived-EVs.

In conclusion, imaging analysis of fractions derived from 2 different cell lines confirmed:

1) The decrease of the diameter according to different centrifugation speed and times;
2) The presence of particles of different dimensions among centrifugation steps;
3) Common characteristics between EVs derived from 2 different cell lines.

Unfortunately, we did not have the opportunity to collect EM picture of MDA-MB231 derived-EVs.

Zetasizer analysis

During my period abroad at Norwegian Institute for Cancer Research, we set the Zetasizer instrument to discriminate from a dimensional point of view the size of particles obtained by the 5 different centrifugations, thus once back in Milan I had the opportunity to set experimental conditions in order to carry out the same dimensional analysis on the main topic of my research work, the LM-16 cells.

In the first step we set-up the correct parameters in the Zetasizer software.

Sample Name:	50-80mean		
SOP Name:	Alicia prostasomes_fixed.sop		
File Name:	50-80 tripli.dts	**Dispersant Name:**	NaCl 0.9%
Record Number:	238	**Dispersant RI:**	1,335
Material RI:	1,45	**Viscosity (cP):**	1,0211
Material Absorbtion:	0,010	**Measurement Date and Time:**	mercoledì 22 gennaio 2020 10:59:...
Temperature (°C):	25,0	**Duration Used (s):**	70
Count Rate (kcps):	222,1	**Measurement Position (mm):**	3,00
Cell Description:	Disposable micro cuvette (40µl)	**Attenuator:**	9

Figure 102 – Zetasizer settings.

To obtain a correct size distribution we set the material refractive index RI to 1,45 (Lipid-cholesterol bilayer), the material absorbtion to 0,01, the RI of saline solution to 1,335 and its viscosity expressed in cP to 1,0211. The count rate is optimal between 100 and 1000, each sample was diluted to reach this value.

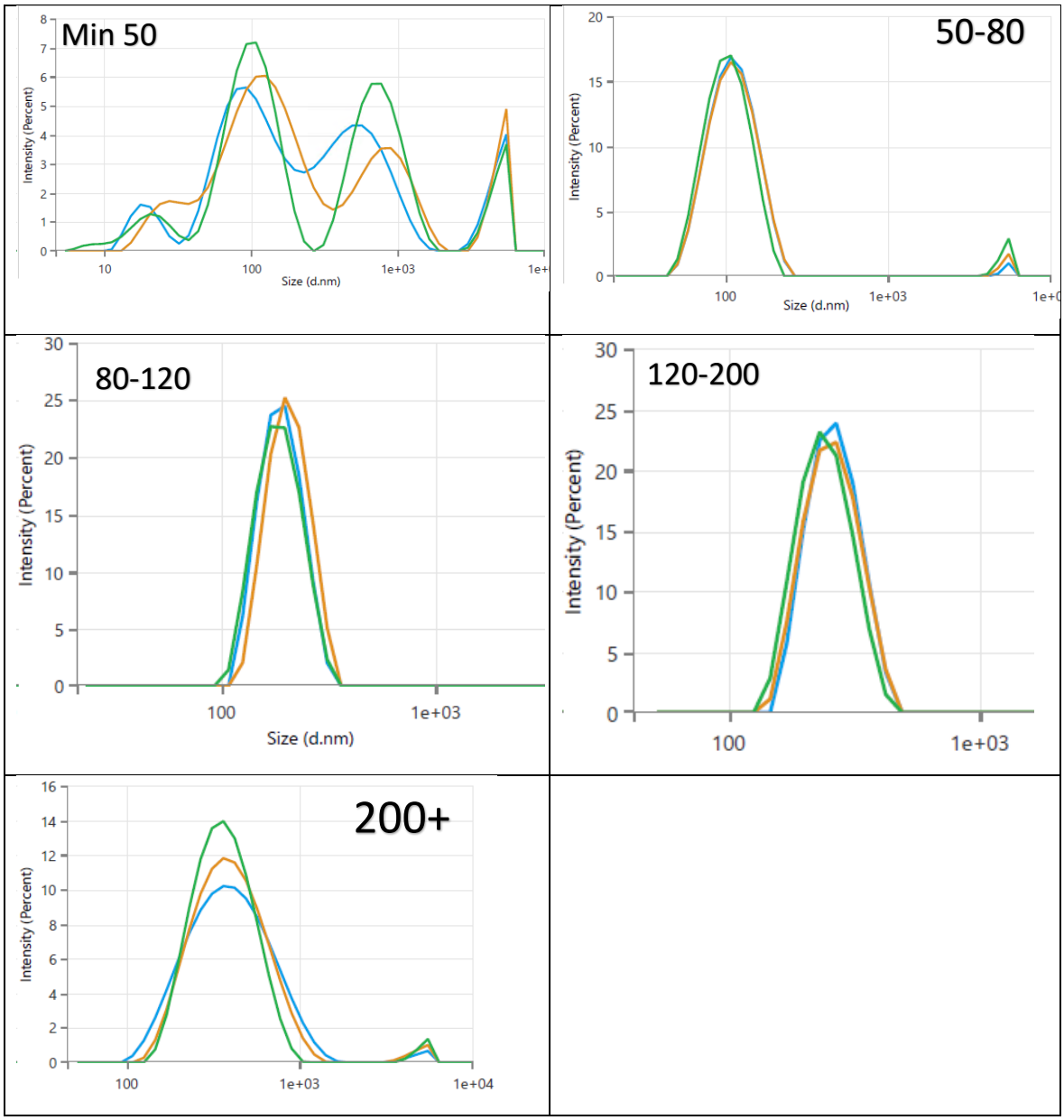

Table 11 – Zetasizer distributions of the 5 different fractions derived from LM-16 cells.

	Z average (nm)	Polydispersity Index
F1 (min50)	158 ± 8	0.66
F2 (50-80)	113.3 ± 0.7	0.29
F3 (80-120)	179.6 ± 9	0.11
F4 (120-200)	248.2 ± 10	0.17
F5 (200+)	347.8 ± 8	0.25

Table 12 – Z average value and Polydispersity index of the 5 different fractions derived from LM-16 cells.

Zetasizer analysis for LM-16 derived EVs have been performed by Alfatest Srl (Cinisello Balsamo, Italy) with Zetasizer Ultra. Zetasizer analysis gives a mean particle size (z-average) and an estimate of the width of the distribution (polydispersity index).

Tables 11 and 12 show that the decrease of the Z average is paralleled by the decrease of the theoretical dimensional range (excepted for the small size fraction). All particles clearly show a mid-range polydispersity index, suggesting the homogeneity of each sample, except for the smallest fraction which is the closest to the >0.7 limit which indicates a broad distribution of particle size. In conclusion DLS analysis of our samples are represented by differences in terms of dimension of suspended particles and confirms the previous imaging data obtained by Electron Microscopy.

Zetasizer analysis of PC-3 cell lines

Zetasizer experiments have been carried out in the lab of Exosomes and Prostate Cancer – Oslo University Hospital – Prof A. Llorente.

Min 50

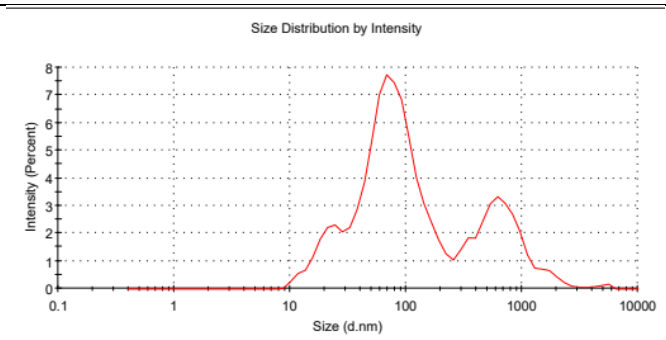

50-80

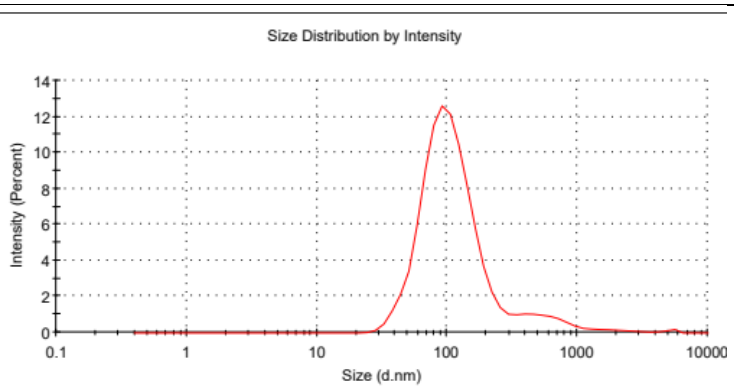

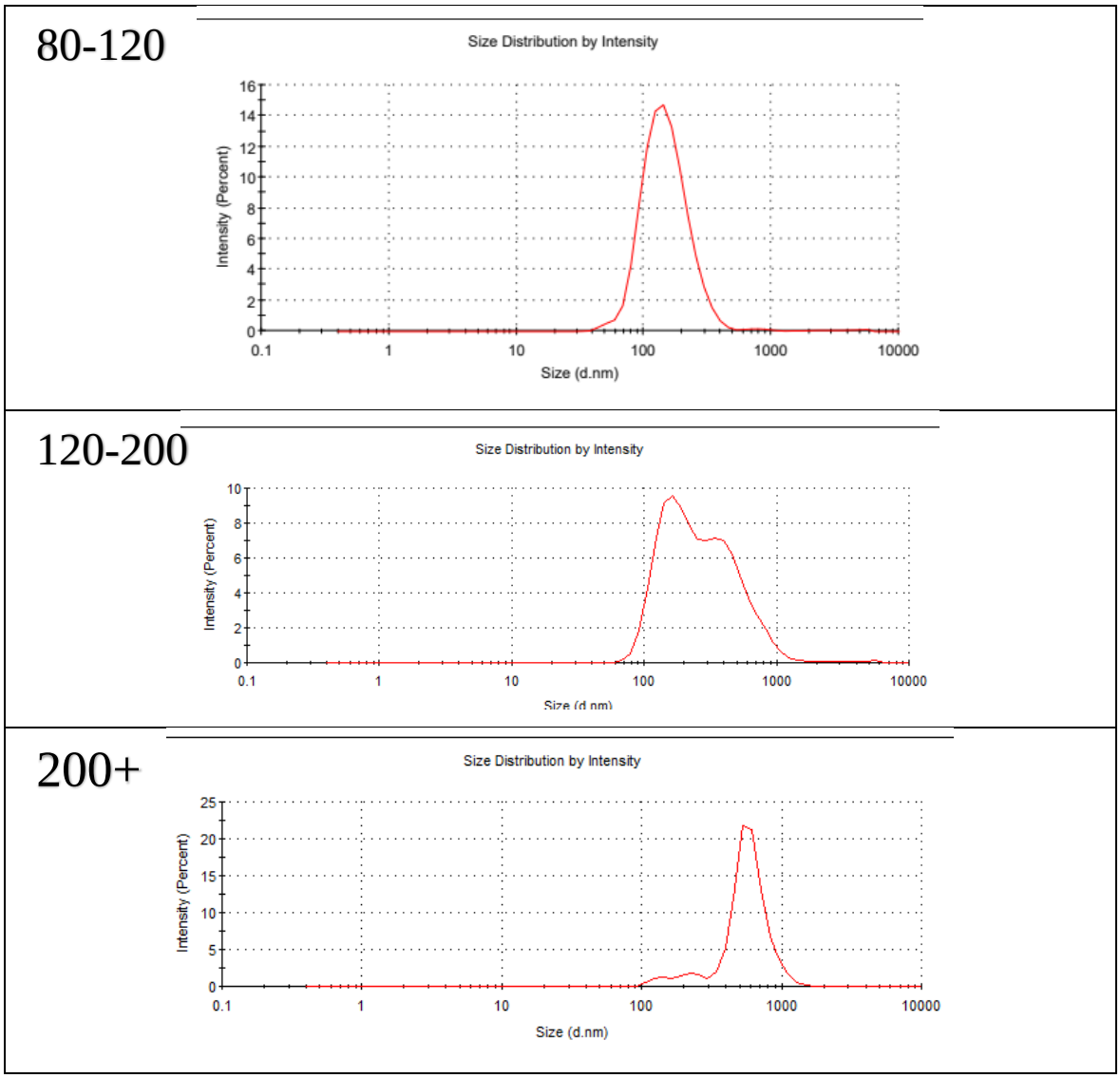

Tab 13 – Zetasizer distribution graphs of the 5 different fractions derived from PC-3 cells.

The table 13 clearly resumes the data obtained by the Zetasizer distributions; as seen with the LM-16 derived EVs, the hydrodynamic radius measured by DLS analysis decreases with the increase of speed and centrifugation times. All particles (excepted for the smallest ones) clearly show a low and comparable polydispersity index, suggesting the homogeneity of each sample.

In addition to our fractions, thanks to the collaboration with Dr. Sagini, we compared dimensional distributions obtained by our centrifugation method with those of the classical Thery's one (resulting into two different pellets, 100k for exosomes and 10k for microvesicles). The hydrodynamic radius of the 100k pellet mainly corresponds to F3 fraction.

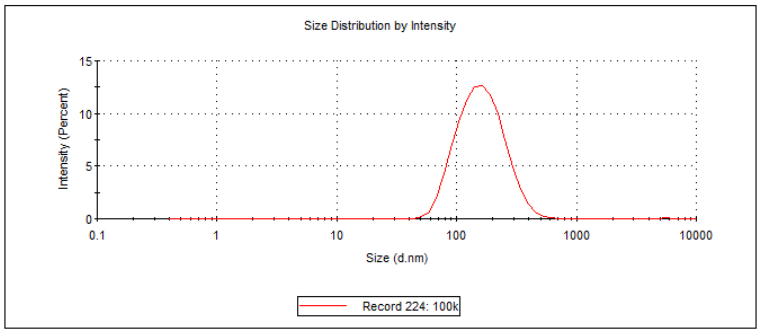

Figure 103 – Zetasizer distribution of 100K pellet (exosomes).

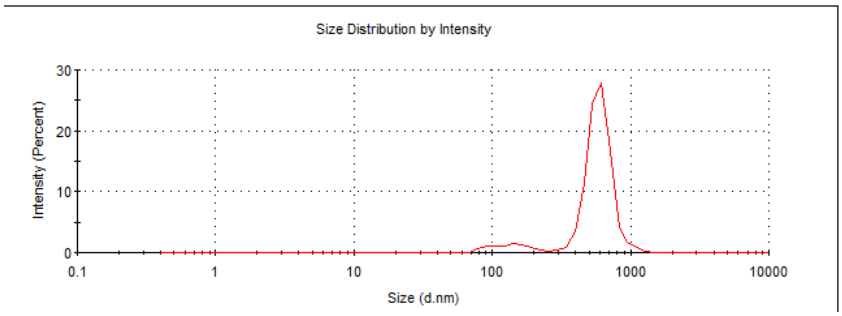

Figure 104 – Zetasizer distribution of 10k pellet (microvesicles).

10K pellet mainly correspond to our biggest fraction.

	PDI	**Z Avg (nm)**	**sd**
F1 (min 50)	0,55	116	54,91
F2 (50-80)	0.28	102,80	12,41
F3 (80-120)	0.17	139,50	15,25
F4 (120-200)	0.27	232,28	36,03
F5 (200+)	0.23	498,8	72,83
10K	0.317	515,6	63,3
100K	0.199	149,2	11,2

Table 14 – Results obtained by dimensional analysis of 5 different fractions and 10k and 100k isolated according to Thery from cell media of PC-3 cells.

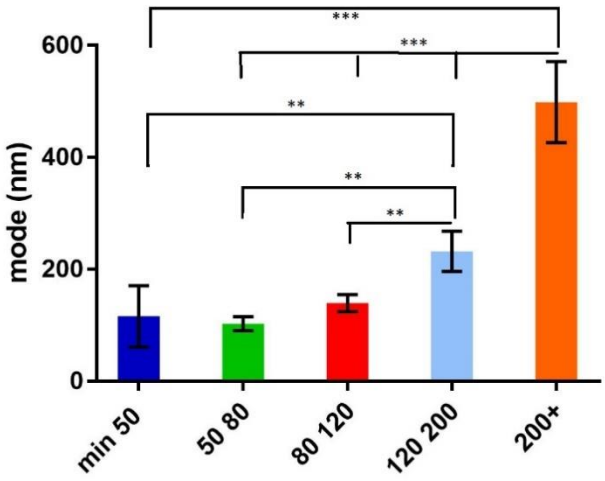

Figure 105 – significant changes in z averages from the 5 different fractions.

In conclusion as resumed by table 14 and figure 100 demonstrated significant dimensional changes among the 5 fractions through Zetasizer analysis of the 5 fractions.

Nanosight analysis.

To further characterize these fractions, we carried out also Nanosight analyses. For our particular set of experiments Alfatest srl recommended us to be more confident with Zetasizer analyses, since Nanosight is less able to discriminate among samples with close dimensional intervals. We performed analyses only on PC-3 cells (n=5).

	F1 (nm)	sd	F2(nm)	sd	F3(nm)	sd	F4(nm)	sd	F5(nm)	sd	100k	sd
Mean	130,1	14,71	113,65	7,51	135,58	9,07	187,62	13,03	272,42	32,78	153,05	0,29
Mode	89,94	11,34	85,65	9,03	108,17	16,76	140,55	11,77	254,13	119,70	121,37	2,36
D10	78,19	10,31	75,73	10,78	88,97	12,50	118,81	6,11	151,41	20,46	104,45	2,61
D50	111,07	13,81	98,95	8,79	119,88	15,89	168,81	11,62	244,90	38,66	136,16	0,37
D90	211,82	35,64	168,72	15,12	200,57	13,56	285,56	26,22	433,28	34,26	220,75	0,63

Table 15 – dimensional data obtained by Nanosight analysis of the 5 different fractions together with classical 100K.

Table 15 resumes the 5 different experiments performed on PC-3 cells confirming the dimensional obtained by two other methods. We obtained a clear dimensional distinction of each subset of particle, and even in Nanosight 100K appears the most similar to F3.

Proteomics of 5 different fractions and parental cells

Analysis of protein purity

Thanks to our collaboration with prof P. Bergese of Università Degli Studi di Brescia we were able to utilize the Colorimetric NAnoplasmonic Assay, which was developed by his research group. Thanks to this assay we have been able to assess the purity grade of our preparations [76].

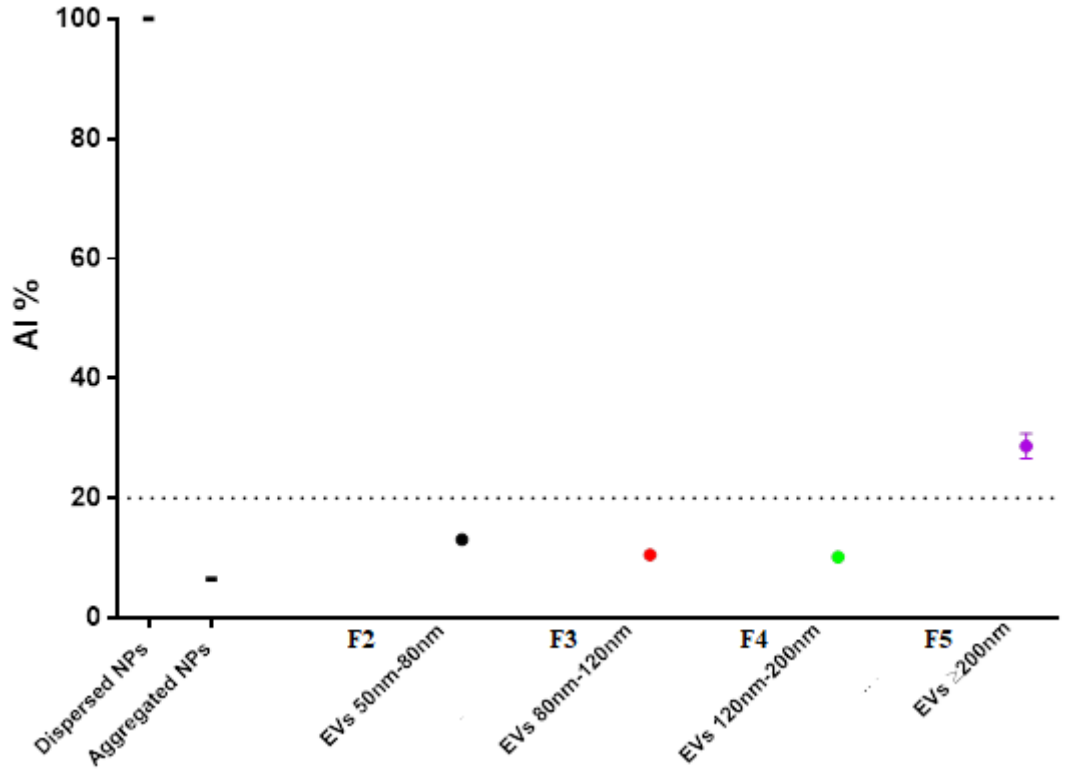

Figure 106 - Analysis of protein purity with CONAN. AI= aggregation index.

CONAN assay has been carried out in presence of dispersed and aggregated Nanoparticles (NPs) as internal control. An aggregation index (AI) below 20% indicates the purity of preparations devoid of free protein contaminants. As clearly seen in the graph, only F5 fraction (>200 nm) contains free protein contaminants, while the remaining fractions are below 20% AI. F1 was not processed due to the little dimension of the particles which can interfere with the analysis. In conclusion, the fractions are free of protein contaminants therefore each protein that we are going to find in each fraction is very likely contained in EVs, except for F5.

Comparison of protein numbers recovered in different EVs fractions

After lipid profile and dimensional characterization of 5 fractions we performed a complete proteomics analysis to unravel possible differences in terms of protein pattern carried by different populations of EVs. Thanks to Dr. G. Garrone and Dr F. Farè of Filarete Foundation of Università Degli Studi di Milano, we performed mass spectrometry analysis and set up the parameters for the best possible analysis. We decided to search "differential" and "common" proteins among the 5 fractions. We made also an analysis of 10K and 100K canonical pellets isolated by ultracentrifugation according to Thery's method to make comparisons with the different fractions. We also analyzed whole cells protein extract to unravel possible functional enrichment between cell and each fraction. All samples have been analyzed in biological triplicates. We found a total of 2003 proteins among all 5 fractions; each fraction is characterized by the presence of both common and unique proteins as explained by following tables.

	Total proteins	**Common proteins**	**Unique proteins**
F-1	697	600	97
F-2	819	802	17
F-3	1079	1065	14
F-4	1621	1480	141
F-5	1654	1402	252

Table 13 –Proteins recovered in 5 fractions.

	Total proteins	**Common proteins**	**Unique proteins**
10k	1192	889	303
100k	1293	889	404

Table 14 - Proteins recovered in canonical pellets (10K and 100K).

We identified different proteins for each fraction, ranging from 697 to 1654 protein from F-1 to F-5. They are also characterized by the presence of unique proteins that thus characterize each fraction. In addition, we found a total of 2008 proteins in LM-16 cells.

We made a comparison between the protein profile of each fraction with that of parental cell. We found that dimension size is paralleled by an increased number of common proteins, ranging from 23.6% for smallest particles to 46.1% of bigger ones.

	% Proteins in common with Parental Cell
F-1	23,6%
F-2	24,4%
F-3	29,8%
F-4	41,8 %
F-5	46,1%

Table 15 - % of proteins in common between each fraction and parental cell.

We also compared protein profiles of each fraction with proteomics derived from 100K and 10K pellet according to Thery's method.

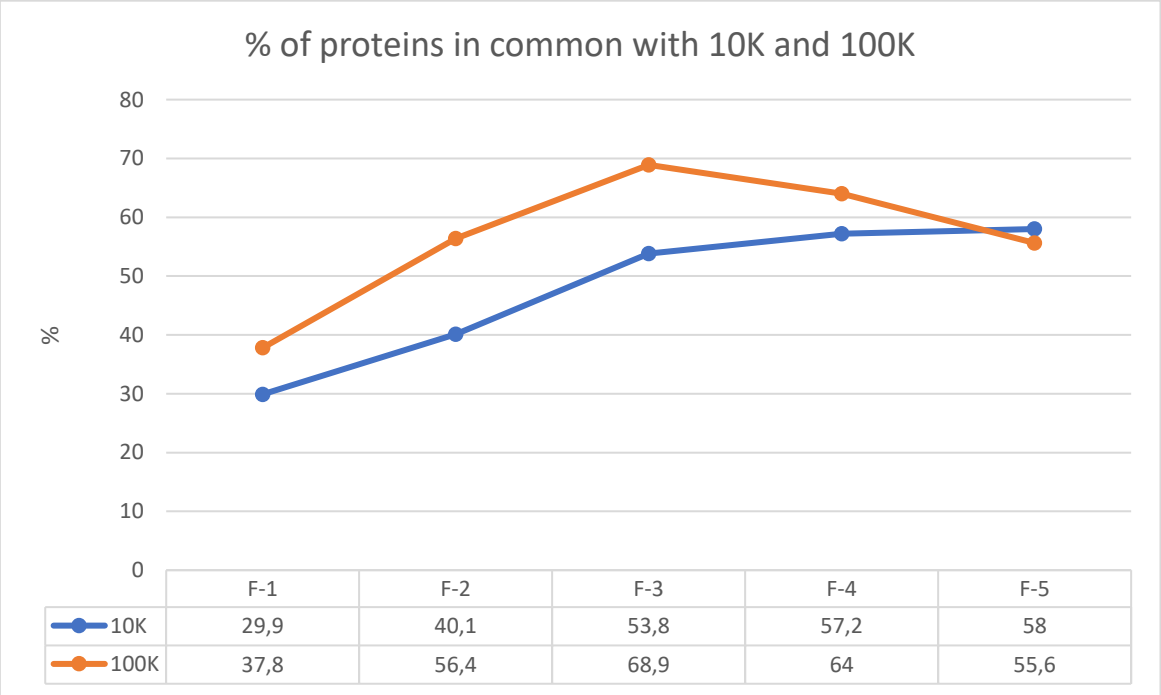

Figure 107 - % of proteins in common among each fraction and 10K/100K canonical pellets.

10K protein profile shows a constant increase in % of proteins in common from F1 to F5 with a maximum of 58%. In contrast 100K has a distribution with a peak of 68,9% on F3. In conclusion, our 5 fractions are different in term of protein content if compared with both 100 and 10k pellet protein profile. F3 fraction is the most similar to 100K while F5 to 10K.

Evaluation of protein enrichment in different fractions based on their parental cell origin

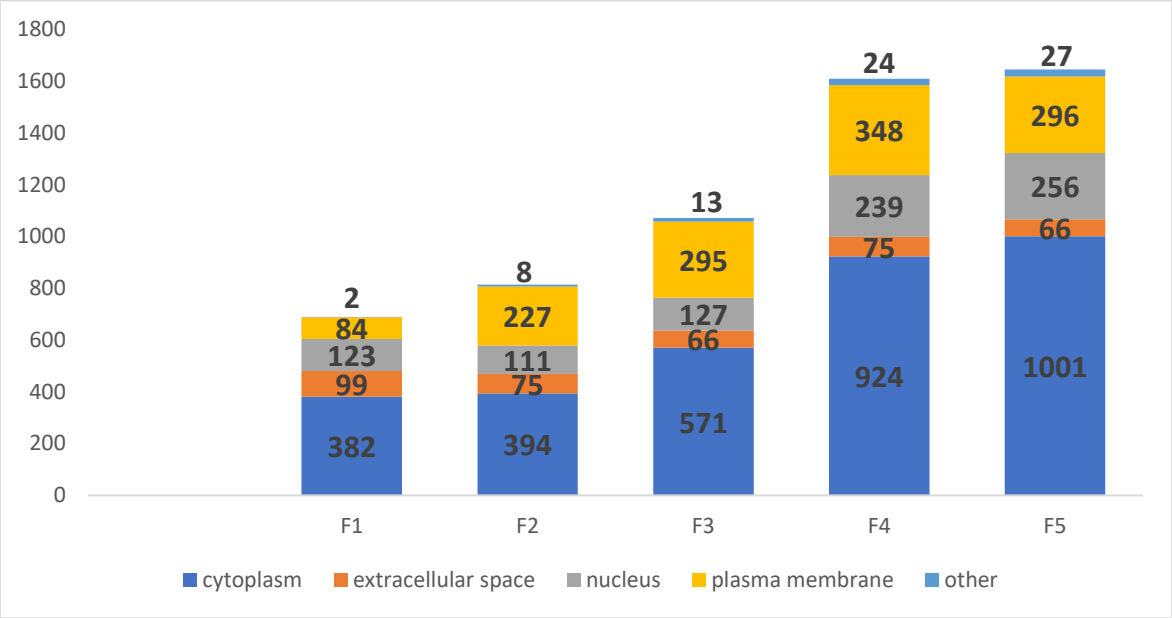

Figure 108 – Numbers of proteins derived from different cell sites recovered in each fraction.

As shown in the graph we reported that F1 and F2 contain similar amounts of nuclear protein while from F3 to F5 we reported an increase of nuclear protein number, particularly from F3 to F4. Proteins from extracellular space appear to be similar, except for F1. Nuclear proteins are quite comparable from F1 to F3 and from F4 to F5. Plasma membrane-derived proteins have a unique pattern; the lowest value is in F1, followed by F2; interestingly F3 and F5 have the same number of proteins in common. The highest value is reported in F4. In conclusion fractions are differently enriched in proteins derived from different sites of the cell.

IPA analysis of proteins recovered in 5 fractions

The differentially expressed proteins were categorized to IPA canonical pathways:

1) to obtain an elementary investigation about the functionality of the 5 different fractions;
2) to unravel possible different functions involved in growth, proliferation and invasion of melanoma through EVs.

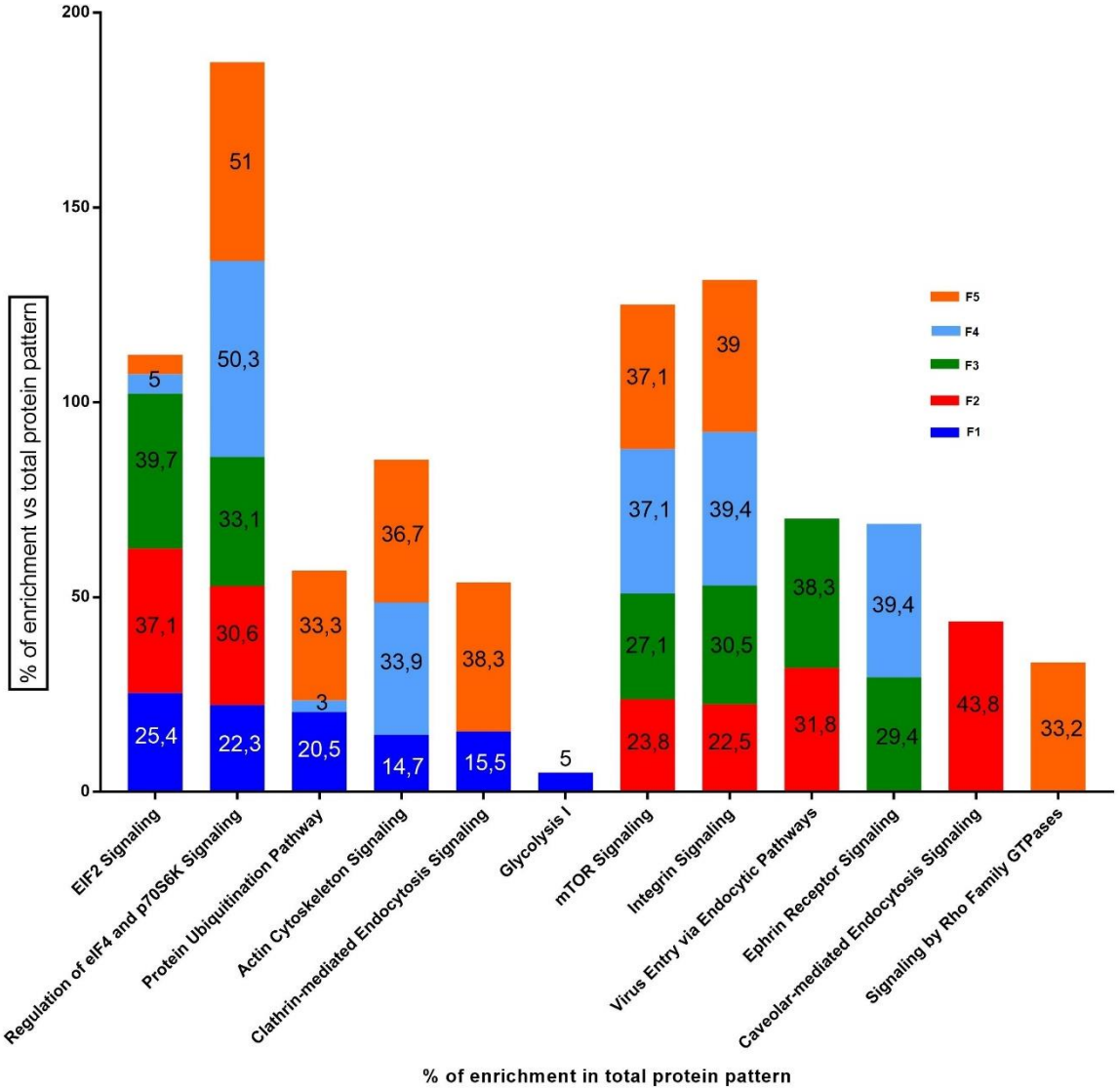

Figure 109 – % of enrichment in proteins which encoding for a determined function vs total protein pattern for each fraction. Data are independent of protein quantity recovered in each fraction.

EIF2 signaling and regulation of eIF4 and p70S6K signaling are used to be common pathways involved in protein synthesis; they are the only two canonical pathways which are present in all the 5 fractions. Particularly EIF2 signaling is codified in F2 and F3, less in F-1 and in small amount (5%) in the remaining two fractions.

Ubiquitination seems to be a function which is preferentially and exclusively expressed by F-5 and F-1. 3 % of F-4 is probably due to contamination (or maybe improper cutoff settings) of the closest fraction.

Cytoskeleton organization, through actin cytoskeleton signaling is a function preferentially encoded by bigger vesicles, F4 and F5 and also even if in less extent, by smallest ones. F2 and F3 seem to utilize virus entry via endocytic pathway for their internalization into recipient cells, maybe sharing this mechanism with viruses. Particularly Caveolar-mediated Endocytosis signaling is a unique functionality of F2. Interestingly, clathrin-mediated endocytosis signaling seems to be the preferential "eat-me" signal of F5 (microvesicles) and F1 (exomeres) maybe indicating different internalization pathways from microvesicles and exosomes. Proteins codifying for glycolysis seem to be present only in exomeres. This is in line with previous observations which stated that exomeres show an enrichment in metabolic enzymes and above all the glycolytic ones[19]. mTOR and integrin signaling have similar profiles of enrichment for each fraction. Integrin signaling is enriched in F-4 and in F-5.

The ephrin-Eph signaling system is a bidirectional cell–cell communication device mediated by membrane-tethered ligand–receptor interactions. Ephs and ephrins are involved in many different physiological processes, including boundary formation and axon guidance, as well as pathological processes such as cancer [77].

Signaling by RHO family GTPases is found only in F-5, which is the fraction composed by Microvesicles. Our data corroborates previous findings in literature[78]. Particularly the small GTPase RhoA triggers a specific pathway for the biogenesis of microvesicles in various human cancer cells. Inhibition of the activity of this pathway blocks microvesicles biogenesis cancer cells and prevents oncogenic transformation in cell culture as well as tumor growth in mice [79].

Canonical exosomal markers

We then focused on the most enriched GO-term in all the 5 fractions GO:0070062 which identifies: “A vesicle that is released into the extracellular region by fusion of the limiting endosomal membrane of a multivesicular body with the plasma membrane. Extracellular exosomes, also simply called exosomes, have a diameter of about 40-100nm”.

	% of proteins codifying for “extracellular exosome” vs total ones	**Number of proteins**	**Bonferroni’s test**
F-1	65,4	455	1.5x10-202
F-2	70.2	575	1.1x10-287
F-3	68,7	741	0
F-4	58,7	951	0
F-5	56,9	941	0

Table 16 - % of enrichments in proteins inserted into the “extracellular exosome” category of the Gene Ontology Consortium.

According to table 16, we found a huge enrichment in proteins encoding for “Extracelluar Exosome”, ranging from 70.2 (F2) to 56.9% (F5). The highest values (>65%) characterize the fractions from F1 to F3 meaning that these fractions are the most enriched in “extracellular exosome” markers. All statistics have been mate made with Bonferroni’s test, with DAVID tool.

We then compared each fraction with the 100 canonical exosome markers list obtained by www.vesiclepedia.org

	TOP 100 canonical exosomes markers in common with each fraction
F-1	73
F-2	90
F-3	89
F-4	90
F-5	90

Table 17 – Proteins in common among each fraction and the top 100 canonical EVs marker found on www.vesiclepedia.org.

Interestingly almost all exosomes canonical markers are present in the 5 different fractions.

We compared the lists of canonical markers contained in each fraction in order to evaluate possible biomarkers for 5 fractions; surprisingly the only match was the CD63; this tetraspanin is indeed the only molecule, among the top 100, which is unique for a determined fraction, the F-2.

All the other markers are expressed in all the 5 fractions. Ezrin, Annexin-A1, A6 A7 and A11 (ANXA1, ANXA6, ANXA7, ANXA11), Flotillin-1, Guanine nucleotide-binding protein 1 and 2 (GNB1) (GNAI2), Tumor susceptibility gene 101 (TSG101), cell division control protein 42 homolog (CDC42), G protein subunit beta2 (GNB2), Ras-related protein Rab-5C (RAB5C), GDP Dissociation inhibitor 2 (GDI2) , G protein subunit alpha S (GNAS), Ras homolog family member A (RHOA), Ras-related C3 botulinum toxin substrate 1 (RAC1), Ras-related protein Ral-A (RALA), and Annexin a-11 are present in F2, F3, F4 and F5 while not in F1; Filamin-A (FLNA) is present in F1, F4 and F5.

Effect of the pharmacological modulation of LM-16 cells on EVs.

To evaluate if the pharmacological modulation of the two crucial lipids involved in EVs biosynthesis and functionality, namely Cholesterol and BisMonoacylGlycerophosphate can affect EVs characteristics, we decided to administer simvastatin and KT182 to LM-16 cells. Simvastatin is an inhibitor of HMG-CoA reductase, the rate limiting enzyme of cholesterol biosynthesis while KT-182 is a small molecule which impairs BMP degradation through inhibition of ABHD6 (enzyme responsible of BMP hydrolyzation).

Dose-finding experiments

Our goal was to set the experimental conditions in order to affect exclusively the homeostasis of the two lipids, without affecting cell proliferation and vitality.

We first performed proliferation assays, counting cells with coulter counter; cells have been incubated with different doses of the compounds. We set the experimental conditions as follows:

- Day 0 – seeded 70000 cells x 35mm wells, with 10% FCS
- Day 1 – replaced media with MEM + 10% FCS + compounds + 0.1% DMSO in ctrl and simvastatin group
- Day 3 – replaced media with serum free one + compounds + 0.1% DMSO in ctrl and simvastatin group
- Day 6 – proliferation assay, MTT and de novo cholesterol biosynthesis.

As shown in following graphs, simvastatin inhibits cell proliferation at 0.3 uM; kt 182 shows no significant inhibition of cell growth up to 50nM.

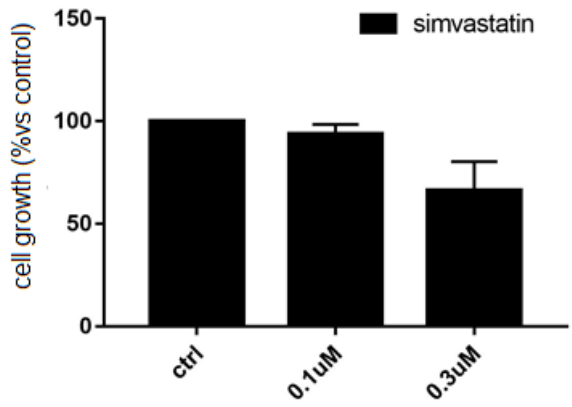

Figure 110- Simvastatin dose-finding by cell proliferation assay.

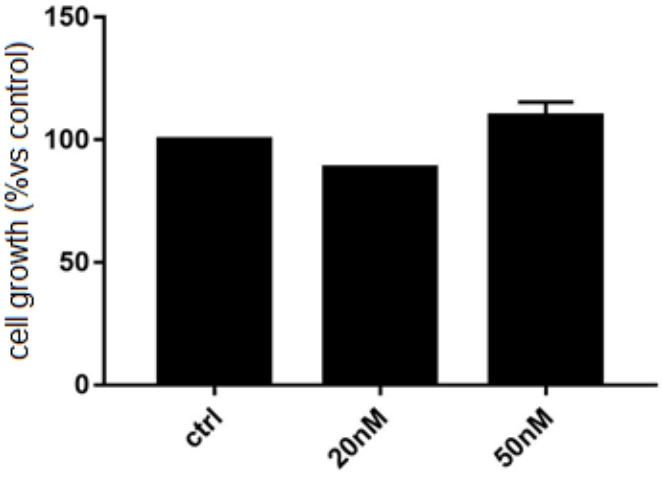

Figure 111 - KT182 dose-finding by cell proliferation assay.

We also decided also to administer both compounds to cells in order to assess whether the two drugs could exert an additive or synergistic effect.

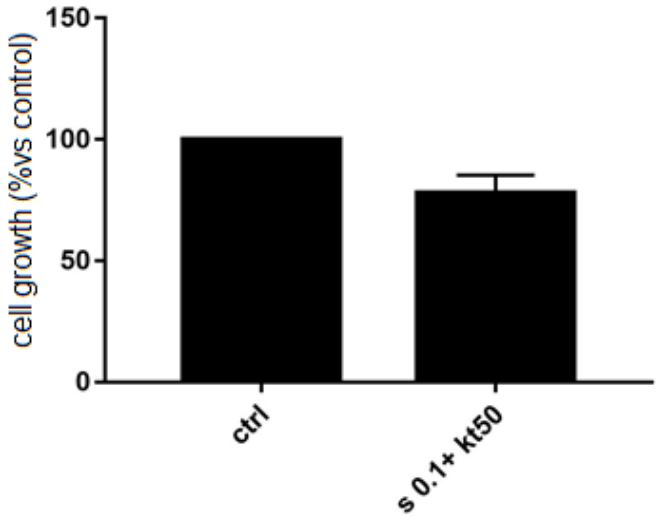

Figure 112 – Cell proliferation assay with simvastatin 0.1uM+ KT182 50nM.

Altogether these data demonstrated that while treatments alone do not produce relevant effect on cell proliferation, their combination leads to a proliferation decrease.

In addition to assess cell vitality, we carried out MTT assays in the same experimental conditions.

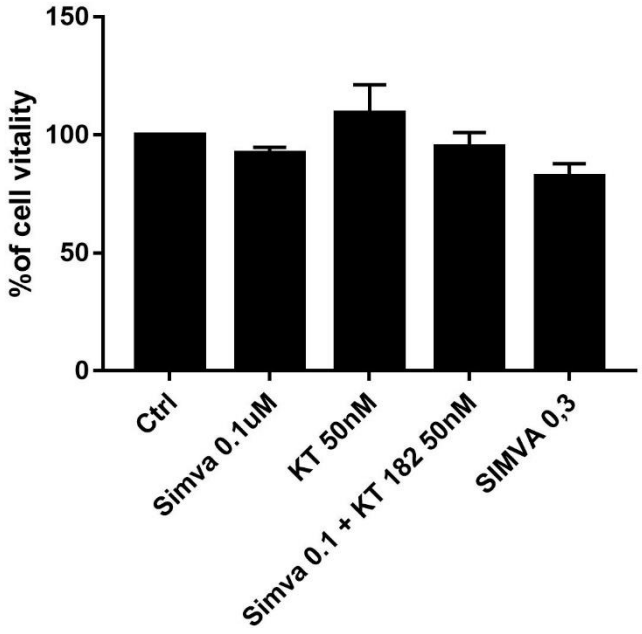

Figure 113 – Cell vitality of LM-16 cells under pharmacological treatment measured by MTT assay.

MTT assay demonstrated the absence of toxicity exerted by compounds.

We then evaluated the effect of the compounds on de novo cholesterol biosynthesis, through the incorporation of 14C acetate in cells and subsequent incorporation in cholesterol.

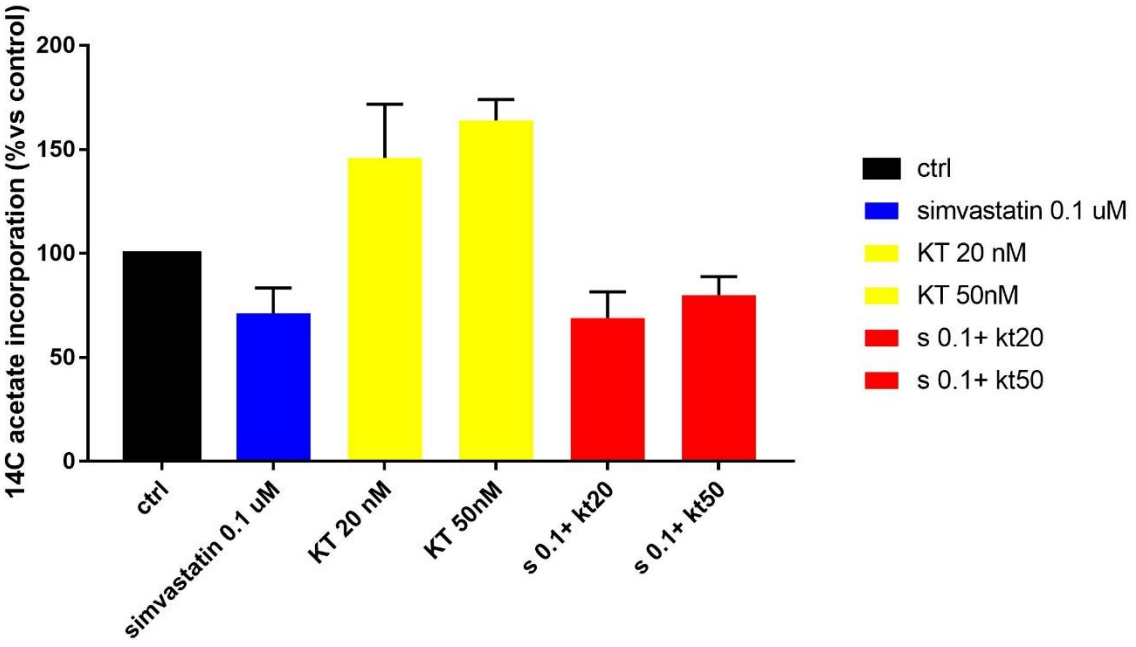

Figure 114 – Effect of KT182 and Simvastatin on de-novo cholesterol biosynthesis in LM-16 cells.

As expected, 0.1 µM of simvastatin reduces the biosynthesis of cholesterol by 28.7 % without affecting cell proliferation (as described in the previous part of this chapter). Interestingly we reported a dose-dependent increase of de novo cholesterol biosynthesis with KT182 of respectively 45.8% and 64%. When co-administered the effect of KT182 is reverted by the 0.1 µM dose of simvastatin, with a decrease of biosynthesis of 31 and 21,1%, respectively for 20nM and 50nM of KT182.

Altogether these data lead us to choose the dose range of the two compounds for further experiments: Simvastatin 0.1uM, KT182 50nM and their association, since we affected cholesterol homeostasis while not cell proliferation. We are planning to measure BMP levels and to pursue this aim Prof. E. Valoti and Dr V. Straniero of the Department of Chemistry of University of Milan are now synthesizing a deuterate BMP internal standard.

Dimensional Analysis

Once established the non-toxic doses of drugs for our experimental conditions and cell model, we aimed to evaluate the effect on the different EVs populations. We took in consideration only the 10K (microvesicles) and the 100K (exosomes) pellet, since we wanted to evaluate a possible "switch" among different EVs populations. We seeded 1x10^6 cells in 150mm plates and after 3+3days of incubation we isolated EVs following Thery's protocol. The first step was to evaluate differences in terms of EVs dimension. All measurements have been performed with Nanosight LM300 at the Istituto Nazionale dei Tumori.

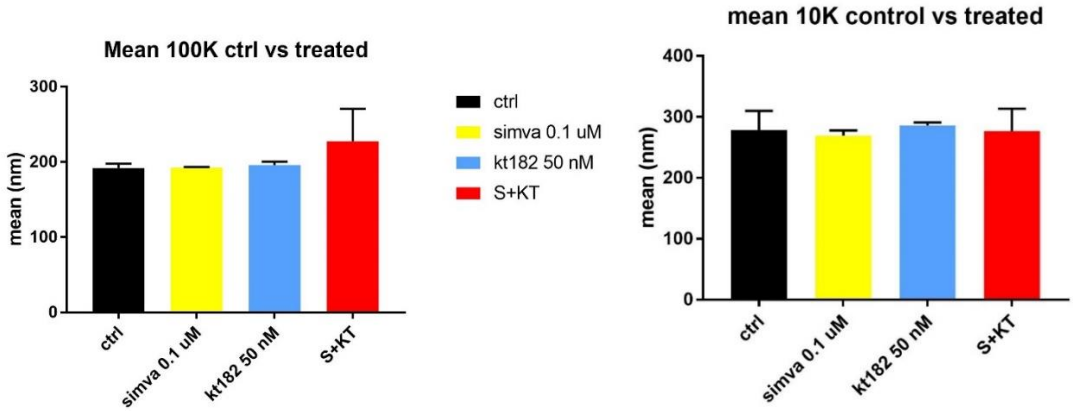

Figure 115 – Means of the diameters in nanometers of particles recovered from EVs derived from pharmacologically treated LM-16 cells, 100K exosomes (left) and 10K microvesicles (right).

As shown in the figures, we did not find any significant difference in terms of the mean of the hydrodynamic radius of Evs, both in 100K and in 10K groups. There is a small increase in simvastatin + KT 182 group, but this group is characterized by a high standard deviation.

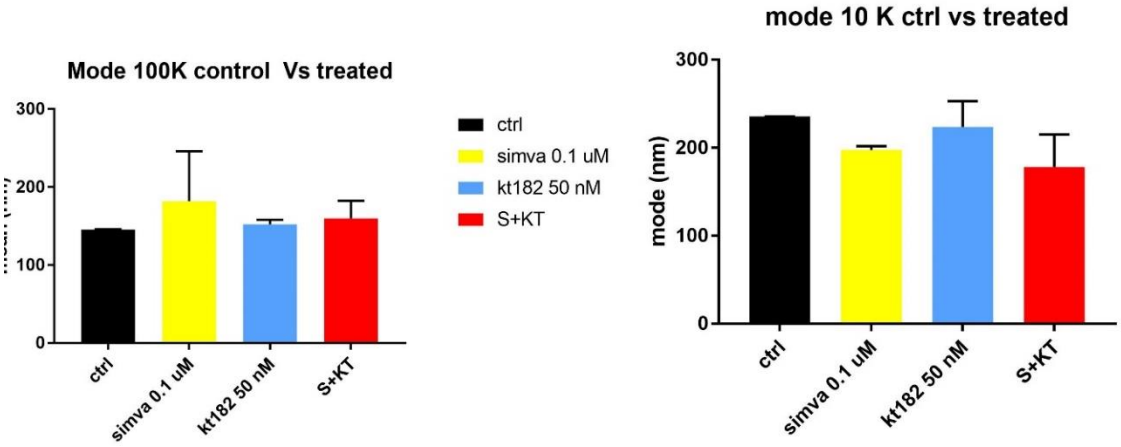

Figure 116 – Modes (most frequent particle) recovered from EVs derived from pharmacologically treated LM-16 cells, 100K exosomes (left) and 10K microvesicles (right).

We also measured the modes (e.g. most frequent particle in samples). Even in this case, we did not report any significant difference of the other dimensional value reported by Nanosight. These data corroborate the observation made by measurements of the mean: we can conclude that pharmacological treatments did not affect EVs dimensions.

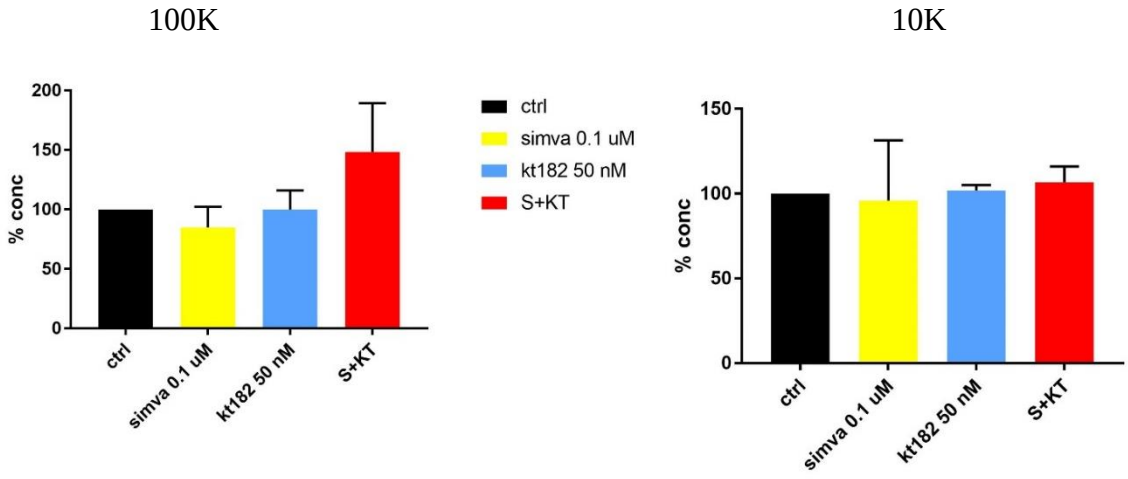

Figure 117 – % of increase (or decrease) of particle numbers vs controls, 100K exosomes (left) and 10K microvesicles (right).

In order to have more reliable and comprehensive data, we prefer to show the % of increase (or decrease) of particle vs controls, due to huge variations between the concentration

measurements with Nanosight among different experiments. In this case, assuming control as 100%, we did not report significant variations of particle concentration with simvastatin 0.1uM and kt182 50nM, both in exosomes and in microvesicles fractions. For as concern the association of the two treatments, we report an increase of particle concentration of 100K fraction.

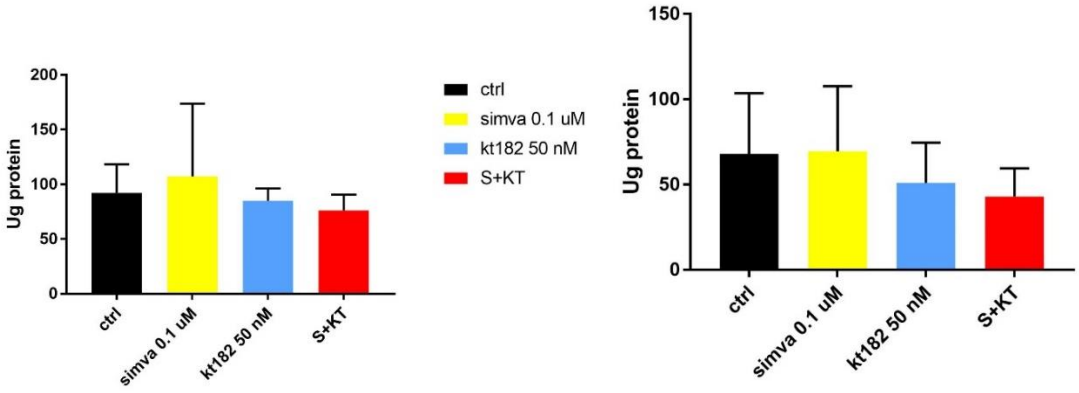

Figure 118 – Micrograms of proteins of EVs recovered from pharmacologically treated LM-16 cells, 100K exosomes (left) and 10K microvesicles (right).

In these graphs we are showing the µgrams of total protein measured with BCA assay. Also in this case, we did not find any significant variations in protein content after treatments.

Altogether after the cross-analysis of these data, we can conclude that pharmacological treatment with simvastatin 0.1uM and kt182 50nM, alone or together, did not significantly affect exosomes and microvesicles dimensions, concentration, and total protein content.

Confocal microscopy analysis.

In order to assess if treatments can modify the endolysosomal system structure/motility, we run an experiment with super resolution microscopy. We stained cells with DAPI (blue, nucleus) and antibodies for RAB7, a late endosomal marker (red) and Bismonoacylglycerophosphate (green).

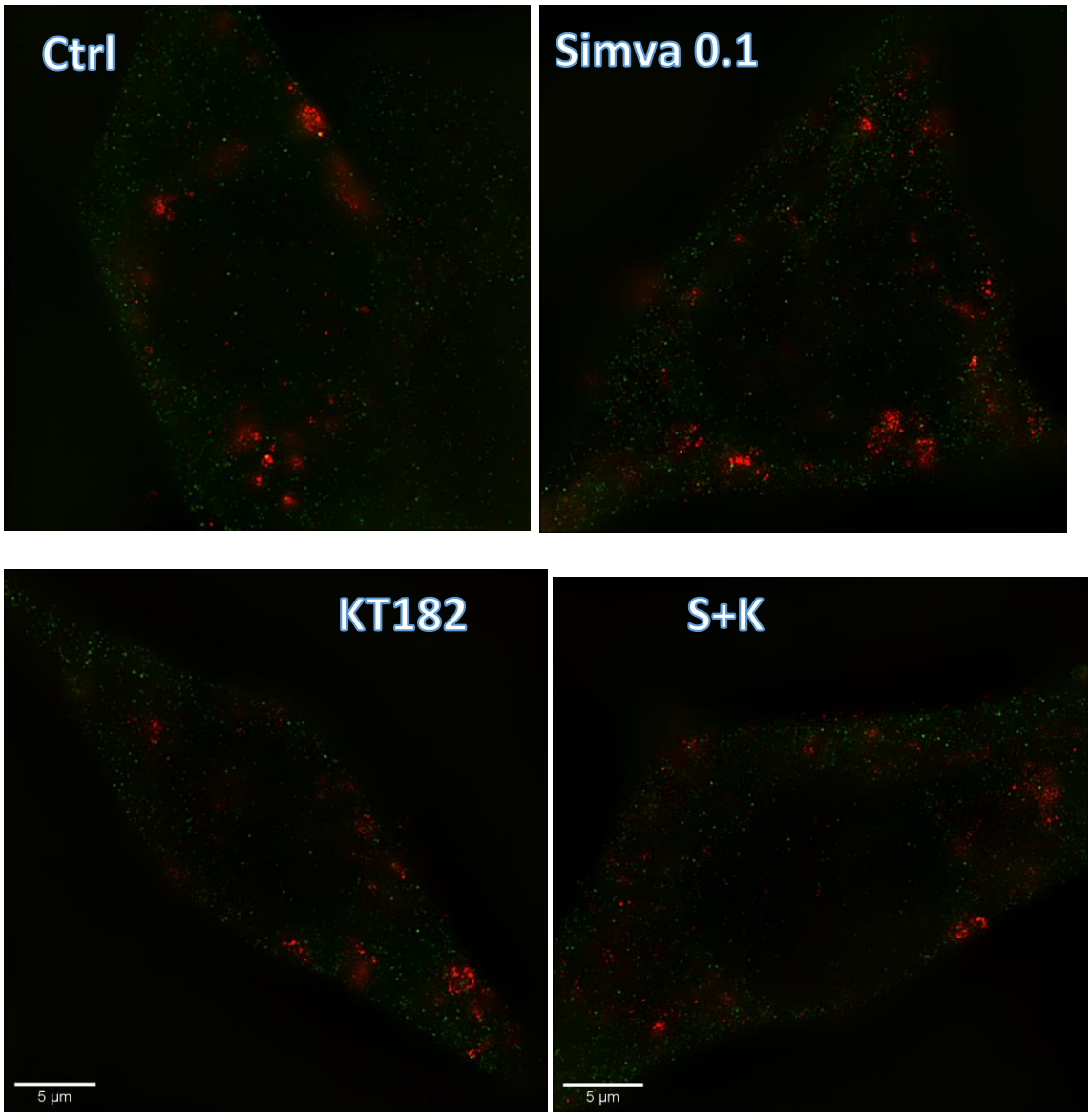

Figure 119 – Super resolution microscopy of pharmacologically treated LM-16 cells analyzed by Dr M. Ascagni.

Even if pictures are of difficult interpretation, we can conclude that treatments seem to not change the morphology of the cell and of the endosomal system visible in red.

In order to further investigate the effect of three different treatments on endolysosomal system we carried out a confocal microscopy experiment on LM-16 cells incubating them with three different antibodies reacting respectively with:

1) Rab7, Late Endosomal marker (red signal);
2) BMP, phospholipid, (green signal);
3) LAMP-1, Lysosomal marker (white signal).

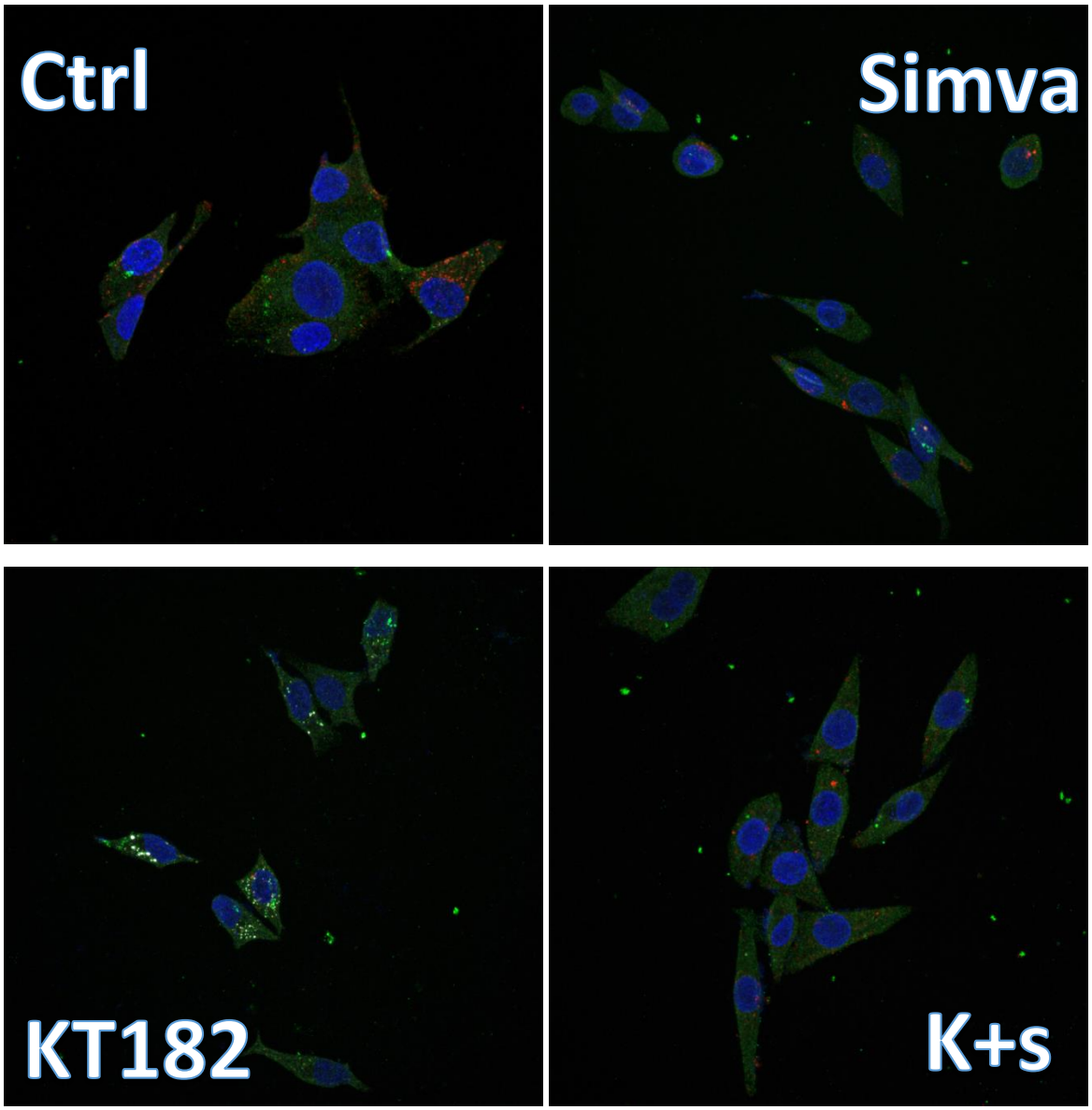

Figure 120 – Confocal microscopy analysis of LM-16 cell upon different pharmacological treatments.

Our first end-point was to evaluate the intensity of the green signal (BMP) in order to understand whether different compounds were able to affect BMP concentration in cells. Analysis performed by Dr. Ascagni unraveled no significant differences of BMP signal intensity among different conditions.

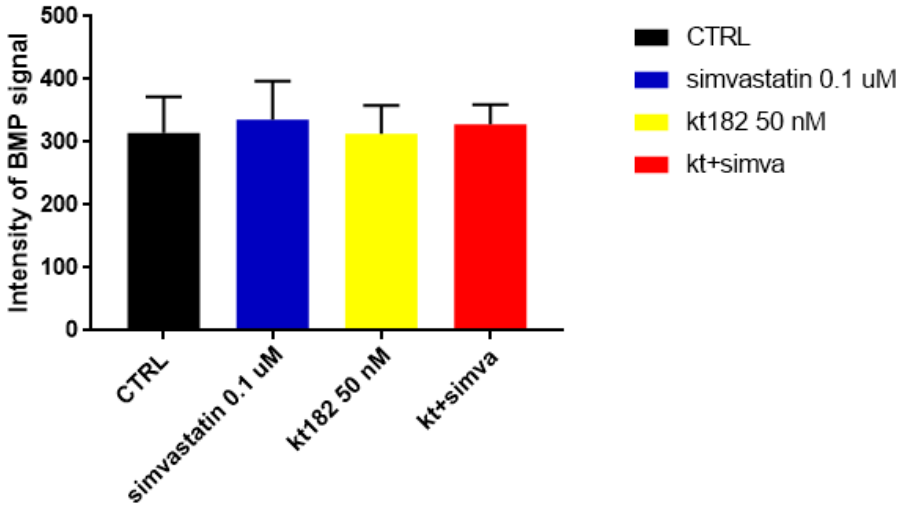

Figure 121 – Distribution of BMP signal upon different treatments in LM-16 cells unraveled no significant changes among different treatments.

Our second end point was to evaluate the co-localization of BMP with lysosomes. As shown in figure 122 lysosomal signal (white) is present only in KT182-treated cells; furthermore LAMP-1 seems to co-localize mainly with BMP. We then splitted signals to better visualize and evaluate the co-localization between BMP and LAMP-1.

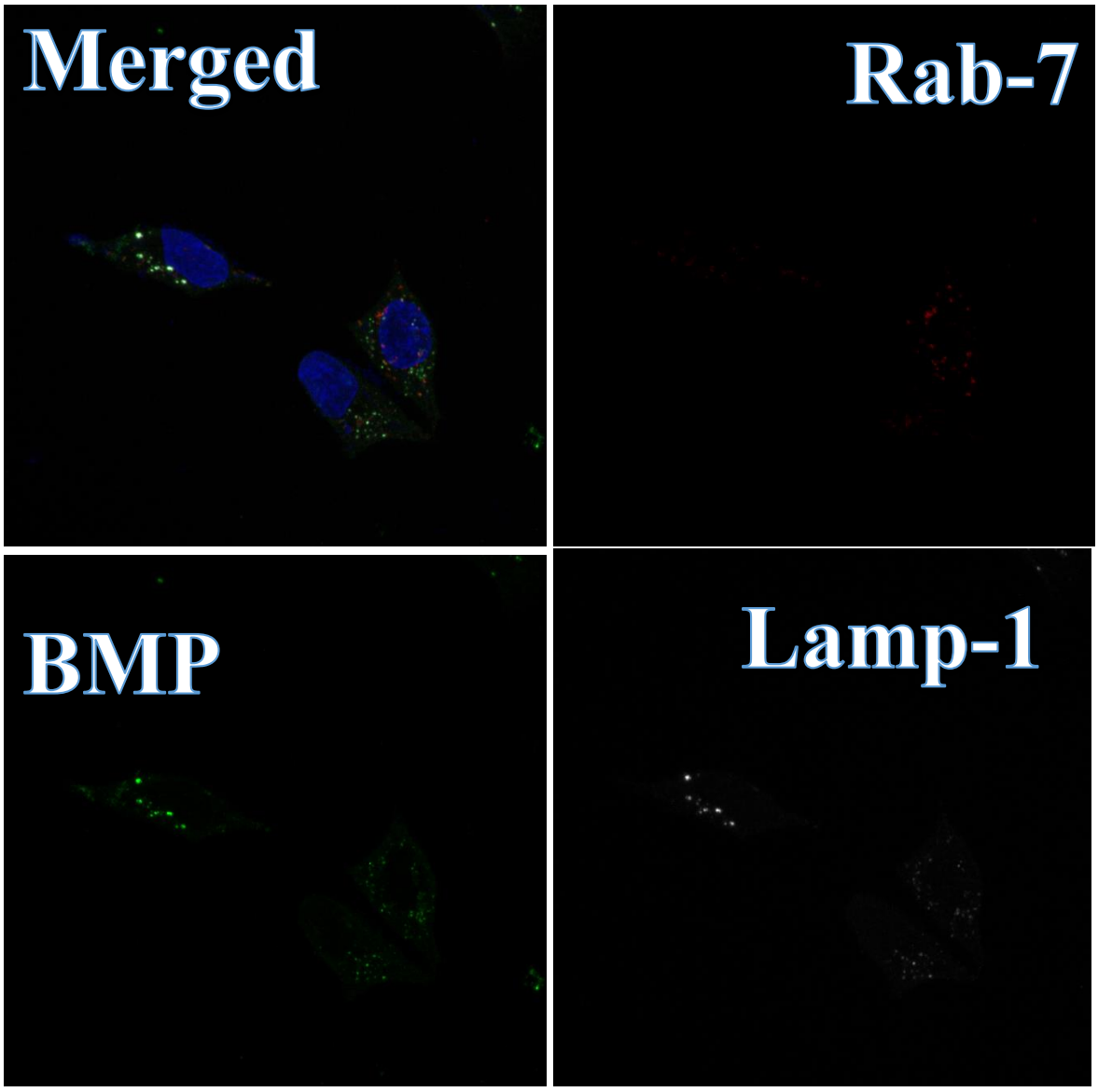

Figure 122 – KT 182 treated cells splitted signals.

As shown in figure 122 LAMP-1 mainly co-localizes with BMP, while no co-localization with other markers have been observed with Rab7.

In conclusion KT182 seems to re-organize the intracellular distribution of BMP without affecting its overall concentration, increasing BMP levels in lysosomes. Furthermore KT-182 strongly increases the expression of LAMP-1 lysosomal marker.

Proteomics and IPA analysis of EVs derived by pharmacologically-modulated LM 16 cells

After dimensional and total protein content characterization of EVs, we decided to perform a deep proteomic analysis (by mass spectrometry) in order to assess if a pharmacological treatment addressed to two important lipids, (simvastatin 0.1µM for cholesterol and KT182 50nM for BMP) may modulate EVs in terms of:

1) release (altered number of secreted EVs;

2) functionality through changes in protein content (or cargo).

Only few literature data utilize simvastatin to unravel differences in term of secreted EVs, whilst no data are present on behavior of EVs after BMP pharmacological modulation. As reported previously we performed a deep dose-finding for simvastatin concentration, since we wanted only to inhibit biosynthesis of cholesterol without affecting protein prenylation, while we chose the proper KT182 concentration after assessing the toxicity of the molecule by MTT and proliferation assays.

Equal concentration of protein lysate has been injected in mass spectrometry and increases or decreases of protein levels vs controls were reported. We found a total of 1293 in the 100K, and 1192 in 10K fraction.

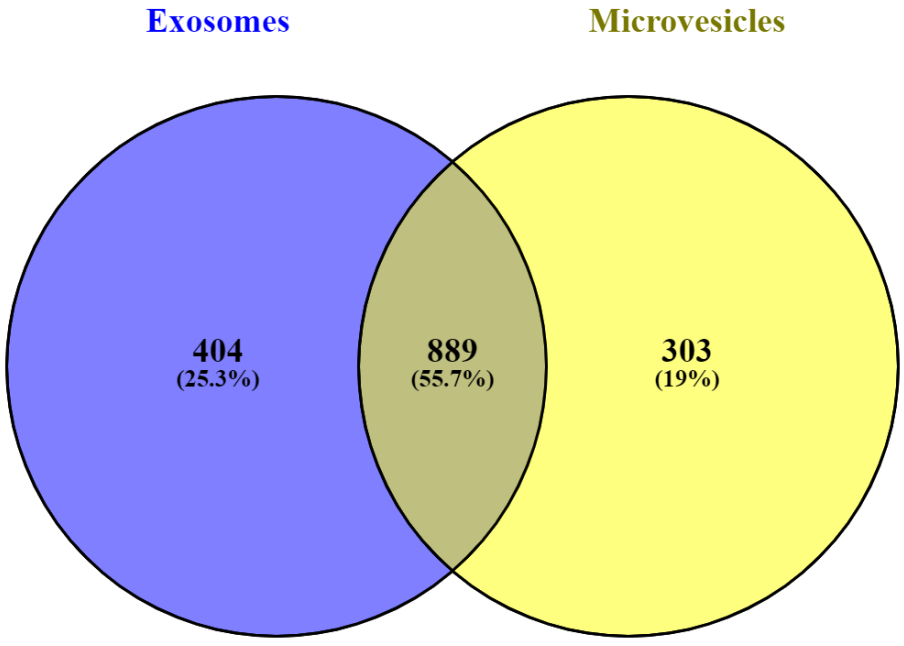

Figure – 123 venn diagram of proteins recovered in 10 and 100K fractions.

	100K	**100K**	**10K**	**10K**
	Significantly upregulated	Significantly downregulated	Significantly upregulated	Significantly downregulated
Simvastatin 0.1uM	65	6	36	27
KT182 50nM	60	4	46	17
Simvastatin+kt182	41	7	24	29

Table 18 – Proteins significantly upregulated/downregulated found in 10K and 100K fractions after pharmacological treatment of parental cells.

As shown in table 18 we found proteins significantly upregulated ($p>0.01$) comparing treatments vs controls, while less proteins were significantly downregulated. Afterwards we utilized Ingenuity Pathway Analysis in order to evaluate all the cross-links, connections and meaning of the total different protein pattern.

a) Effect on 100K

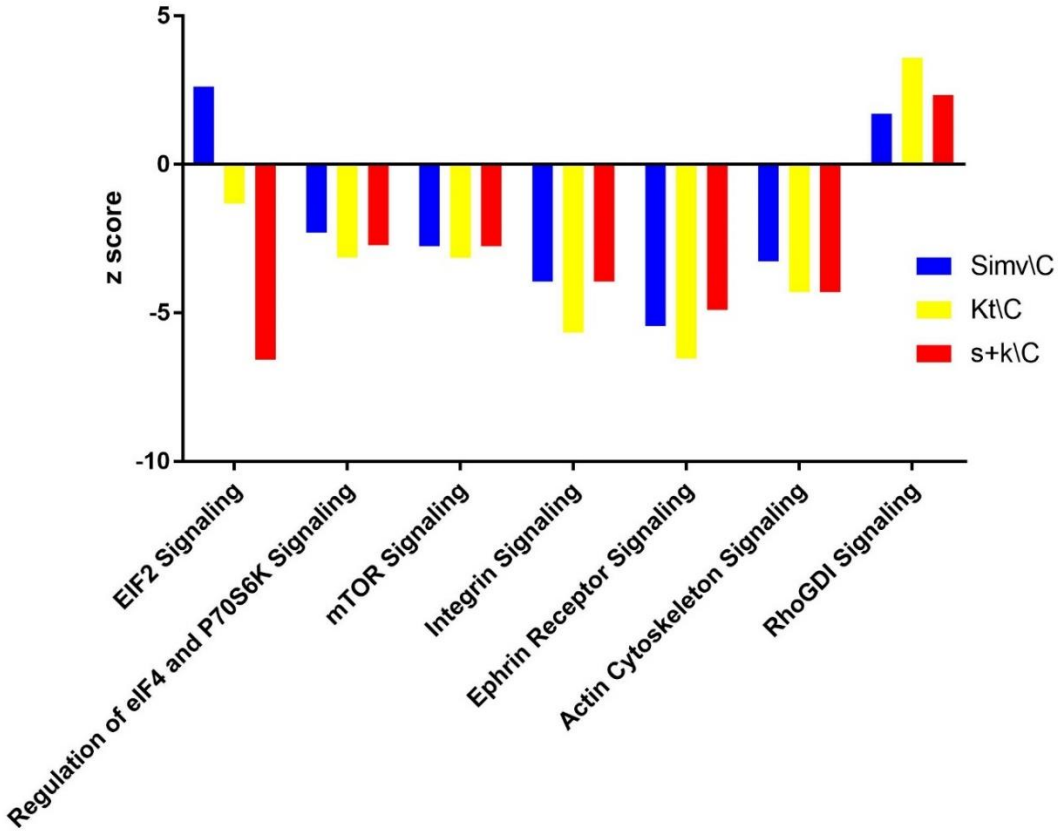

Figure 124 – Downregulated and upregulated pathways after IPA analysis of proteomics of 100K pellet. All data are expressed as variations of z scores of treated vs ctrls.

Figure 116 summarizes the effect of different treatments on 100K of IPA canonical pathways through the expression of the z score which reflects an overall predicted activation/inhibition state of the biological function (negative values: inhibited; positive values: activated). All treatments seem to go towards the same direction, except for EIF2 signaling, whose activity increases with simvastatin, decreases with kt182 and dramatically dropped with both treatments. Interestingly rhoGDI signaling is the only function increased by treatments.

b) Effect on 10K

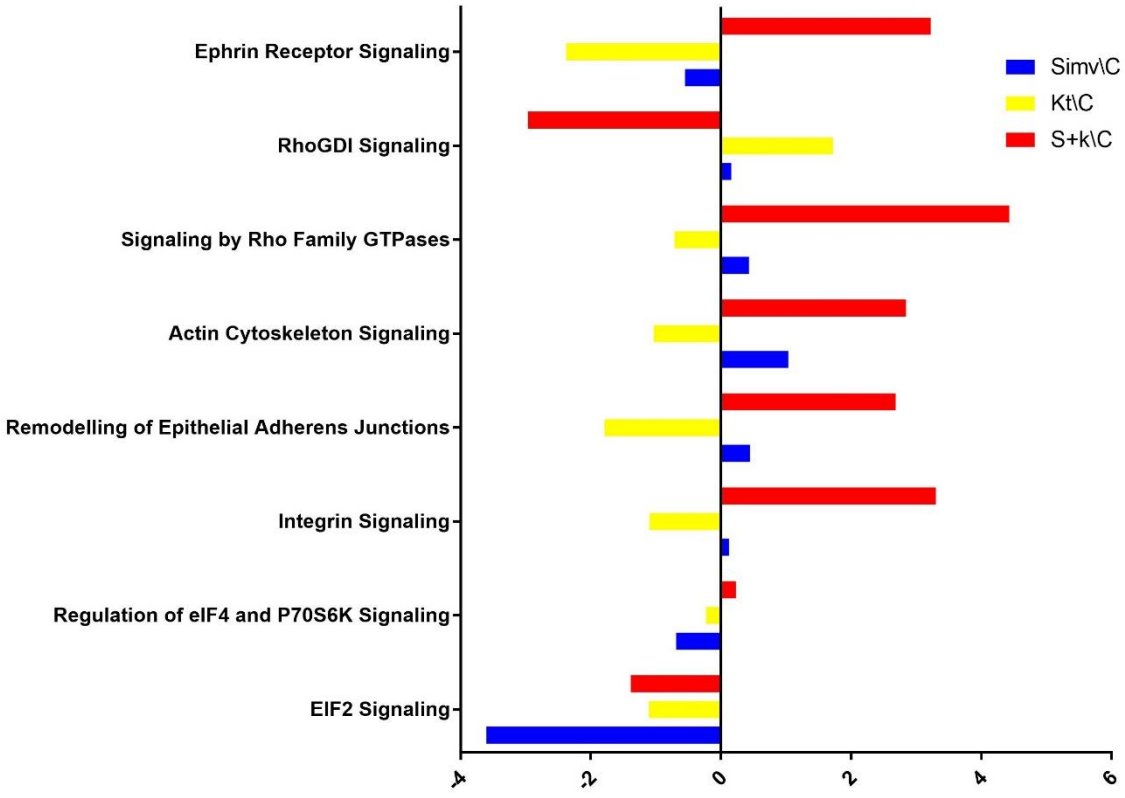

Figure 125 – Downregulated and upregulated pathways after IPA analysis of proteomics of 10K pellet. All data are expressed as variations of z scores of treated vs ctrls

Treatments affect 10K and 100K z scores of canonical pathways in different ways. For as concern 10K ephrin receptor signaling is downregulated by treatments alone while is increased with the combination, while RhoGDI has an opposite behavior (increases in treatments alone and decreases with the combination. Signaling by Rho Family GTPases, actin cytoskeleton signaling, remodeling of epithelial adherens junctions and integrin

signaling increased their functionality with simvastatin and combination while decreased with kt182. We reported a very small increase of the z score of Regulation of eIF4 and P70S6K with the combination and a decrease in KT182 and simvastatin group. EIF2 signaling is downregulated in all the 3 different conditions.

c) Comparison between effects of treatments in 10K and 100K group

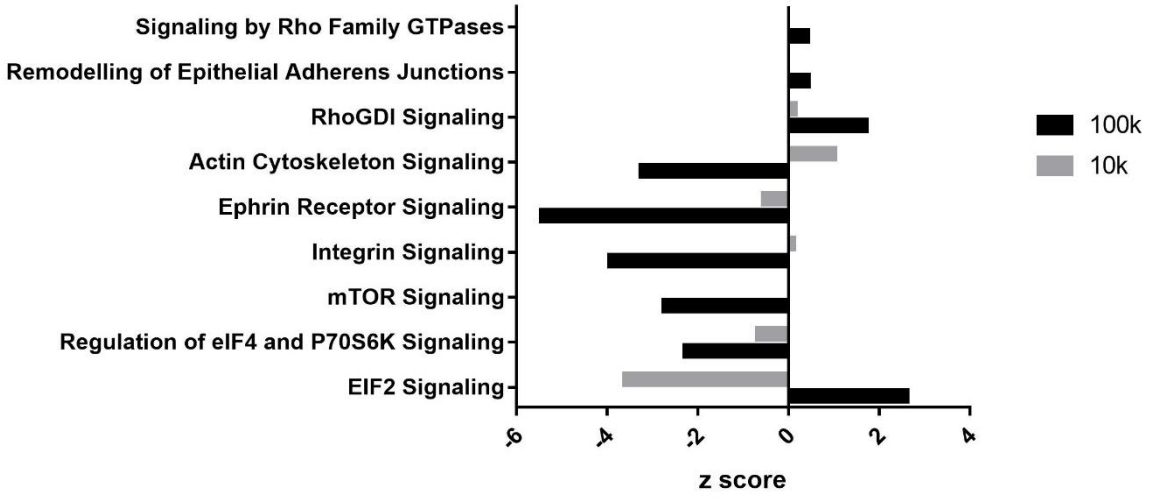

Figure 126 – Comparison between simvastatin treatment in 10K and 100K.

It is also interesting to assess the differences of the activity exerted by the treatments on the two different fractions (microvesicles for 10K and exosomes for 100K). For example EIF2 signaling is really different between the two groups; simvastatin indeed increases EIF2 functionality in 100K while decreases it in microvesicles group. Actin cytoskeleton signaling has an opposite behavior, with a decrease in 100K and an increase in 10k group. Regulation of eIF4 and p70S6 is decreased mostly in 100K rather than in 10K while mTOR signaling is absent in 10K and downregulated in 100K pellet. Integrin signaling and ephrin receptor signaling is downregulated in 100K and little upregulation is recorded in 10K. RhoGDI, remodeling of epithelial adherens junctions and signaling by RhoFamily GTPases are increased in 100K but not in 10K.

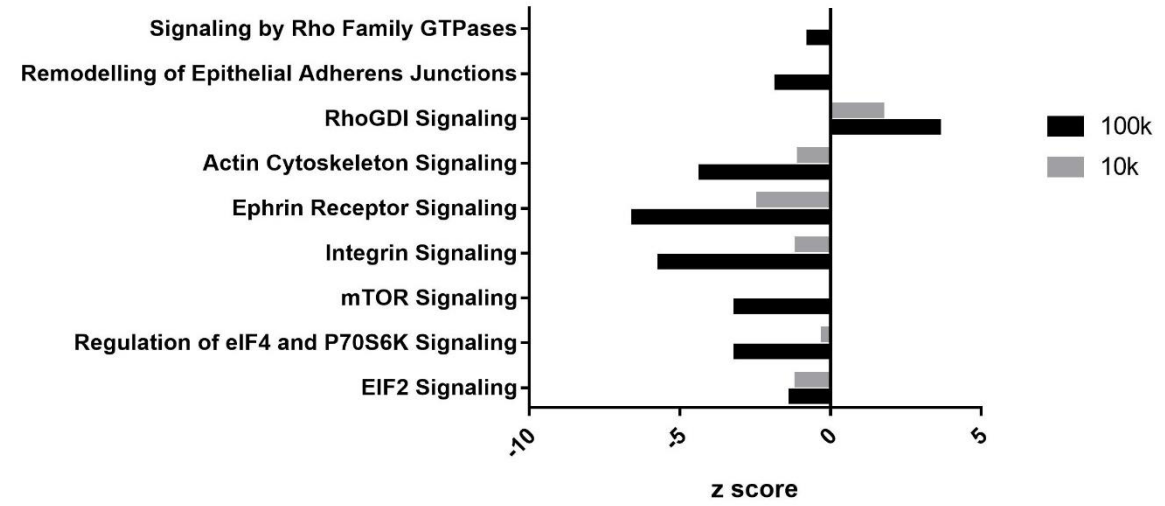

Figure 127 – Comparison between kt182 treatment in 10K and 100K.

KT182 seems to alter EVs functionality in a more homogeneous fashion compared to simvastatin (figure 120). Almost all functionalities are downregulated (except for RhoGDI signaling). We have to mention that even if functionalities go towards the same direction, the entity the downregulation is really more evident in 100K group than 10K one.

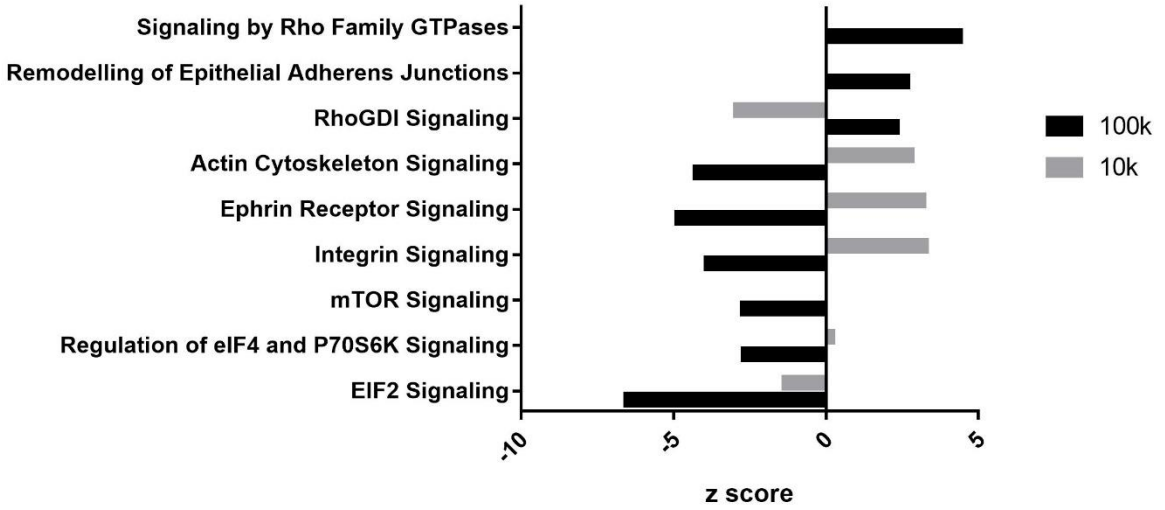

Figure 128 – Comparison between simvastatin + KT182 treatment in 10K and 100K groups.

The association of the two drugs differently alters functionalities of both 100K and 10K. We reported an opposite behavior with integrin signaling, ephrin receptor signaling and actin cytoskeleton signaling, with an increase in 10K and a decrease in 100K. RhoGDI signaling is increased in 100K while it is decreased in 10K. Signaling by Rho Family GTPases and

remodeling of epithelial adherens junctions are increased in 100K while drug treatments does not affect 10K. EIF2 and EF2 signaling is downregulated in both groups.

In addition to these data, we performed an analysis on IPA molecular and cellular functions.

100K		Simva/C	KT/C	S+KT/C
cellular movement				
migration				
cell growth and proliferation				
cell death				

Table 19 – IPA molecular and cellular functions in 100K. Blue=downregulated, orange = upregulated vs ctrls.

As reported in table 19 we found that treatment of parental cells with treatments leads to the secretion of a 100K pellet which possesses reduced capacity to enhance cellular movement, migration, cell growth and proliferation and cell death, excepted for association of the two treatments, which promote cell death.

10K		Simva/C	KT/C	S+KT/C
cell death (cell survival inhibition				
protein synthesis				
cellular movement				
cellular assembly and organization				

Table 20 – IPA molecular and cellular functions in 100K. Blue=downregulated, orange = upregulated vs ctrls.

Proteins contained in 10K lead to different IPA molecular and cellular functions compared with 100K. In this case simvastatin and KT182 increase cell death through the decrease of proteins involved in the promotion of cell survival while protein synthesis is downregulated by all the treatments. Cellular movement cellular assembly and organization are decreased by the drugs alone and increased with the association.

Distribution of up and downregulated canonical EV markers

As we did for the 5 fractions described in the previous chapter of this thesis, we compared the distribution of the canonical EV markers in 10 and 100K. We first made a comparison

between the protein list obtained by the analysis of both samples and the top 100 canonical EV markers of www.vesiclepedia.org; afterwards we took in consideration only those ones which were significantly up/down regulated.

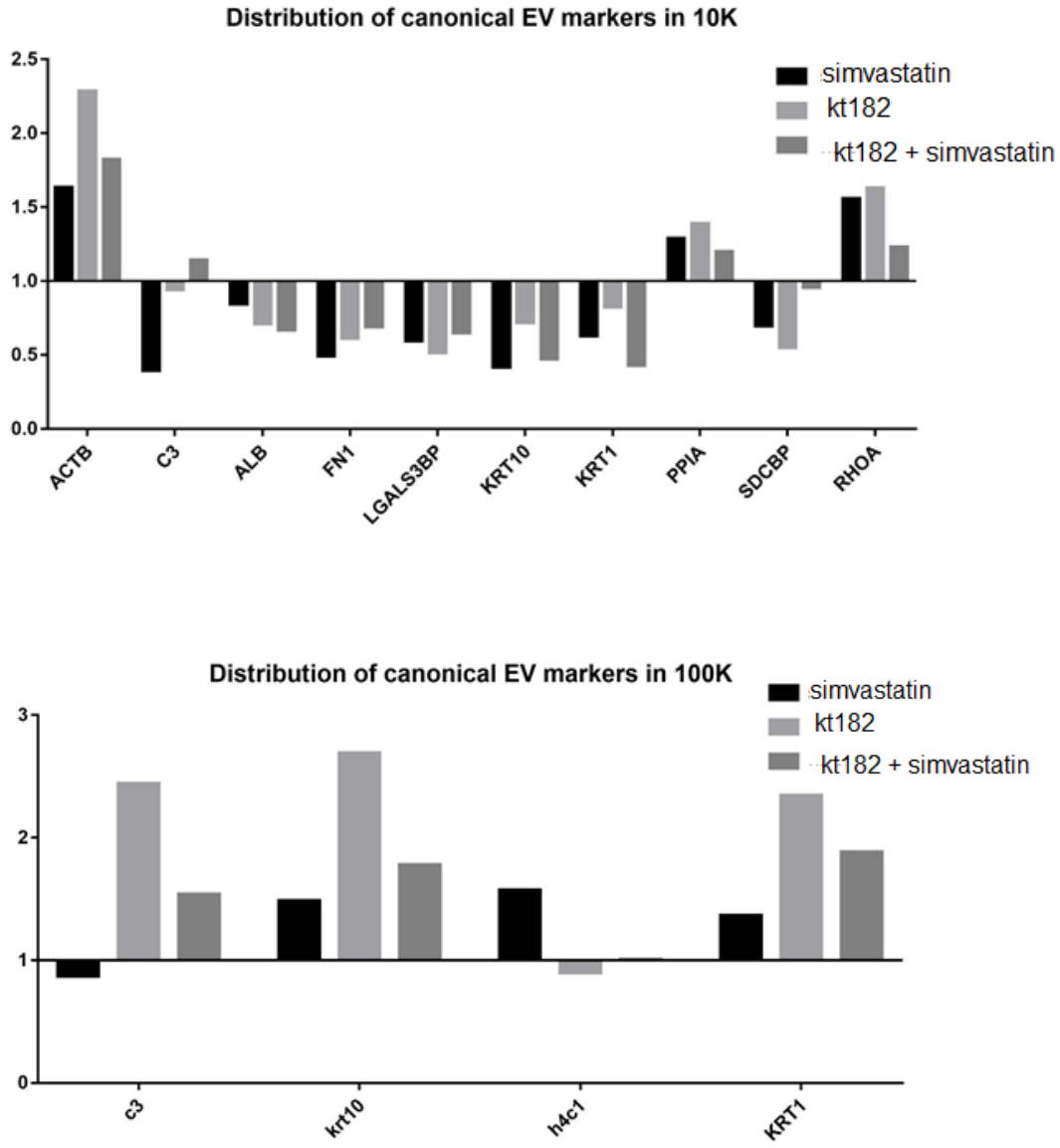

Figure 129 – Fold increase/decrease of common canonical EVs markers from www.vesiclepedia.org recovered from cell media of pharmacologically treated LM-16 cells. we took in consideration only significantly up/downregulated proteins.

Canonical markers of EVs as TSG101, CD9, CD81, ALIX were found in both fractions, and their expression is not significantly altered by both treatments.

Discussion

EVs are small bilayer vesicles produced in physiological and (mostly) in pathological conditions, which can be classified according to their dimension and origin [80], while exomeres are still very little characterized to draw any conclusion and to assess if they belong to extracellular vesicle family. EVs represent definitively one of the "hot topic" in modern science; they are indeed very attractive since they can be utilized as excellent biomarker [81] of pathological states, drug delivery systems [82] [83] or they can have also a therapeutic role [84] in some cases. Their role in disseminating pathological conditions from one cell to another has been demonstrated during last years, thanks to the characterization of the nucleic acids, lipids and proteins contained in EVs and involved in several pathological signalling [15]. All these properties make EVs as actors of the development of various pathologies, particularly cancer, making them attractive pharmacological targets [81][85][86][87]. Unfortunately, although a huge number of publications can be found, they are very heterogeneous and variegated in terms of results and method utilized for EVs isolation, leading to an uncertain knowledge about their characterization and functionality. Particularly the presence of a huge heterogeneity of EVs isolation and characterization methods impairs the possible comprehension and development of their pharmacological and pharmaceutic development. Several works[88] [18] and guidelines [7] aimed at EVs dimensional characterization and categorization but with lack of accordance. Indeed it was first reported that EVs were divided in Exosomes (50-150nm) and Microvesicles (50-1000nm), which can be isolated with two different ultracentrifugation steps, the so called 100K for exosomes and 10K for microvesicles [18].

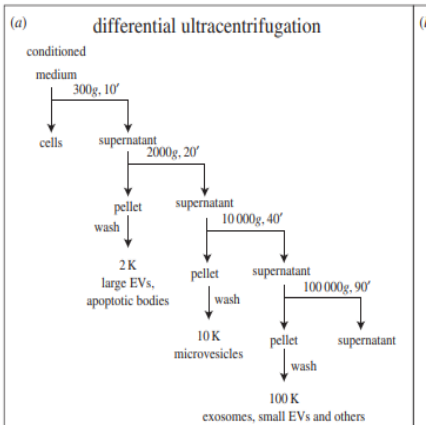

Figure 130 - Canonical method of isolation by Thery 2006 [18].

MISEV 2018 instead proposed another kind of size-based classification, in which EVs were divided in “small EVs” (sEVs) and “medium/large EVs” (m/lEVs), with ranges defined, for instance, respectively, < 100nm or < 200nm [small], or > 200nm [large and/or medium][7]. Zhang work after Flow Field Fractionation of EVs proposed a classification in small-Exosomes (exo-s) 60-80 nm, large-exosomes (exo-L) 90-120 nm, Microvesicles minor than 1000nm and exomeres, which are a new population, still unknown if part of EVs family, with a diameter of 35nm.

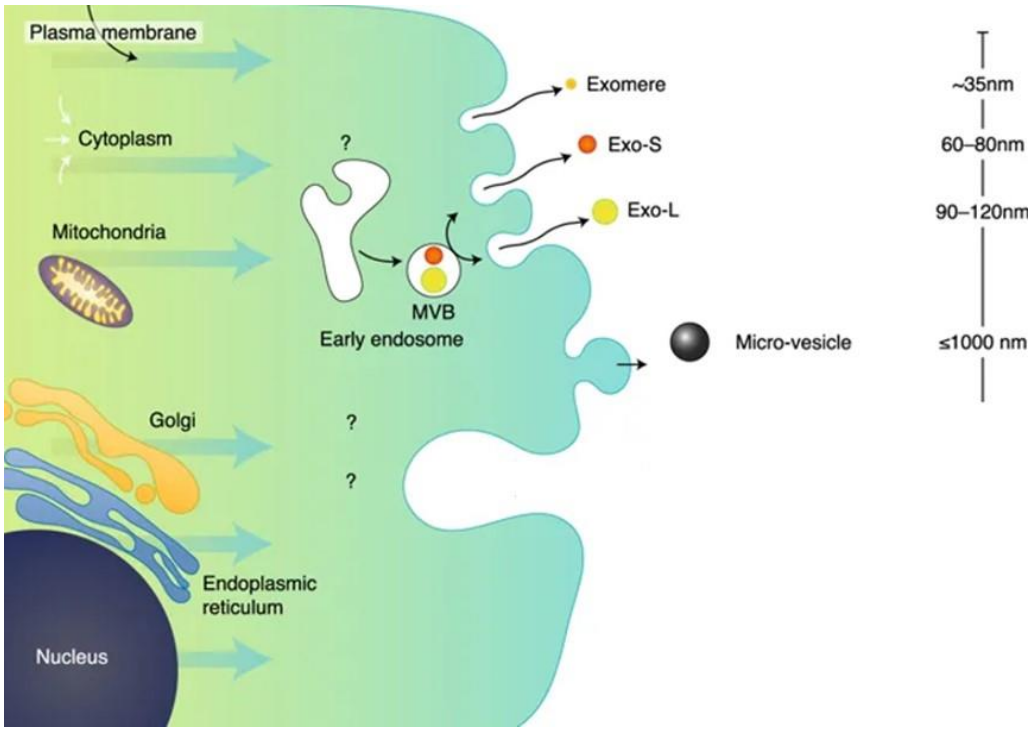

Figure 131 – Dimensional classification of Extracellular Vesicles [20].

As previously mentioned, one of the most important problem is the lack of accordance for EVs classification, since overlap in physical and chemical characteristics makes very difficult their correct characterization. In addition, the absence of a standardized technology for EVs isolation, and characterization impairs knowledge in EV research. From an “operative” point of view of this PhD project we improved the separation method developing the “sequential ultracentrifugation” rather than utilizing the canonical “differential one”. We developed our method utilizing Livshits’ tool [68], which allowed us to set the more appropriate centrifugation time and g forces to obtain a pellet which could contain particles of the desired dimensional interval. We tried first the dimensional interval (as proposed by MISEV) of min 50, 50-100, 100-150, 150-200 and >200. Analyzing the fatty acids profile

of the 5 different fractions, we did not report significant differences among the SFA/UFA ratios of the 50-100, 100-150 and 150-200, leading to two different conclusions:

1. The three aforementioned populations must be considered one
2. The dimensional cut offs are set incorrectly, since we did not find significant differences among three populations (50-100, 100-150, 150-200).

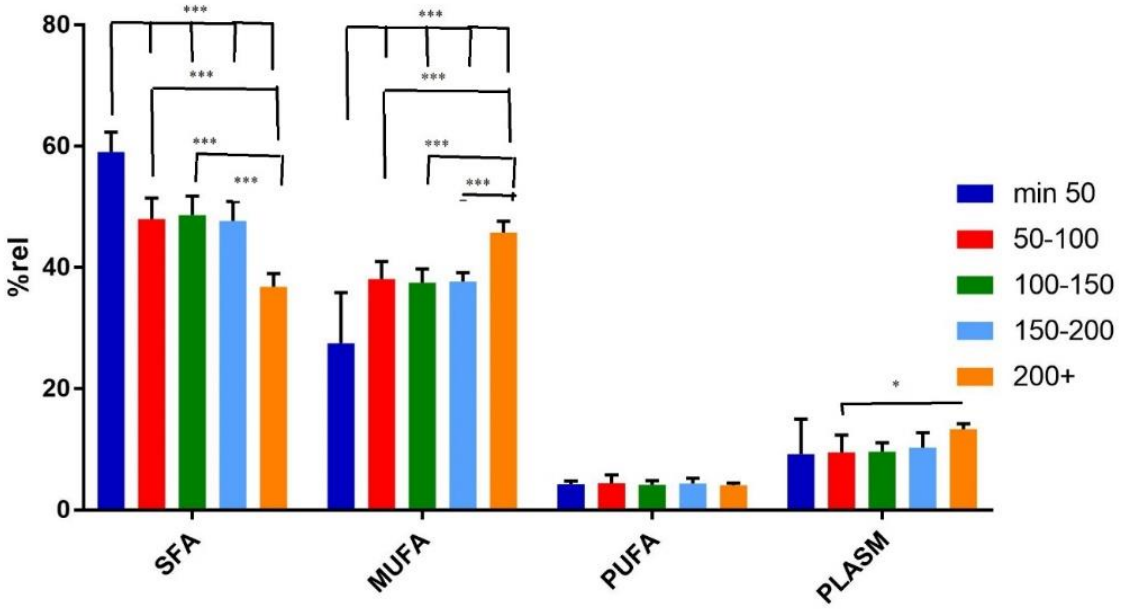

Figure 132 – relative % of saturated, monounsaturated and polyunsaturated fatty acids and plasmalogens among different fractions isolated by ultracentrifugation according to MISEV guidelines.

For these reasons, we changed the centrifuges set-up to obtain particles according with Zhang's observation [19].

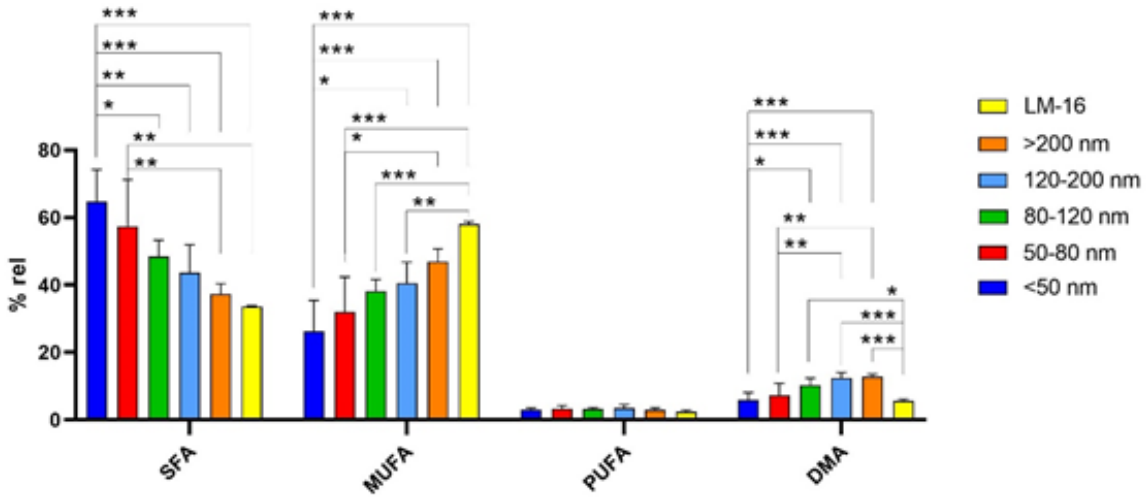

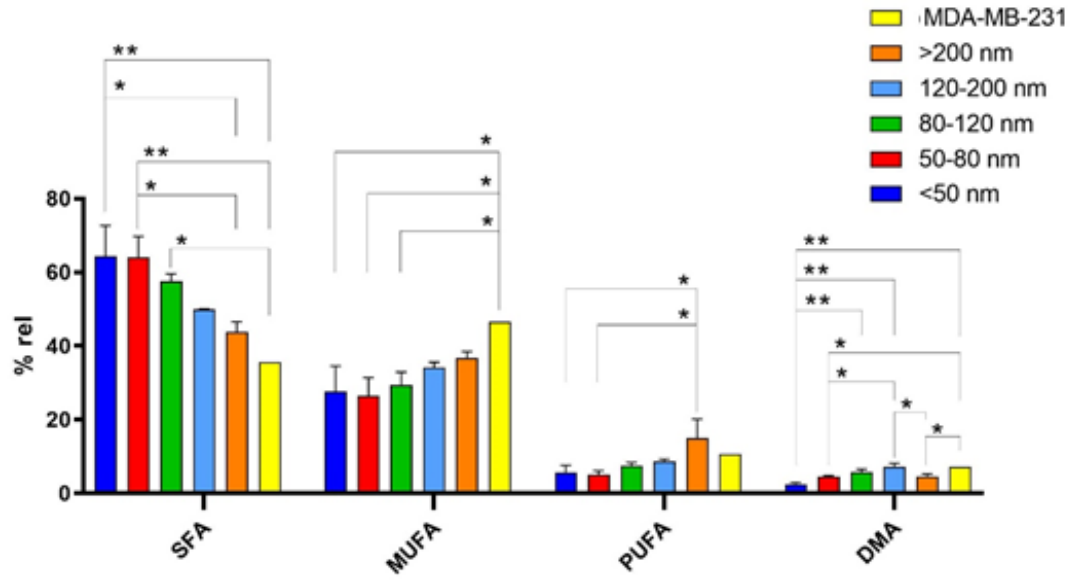

.

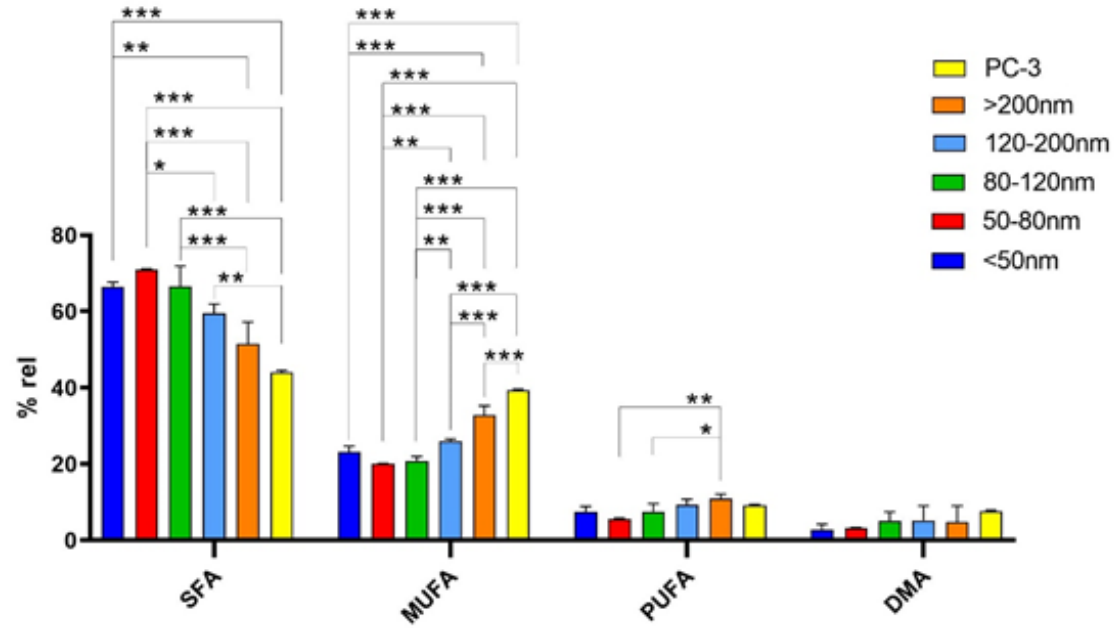

Figure 133 – Relative % of saturated, monounsaturated and polyunsaturated fatty acids and plasmalogens among different fractions isolated by ultracentrifugation according to Zhang's observations in three different cell lines.

Despite with different %, as expected, the striking and common feature was the relative, significant and continuous increase of saturated fatty acids from big particles toward smaller ones, counterbalanced by a decrease in unsaturated ones. These data have been further

confirmed in EVs derived from two other tumoral cell lines, MDA-MB231 and PC-3 concluding that differences in % rel of fatty acids among different EVs population can be considered as a common and new EVs characteristic.

In addition our results indicated that parental cell fatty acid lipid profile is more similar in bigger vesicles than in the smaller ones. It was already known that EVs were more enriched in saturated fatty acids compared to cells, but it was still unknown that there are "some vesicles that are more saturated than other ones". These differences can be reflected in different EV behavior in biological fluid and in their interaction with recipient cells due to their different rigidity and electronegativity. EVs size can be also important to ascertain their origin: it is known indeed that Multi Vesicular Bodies, which are the intracellular compartment in which EVs are generated, are larger than 250 nm diameter and they contain 50-80 nm diameter internal vesicles [21]. Therefore is it possible to exclude EVs of a dimension larger than 80 nm as "intracellular-derived EVs"?

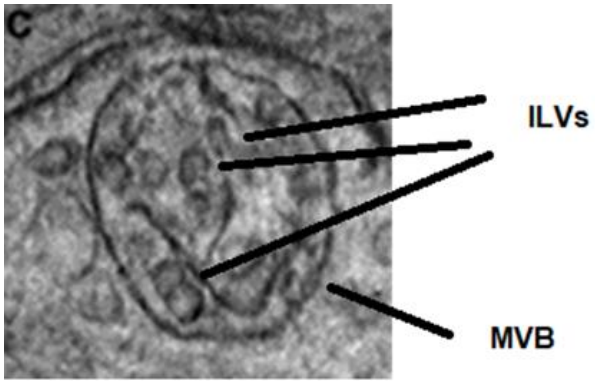

Figure 134 – Intraluminal Vesicles inside a multivesicular body.

To further prove the goodness of our separation method, we processed samples with Zetasizer, Nanosight, electron microscopy plus atomic force microscopy for exomeres. Both Dynamic Light Scattering analyses made with Nanosight and Zetasizer unraveled the presence of bigger particles compared to the theoretical ones. This can be due to the fact that both these systems measure the hydrodynamic radiuses of each particle. Indeed each particle has an electric charge over its surface, which attracts water molecules, which provoke a different refraction of the light leading the instrument to measure the real radius of the particle plus that of the water coupled to the bilayer surface. In contrast EM makes particles splattered on a copper surface leading to their deformation in some way. In order to have a more reliable and as much as possible correct analysis, in my period is Oslo at the Norwegian

Institute for Cancer Research, Research group of A. Llorente, we tried to compare the 3 aforementioned methods.

Which is the correct dimension?

. Comparison among three different classic method for EVs dimensional characterization shows that it is really tricky to dimensionally characterize EVs.

	nanosight	zetasizer	Electron microscopy
Min 50	89,94	116	28,45
50-80	85,65	102,80	48,50
80-120	108,17	139,50	47,25 (mean 62)
120-200	140,55	232,28	221,57
200+	254,13	498,8	n.d.

Table 21 – Comparison among different measurements methods of EVs derived from PC3 cells

As reported in table 21, a dimensional shift from high to low centrifugations speed and time is clearly shown but the results (even if performed on the same sample) are very different depending the method utilized. We also reported these results to Alfatest SRL, Italian distributors of Nanosight and Zetasizer asking them the reasons of the differences of the results obtained by their instruments. This should be due to an enhanced focus of Nanosight of the particles around 100nm. In addition, Nanosight technology is more indicated to measure monodisperse samples rather than polydisperse one (e.g. EVs from cell media or biological fluids which contains a broad amount of particles of different physical and chemical characteristics). In contrast Zetasizer software and algorithms are more prone to measure differences among very dimensionally different fractions, thus we decided to utilize it for LM-16 analysis, which has been directly performed by Dr Moretto of Alfatest SRL. Differences between theoretical and real radius can also be due to intrinsic limitations of the centrifugation method; the first issue is the EVs density. We indeed take in consideration the mean density value of that can be found in literature [68], even if we do not know if all

particles of a given size are characterized by the same density. In addition, centrifugation is not a very clean method for EVs isolation due to the co-isolation of smaller particles than those of the desired dimensional interval and protein contaminants of the cell media.

We have also to report that the smallest fraction (exomeres) is more visible by Electron and Atomic Force microscopy since their dimensions are below the detection limit of DLS technologies. EVs correct size determination is of paramount interest since it can explain important features of small vesicles; it has been demonstrated that nanoparticles behavior (e.g. synthetic lipidic nanoparticles which mimic extracellular vesicles) in bloodstream is dependent on their dimension. Larger particles (microscale) possess higher probability of localizing to vessel walls as well as non-spherical nanoparticles compared to spherical ones [82]. Small nanoparticles are able to better cross the capillary walls easily than larger ones. Interestingly in vitro studies demonstrated that cells only take up nanoparticles of 10-60 nm and that smaller NPs better internalize [82].The other big issue is the absence of methods that nowadays allow us to proper count the vesicles.

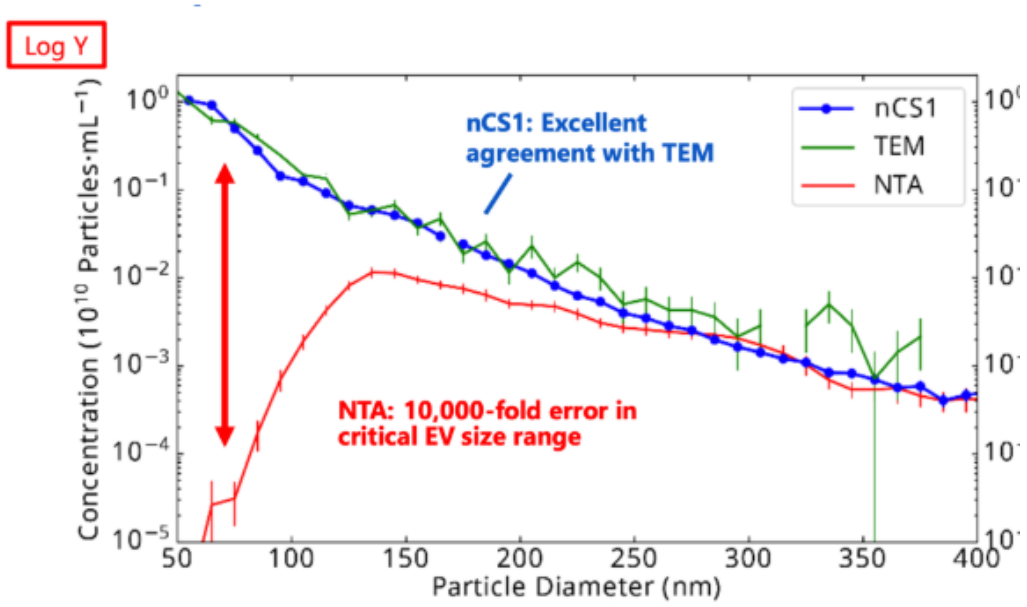

Figure 135 - EV sample measured by Cryo-TEM, NTA and Microfluidic Resistive Pulse Sensing (MRPS or "nCS1").

EV sample measured by Cryo-TEM, NTA and Microfluidic Resistive Pulse Sensing (MRPS or "nCS1") unraveled that the Nanotracking particle analysis (Nanosight) data under-reports concentration by 10,000-fold in the canonical range of small exosomes. This error leads to the impossibility to count the vesicles, and therefore to normalize any data regarding the fractions. It is indeed imperative to find a quick, easy and affordable method normalize each

data (cholesterol, phospholipids, total protein content etc). Up to now it is quite impossible to normalize data for total protein content since we do not know if microvesicles, large/small exosomes and exomeres are equally or differentially enriched in total protein content. For these reasons, to overcome the problem, we analyzed:

1) The relative % of fatty acid of each fraction since it is independent of normalization, so the differences among all fractions are true

2) The relative % of the proteins involved in molecular pathways, independently of their expression rates for proteomics of the 5 fractions.

Once we were sure of the presence of particles of different size in all fractions we performed their proteomics (in biological triplicates). We first carried out COlorimetric NANoplasmonic assay in collaboration with prof P. Bergese of University of Brescia; thanks to this assay we confirmed the absence of free protein contaminant in our samples: therefore we are confident that each protein found by proteomics is contained in EVs or expressed on their surface. Fractions differ by the presence of:

1) A different number of proteins, respectively 697, 819, 1079, 1621 and 1654 from F1 (smaller) to F5 (bigger);
2) Common and unique proteins, respectively 97, 17, 14, 141 and 252 from F1 to F5.

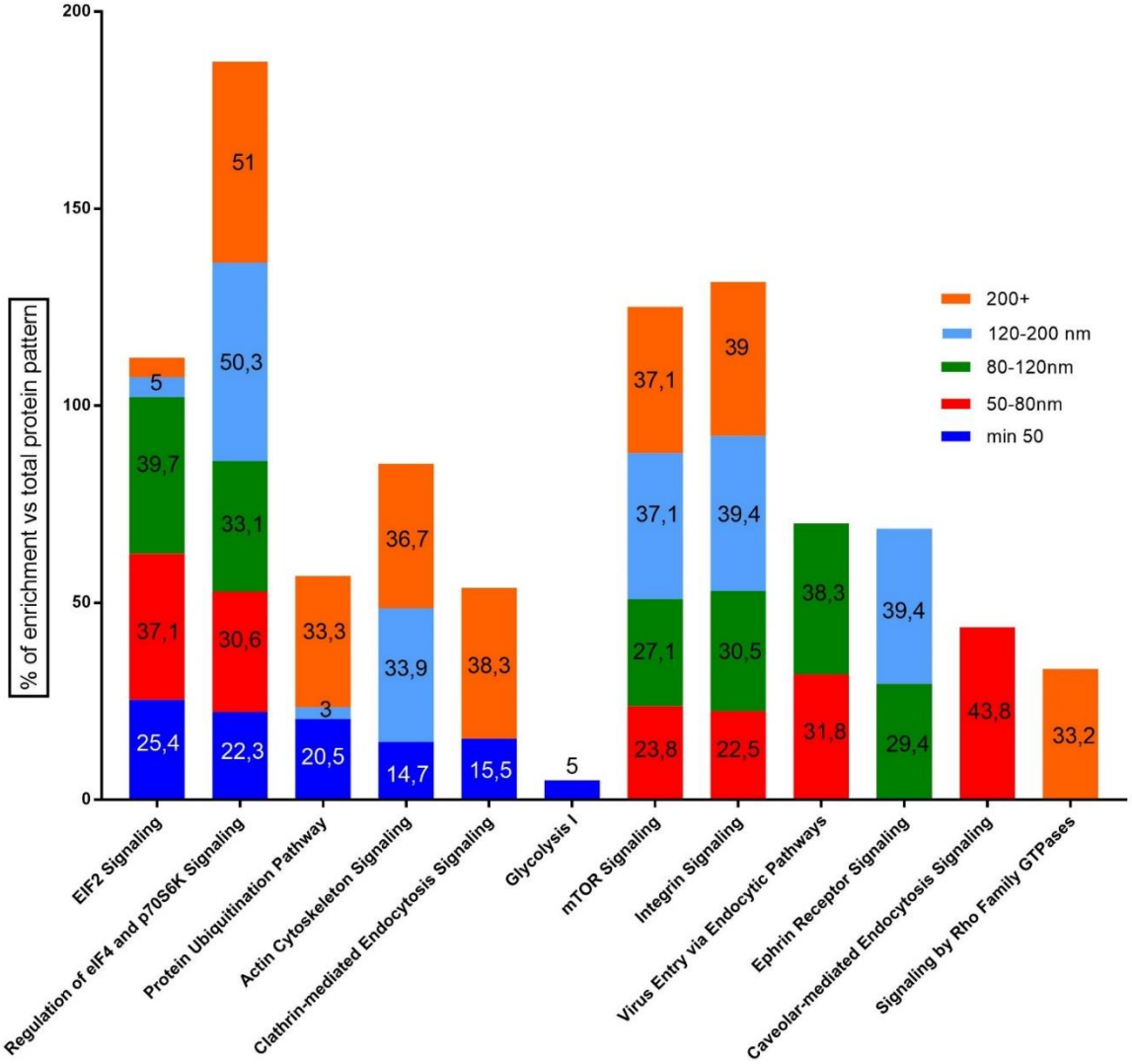

Figure 136 – % of enrichment in proteins which encode from a determined function vs total protein pattern for each fraction. Data are independent of protein quantity recovered in each fraction.

Protein patterns were quite surprising. Each fraction seems to be enriched differentially in pathways involved in various signaling. Proteins codifying for glycolysis seem to be present only in exomeres. This is in line with previous observations which stated that exomeres show an enrichment in metabolic enzymes and above all the glycolytic ones [19]. mTOR and integrin signaling have similar profiles of enrichment for each fraction. Particularly mTOR is dysregulated in several types of cancer, and maybe its action is driven by extracellular vesicles [89] [90]. Integrin signaling is enriched in F-4 and in F-5, meaning that these two fractions may be more prone in disseminating metastasis by the adhesion through integrins to extracellular matrix [85][91]. Particularly in melanomas integrins are associated with metastasis and cell migration [92]. The ephrin-Eph signaling system is a bidirectional cell–

cell communication device mediated by membrane-tethered ligand–receptor interactions. Ephs and ephrins function in many different physiological processes, including boundary formation and axon guidance, as well as pathological processes such as cancer [77]. Signaling by rho family GTPases is found only in F-5, which is the fraction composed by Microvesicles. Our data corroborates previous findings in literature[78]. Particularly the small GTPase RhoA triggers a specific pathway for the biogenesis of microvesicles in various human cancer cells. Inhibition of the activity of this pathway blocks microvesicles biogenesis cancer cells and prevents oncogenic transformation in cell culture as well as tumor growth in mice [79].

One of the most important and interesting feature of EVs is their internalization into recipient cells [93]; a better understanding of the mechanisms involved in their internalization (both physical and biochemical) can be useful to:

1) develop promising drug delivery system which are able to target only desired cells;
2) impair the uptake of cancer-derived EVs in healthy cells.

EVs are recently emerging as high-complexity drug delivery systems; indeed integrate knowledge about EVs biology may have important clinical insights in manufacturing synthetic EVs-like particles [6]. Design and manufacturing challenges can be overcome by exploring EVs structures for the transport of molecular cargo throughout the body. However, the potential of all EVs as delivery tool it is still uncertain because of the aforementioned challenges in their isolation and characterization.

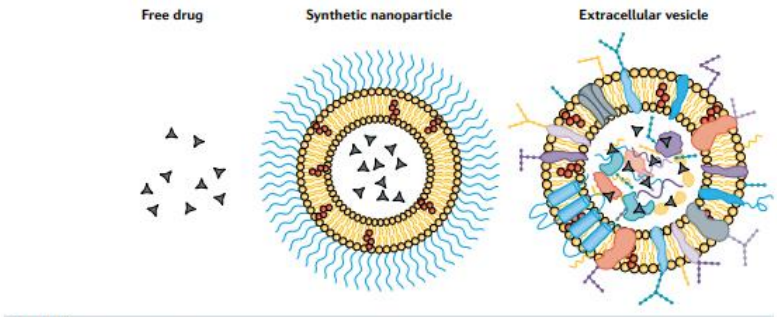

Complexity	+	++	+++
Variability	+	++	+++
Manufacturing expertise	+++	++	+
Safety	+	++	++
Circulation time	+	+++	++
Multifunctionality	+	++	+++

Figure 137 from [6] *- Characteristics of free drugs, clinically approved synthetic nanoparticles and extracellular vesicles. Low (+) medium (++) high (+++).*

As clearly seen in figure 129, EVs are much more complex structure compared to classical small lipid nanoparticle. Indeed while synthetic nanoparticles are composed by phospholipids, cholesterol and PEG, EVs express several proteins on their surface which are involved in signaling and internalization processes [80].

One of the most important problems related to synthetic nanoparticles, as demonstrated by clinical trials is their hepatic clearance from the circulation [94]. A great example of engineered EV was made by Alvarez-Erviti et al., whose research group conduced a very fascinating study [95]. To obtain immunologically inert vesicles, they harvested bone marrow cells from mice with a homogenous major histocompatibility complex haplotype; immature dendritic cells produce indeed EVs devoid of T cell activators. With this strategy, the rapid clearance of exogenous nanoparticles in liver and spleen is strongly reduced. Targeting was achieved by engineering the dendritic cells to express Lamp2b fused to the neuron-specific RGV (rabies viral glycoprotein) peptide. To demonstrate the targeting of these EVs, they loaded them by electroporation with GADPH siRNA. Intravenously injected in mice, RVG-modified exosomes silenced specifically GADPH in neurons, microglia and oligodendrocyte in the brain, while they did not observe aspecific uptake in other tissues.

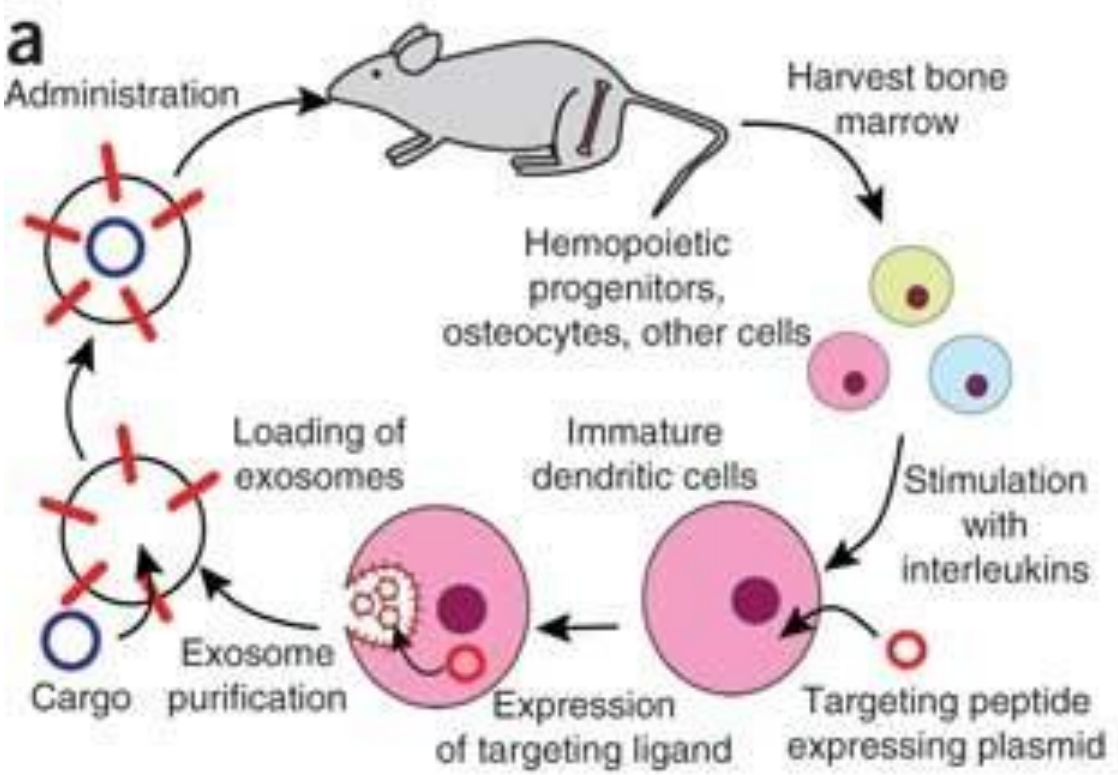

Figure 138 – Schematic representation of Alvarez- Erviti and colleagues' experiment.

In another study conducted in mice by the group of Luo W et al., they tracked CD63+ cardiac EVs demonstrating that in physiological conditions they accumulate first in thymus, testes, lung and kidneys with minor uptake by liver [96], suggesting that knowledge and characterization of lipids and proteins of natural-released EVs can give very useful information to build synthetic particles to be used in clinic as efficient drug delivery systems, with a defined organotropism, which would let therapeutic compounds to concentrate only in its action site.

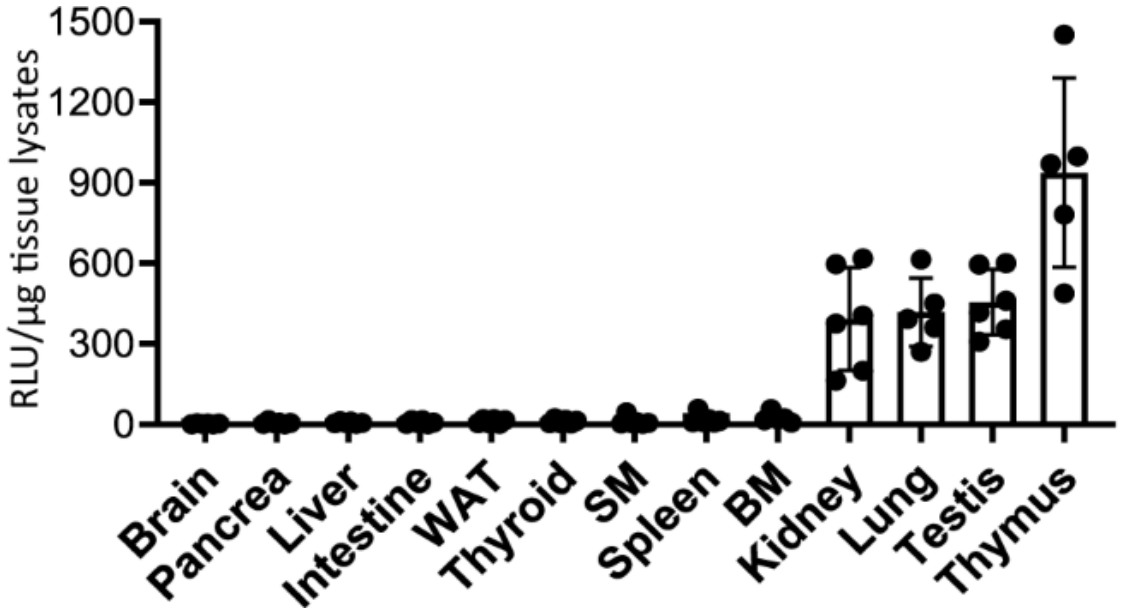

Figure 139 - Tissue uptake of cardiomyocyte-derived exosomes has been detected by luciferase activity in 13 mouse organs. WAT: White adipose tissue. SM Skeletal muscle. BM Bone marrow [96].

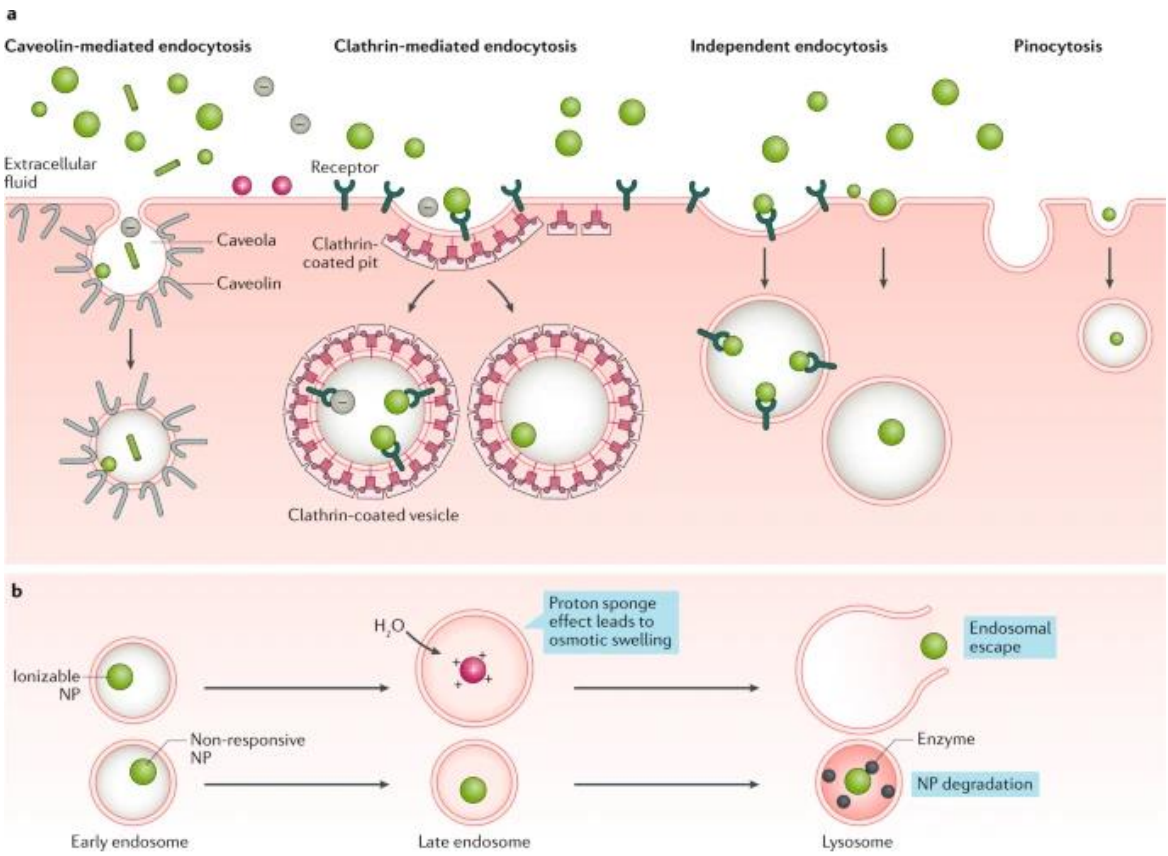

Figure 140 from [82] - *Different endocytosis mechanisms for lipid nanoparticles (NPs) (B) Inside the cell, NPs remain trapped within endosomes. To achieve functional delivery, most NPs must escape from these compartments before they acidify. NPs can remain trapped and are destroyed by lysosome acidity and proteolytic enzymes.*

As unraveled by IPA analysis we found that caveolar endocytosis pathways is preferentially exerted by F2 fraction, while clathrins seems to be involved in internalization of F1 and F5 (smallest and biggest fraction) suggesting different mechanisms of internalization for each fraction of a given size. In a world in which nanotechnologies are increasing in importance (e.g. covid vaccines are nanoparticle-based) it should be useful to ascertain if different sizes of EV are correlated with different mechanism of internalization, (caveolae for bigger vesicles while clathrins for small ones as reported in our findings). A possible final goal should be to replicate EVs functionality in exosome-like synthetic nanoparticles inserting proteins encoding for caveolae or clathrins according to their dimension. In addition the increase of the %rel in saturated fatty acids from the biggest to the smallest fraction may explain different EVs features. Saturated fatty acids make vesicle thicker and rigid probably conferring different physical behaviour in bloodstream and in interactions with recipient

cells. The increased membrane rigidity of EVs could be important in ensuring that EVs are not easily degraded and are readily able to circulate in biological fluids [29].

Another interesting protein found only in F5, the EEA-1 (early endosome antigen 1), a proteic marker for early endosomes. It is really intriguing to speculate about the presence of this protein in only in F5 fraction, that contains bigger vesicles which are used to derive from plasma membrane budding and not from the endosomal system. It is possible to speculate a role of early endosomes also in microvesicles (plasma derived vesicles) biogenesis?

In addition, we aimed to characterize the canonical exosomal marker contained in the fractions. To achieve this purpose we took in consideration the top 100 markers of www.vesiclepedia.org. All canonical markers overlap among the fractions, except CD63, a tetraspanin which is associated to small vesicles [66] and is found in F2 fraction in our experimental conditions, leading to the conclusion that a revision of all markers contained in EVs is imperative.

After EVs characterization, we decided to modulate two important lipids fundamental for EVs biogenesis and fate, as extensively reported in the chapter "Lipids as pivotal component for EVs Biogenesis and Functions". We aimed to understand if a pharmacological modulation of these important actors of EVs life could be useful and therefore considered as scientific tool to better understand EVs functionality and a pharmacological tool for cancer treatment. At the beginning of the project, since these data were not available, the question was: do pharmacological modulation of BMP metabolism and Cholesterol biosynthesis lead to dysfunctional EVs or to reduced/increased biogenesis? In order to investigate about this question, we decided to utilize simvastatin to lower cholesterol biosynthesis and KT182 to impair ABHD6 activity, which is the enzyme contained in late endosomes responsible of the 90% of BMP hydrolysis. To pursue this goal we run the de-novo cholesterol biosynthesis, coupled with cell proliferation. In our experimental conditions a concentration of 0.1µM of simvastatin administered for 3days in FCS10% + 3 days w/o serum was able to reduce de-novo cholesterol biosynthesis by 30% without affecting cell proliferation. In the same experimental conditions, we reported an increase of more than 50% of cholesterol biosynthesis upon KT182 50nM treatment. Unfortunately it was not possible to assess the synthesis of de novo BMP, neither its concentration, since internal standard was not available, so the dose finding of KT182 was made taking in consideration the first dose in

which we did not report any proliferation inhibition. Thanks to our collaboration with Prof. E. Valoti, they are now synthetizing it for future analyses.

Confocal Microscopy Analysis of treated cells with antibodies reacting with BMP (late endosomal marker), LAMP-1 (Lysosomal Marker) and Rab-7 (Late Endosomal Marker) showed us important results. Quantification of BMP signal did not unravel any significant variation of BMP levels among the different treatments; remarkably LAMP-1 signal is present only in KT-182 treated cells which display an increased number of Lysosomes compared to control and to the other conditions. Furthermore LAMP-1 signal co-localizes with BMP, indicating a different intracellular distribution of the phospholipid, since overall concentration did not change significantly.

Lysosomes play an important role in exosome biogenesis and release as suggested by several evidences; for example alkalinization of lysosomal pH with bafilomycin A or Chrloroquine impairs lysosomal function increasing the release of EVs, as well as in lysosomal storage diseases as Niemann Pick Type C in which an increased release of EVs was reported due to the impairment of lysosomal functionality [97]. It is well known that EVs secretion is increased in cancer as demonstrated both *in vivo* and *in vitro* [98] thus a drug which is able to increase EVs degradation may be considered as a new and alternative therapeutic strategy.

After pharmacological treatment we isolated EVs; in this case, since it was a preliminary study, we only isolated the two canonical fractions 10K (microvesicles) and 100K (exosomes), to have a general idea about the effect of these drugs and therefore cholesterol and BMP modulation on EVs. Surprisingly even if we found an increased LAMP-1 expression in KT182 treated cells we did not report any significant change in EVs number both in 100K and 10K EVs as previously reported raising different questions; we strongly believe that further studies are still needed to evaluate the effects of the compounds on the degradation of different EVs populations.

After EVs dimensional characterization we performed proteomics analysis, followed by IPA analysis since it would be indeed very fascinating and intriguing if a modulation of two lipids, without affecting cell proliferation and vitality and EVs size and counts could alter their protein pattern and therefore their functionality. Several proteins in both fractions were significantly up- and down- regulated in different proteins compared to control.

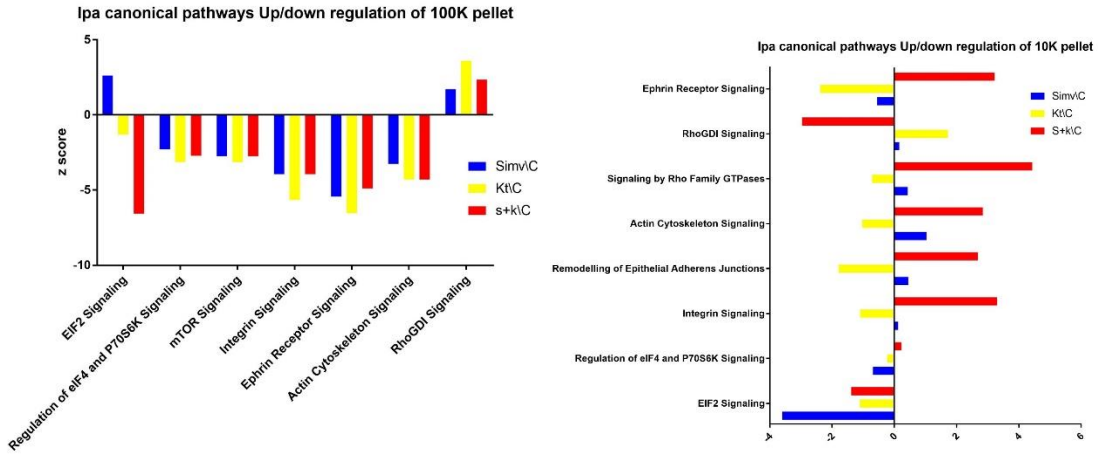

Figure 141 – Up- and down-regulation of IPA canonical pathways of 10K and 100K EVs pellet after treatments in our experimental conditions.

As clearly reported in the graphs we obtained important modulations in terms of z score of several 100K and 10K functions. All pathways found in both EV categories are involved in melanoma, as previously reported. Increased levels of EIF2α have been related to a worst melanoma prognosis and to the invasive phase of melanoma [99]. Integrin signaling is responsible for metastasis dissemination by the adhesion through integrins to extracellular matrix thus a therapeutic strategy involved in lowering its expression in both categories of vesicles secreted by a tumoral cell line is certainly an attractive therapeutic strategy, as well as the reduction of ephrin receptor signaling. In addition our treatments can be utilized as research tool to better understand if different vesicles populations have different roles in melanoma. Treatments indeed act differentially in the two groups, sometimes leading to opposite effects supporting to speculate about different biogenesis mechanism beyond 10 and 100K which are strongly and differentially dependent on cholesterol and BMP.

100K		Simva/C	KT/C	S+KT/C
cellular movement				
migration				
cell growth and proliferation				
cell death				

10K		Simva/C	KT/C	S+KT/C
cell death and survival				
protein synthesis				
cellular movement				
cellular assembly and organization				

Figure 142 – IPA molecular and cellular functions in 100K and 10K after pharmacological treatments. Blue=downregulated, orange = upregulated.

In addition, IPA analysis unraveled that the 100K and 10K share patterns that regulate several important cell features, as cellular movement and cell death which are common between the two fractions. On other hands we found also differences; 100K are indeed prone to promote cell growth, proliferation and migration, while 10K are involved in protein synthesis and cellular assembly and organization. Regarding 100K fraction all treatments reduced all functional categories involved in cancer pathogenesis. Interestingly, the association of the two treatments induces the generation of vesicles which transport genes involved in the induction of cell death. Even in 10K pellet we found a reduction of protein synthesis, cellular movement and cellular assembly and organization with an increased cell death. In conclusion it should be of paramount interest to develop a therapeutic strategy which confers reduced pro-tumoral characteristics to EVs directly produced by tumoral cell lines. IPA let us also to obtain a “graphical summary report” of the analysis; as previously mentioned pathways in blue are downregulated while those in orange ones are upregulated, in terms of z-score enrichment analysis, which accounts for total protein pattern functional enrichment.

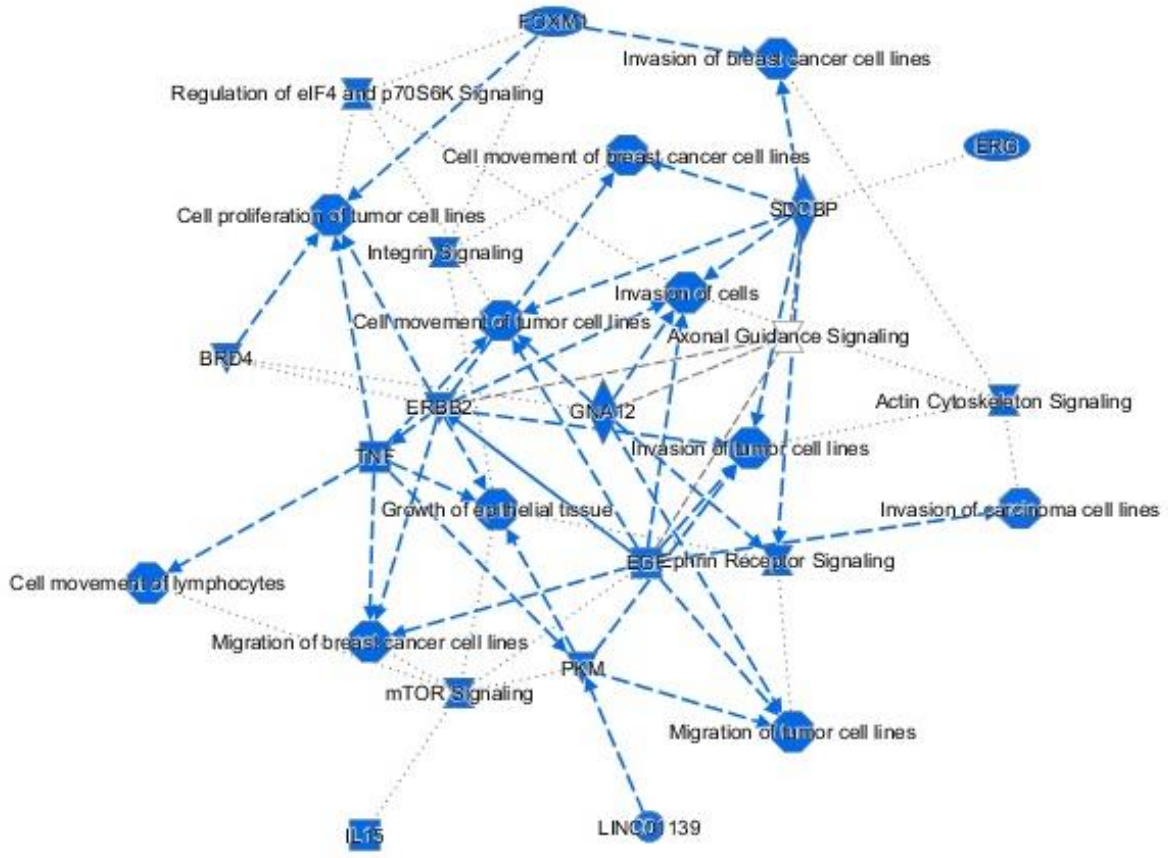

Figure 143 - Simvastatin effect on 100K pellet.

Simvastatin treatment significantly decreases several typical cancer behaviors which are part of 100K (exosomes) pellet functionality; EVs are indeed used to transport proteins, lipids and genetic material to close and distant cells, and they are one of the main reasons of metastasis progression of tumors and melanoma [100] [87] [101]; Simvastatin treatment significantly inhibits several cancer-related pathways as cell proliferation, mTOR signaling, cell movement of tumoral cell lines, invasion of carcinoma cell lines. Interestingly we found also other tumors in the list, particularly breast cancer; simvastatin inhibits ERBB2 signaling in EVs, which is one of the most important protein involved in breast cancer [102], which is strongly corroborated by the reduction of other protein functionalities related to breast cancer cells, as migration and cell movement of breast cancer cell lines. This is also in line with previous observations in which Melanoma can spread to lymph nodes, secondary sites in the skin, and distant organs such as the breast [103]. Melanoma in the breast could be primary in the breast skin, primary in the breast tissue, metastasis in the breast, or in-transit metastases to breast tissue and breast skin [103]. Graphical summary did not unravel any nodes significant upregulation.

Simvastatin is able to reduce caveolar and clathrin-mediated endocytosis signaling, which, as mentioned before, are involved in internalization in recipient cells. (green indicates the % of downregulation while red means upregulation). Altogether these data lead to the conclusion that simvastatin can act on two fronts: 1) the impaired capacity of transfer cancer related genes, some of them related to breast metastasis 2)reduced capacity of internalization in recipient cells.

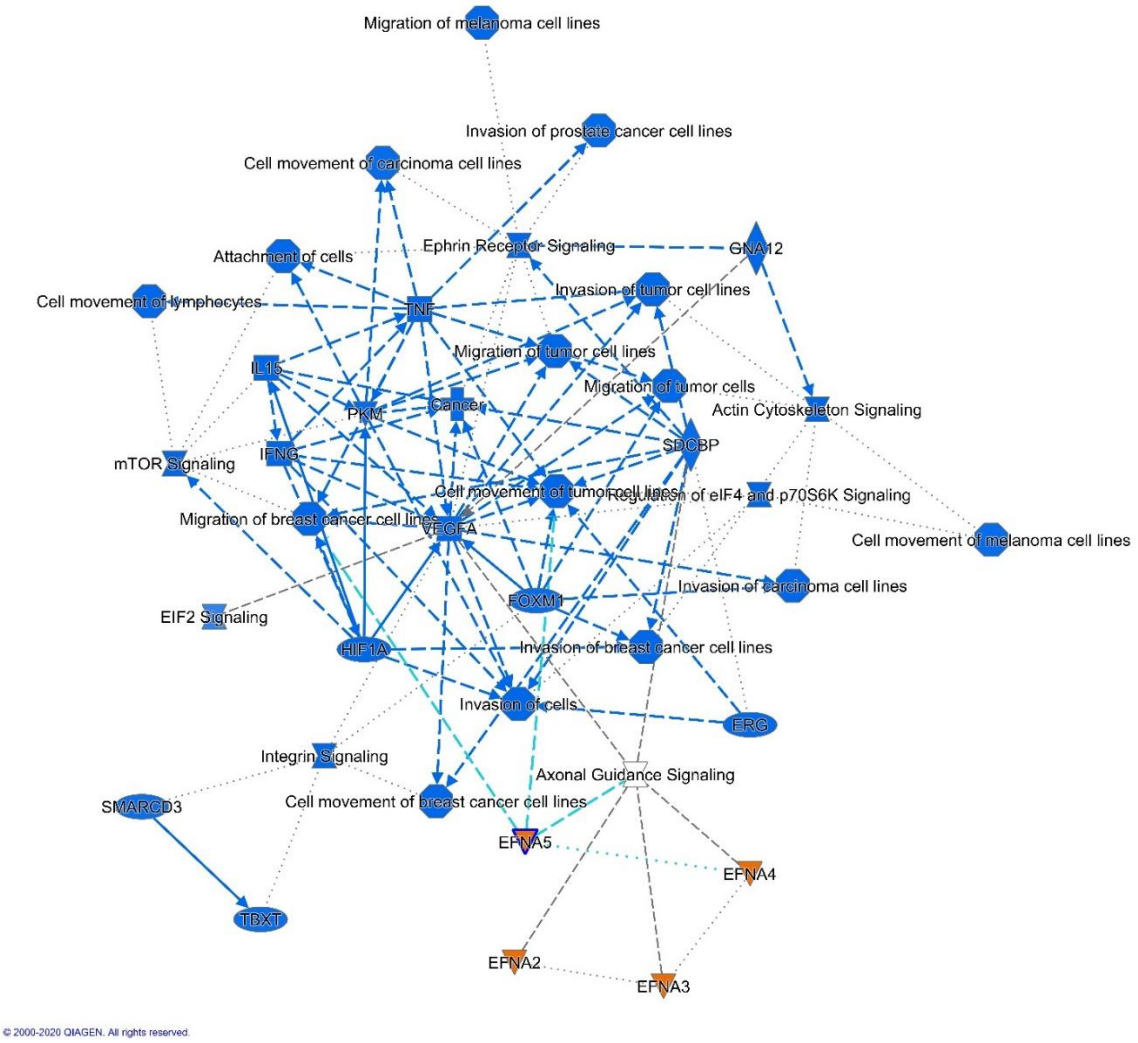

Figure 144 - Altered functionalities after KT182 treatment of 100K pellet.

As well as simvastatin, KT 182 impairs migration of melanoma cell lines, cell movement of carcinoma cell lines, cytoskeleton signaling, cell movement of melanoma cell lines, mTOR,

integrins, all functionalities related to metastatic behavior of melanoma. KT182 reduces also inflammatory pathways which involve IL-15 and TNF alpha. Another remarkable observation is the significant reduction of migration of breast cancer cell line. It has been reported that melanoma can spread first in lymph nodes and then in secondary sites in the skin and distant organs as the breast [103]. In addition, KT182 inhibits the vascular endothelial growth factor (VEGF), which is crucial for tumor neo-vascularization during metastasis formation and tumoral growth [104]. We found also upregulated functionality of EFNA family, which has been reported to be overexpressed in various cancers as melanoma, and promotes exosome-mediated chemoresistance to pharmacological treatment [105].

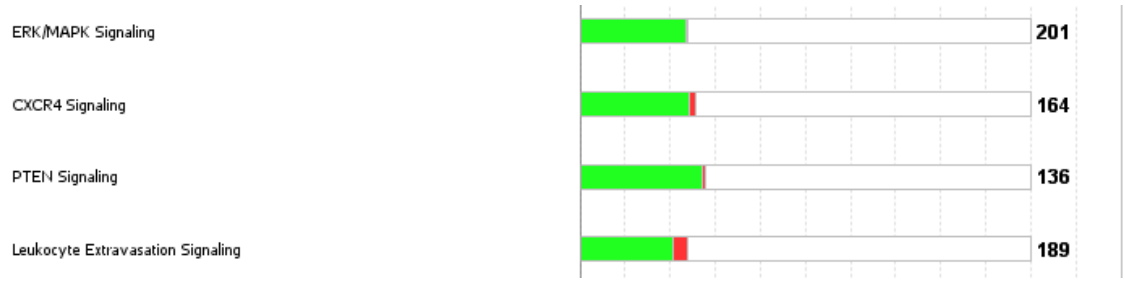

Kt182 is also able to exerts a significant downregulation of several cancer-related genes and kinases involved in cancer progression such as ERK/MAPK [63], CXCR4[106], PTEN [69] and leukocyte extravasation signaling. (green indicates the % of downregulation while red is the upregulation).

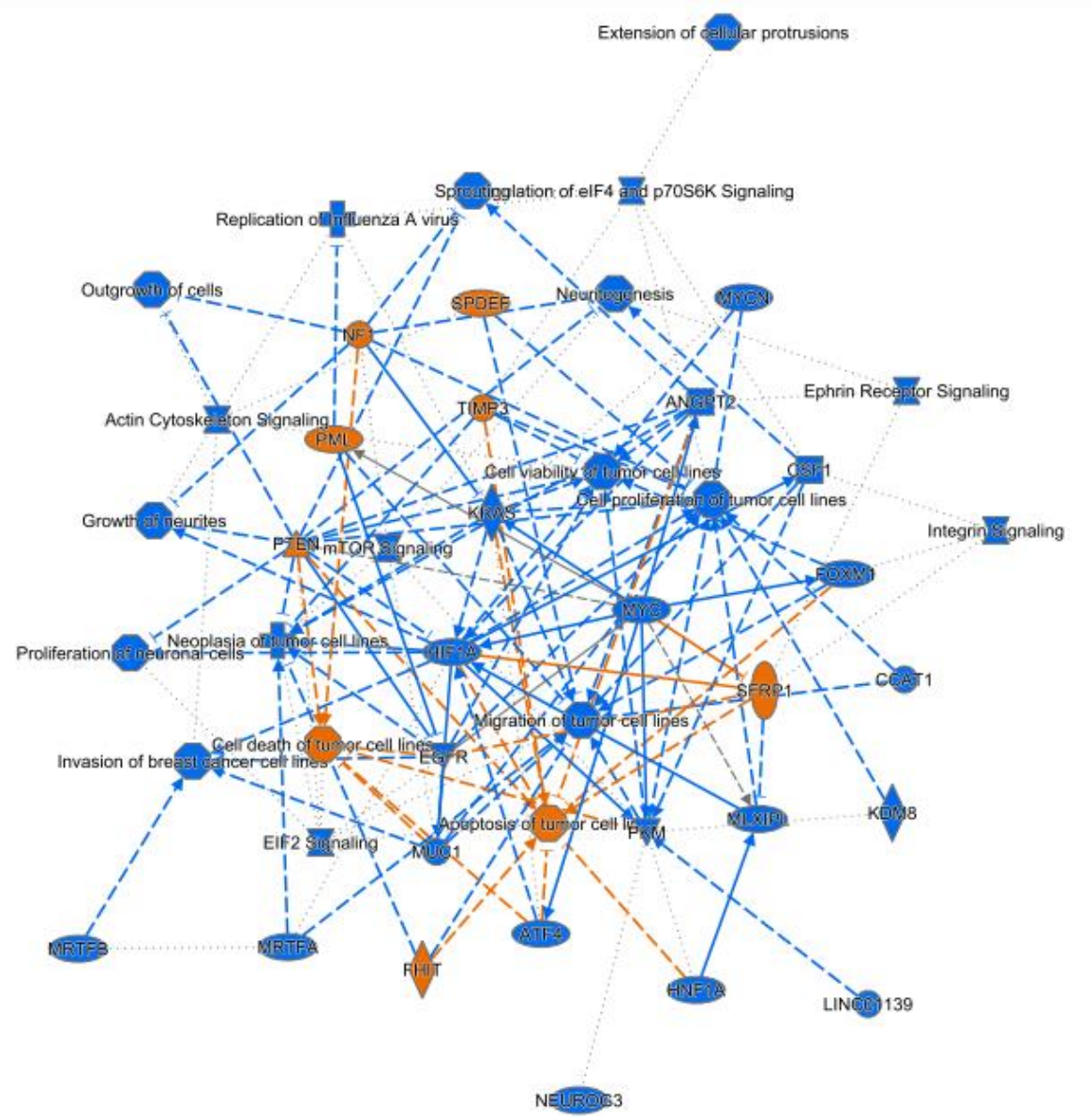

Figure 145 - Altered functionalities after KT182+ simvastatin treatment of 100K pellet.

KT182+simvastatin in our experimental conditions also reduced particular cancer related metastatic behavior, as neoplasia of tumor cell lines, migration, cell viability and cell proliferation. Interestingly in this case association of the two drugs increases cell death and apoptosis selectively of tumoral cell line (as reported in IPA); this feature is of paramount interest since it can be translated in an interesting therapeutic target. Indeed one of the most important limit of actual chemotherapy is that drugs do not distinguish between healthy and tumoral cells; in this case treatments seems to selectively inhibit tumoral cell lines proliferation.

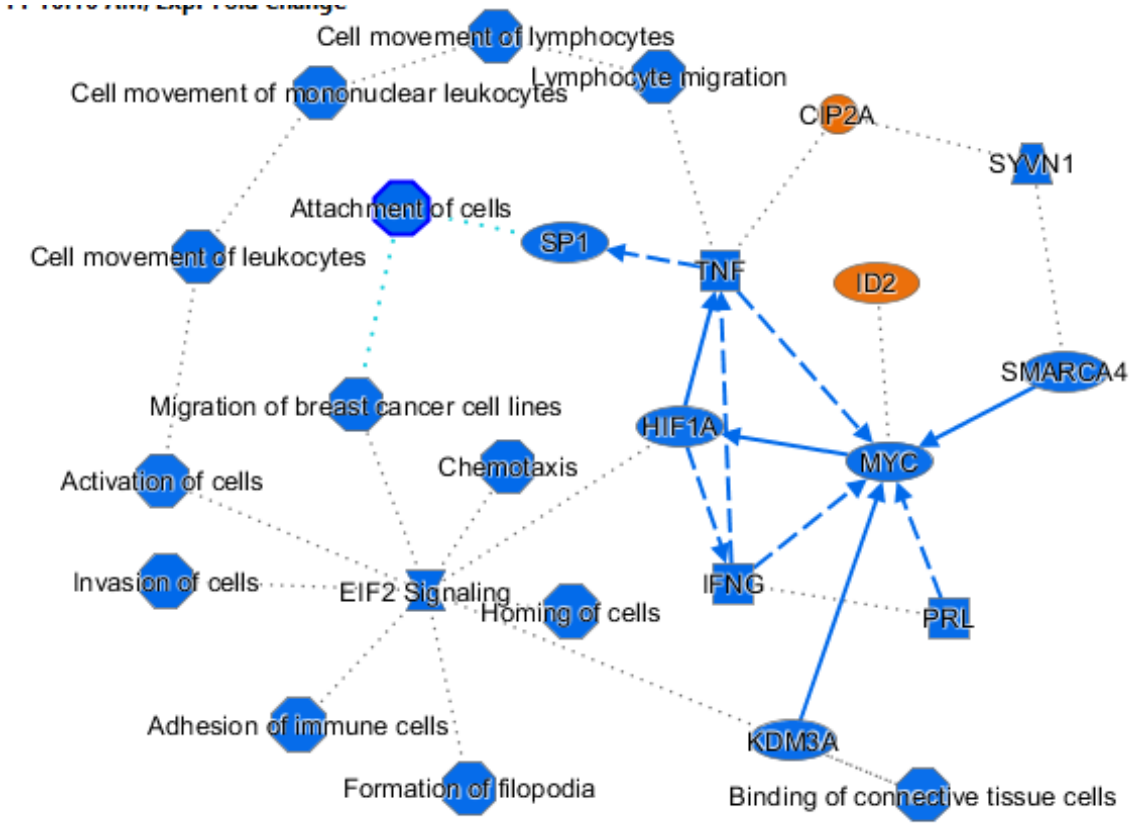

Figure 146 – Effects of simvastatin treatment in 10K pellet.

Simvastatin treatment in the same experimental conditions seems to decrease several immune system response functionalities, through the inhibition of lymphocyte and leukocytes migration and movement. These functionalities were absent in 100K pellet. Even in 10K pellet several and important cancer functionalities are downregulated, as activation, invasion, homing of cells. In addition, even in 10K migration of breast cancer cell lines is reduced, as well as TNF signalling.

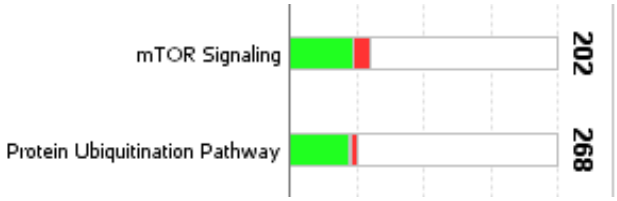

Ubiquitination is involved in the development of different tumors by regulation important genes or signaling pathways, above all melanomas. Targeting the ubiquitin-proteasome system (UPS) has recently been proposed as a new therapeutic strategy [107].

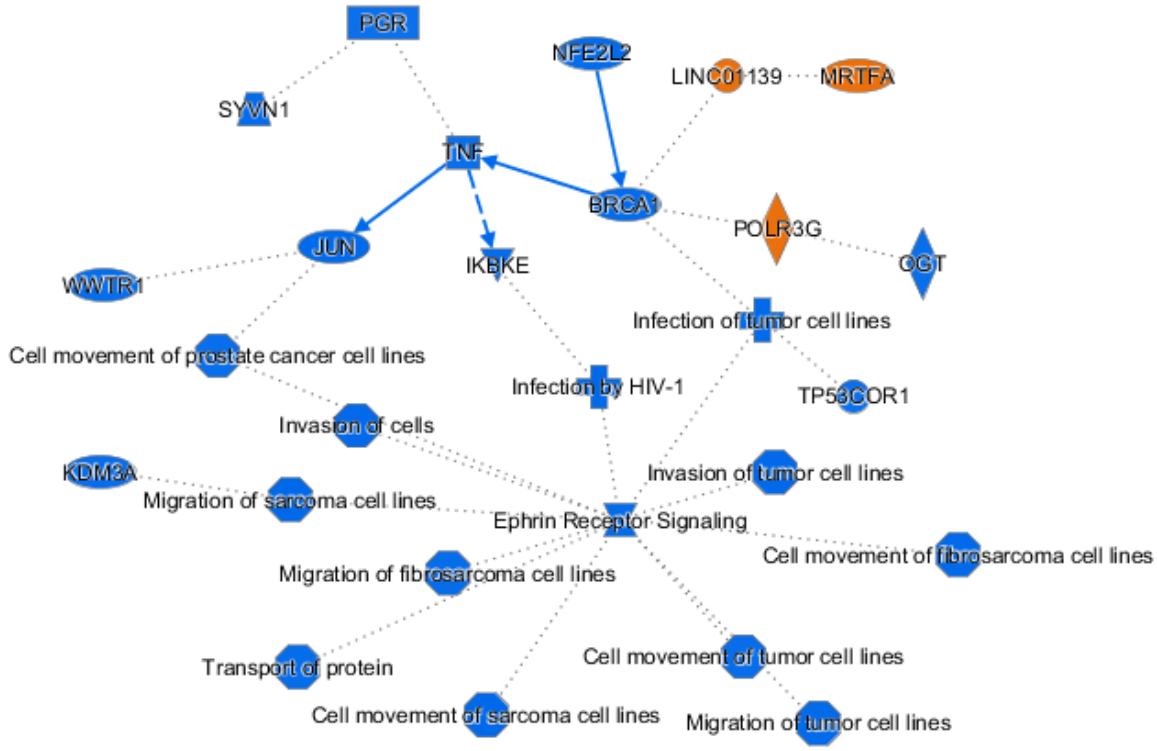

Figure 147 – Effects of KT182 treatment in 10K pellet.

Treatment with KT-182 also reduces some important and interesting aspect of cancer as cellular movement, invasion, infection and migration of tumor cell lines. Particularly KT182 reduces genes involved in migration of prostate cancer cell lines, whose relationship with melanoma was established in 2015 [108].

As well as in the other categories, we found a decrease of ephrin receptor, mTOR signaling and protein ubiquitination pathways.

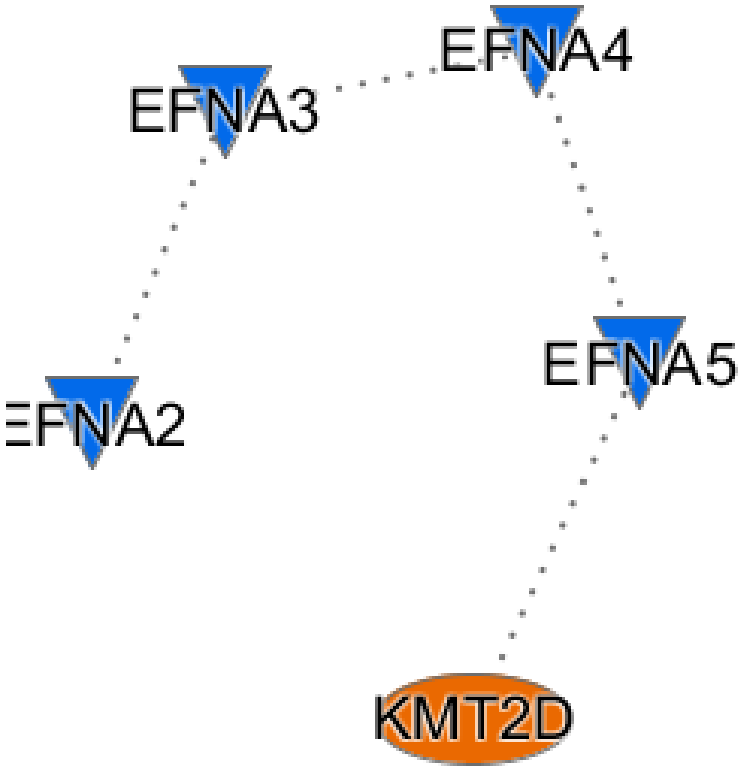

Figure 148 – Effects of KT182+ simvastatin treatment in 10K pellet.

In this case IPA reported reduction of Ephrin protein families, whose functionality has been extensively discussed before and the upregulation of (lysine (K)-specific methyltransferase 2D). Particularly KMT2D is as a potent tumor suppressor in melanoma [109]; its deficiency upregulates glycolysis enzymes, intermediate metabolites, and glucose consumption rates promoting tumorigenesis, thus its increase can be considered as a promising therapeutic strategy.

May Lipids can be useful for EVs quantification?

As mentioned, phospholipids represent one of the main components of extracellular vesicles and are part of their membrane. It is well known that there are about 5000000 lipid molecules in 1μm^2 of lipid bilayer[110], so the idea was to measure the phospholipid content of each fraction to try to obtain the number of the vesicles contained in the sample. The method proposed has several limitations: it does not account of the other lipids that can modify the shape of the vesicles, and of the really high curvature of the membrane that can impair the tabulated value. Anyway if it should be possible to overcome these limitations (maybe with a software-based reconstruction of the EVs membrane) it will be possible to propose a new and alternative method to count extracellular vesicles. These experiments have been based with PC-3 derived 5 fractions. Firstly the phosphorus content have been measured in 3 different experiments of the 5 fractions, with the Ames' assay.

	nmoles P	**SD**
Min 50	6,901753	2,358717
50-80	8,091498	1,353727
80-120	8,388646	1,604456
120-200	9,127821	3,004816
200+	9,650139	2,701786

Table 22 – nMoles of phosphorus contained in PC-3 derived fractions (mean of 3 different experiments, n=3).

Afterwards number of molecules of phosphorus have been obtained by utilizing the Avogadro's number (6,022x10^{23}) after the conversion of nmoles in moles.

	nmoles P	**Molecules P**
Min 50	6,901753	4,15x10^14
50-80	8,091498	4,87x10^14
80-120	8,388646	5,046x10^14
120-200	9,127821	5,49x10^14
200+	9,650139	5,81x10^14

Table 23 – nMoles of phosphorus converted in molecules of phosphorus contained in PC-3 derived fractions (n=3)

After that the surface of each fraction have been calculated through the the diameter (expressed by the Z-vg) of the particles calculated with the zetasizer, by utilizing the simple formula $4\pi r^2$.

	Z Avg Diameter (nm)	**Radius (nm)**	**Surface of the single EV**
Min 50	116	58	42,25 μm^2
50-80	102,80	51,4	33,183 μm^2
80-120	139,50	69,75	61,105 μm^2
120-200	232,28	116,14	169,415 μm^2
200+	498,8	249,4	781,236 μm^2

Table 24 – surface of the single EVs calculated on z avg diameter measured by Zetasizer

The total surface of the sum of the EVs contained in the sample from the phosphorus content have been calculated.

	Surface of total EVs
Min 50	83x10^6 μm^2
50-80	97x10^6 μm^2
80-120	100x10^6 μm^2
120-200	109x10^6 μm^2
200+	116,2x10^6 μm^2

Table 25 – surface of the total EVs calculated from phosphorus content.

At this point, by knowing the surface of the total EVs obtained nmoles of phosphorus and

the surface of the single EV measured by zetasizer we are able to calculate the number of Vesicles contained into the sample.

	Surface of total EV	**Surface of single EV**	**Number of particles**
Min 50	83x10^6 μm^2	42,25 μm^2	1,96x10^6
50-80	97x10^6 μm^2	33,183 μm^2	2,92x10^6
80-120	100x10^6 μm^2	61,105 μm^2	1,63x10^6
120-200	109x10^6 μm^2	169,415 μm^2	6,43x10^6
200+	116,2x10^6 μm^2	781,236 μm^2	1,48x10^6

Table 26 – Calculation of number of particles.

It would be really interesting to corroborate phospholipid measures with that of cholesterol since they are the main "lipid" components of EVs, and to try to develop an algorithm that considering lipid content may allow to calculate the number of EVs contained in a given sample.

Conclusions

Extracellular vesicles represent a very attractive field of research during last years. As previously mentioned EVs participate to several transduction signal pathways, and it has been demonstrated that the impairment of their functions leads to altered pathological states.

Since there is lack of accordance in EVs separation methods, which impairs their correct characterization and therefore the comprehension of their functions, we first decided to develop a new subsequent ultracentrifugation protocol which took in consideration the size-based guidelines.

In addition, since EVs are the "naturally" transporters of proteins, molecules, nucleic acids and so on in biological fluids, used to achieve cell-cell communications, studies on the comprehension of their protein/lipid/dimensions characterization may help in create synthetic lipid nanoparticles for efficient drug delivery systems. Most drugs fail indeed in clinical stages even though they showed good biological activity in in vitro studies, probably due to the lack of a physiological environment as that of human body and because of selectivity, bioavailability and specificity. These elements lead to the conclusion that is imperative to focus on alternative ways to carry drugs in biological fluids. Lipid nanoparticles (LNPs) represent a great technique that has been developed during last years as drug delivery. LNPs share several characteristics with EVs; they possess indeed comparable dimensions, they are surrounded by a lipid membrane and transport molecules in biological fluids. Naturally occurring EVs have been of interest due to their ability to communicate and deliver compounds to other cells. However LNPs lack of proteins in their structure, compared to natural EVs, and proteins are a prerequisite for targeted delivery; indeed surface proteins enable recognition and targeting capability.

As previously reported, in our studies we found several differences in terms of lipid and protein composition for 5 populations of naturally-occured EVs; several protein patterns are involved in EVs-specific mechanisms of internalization in recipient cells, as well as the different enrichment in saturated fatty acids among the different populations.

We strongly believe that our findings may pave the way to studies aimed at building efficient synthetic nanoparticles which accounts not only of EVs lipid composition but also of the proteic one. In addition, we found that Melanoma-released EVs include vesicles of different size, fatty acid and protein; these differences may translate into distinct behaviors and functions in biological fluids and help to define the role of specific EV populations in

physiological and pathological processes. To further improve our analyses we are now setting up conditions to perform IPA analysis utilizing not only the % of proteins encoding for a determined function but also their expression ratios.

Targeting EVs biogenesis and release may have potential clinical relevance for several diseases therapy, particularly in cancer since their circulating levels are elevated in patients with aggressive disease. Altering the release or the functionality of EVs in pathological states represent a new possible pharmacological strategy.

In order to pursue these aims we decided to modulate the levels of two important lipids involved in EVs biogenesis, namely cholesterol and BisMonoacylglycerophosphate in order to answer different questions: May Cholesterol and/or BMP modulation lead to:

1. altered number of EVs secretion?
2. differences in terms of EVs size?
3. different functionality due to different recruitment of proteins during EVs biogenesis.

Our results indicated that in our experimental conditions we did not affect cell proliferation; in addition Nanosight analysis of Exosomes (100k) and Microvesicles (10k) did not alter the number of secreted EVs and their size. Cholesterol and BMP modulation of melanoma cells dramatically alters the protein content of released EVs, possibly leading to altered EVs functionality, suggesting the potential of lipid modulation in reshaping tumor cell-released EVs to develop new therapeutic approaches. It is really intriguing to think that a modulation of lipid levels alters the proteic content of secreted EVs. To better understand mechanisms beyond these effects we are now performing a lipidomics analysis of cells and secreted EVs, to unravel possible changes in their lipid compositions.

Finally, these results pave the road to new pharmacological treatments to modulate EVs functions in cancer and may provide a new pharmacological tool to better understand EVs protein loading during their biogenesis.

References.

[1] "CORE CURRICULUM ONCOLOGIA CLINICA 2/ED." [Online]. Available: https://www.mheducation.it/core-curriculum-oncologia-clinica-2-ed-9788838639845-italy. [Accessed: 09-Feb-2021].

[2] M. Mandalà and D. Massi, "Tissue prognostic biomarkers in primary cutaneous melanoma," *Virchows Archiv*, vol. 464, no. 3. Springer Verlag, pp. 265–281, 2014, doi: 10.1007/s00428-013-1526-x.

[3] S. Gandini *et al.*, "Meta-analysis of risk factors for cutaneous melanoma: I. Common and atypical naevi," *Eur. J. Cancer*, vol. 41, no. 1, pp. 28–44, 2005, doi: 10.1016/j.ejca.2004.10.015.

[4] G. Van Niel, G. D'Angelo, and G. Raposo, "Shedding light on the cell biology of extracellular vesicles," *Nature Reviews Molecular Cell Biology*, vol. 19, no. 4. Nature Publishing Group, pp. 213–228, 01-Apr-2018, doi: 10.1038/nrm.2017.125.

[5] Y. W. Yi *et al.*, "Advances in analysis of biodistribution of exosomes by molecular imaging," *International Journal of Molecular Sciences*, vol. 21, no. 2. MDPI AG, p. 665, 02-Jan-2020, doi: 10.3390/ijms21020665.

[6] K. W. Witwer and J. Wolfram, "Extracellular vesicles versus synthetic nanoparticles for drug delivery," *Nat. Rev. Mater.*, 2021, doi: 10.1038/s41578-020-00277-6.

[7] C. Théry *et al.*, "Minimal information for studies of extracellular vesicles 2018 (MISEV2018): a position statement of the International Society for Extracellular Vesicles and update of the MISEV2014 guidelines," *J. Extracell. Vesicles*, vol. 7, no. 1, 2018, doi: 10.1080/20013078.2018.1535750.

[8] J. De Toro, L. Herschlik, C. Waldner, and C. Mongini, "Emerging roles of exosomes in normal and pathological conditions: New insights for diagnosis and therapeutic applications," *Front. Immunol.*, vol. 6, no. MAY, pp. 1–12, 2015, doi: 10.3389/fimmu.2015.00203.

[9] M. Colombo, G. Raposo, and C. Théry, "Biogenesis, Secretion, and Intercellular Interactions of Exosomes and Other Extracellular Vesicles," *Annu. Rev. Cell Dev. Biol.*, vol. 30, no. 1, pp. 255–289, Oct. 2014, doi: 10.1146/annurev-cellbio-101512-122326.

[10] K. J. McKelvey, K. L. Powell, A. W. Ashton, J. M. Morris, and S. A. McCracken, "Exosomes: Mechanisms of Uptake," *Journal of Circulating Biomarkers*, vol. 4. SAGE Publications Ltd, 29-Jan-2015, doi: 10.5772/61186.

[11] B. Adem, P. F. Vieira, and S. A. Melo, "Decoding the Biology of Exosomes in Metastasis," *Trends in Cancer*, vol. 6, no. 1, pp. 20–30, 2020, doi: 10.1016/j.trecan.2019.11.007.

[12] F. Colotta, P. Allavena, A. Sica, C. Garlanda, and A. Mantovani, "Cancer-related inflammation, the seventh hallmark of cancer: Links to genetic instability," *Carcinogenesis*. 2009, doi: 10.1093/carcin/bgp127.

[13] W. Mu, S. Rana, and M. Zöller, "Host matrix modulation by tumor exosomes promotes motility and invasiveness," *Neoplasia (United States)*, 2013, doi:

10.1593/neo.13786.

[14] M. Y. Fong *et al.*, “Breast-cancer-secreted miR-122 reprograms glucose metabolism in premetastatic niche to promote metastasis,” *Nat. Cell Biol.*, 2015, doi: 10.1038/ncb3094.

[15] H. G. Zhang, *Emerging concepts of tumor exosome–mediated cell–cell communication*. 2013.

[16] T. Skotland, K. Sagini, K. Sandvig, and A. Llorente, “An emerging focus on lipids in extracellular vesicles,” *Adv. Drug Deliv. Rev.*, Mar. 2020, doi: 10.1016/j.addr.2020.03.002.

[17] D. K. Jeppesen *et al.*, “Reassessment of Exosome Composition,” *Cell*, vol. 177, no. 2, pp. 428-445.e18, Apr. 2019, doi: 10.1016/j.cell.2019.02.029.

[18] C. Théry, A. Clayton, S. Amigorena, and and G. Raposo, “Isolation and Characterization of Exosomes from Cell Culture Supernatants,” *Curr. Protoc. Cell Biol.*, pp. 30:3.22:3.22.1–3.22.29, 2006.

[19] H. Zhang *et al.*, “Identification of distinct nanoparticles and subsets of extracellular vesicles by asymmetric flow field-flow fractionation,” *Nat. Cell Biol.*, vol. 20, no. 3, pp. 332–343, 2018, doi: 10.1038/s41556-018-0040-4.

[20] A. Zijlstra and D. Di Vizio, “Size matters in nanoscale communication,” *Nat. Cell Biol.*, vol. 20, no. 3, pp. 228–230, Mar. 2018, doi: 10.1038/s41556-018-0049-8.

[21] A. L. Altick, L. M. Baryshnikova, T. Q. Vu, and C. S. Von Bartheld, “Quantitative analysis of multivesicular bodies (MVBs) in the hypoglossal nerve: Evidence that neurotrophic factors do not use MVBs for retrograde axonal transport,” *J. Comp. Neurol.*, vol. 514, no. 6, pp. 641–657, Jun. 2009, doi: 10.1002/cne.22047.

[22] C. V. Harding, J. E. Heuser, and P. D. Stahl, “Exosomes: Looking back three decades and into the future,” *Journal of Cell Biology*, vol. 200, no. 4. The Rockefeller University Press, pp. 367–371, Feb-2013, doi: 10.1083/jcb.201212113.

[23] J. Kowal, M. Tkach, and C. Théry, “Biogenesis and secretion of exosomes,” *Current Opinion in Cell Biology*, vol. 29, no. 1. Elsevier Ltd, pp. 116–125, 01-Aug-2014, doi: 10.1016/j.ceb.2014.05.004.

[24] G. Raposo and W. Stoorvogel, “Extracellular vesicles: Exosomes, microvesicles, and friends,” *Journal of Cell Biology*. 2013, doi: 10.1083/jcb.201211138.

[25] N. P. Hessvik and A. Llorente, “Current knowledge on exosome biogenesis and release,” *Cellular and Molecular Life Sciences*, vol. 75, no. 2. Birkhauser Verlag AG, pp. 193–208, 01-Jan-2018, doi: 10.1007/s00018-017-2595-9.

[26] H. Stenmark, “Rab GTPases as coordinators of vesicle traffic,” *Nature Reviews Molecular Cell Biology*, vol. 10, no. 8. Nature Publishing Group, pp. 513–525, 15-Aug-2009, doi: 10.1038/nrm2728.

[27] P. D. Robbins and A. E. Morelli, “Regulation of immune responses by extracellular vesicles,” *Nature Reviews Immunology*. 2014, doi: 10.1038/nri3622.

[28] W. M. Henne, H. Stenmark, and S. D. Emr, “Molecular mechanisms of the membrane sculpting ESCRT pathway,” *Cold Spring Harb. Perspect. Biol.*, vol. 5, no. 9, Sep. 2013, doi: 10.1101/cshperspect.a016766.

[29] M. Record, S. Silvente-Poirot, M. Poirot, and M. J. O. Wakelam, “Extracellular vesicles: Lipids as key components of their biogenesis and functions,” *J. Lipid Res.*, 2018, doi: 10.1194/jlr.E086173.

[30] T. Skotland, K. Sandvig, and A. Llorente, “Lipids in exosomes: Current knowledge and the way forward,” *Progress in Lipid Research*. 2017, doi: 10.1016/j.plipres.2017.03.001.

[31] P. D. Robbins and A. E. Morelli, “Regulation of immune responses by extracellular vesicles,” *Nature Reviews Immunology*, vol. 14, no. 3. Nature Publishing Group, pp. 195–208, 25-Mar-2014, doi: 10.1038/nri3622.

[32] C. Tricarico, J. Clancy, and C. D’Souza-Schorey, “Biology and biogenesis of shed microvesicles,” *Small GTPases*, vol. 8, no. 4, pp. 220–232, 2017, doi: 10.1080/21541248.2016.1215283.

[33] H. Kalra, G. P. C. Drummen, and S. Mathivanan, “Focus on extracellular vesicles: Introducing the next small big thing,” *International Journal of Molecular Sciences*. 2016, doi: 10.3390/ijms17020170.

[34] J. Boyle, “Lehninger principles of biochemistry (4th ed.): Nelson, D., and Cox, M.,” *Biochem. Mol. Biol. Educ.*, 2005, doi: 10.1002/bmb.2005.494033010419.

[35] M. Tkach, J. Kowal, and C. Théry, “Why the need and how to approach the functional diversity of extracellular vesicles,” *Philos. Trans. R. Soc. B Biol. Sci.*, vol. 373, no. 1737, 2018, doi: 10.1098/rstb.2016.0479.

[36] E. Boilard, “Extracellular vesicles and their content in bioactive lipid mediators: More than a sack of microRNA,” *Journal of Lipid Research*, vol. 59, no. 11. American Society for Biochemistry and Molecular Biology Inc., pp. 2037–2046, 01-Nov-2018, doi: 10.1194/jlr.R084640.

[37] A. Llorente *et al.*, “Molecular lipidomics of exosomes released by PC-3 prostate cancer cells,” *Biochim. Biophys. Acta - Mol. Cell Biol. Lipids*, vol. 1831, no. 7, pp. 1302–1309, Jul. 2013, doi: 10.1016/j.bbalip.2013.04.011.

[38] C. A. Haynes, J. C. Allegood, H. Park, and M. C. Sullards, “Sphingolipidomics: Methods for the comprehensive analysis of sphingolipids,” *Journal of Chromatography B: Analytical Technologies in the Biomedical and Life Sciences*, vol. 877, no. 26. NIH Public Access, pp. 2696–2708, 15-Sep-2009, doi: 10.1016/j.jchromb.2008.12.057.

[39] N. E. Braverman and A. B. Moser, “Functions of plasmalogen lipids in health and disease,” *Biochimica et Biophysica Acta - Molecular Basis of Disease*. 2012, doi: 10.1016/j.bbadis.2012.05.008.

[40] A. A. Farooqui, L. A. Horrocks, and T. Farooqui, “Glycerophospholipids in brain: Their metabolism, incorporation into membranes, functions, and involvement in neurological disorders,” *Chemistry and Physics of Lipids*. 2000, doi: 10.1016/S0009-3084(00)00128-6.

[41] W. W. Christie and X. Han, “Lipid Analysis,” *Lipid Anal.*, pp. 305–338, 2010, doi: 10.1533/9780857097866.305.

[42] T. Rog and A. Koivuniemi, “The biophysical properties of ethanolamine plasmalogens revealed by atomistic molecular dynamics simulations,” *Biochim.*

Biophys. acta, 2016.

[43] F. Simbari *et al.*, "Plasmalogen enrichment in exosomes secreted by a nematode parasite versus those derived from its mouse host: Implications for exosome stability and biology," *J. Extracell. Vesicles*, 2016, doi: 10.3402/jev.v5.30741.

[44] S. Phuyal *et al.*, "The ether lipid precursor hexadecylglycerol stimulates the release and changes the composition of exosomes derived from PC-3 cells," *J. Biol. Chem.*, 2015, doi: 10.1074/jbc.M114.593962.

[45] M. R. Teli, O. F. W. James, A. D. Burt, M. K. Bennett, and C. P. Day, "The natural history of nonalcoholic fatty liver: A follow-up study," *Hepatology*, 1995, doi: 10.1002/hep.1840220616.

[46] F. W. Pfrieger and N. Vitale, "Thematic review series: Exosomes and microvesicles: Lipids as Key Components of their Biogenesis and Functions Cholesterol and the journey of extracellular vesicles," *Journal of Lipid Research*, vol. 59, no. 12. American Society for Biochemistry and Molecular Biology Inc., pp. 2255–2261, 01-Dec-2018, doi: 10.1194/jlr.R084210.

[47] J. Gruenberg, "Life in the lumen: The multivesicular endosome," *Traffic*, vol. 21, no. 1, pp. 76–93, Jan. 2020, doi: 10.1111/tra.12715.

[48] T. Kobayashi, E. Stang, K. S. Fang, P. De Moerloose, R. G. Parton, and J. Gruenberg, "A lipid associated with the antiphospholipid syndrome regulates endosome structure and function," *Nature*, vol. 392, no. 6672, pp. 193–197, 1998, doi: 10.1038/32440.

[49] J. Chevallier *et al.*, "Lysobisphosphatidic acid controls endosomal cholesterol levels," *J. Biol. Chem.*, vol. 283, no. 41, pp. 27871–27880, Oct. 2008, doi: 10.1074/jbc.M801463200.

[50] T. Kobayashi, K. Startchev, A. J. Whitney, and J. Gruenberg, "Localization of lysobisphosphatidic acid-rich membrane domains in late endosomes," *Biol. Chem.*, vol. 382, no. 3, pp. 483–485, Mar. 2001, doi: 10.1515/BC.2001.059.

[51] G. F. Grabner *et al.*, "Metabolic regulation of the lysosomal cofactor bis(monoacylglycero)phosphate in mice," *J. Lipid Res.*, vol. 61, no. 7, p. jlr.RA119000516, Jul. 2020, doi: 10.1194/JLR.RA119000516.

[52] K. Laulagnier *et al.*, "Mast cell- and dendritic cell-derived display a specific lipid composition and an unusual membrane organization," *Biochem. J.*, 2004, doi: 10.1042/BJ20031594.

[53] C. Bissig and J. Gruenberg, "ALIX and the multivesicular endosome: ALIX in Wonderland," *Trends in Cell Biology*, vol. 24, no. 1. Elsevier Current Trends, pp. 19–25, 01-Jan-2014, doi: 10.1016/j.tcb.2013.10.009.

[54] W. Möbius *et al.*, "Recycling compartments and the internal vesicles of multivesicular bodies harbor most of the cholesterol found in the endocytic pathway," *Traffic*, vol. 4, no. 4, pp. 222–231, Apr. 2003, doi: 10.1034/j.1600-0854.2003.00072.x.

[55] K. Strauss *et al.*, "Exosome secretion ameliorates lysosomal storage of cholesterol in Niemann-Pick type C disease," *J. Biol. Chem.*, vol. 285, no. 34, pp. 26279–26288, Aug. 2010, doi: 10.1074/jbc.M110.134775.

[56] A. Kulshreshtha *et al.*, “Simvastatin mediates inhibition of exosome synthesis, localization and secretion via multicomponent interventions,” *Sci. Rep.*, vol. 9, no. 1, pp. 1–10, Dec. 2019, doi: 10.1038/s41598-019-52765-7.

[57] T. Kobayashi *et al.*, “Separation and characterization of late endosomal membrane domains,” *J. Biol. Chem.*, 2002, doi: 10.1074/jbc.M202838200.

[58] M. Catalano and L. O’Driscoll, “Inhibiting extracellular vesicles formation and release: a review of EV inhibitors,” *J. Extracell. Vesicles*, vol. 9, no. 1, 2020, doi: 10.1080/20013078.2019.1703244.

[59] M. A. Antonyak and R. A. Cerione, “Microvesicles as mediators of intercellular communication in cancer,” *Methods Mol. Biol.*, 2014, doi: 10.1007/978-1-4939-0856-1_11.

[60] K. Essandoh *et al.*, “Blockade of exosome generation with GW4869 dampens the sepsis-induced inflammation and cardiac dysfunction,” *Biochim. Biophys. Acta - Mol. Basis Dis.*, vol. 1852, no. 11, pp. 2362–2371, 2015, doi: 10.1016/j.bbadis.2015.08.010.

[61] S. Phuyal, N. P. Hessvik, T. Skotland, K. Sandvig, and A. Llorente, “Regulation of exosome release by glycosphingolipids and flotillins,” *FEBS J.*, vol. 281, no. 9, pp. 2214–2227, 2014, doi: 10.1111/febs.12775.

[62] M. . Raiteri *et al.*, “Pharmacological control of the mevalonate pathway: Effect on arterial smooth muscle cell proliferation,” *J. Pharmacol. Exp. Ther.*, vol. 281, no. 3, pp. 1144–1153, 1997.

[63] T. Wang *et al.*, “Simvastatin-induced breast cancer cell death and deactivation of PI3K/Akt and MAPK/ERK signalling are reversed by metabolic products of the mevalonate pathway.,” *Oncotarget*, vol. 7, no. 3, pp. 2532–44, 2016, doi: 10.18632/oncotarget.6304.

[64] J. K. Cao, J. Kaplan, and N. Stella, “ABHD6: Its Place in Endocannabinoid Signaling and Beyond,” *Trends in Pharmacological Sciences*, vol. 40, no. 4. Elsevier Ltd, pp. 267–277, 01-Apr-2019, doi: 10.1016/j.tips.2019.02.002.

[65] P. Poursharifi, S. R. M. Madiraju, and M. Prentki, “Monoacylglycerol signalling and ABHD6 in health and disease,” *Diabetes, Obes. Metab.*, vol. 19, pp. 76–89, Sep. 2017, doi: 10.1111/dom.13008.

[66] J. Kowal *et al.*, “Proteomic comparison defines novel markers to characterize heterogeneous populations of extracellular vesicle subtypes,” *Proc. Natl. Acad. Sci. U. S. A.*, vol. 113, no. 8, pp. E968–E977, 2016, doi: 10.1073/pnas.1521230113.

[67] R. Crescitelli *et al.*, “Subpopulations of extracellular vesicles from human metastatic melanoma tissue identified by quantitative proteomics after optimized isolation,” *J. Extracell. Vesicles*, vol. 9, no. 1, p. 1722433, Jan. 2020, doi: 10.1080/20013078.2020.1722433.

[68] M. A. Livshts *et al.*, “Isolation of exosomes by differential centrifugation: Theoretical analysis of a commonly used protocol,” *Sci. Rep.*, vol. 5, no. October, pp. 1–14, 2015, doi: 10.1038/srep17319.

[69] M. Daniotti *et al.*, “BRAF alterations are associated with complex mutational profiles in malignant melanoma,” *Oncogene*, vol. 23, no. 35, pp. 5968–5977, Aug.

2004, doi: 10.1038/sj.onc.1207780.

[70] J. FOLCH, M. LEES, and G. H. SLOANE STANLEY, “A simple method for the isolation and purification of total lipides from animal tissues.,” *J. Biol. Chem.*, 1957, doi: 10.3989/scimar.2005.69n187.

[71] F. A. W. Coumans *et al.*, “Methodological guidelines to study extracellular vesicles,” *Circ. Res.*, vol. 120, no. 10, pp. 1632–1648, 2017, doi: 10.1161/CIRCRESAHA.117.309417.

[72] Politecnico di Milano, “Microscopia elettronica a trasmissione (TEM),” *http://samm.chem.polimi.it/microscopia-elettronica-a-trasmissione-tem*, 2020. .

[73] Alfatest, “Zetasizer Nano,” *https://www.alfatest.it/prodotti/zetasizer-nano*, p. 36, 2009.

[74] Malvern Panalytical Ltd., “Dynamic light scattering: An introduction in 30 minutes. Tecnical note (MRK656-01),” pp. 1–8, 2018.

[75] Catalog, “Nanosight Range,” *Malvern Instruments*, 2014.

[76] D. Maiolo *et al.*, “Colorimetric nanoplasmonic assay to determine purity and titrate extracellular vesicles,” *Anal. Chem.*, 2015, doi: 10.1021/ac504861d.

[77] R. Klein and A. Kania, “Ephrin signalling in the developing nervous system,” *Current Opinion in Neurobiology*, vol. 27. Elsevier Ltd, pp. 16–24, 2014, doi: 10.1016/j.conb.2014.02.006.

[78] M. A. Antonyak, K. F. Wilson, and R. A. Cerione, “R(h)oads to microvesicles,” *Small GTPases*, vol. 3, no. 4. Taylor and Francis Inc., p. 219, 2012, doi: 10.4161/sgtp.20755.

[79] B. Li, M. A. Antonyak, J. Zhang, and R. A. Cerione, “RhoA triggers a specific signaling pathway that generates transforming microvesicles in cancer cells,” *Oncogene*, vol. 31, no. 45, pp. 4740–4749, Nov. 2012, doi: 10.1038/onc.2011.636.

[80] G. van Niel, G. D’Angelo, and G. Raposo, “Shedding light on the cell biology of extracellular vesicles,” *Nat. Rev. Mol. Cell Biol.*, 2018, doi: 10.1038/nrm.2017.125.

[81] Y. H. Soung, S. Ford, V. Zhang, and J. Chung, “Exosomes in cancer diagnostics,” *Cancers*. 2017, doi: 10.3390/cancers9010008.

[82] M. J. Mitchell, M. M. Billingsley, R. M. Haley, M. E. Wechsler, N. A. Peppas, and R. Langer, “Engineering precision nanoparticles for drug delivery,” *Nat. Rev. Drug Discov.*, 2020, doi: 10.1038/s41573-020-0090-8.

[83] D. Ha, N. Yang, and V. Nadithe, “Exosomes as therapeutic drug carriers and delivery vehicles across biological membranes: current perspectives and future challenges,” *Acta Pharm. Sin. B*, vol. 6, no. 4, pp. 287–296, 2016, doi: 10.1016/j.apsb.2016.02.001.

[84] J.-S. Kang, “The potential of exosomes as theragnostics in various clinical situations,” in *Exosomes*, Elsevier, 2020, pp. 467–486.

[85] A. Hoshino *et al.*, “Tumour exosome integrins determine organotropic metastasis,” *Nature*, 2015, doi: 10.1038/nature15756.

[86] A. Li, T. Zhang, M. Zheng, Y. Liu, and Z. Chen, “Exosomal proteins as potential markers of tumor diagnosis,” *Journal of Hematology and Oncology*. 2017, doi: 10.1186/s13045-017-0542-8.

[87] A. L. Isola, K. Eddy, and S. Chen, “Biology, therapy and implications of tumor exosomes in the progression of melanoma,” *Cancers*. 2016, doi: 10.3390/cancers8120110.

[88] A. Zijlstra and D. Di Vizio, “Size matters in nanoscale communication,” *Nat. Cell Biol.*, vol. 20, no. 3, pp. 228–230, 2018, doi: 10.1038/s41556-018-0049-8.

[89] A. P. Madigan, B. Gallant, M. P. Clark, Y. Wan, W. Zhang, and H. Lu, “Exosomes-mediated mTOR activation is involved in ovarian cancer cell aggression and migration,” *FASEB J.*, vol. 31, pp. 614.23-614.23, doi: 10.1096/FASEBJ.31.1_SUPPLEMENT.614.23.

[90] W. Zhang *et al.*, “The exosome-mediated PI3k/Akt/mTOR signaling pathway in cervical cancer.,” *Int. J. Clin. Exp. Pathol.*, vol. 12, no. 7, pp. 2474–2484, 2019.

[91] S. Rana, S. Yue, D. Stadel, and M. Zöller, “Toward tailored exosomes: The exosomal tetraspanin web contributes to target cell selection,” *Int. J. Biochem. Cell Biol.*, 2012, doi: 10.1016/j.biocel.2012.06.018.

[92] S. M. Arias-Mejias, K. Y. Warda, E. Quattrocchi, H. Alonso-Quinones, S. Sominidi-Damodaran, and A. Meves, “The role of integrins in melanoma: a review,” *International Journal of Dermatology*, vol. 59, no. 5. Blackwell Publishing Ltd, pp. 525–534, 01-May-2020, doi: 10.1111/ijd.14850.

[93] T. K. Howcroft, H. G. Zhang, M. Dhodapkar, and S. Mohla, “Vesicle transfer and cell fusion: Emerging concepts of cell-cell communication in the tumor microenvironment,” in *Cancer Biology and Therapy*, 2011, doi: 10.4161/cbt.12.3.17032.

[94] J. Wolfram and M. Ferrari, “Clinical cancer nanomedicine,” *Nano Today*, vol. 25. Elsevier B.V., pp. 85–98, 01-Apr-2019, doi: 10.1016/j.nantod.2019.02.005.

[95] L. Alvarez-Erviti, Y. Seow, H. Yin, C. Betts, S. Lakhal, and M. J. A. Wood, “Delivery of siRNA to the mouse brain by systemic injection of targeted exosomes,” *Nat. Biotechnol.*, vol. 29, no. 4, pp. 341–345, 2011, doi: 10.1038/nbt.1807.

[96] W. Luo, Y. Dai, Z. Chen, X. Yue, K. C. Andrade-Powell, and J. Chang, “Spatial and temporal tracking of cardiac exosomes in mouse using a nano-luciferase-CD63 fusion protein,” *Commun. Biol.*, vol. 3, no. 1, pp. 1–9, Dec. 2020, doi: 10.1038/s42003-020-0830-7.

[97] S. Buratta *et al.*, “Lysosomal exocytosis, exosome release and secretory autophagy: The autophagic- and endo-lysosomal systems go extracellular,” *Int. J. Mol. Sci.*, vol. 21, no. 7, Apr. 2020, doi: 10.3390/ijms21072576.

[98] M. Logozzi, D. Mizzoni, R. Di Raimo, and S. Fais, “Exosomes: A source for new and old biomarkers in cancer,” *Cancers*, vol. 12, no. 9. MDPI AG, pp. 1–18, 01-Sep-2020, doi: 10.3390/cancers12092566.

[99] I. Maida *et al.*, “Translational control mechanisms in cutaneous malignant melanoma: the role of eIF2α,” *J. Transl. Med.*, vol. 17, no. 1, p. 20, Dec. 2019, doi: 10.1186/s12967-019-1772-z.

[100] M. Tucci, F. Mannavola, A. Passarelli, L. S. Stucci, M. Cives, and F. Silvestris, "Exosomes in melanoma: A role in tumor progression, metastasis and impaired immune system activity," *Oncotarget*, vol. 9, no. 29. Impact Journals LLC, pp. 20826–20837, 17-Apr-2018, doi: 10.18632/oncotarget.24846.

[101] A. A. Patil and W. J. Rhee, "Exosomes: Biogenesis, Composition, Functions, and Their Role in Pre-metastatic Niche Formation," *Biotechnol. Bioprocess Eng.*, vol. 24, pp. 689–701, 2019, doi: 10.1007/s12257-019-0170-y.

[102] B. N. Hannafon, K. J. Carpenter, W. L. Berry, R. Janknecht, W. C. Dooley, and W. Q. Ding, "Exosome-mediated microRNA signaling from breast cancer cells is altered by the anti-angiogenesis agent docosahexaenoic acid (DHA)," *Mol. Cancer*, vol. 14, no. 1, pp. 1–13, 2015, doi: 10.1186/s12943-015-0400-7.

[103] A. Al Samaraee, H. Khout, T. Barakat, and T. Fasih, "Breast metastasis from a melanoma," *Ochsner J.*, vol. 12, no. 2, pp. 149–151, 2012.

[104] E. J. Ekström *et al.*, "WNT5A induces release of exosomes containing pro-angiogenic and immunosuppressive factors from malignant melanoma cells," *Mol. Cancer*, 2014, doi: 10.1186/1476-4598-13-88.

[105] J. Fan *et al.*, "Chemoresistance transmission via exosome-Mediated EphA2 transfer in pancreatic cancer," *Theranostics*, vol. 8, no. 21, pp. 5986–5994, 2018, doi: 10.7150/thno.26650.

[106] J. Kim *et al.*, "Chemokine receptor CXCR4 expression in patients with melanoma and colorectal cancer liver metastases and the association with disease outcome," *Ann. Surg.*, vol. 244, no. 1, pp. 113–120, Jul. 2006, doi: 10.1097/01.sla.0000217690.65909.9c.

[107] J. Guo and J. Zhang, "Ubiquitination and Deubiquitination in Melanoma Research and Clinically Relevant Outcomes," in *Ubiquitin - Proteasome Pathway*, IntechOpen, 2020.

[108] A. Goldenberg, S. I. B. Jiang, and P. R. Cohen, "A possible association between melanoma and prostate cancer. Results from a case-control-study," *Cancers (Basel).*, vol. 7, no. 2, pp. 670–678, Apr. 2015, doi: 10.3390/cancers7020670.

[109] M. Maitituoheti *et al.*, "Enhancer Reprogramming Confers Dependence on Glycolysis and IGF Signaling in KMT2D Mutant Melanoma," *Cell Rep.*, vol. 33, no. 3, Oct. 2020, doi: 10.1016/j.celrep.2020.108293.

[110] B. Alberts, A. Johnson, J. Lewis, M. Raff, K. Roberts, and P. Walter, "The Lipid Bilayer," 2002.

[111] Q. Zhang *et al.*, "Transfer of Functional Cargo in Exomeres," *Cell Rep.*, vol. 27, no. 3, pp. 940-954.e6, 2019, doi: 10.1016/j.celrep.2019.01.009.

[112] M. Tkach, J. Kowal, and C. Théry, "Why the need and how to approach the functional diversity of extracellular vesicles," *Philos. Trans. R. Soc. B Biol. Sci.*, vol. 373, no. 1737, p. 20160479, Jan. 2018, doi: 10.1098/rstb.2016.0479.

Introduction and main problems about EVs studies

Extracellular vesicles (EVs) are lipid bilayer particles physiologically secreted by cells, used to transport proteins, lipids and nucleic acid, and classified by origin: Microvesicles from plasma membrane and Exosome from MultiVesicularBodies (intracellular compartment in which intraluminal vesicles are generated). Newest works suggest classifications in small-(50-80nm), large(80-120nm) exosomes and microvesicles(120-1000nm) and exomeres<50 nm.

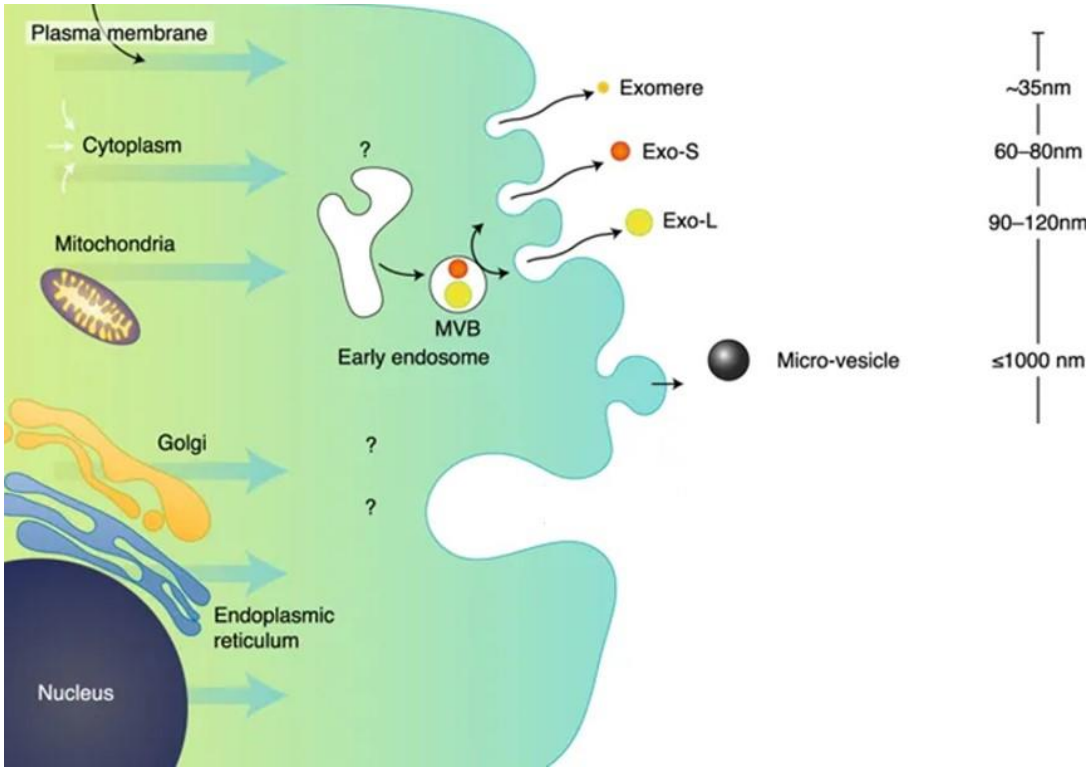

EVs dimensions interest aroused during last years as reviewed by Zijlstra et al.

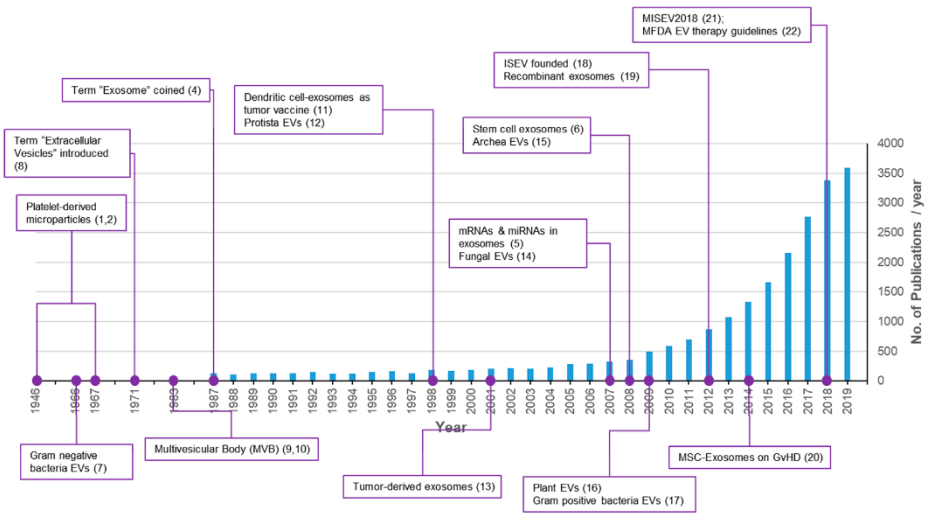

During last years a huge interest in this field emerged. The term "exosome" became unusual, being substituted with EVs, classified in exosomes, microvesices, microparticles, ectosomes, oncosomes, apoptotic bodies and many others. Specific issues arise when working with these "entities" whose size and amount make them difficult to obtain as pure preparation and to characterize them properly. In the current stage of EV field there is lack of precision knowledge.

For these reasons, it was so hard and compelling to start a new PhD project (since I was the first one to study EVs in my lab). The figure above represents EVs publications during last years, published with "lack of precision knowledge" as stated by Théry; We were at the beginning and we had first to study literature; it was really difficult to discriminate "the most precise works" to build the project. Therefore in the light of this situation we had to find, learn and optimize all methods for EVs isolation, characterization and a future pharmacological modulation, so most of experimental conditions can be considered as real "results" of this project.

During last year I visited the lab of exosome and prostate cancer, under supervision of Prof: Llorente where I highly refined my knowledge and techniques in EVs isolation and characterization, filling my gaps, and I learned to use several instruments as Electron Microscopy, Nanosight, zetasizer.

In addition, we utilized all the data of my project to write the Bando Seed called "New lipid-oriented pharmacological and chemical approaches to discriminate and unravel extracellular vesicles biological functions" which has recently been funded, in collaboration with Proff Valoti and Puglisi.

Aims, materials, methods development and optimization

1) **Cell models**

Since EVs are released from all cells but mostly from cancer cells[5] we utilized a lymph-node melanoma metastatic cell line (LM-16), breast adenocarcinoma (MDA-MB231) and. Prostate Cancer cell line (PC3)

2) **Isolation**

Given the inefficacy of current exosome isolation protocols to provide pure populations of EVs subtypes, all studies analyze the functions of mixtures of EVs, either a heterogeneous population of small EVs or mixtures of EVs of all sizes.

Canonical Differential ultracentrifugation(DC)[71] isolates EVs based on their size and density by increasing the centrifugal force to pellet debris (<1500g), large EVs (10K pellet), and small EVs (100K pellet).

The group of Livshits and colleagues developed a formula to theoretically calculate the expected size portion of the pelleted particles[7].To overcome aforementioned limitations, following dimensional guidelines, for the first time in EV studies we set the parameters to pellet five different EV fractions in our experimental conditions, respectively <50nm, 50-80nm, 80-120nm, 120-200nm and >200 performing a size-based EVs isolation through DC.

3) Characterization

W aimed to analyze their lipid composition because quantifying lipids in EV preparations, takes into account the defining component of EVs: the lipid bilayer that defines them as vesicles, resulting in an interesting possibility for their characterization.

Thanks to the collaboration of Dr. Sagini and the facility of Electron Microscopy in Oslo, we optimized the classical method to better stain the 5 different fractions. We also analysed dimensional data from pictures through TEM exosome analyser software.

Further dimensional analysis was performed in Oslo with Nanoparticle tracking analysis (Nanosight) and dynamic light scattering (Zetasizer), thanks to the collaboration with Alfatest srl, whose scientists (Dr. Moretto and Dr. Santoliquido) helped us to set as much as possible correct instrument for our particular analysis.

Proteomic analysis was performed through High Resolution Mass Spectrometry Analysis (nLC-HRMS).

Dimensional analysis

1) Zetasizer

	PDI	Z Avg (nm)	sd
Min 50	0,55	116	54,91
50-80	0.28	102,80	12,41
80-120	0.17	139,50	15,25
120-200	0.27	232,28	36,03
200+	0.23	498,8	72,83
10K	0.208	515,6	63,3
100K	0.199	149,2	11,2

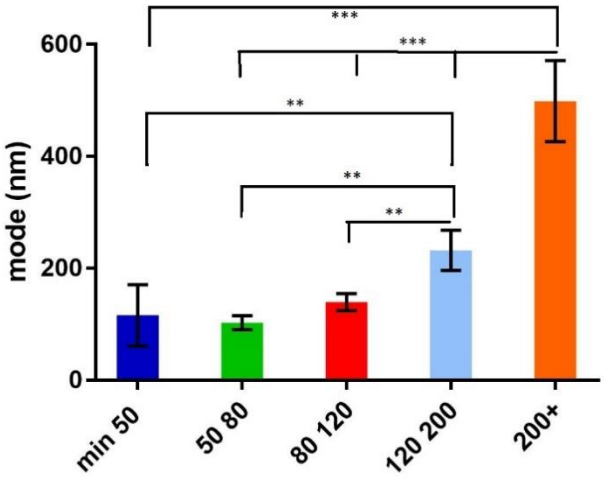

These experiments have been performed in Oslo with PC-3 cells (n=5). The table clearly shows as the Z average (which is the best way to represent the intensity average particle diameter) hydrodynamic radius is paralleled by the theoretical one, setup by the different centrifugation forces and times with significant differences (2-way anova). In addition to this, except for the smallest fraction (maybe for particle aggregation of instrument resolution), all particles clearly show a low and comparable polydispersity index, suggesting the homogeneity of each sample. 10K and 100K represent the “Canonical” pellets respectively microvesicles and exosomes.

	PDI	Z Avg (nm)	sd
Min 50	0,57	207,95	69,36
50-80	0.32	145,7	46,24
80-120	0.28	198,3	26,44
120-200	0.17	254,2	8,76
200+	0.29	337,4	13,70

The same trend is also documented in LM-16 cells

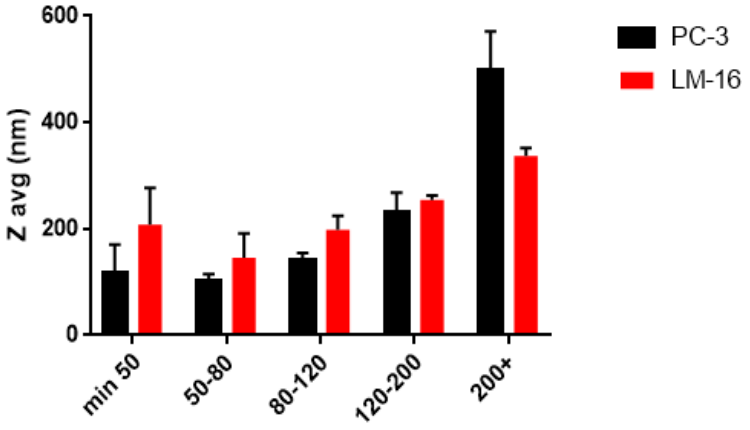

The graph summarizes the dimensional analysis of the two different cell lines. Interestingly, by performing the (two-way anova), there are no significant differences between the correspondently fractions of the two cell lines, but there is significant difference between the two 200+'s.

2) Nanosight

	min 50 nm	sd	50-80 nm	sd	80-120 nm	sd	120-200 nm	sd	200+ nm	sd	100k	sd
Mean	130,1	14,71	113,65	7,51	135,58	9,07	187,62	13,03	272,42	32,78	153,05	0,29
Mode	89,94	11,34	85,65	9,03	108,17	16,76	140,55	11,77	254,13	119,70	121,37	2,36

Nanosight mean and mode (most frequent particle) confirm the dimensional trend observed with zetasizer analysis (n=5)

3) Electron microscopy

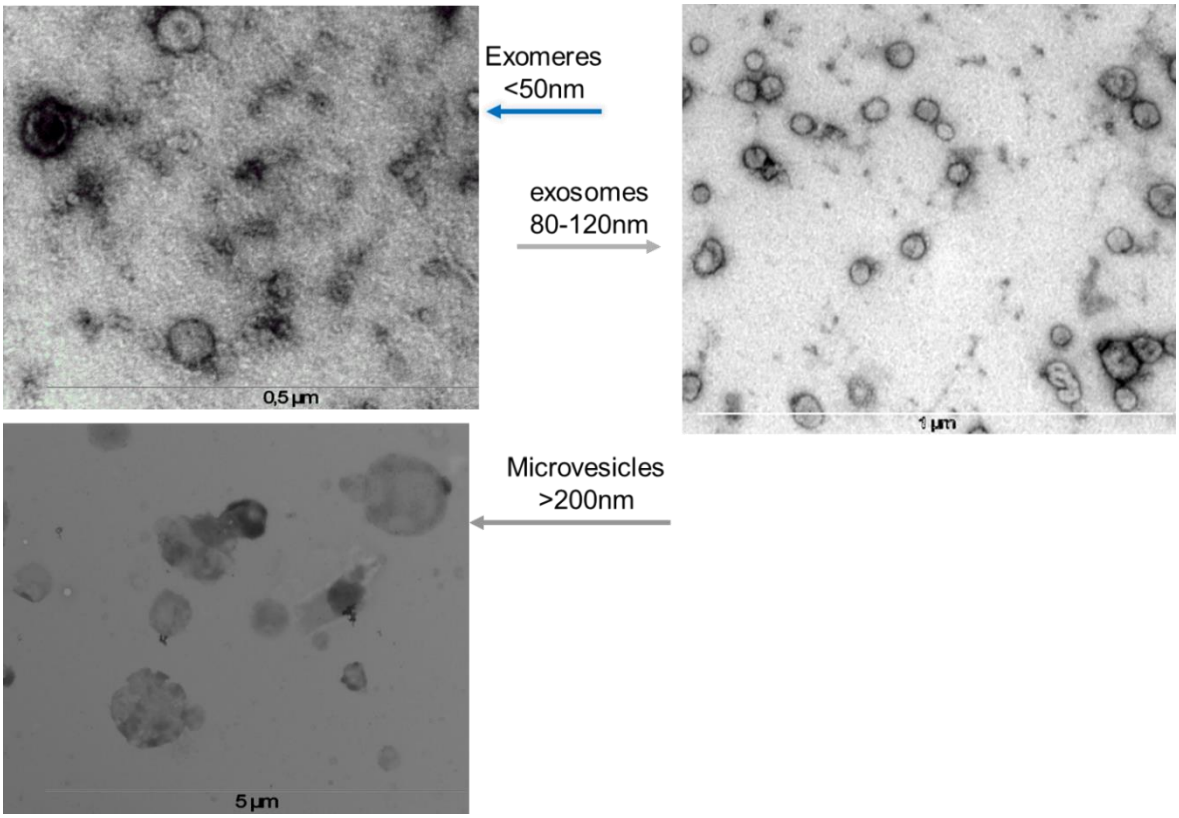

EM images confirmed the dimensions of particles subfractions

	nanosight	zetasizer	Electron microscopy
Min 50	89,94	116	28,45
50-80	85,65	102,80	48,50
80-120	108,17	139,50	47,25 (mean 62)
120-200	140,55	232,28	221,57
200+	254,13	498,8	n.d.

Comparison among three different classic method for EVs characterization shows that it is really tricky to dimensionally characterize EVs since it highly depends on isolation method and afterwards on dimensional characterization method which is utilized.

Characterization

1) Lipids

We deeply analyzed the lipid composition of parental cells (LM-16, PC-3 and MDA-MB-231), performing quali-quantitative analysis of most relevant lipid classes (data not shown)

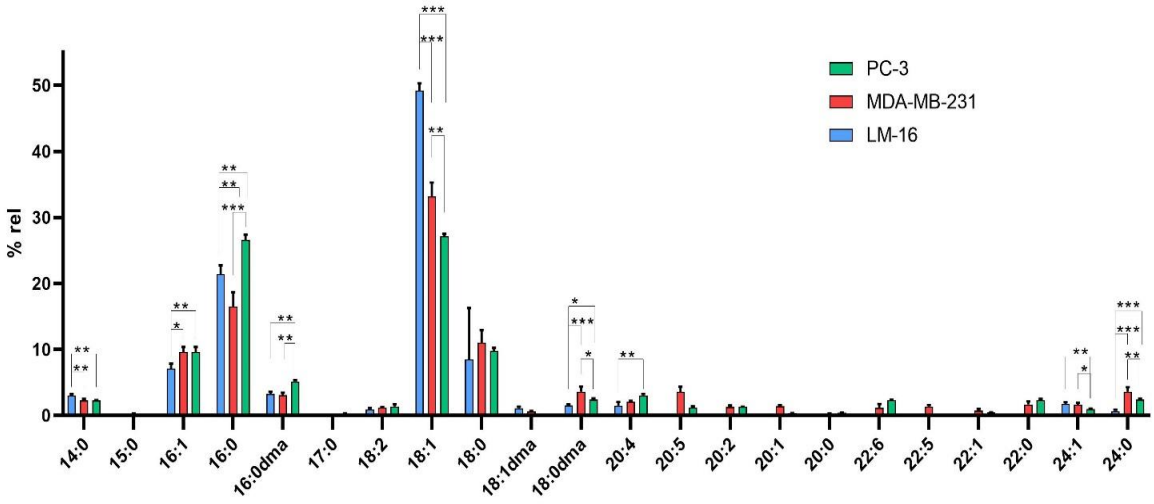

.

As expected and as clearly showed, each cell line possess its unique profile of fatty acids, which confers the functions of the different tissues.

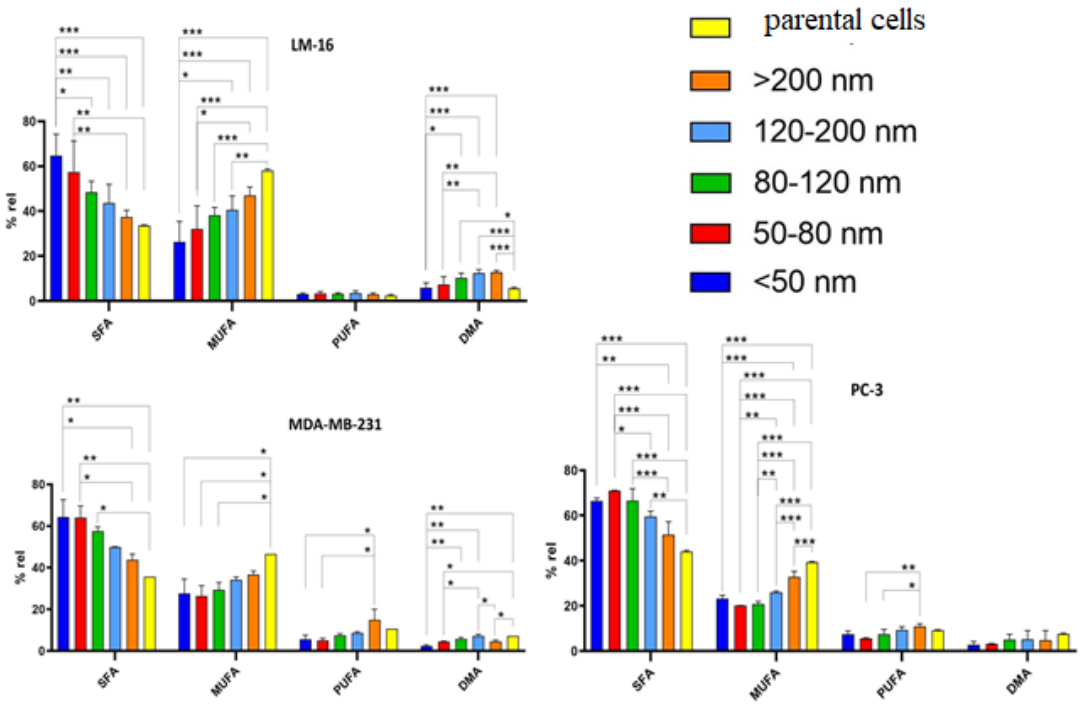

Here are represented fatty acid summarized for their grade of insaturation and fatty alcohols derived from total lipid extracts. Even if the 5 fractions derive from different cell lines (which are different in their total composition) they have the same pattern, EVs radius is paralleled by increased %rel of saturated fatty acids counterbalanced by a decrease in monounsaturated ones. This can be explained

not only by their tightness and curvature radius, but also from their different origin (since EVs are generated from lipid membrane budding).

We also measured Phosphorus and cholesterol even if it is not possible to normalize data due to the lack of precise methods to count vesicles; therefore we are more confident with fatty acids %rel because it is independent from any kind of normalization.

2)Proteomics

Protein characterization is fundamental for EVs studies, and we therefore decided to further investigate also in this field. We recently performed a deeply proteomic analysis of the fractions on LM-16 cell lines (n=3). Thanks to our collaboration with Prof P. Bergese (Università degli Studi di Brescia) through the Colorimetric NANoplasmonic Assay we were able to determine the purity grade of EVs preparations. The assay is indeed aimed at determining the presence of free protein contaminants in EVs preparations.

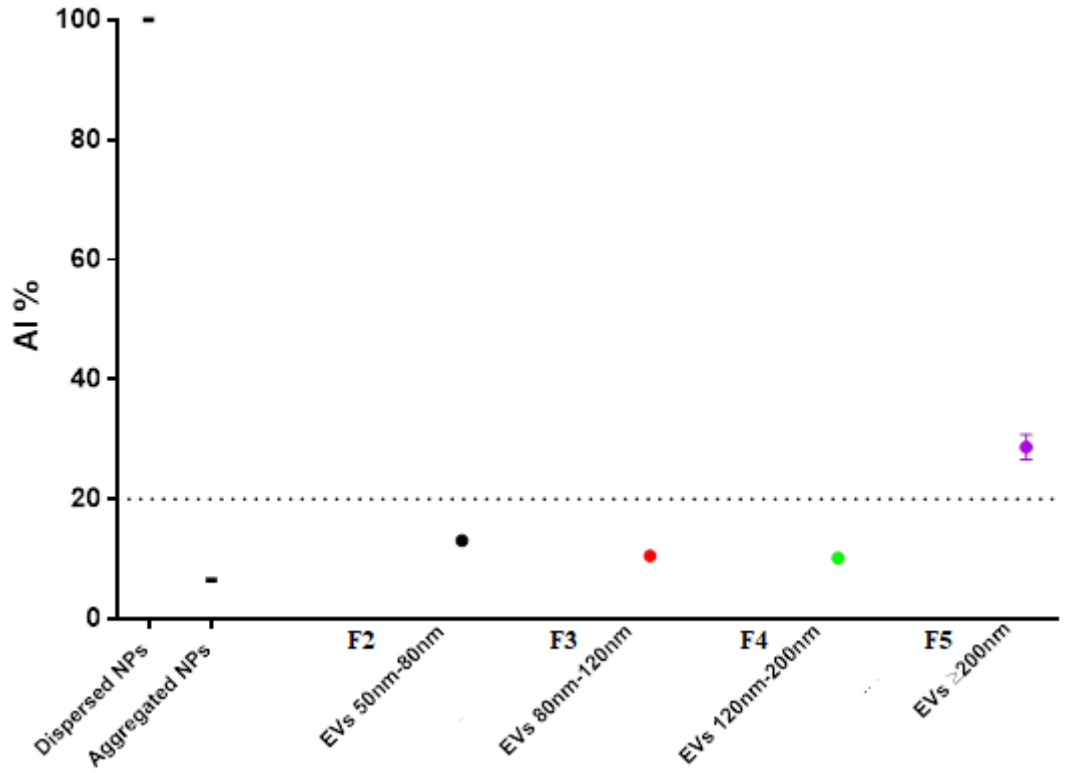

In our case, the fractions were free of protein contaminants, except for F5.

We then performed proteomics of 5 fractions , in order to unravel possible differences in terms of protein pattern carried by diferent EVs populations, thanks to our collaboration with Filarete foundation of UNIMI.

	Total proteins	**Common proteins**	**Unique proteins**
F-1	697	600	97

F-2	819	802	17
F-3	1079	1065	14
F-4	1621	1480	141
F-5	1654	1402	252

Number of proteins recovered in 5 fractions

As reported in the table we were able to find several proteins among the 5 fractions. Proteins have been separated in common proteins (present in more than one fraction) and unique (present only in that particular fraction).

Analysis of data have been further carried out by Ingenuity Pathway Analysis software.

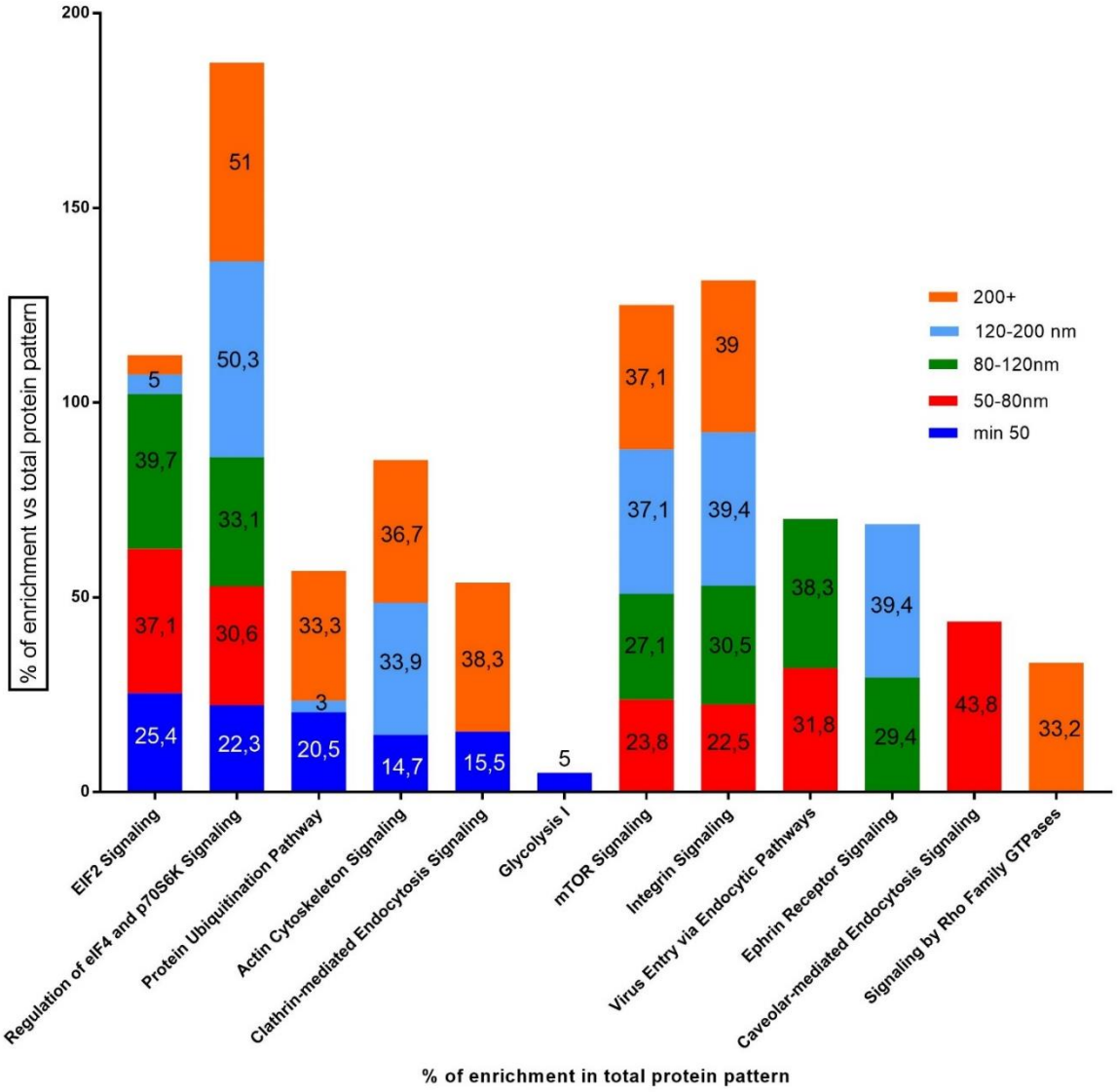

The differentially expressed proteins were categorized to related IPA canonical pathways

1) to obtain an elementary investigation about the functionality of the 5 different fractions

2) to unravel possible different functions involved in growth, proliferation and invasion of melanoma through EVs.

Protein patterns were quite surprising. Each fraction seems to be enriched differentially in pathways involved in various signaling. Proteins codifying for glycolysis seem to be present only in exomeres. mTOR and integrin signaling have similar profiles of enrichment for each fraction. Particularly mTOR is dysregulated in several types of cancer, and maybe its action is driven by extracellular vesicles. Integrin signaling is enriched in 120-200 and in 200+, meaning that these two fractions may be more prone in disseminating metastasis by the adhesion through integrins to extracellular matrix. Particularly in melanomas integrins are associated with metastasis and cell migration [92]. The ephrin-Eph signaling system is a bidirectional cell–cell communication device mediated by membrane-tethered ligand–receptor interactions. Ephs and ephrins function in many different physiological processes, including boundary formation and axon guidance, as well as pathological processes such as cancer [77]. Signaling by rho family GTPases is found only in 200+, which is the fraction composed by Microvesicles.

Pharmacological modulation

Since EV generation depends on lipid exchanges between different membranes involved in the pathway, it is reasonable to think that a modulation of lipid composition of parental cells may alter their release or functionality. In addition to this, cholesterol and BisMonoacylGlyceroPhosphate seems to co-operate for EVs biogenesis and release[29]. Since it is well known that simvastatin is able to reduce de-novo cholesterol biosynthesis while KT182 is a compound able to impair BMP degradation, we decided to treat parental cells with these two compounds.

We wanted to assess if pharmacological modulation of these two lipids may interfere with EVs release (number of vesicles released by the cell) or impair EVs functionality.

For the “pharmacological” part of the project, we utilized classical Thery’s ultracentrifugation method obtaining only two pellets, namely 10K Microvesicles and 100K Exosomes. We set the experimental conditions as follows:

- Day 0 – seeded 70000 cells x 35mm wells, with 10% FCS
- Day 1 – replaced media with 10% FCS + 0.1uM of simvastatin, 50nM of KT182 alone or in combination + 0.1% DMSO in ctrl and simvastatin group
- Day 3 – replaced media with serum free one + 0.1uM of simvastatin, 50nM of KT182 alone or in combination + 0.1% DMSO in ctrl and simvastatin group
- Day 6 – proliferation assay, MTT and de novo cholesterol biosynthesis.

In order to assess if treatments lead to a different concentration or dimensions of EVs secreted by cells we carried out nanosight analysis.

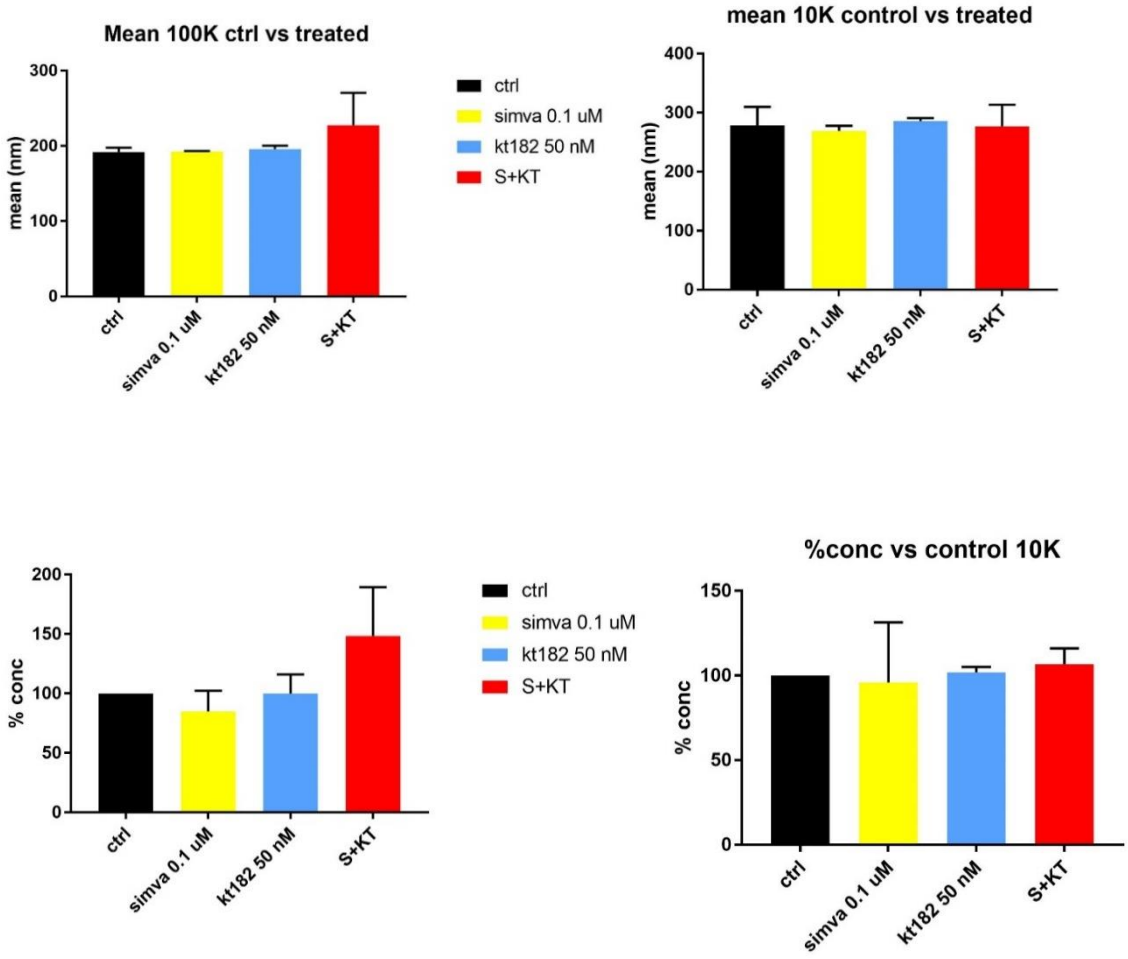

Graphs report that treatments did not affect dimensions and particle concentration in significant manner.

After dimensional analysis we carried out proteomics analysis in order to assess if modulation the aforementioned lipids may change EVs functionality through modulation of their protein content.

We found a total of 1293 for 100K, while 1192 in 10K fraction.

	100K	**100K**	**10K**	**10K**
	Significantly upregulated	Significantly downregulated	Significantly upregulated	Significantly downregulated
Simvastatin 0.1uM	65	6	36	27
KT182 50nM	60	4	46	17
Simvastatin+kt182	41	7	24	29

As reported in the table, we found that treatments significantly up and downregulated different proteins in both EVs populations.

In order to answer to the "functionality" question, we performed IPA analysis of the protein pattern obtained by our experiments.

100K	Simva/C	KT/C	S+KT/C
cellular movement			
migration			
cell growth and proliferation			
cell death			

10K	Simva/C	KT/C	S+KT/C
cell death (cell survival inhibition			
protein synthesis			
cellular movement			
cellular assembly and organization			

As reported in tables we found that treatment of parental cells with simvastatin, kt182 and their combination least to the secretion of exosomes (100k) which possesses reduced capacity to enhance cellular movement, migration, cell growth and proliferation and cell death, excepted for treatments association. In addition treatments are able to make also effects on microvesicles, reducing proteins involved in the promotion of cell survival, cellular movement and cellular assembly and organization.

Conclusions

We set up a valid and reproducible method to perform a size-based EVs isolation through ultracentrifugation. Differences in term of size have been confirmed by different dimensional analysis through TEM, AFM, Zetasizer and Nanosight. As previously reported, in our studies we found several differences in terms of lipid and protein composition for 5 populations of naturally-occured EVs; several protein patterns are involved in EVs-specific mechanism of internalization in recipient cells, as well as the different enrichment in saturated fatty acids among the different populations.

We strongly believe that our findings may pave the way to studies aimed at building efficient synthetic nanoparticles which accounts not only of EVs lipid composition but also of the proteic one. In addition we found that Melanoma-released EVs include vesicles of different size, fatty acid and protein; these differences may translate into distinct behaviors and functions in biological fluids and help to define the role of specific EV populations in physiological and pathological processes.

In addition we modulated the levels of two important lipids involved in EVs biogenesis, namely cholesterol and BisMonoacylglycerophosphate in order to answer different questions: May Cholesterol and/or BMP modulation lead to:

1. altered number of EVs secretion?
2. differences in terms of EVs size?
3. different functionality due to different recruitment of proteins during EVs biogenesis.

Cholesterol and BMP modulation of melanoma cells dramatically alters the protein content of released EVs, possibly leading to altered EVs functionality, suggesting the potential of lipid modulation in reshaping tumor cell-released EVs to develop new therapeutic approaches. To better understand mechanisms beyond these effects we are now performing a lipidomics analysis of cells and secreted EVs, to unravel possible changes in their lipid compositions.

Finally, these results pave the road to new pharmacological treatments to modulate EVs functions in cancer, and may provide a new pharmacological tool to better understand EVs protein loading during their biogenesis.

Congress participations:

1. Milan, Jul 2017, Speaker at Next Step VIII" "Exosomes, new markers of disease".

2. Poster session, "Simvastatin as a possible tool to alter extracellular vesicles functions. In vitro studies" Spring Meeting Gruppi Giovani SIIA, SIMI, SISA, Rimini 6-7 apr 2018.

3. Speaker at 2nd edition Spring School of the PhD of Pharmacological, Experimental and Clinical Science, Extracellular Vesicles: lipid characterization and their pharmacological modulation, Chiesa in Valmalenco, apr 12-15 2018,

4. Speaker at Next Step 9, Isolation, characterization and pharmacological modulation of different Extracellular Vesicles populations, Milan, 3rd Jul 2018

5. Poster session, "May lipid alteration affect extracellular vesicles' characteristics and functionality?" In vitro studies. 41st Annual Scientific Meeting of the European Lipoprotein Club, Tutzing Sep 10-13 2018.

6. Poster session, Convegno monotematico SIF "Cardiovascular Diseases: from population to basic science searching for new therapeutic targets""May lipid alteration affect extracellular vescicles characteristics and functionality? Napoli, 26-27 sep 2018.

7. Speaker at Convegno Regionale SISA Lombardia, XVII Giornata di Studio, Milano, 4-6 Oct 2018 "Studi in vitro per identificazione e caratterizzazione di vescicole extracellulari in base a size e composizione lipidica. Risultati preliminari".

8. Poster at Convegno Nazionale SISA Bologna 25-27 Nov 2018. "In vitro studies to identify and sort exosome based on their size and lipid composition. Preliminary results"

9. Speaker at 3rd edition Spring School of the PhD of Pharmacological, Experimental and Clinical Science, May a lipid signature identify different populations of Extracellular Vesicles? Studies in LM-16 cancer cell line. Chiesa in Valmalenco. 2-5 apr 2020.

10. Speaker at Next Step 10, sep 18th 2019; "separation and characterization of different extracellular vesicles populations. In vitro studies from a lymph node metastatic melanoma cell line.

11. Speaker at 1st EVIta Symphosium, 6-8 november 2019, Palermo, Italy "Size-dependent Extracellular Vesicles lipid composition. In vitro studies from a lymph-node metastatic melanoma cell line"

12. Speaker at 4th edition Spring School of the PhD of Pharmacological, Experimental and Clinical Science, Size-based isolation, characterization and pharmacological modulation of extracellular vesicles release Chiesa in Valmalenco, apr jun 25,28 2020

13. Oral presentation - ISEV 2021 annual meeting "Characterization of size-based isolated EV populations from a metastatic melanoma cell line by lipid analysis and proteomics"

14. Poster session – ISEV 2021 "May a pharmacological lipid modulation of parental cells reduce protumogeric signalling of secreted Extracellular Vesicles? In vitro proteomic studies on a human metastatic melanoma cell line

Grant or application for public/private financing

Co-writer of EXTRALIPO "New lipid-oriented pharmacological and chemical approaches to discriminate and unravel extracellular vesicles biological functions" Bando SEED – PSR 2019

Experience abroad

5 months at Norwegian Institute for Cancer Research (Oslo, Norway), in the group of exosomes and prostate cancer. My supervisor was Prof. Alicia Llorente.